PHOTODEGRADATION OF PHARMACEUTICALS WITH A RECYCLABLE CATALYST COFE2O4/TIO2 IN AQUEOUS PHASE

HAN GONG

Ph.D

The Hong Kong Polytechnic University

2018

The Hong Kong Polytechnic University

Department of Civil and Environmental Engineering

Photodegradation of pharmaceuticals with a recyclable catalyst $CoFe_2O_4/TiO_2$ in aqueous phase

Han GONG

A thesis submitted in partial fulfillment of the requirements for the
degree of Doctor of Philosophy

July 2017

CERTIFICATE OF ORIGINALITY

I hereby declare that this thesis is my own work and that, to the best of my knowledge and belief, it reproduces no material previously published or written, nor material that has been accepted for the award of any other degree or diploma, except where due acknowledgement has been made in the text.

__________________(Signed)

Han GONG (Name of Student)

DEDICATION

I would like to dedicate this thesis

to all those

who care, support, encourage and love me

ABSTRACT

Pharmaceuticals as emerging contaminants receive great concern because of their easy entry to the water body, frequent detection, low biodegradability, and considerable toxicity to the environment. The treatment of pharmaceuticals by advanced oxidation processes (AOPs) was explored due to the low removal efficiency of traditional methods.

In this study, a novel recyclable photocatalyst $CoFe_2O_4/TiO_2$ was developed. Three pharmaceuticals, including sulfamethoxazole (SMX), antipyrine (AP) and ibuprofen (IBP) were selected as the target compounds to evaluate the application of the photocatalyst in the degradation of pharmaceuticals. The effects of reaction parameters (light source, UV light intensity, initial target compound concentration, catalyst dosage and solution pH), anions, and commonly used oxidants on the destruction performance were studied. The reaction mechanism including the organic intermediates, TOC reduction and inorganic ions release was determined. The toxicity of the degradation products to aquatic organisms, including the green alga *Chlorella vulgaris* and the brine shrimp *Artemia salina* was investigated.

Firstly, the characteristic and magnetic property of the obtained catalyst were revealed. The catalyst was demonstrated to be homogenous spherical aggregates. The phases of $CoFe_2O_4$, anatase TiO_2 and rutile TiO_2, and the atomic ratios of Co, Fe, Ti and O from the catalyst were well justified. Reduced band gap energy and increased specific surface area compared to TiO_2 was found for the obtained catalyst. The average particle size and the zero point of charge value was determined to be around 30 nm and 8.0, respectively. The catalyst showed good magnetic property.

Secondly, based on the degradation of SMX, UV wavelength at 350 nm shows the best performance. The pseudo first-order rate constant of SMX destruction becomes predictable by using a proposed model in terms of SMX initial concentration and catalyst dosage. A light attenuation was found and analyzed by a linear correlation between the reaction rate k and transmission via a common factor (i.e. the catalyst dosage). The photocatalyst was found stable within the pH range of 5.2 and 8.8. The photocatalytic activity of the recycled catalyst remained intact after extensive reuses. The reaction mechanism during the treatment was determined. About 50% TOC reduction was detected as SMX was completely removed. Sixteen intermediates were detected, from which four of them were reported for the first time in this study. Four main destruction pathways, i.e. hydroxylation, cleavage of S-N bond, nitration of amino group, and isomerization were proposed. About 45% of the total mass sulfur source transformed to sulfate ion, and around 25%, 1%, and 0.25% of the total nitrogen transformed to ammonium, nitrogen, and nitrite ions. The toxicity of the treated solution was significantly reduced compared to that of the parent compound SMX. A variation of the algae growth was observed, which was due to the combination of generation of toxic intermediates (i.e. sulfanilamide) and the release of inorganic substances and carbon source as additional nutrients. The adverse effect on the clearance rate of the brine shrimp was also observed, but it can be eliminated if longer degradation time is used.

Thirdly, in terms of AP degradation, the catalyst shows the optimal removal efficiency under the conditions of wavelength at 350 nm, the catalyst dosage at 0.5 g/L, and pH value at 5.5. Ten organic intermediates were identified, and five of them were newly reported in AP treatment process. Hydroxylation, demethylation and the cleavage of the pentacyclic ring were included in the decomposition pathways. The ring opening was certified by the 45% TOC reduction and 60% ammonia release during the process. The parent compound AP and its degradation products show positive effects on the growth of the algae. However, acute toxicity of AP was detected on brine shrimps *A. salina*. The toxicity was eliminated gradually with the decomposition of AP and the generation of the byproducts.

Fourthly, for IBP photodegradation, the UV wavelength of 300 nm, the catalyst dosage of 0.5 g/L, and acidic condition were favorable for IBP destruction by photocatalysis. The removal efficiency was significantly elevated with the addition of oxone or persulfate, and the reaction was faster in the presence of oxone than that with the same concentration of persulfate. However, the reaction was significantly slowed down with the introduction of H_2O_2. The anion NO_3^- accelerated the reaction while the anions Cl^-, F^- and CO_3^{2-} slowed down the IBP photodegradation. Approximately 35% TOC reduction was detected when the parent compound IBP was totally removed. The adverse effect of the parent compound IBP to *C. vulgaris* was gradually eliminated with the decomposition of IBP. No adverse effect was detected for the survival and the feeding of *A. salina* exposed to IBP and the degradation products.

Finally, SMX degradation under UV/$CoFe_2O_4/TiO_2$ catalyzed permanganate oxidation was

investigated in detail for the first time. Sole permanganate showed no effect in SMX degradation, while its introduction to the photocatalytic process doubled the reaction rate at the optimal dosage. It is interesting to find that the reaction rate showed a fluctuation trend in terms of permanganate dosage due to the summation of positive effect of permanganate oxidation and the negative effect of the formation of MnO_2 (at catalyst surface) and light attenuation due to overdosed permanganate. The determined intermediates, the higher inorganic ions release and TOC reduction provided a clue on a higher mineralization compared to SMX degradation in the same process without permanganate. Permanganate above 1 μM may pose threat to the algae growth, therefore a good monitoring and control of residual permanganate dosage should be incorporated into the process design. A good toxicity reduction to *A. salina* was observed in the treated effluent; a longer detention is suggested if the complete removal of toxicity is required.

The results indicate that the photocatalysis process is effective in pharmaceutical removal, TOC reduction and toxicity elimination.

Keywords: pharmaceutical, degradation, photocatalyst, $CoFe_2O_4$/ TiO_2

PUBLICATIONS

Journal Papers:

1. Gong, H., and W. Chu. 2015. Photodegradation of sulfamethoxazole with a recyclable catalyst. Ind. Eng. Chem. Res. 54:12763–12769.

2. Gong, H., and W. Chu. 2016. Determination and toxicity evaluation of the generated products in sulfamethoxazole degradation by UV/$CoFe_2O_4$/TiO_2. J. Hazard. Mater. 314: 197–203.

3. Gong, H., W. Chu., M. J. Chen, and Q. X. Wang. 2017. A systematic study on photocatalysis of antipyrine: Catalyst characterization, parameter optimization, reaction mechanism and toxicity evolution to plankton. Water Res. 112:167-175.

4. Gong, H., and W. Chu. 2018. Permanganate with a double-edge role in photodegradation of sulfamethoxazole: Kinetic, reaction mechanism and toxicity. *Chemosphere*. 191:494-502.

Conference Presentation:

1. Gong, H. (presenter), and W. Chu. Sulfamethoxazole removal by UV/$CoFe_2O_4$/TiO_2: intermediates determination and toxicity evaluation. The 4th GIG-PolyU Workshop on Environmental Engineering and Sciences, Shenzhen, China, 18th December, 2015.

2. Gong, H. (presenter), and W. Chu. Photodegradation of sulfamethoxazole by a recyclable catalyst under UV illumination, the 5th International Conference on Emerging Contaminants (EmCon2016) and Micropollutants (WiOW2016) in the Environment, Sydney, Australia, 20th-23rd September, 2016.

3. Gong, H. (presenter), and W. Chu. Characterization and efficiency evaluation of a magnetic catalyst applied to pharmaceutical removal. The 5th Joint Workshop on Environmental Science and Engineering, Zhuhai, China, 1st-3rd June, 2017.

4. Gong, H. (presenter), and W. Chu. Toxicity reduction of antipyrine during photocatalysis. The 33rd International Conference of the Society for Environmental Geochemistry and Health (SEGH 2017), Guangzhou, China, 30th June-4th July, 2017.

ACKNOWLEDGEMENTS

I would like to dedicate the deepest gratitude to my supervisor Prof. Chu, who is always smiling, patient, kind, and gentle. It's one of the luckiest things for me to have such a good teacher. Thank him for his valuable guidance and endless encouragement. Thank him for teaching me so much on research work, paper writing and giving me the freedom to assign my work. I feel especially motivated to be able to keep doing what I enjoy.

I would like to deliver great thanks to the technicians in the Water and Wastewater Laboratory, Mr. Wai Shung Lam, Ms. Celine Che, Mr. Xie, Mr. Chi Wai Lau and Ms. Chloe for their patient assistant and technical support during my research.

I wish to express my heart-felt appreciation to colleagues in my research group, Dr. Meijuan Chen, Dr. Amy Rao, Dr. Rachel Wang, Prof. Fei Qi, Dr. Guoying Gao, Dr. Dan Shao, Dr. Jingzi Beiyuan, Prof. Shengyan Pu for their precious advices and endless encouragement. Special thanks go to Dr. Lucie Xu and Dr. Grace Lin, for their care, support and love. Sincere thanks also due to Prof. Yu Huang, Dr. Lu Gan and Dr. Xiaoliang Liang, for their generous instruction on the catalyst analysis. Great thanks for setting good examples for me and offering generous help.

I would like to express faithful appreciation to the teachers from CEE, Dr. Daniel Tsang, Dr. Henry Lee and Dr. Ben Leu for their great help during my PhD study.

I wish to extend sincere thanks to my dear friends, Dr. Belinda Gao, Dr. Yeejun Tham, Mr. Lomon Cui, Mr. Weihao Wang, Ms. Yan Tan and Ms. Erin Wang for creating such a wonderful environment full of love and happiness, for building so many beautiful memories in my life.

I wish to dedicate the special thanks to my families, for their steadfast love and support.

Especially thanks to my dearest parents, who support my study even in the poorest financial condition. Thank my father for his deepest love, for teaching me to be patient, strong, and responsible. The lessons on “read a million books and travel a million miles” will always be kept in my mind. Thank my mother for teaching me to be kind, honest, generous and gentle. Thank my brother Hero, for giving me uncountable lessons and companying or guiding me growing up. Thank my sister-in-law, Marina, who always gives me brilliant advice on my every important choice. Special thank also due to my little niece, the five-year-old little angel, for the endless happiness and laughter she takes to me especially when I suffered from the most horrible illness. I thank my little brother for teaching me to be brave and curious to explore, which is essential for my research work. Great thanks also belong to my sisters, my uncles and aunts for their warm care, support and encouragement during my growth. I want to express my deepest thanks to my grandparents, especially my grandma in the paradise, who is believed to be looking at me and lighting up the roads I am walking on as one of the shining stars up the sky. Wish our achievements can be seen and taken pride.

I would like to deliver special thanks to my idol, Stefanie Sun, who supports me to go further in my life with peace of mind. Special thanks also due to my best friend, Ms. Xiao Li. Thank them for accompanying me in the darkest time during my youth life, thank them teaching me so much. I would never be so positive without their encouragement and love.

I am grateful for the valuable comments from the reviewers, Prof. Shuncheng Lee, Prof. Xiaoyan Li, and Prof. Tsair-Fuh Lin for the improvement of the thesis.

Lastly, the financial support from the Hong Kong Polytechnic University (RTVG) are highly appreciated.

TABLE OF CONTENTS

5. Chapter five Photodegradation of sulfamethoxazole with the magnetic catalyst 72

LIST OF FIGURES

LIST OF TABLES

LIST OF ABBREVIATIONS

STPs	Sewage treatment plants
EPA	Environmental protection agency
NSAID	Non-steriodal anti-inflammatory drugs
SMX	Sulfamethoxazole
IBP	Ibuprofen
AP	Antipyrine
AOPs	Advanced oxidation processes
UV	Ultraviolet irradiation
US	Ultrasonic
VIS	Visible light irradiation
LC50	The half lethal concentration
EC50	The half effective concentration
IC50	The half inhibitory concentration
NOEC	None observed effective concentration
LOEC	Lowest observed effective concentration
HPLC	High performance liquid chromatography
UPLC	Ultra-high performance liquid chromatography
ESI	Electrospray ionization
LC/MS	Liquid chromatography/mass spectrometry
TOC	Total organic carbon
ACN	Acetonitrile

XRD	X-ray powder diffraction
SEM	Scanning electron microscopy
TEM	Transmission electron microscopy
EDX	Energy dispersive X-ray analysis
BET	Brunauer–Emmett–Teller
DRS	Diffuse reflectance infrared spectrometry
ZPC	Zero point of charge
JCPDS	Joint Committee on Powder Diffraction Standards
SFL	Sulfanilamide
MB	Methylene blue
RhB	Rhodamine B
MO	Methyl orange
2,4-D	2,4-dichlorophenoxyacetic acid
CB	Conduction band
VB	Valence band

1. Chapter one Introduction

1.1 Background

Plankton, including phytoplankton and zooplankton play critical roles in aquatic ecosystem. Firstly, by taking over bottom levels of the food chain, plankton serve as food for organisms at higher tropic levels (Edwards and Yool 2000). As the primary producers, phytoplankton support the survival of zooplankton, shellfish. And as the primary consumers, zooplankton provide food sources for fish (Christofersen et al. 1993). Shellfish and fish constitute important parts of fishery industry, thus are critical to the local economy. Secondly, molecular oxygen (O_2) is released during photosynthesis of phytoplankton, which not only guarantee the diluted oxygen in the water for survival of all aerobic organisms, but also help to control the atmospheric CO_2/O_2 balance (Shirokova et al. 2009). Finally, plankton play an important role in biogeochemical cycles of chemical elements as a biological pump in the carbon cycle (Garcon et al. 2001, Falkowski 2012, Herndl and Reinthaler 2013); where phytoplankton produce organic matter via photosynthesis, then the vertical migration and fecal pellet sedimentation from zooplankton contribute to the export flux (Turner 2015).

However, nowadays, the life activities of the plankton are threatened by various emerging contaminants (Carlsson et al. 2006, Kim et al. 2007). Among them, pharmaceuticals receive extensive concern in recent studies.

Apart from prevention and treatment of diseases, pharmaceuticals are also used in the growth promotion of live-stock (Kemper 2008). There are various ways for the entry of pharmaceuticals into the environment. Pharmaceuticals residues from either humans or animals that are not metabolized are excreted and pass through sewage drainage system (Lapworth et al. 2012). Pharmaceuticals for external use are easily washed off through bathing and transported to sewage treatment plants (STPs) through drainage system. Another important source of pharmaceutical pollutants is the wastewater produced by hospitals (Sarmah et al. 2006). Owing to the intensive use of drugs, the concentrations of pharmaceuticals from hospital effluents may be even higher than domestic sewage although the sewage discharge from the hospitals contributes to a small proportion of the total wastewater production. Additionally, the pharmaceuticals products which are overdue or unused may be disposed into rubbish bin and ended in the landfill (Pal et al. 2010). It is possible that pharmaceuticals are adsorbed in sludge at STPs and transported to the landfill for disposal. The residual pharmaceuticals in soil may further contaminate the groundwater (Maeng et al. 2011).

Currently, pharmaceuticals are not the major removal targets in water and wastewater treatment. Due to the wide use, the casual release and the incomplete treatment in STPs, pharmaceuticals have been detected in surface water, ground water and STPs (Dana W. Kolpin et al. 2002, Ellis 2006, Focazio et al. 2008, Spongberg et al. 2011). The detection levels are usually at ng/L or μg/L (Brown et al. 2006, Barnes et al. 2008).

Antibiotic is one group of the most frequently detected pharmaceuticals (Karthikeyan and Meyer 2006, Kummerer 2009, Yang et al. 2011, Zhou et al. 2013a, Zhou et al. 2013b, Zhang et al. 2015b). Subgroups of antibiotics include sulphonamides (e.g., sulfamethoxazole, SMX), macrolides (e.g., erythromycin), tetracyclines (e.g., tetracycline), fluoroquinolones (e.g., ciprofloxacin), Beta-Lactams (e.g., cefazolin) and phenicols (e., chloramphenicol). Totally twenty-one common antibiotics from the six categories were detected from the urine of school children aged 8–11 years (Wang et al. 2016). The detected antibiotics include both human antibiotics and veterinary antibiotics. The study concluded that some types of antibiotic were mainly from food or drinking water. What's more, the increased risk of obesity in school children was related to the exposure to the antibiotics.

Another important group of pharmaceuticals is the analgesics and non-steriodal anti-inflammatory drugs (NSAID). In this group, ibuprofen (IBP), antipyrine (AP, also known as phenazone), diclofenac, indomethacine, naproxen, acetylsalicylic acid, are widely produced, consumed and commonly detected (Roberts and Thomas 2006, Cooper et al. 2008, Mompelat et al. 2009, Zorita et al. 2009).

Other detected groups of pharmaceuticals include hormones (e.g., estrogens and progestogens), blood lipid regulators (e.g. clofibric acid), cardiovascular drug (e.g. propranolol and atenolol), anti-depressants (e.g. fluoxetine); antiepileptic drugs (e.g. carbamazepine), stimulants (e.g., caffeine) and so on (Mompelat et al. 2009, Zorita et al. 2009, Lapworth et al. 2012).

A number of researches proved that even at trace concentration (ng/L), pharmaceutical molecules may cause adverse impacts on the life activities of aquatic organisms (Farré et al. 2008). The untreated pharmaceutical molecules can further enter the human bodies via the food chain and the concentrations are possibly enhanced as a result of biological magnification via the food chain (Du et al. 2014, Li 2014, Taylor and Senac 2014, Puckowski et al. 2016). Besides, the existence of some antibiotics in the environment may induce the resistance of bacteria and thus the failure of clinic treatment. Therefore, the efficient removal of pharmaceuticals from the environment is a hot topic in recent years.

Traditional treatment technologies are reported to be ineffective in degradation of most pharmaceutical molecules (Gros et al. 2010), hence attempts on the utilization of newly developed technologies such as advanced oxidation processes (AOPs) were made (Klavarioti et al. 2009).

Titania is used widely as a photocatalyst in many processes (Gupta and Tripathi 2011). Several researches have verified that TiO_2 P25, to be specific, the process UV/TiO_2, is effective in degradation of varieties of pharmaceuticals including sulfamethoxazole (SMX), ibuprofen, antipyrine and so on (Calza et al. 2011, Hu et al. 2012, Tong et al. 2012). However, it is difficult for P25 to be widely applied in the practical water treatment because of its high cost and the limitation from being separated from the liquid phase after use. Therefore, how to reuse/recycle the suspended photocatalyst becomes a critical issue.

Magnetic photocatalysts could be effectively recycled by applying an external magnetic field. Therefore, titania-coated magnetic photocatalysts have attracted great attention in water treatment industry (Xu et al. 2007, Wu et al. 2015). Some recyclable titania-coated magnetic photocatalysts were reported and shown to be efficient in the degradation of other classifications of emerging contaminants (Lu et al. 2007, Casbeer et al. 2012, Ahangara et al. 2016, Arora et al. 2016, Bagheri and Julkapli 2016), while whether they are widely applicable in degradation of pharmaceutical molecule is unknown (Bagheria et al. 2016).

$CoFe_2O_4$ is one of the potential magnetic materials for such an application (Kharisov et al. 2014, Zhou et al. 2016). In this study, the $CoFe_2O_4/TiO_2$ was therefore synthesized by doping the commercial P25 with $CoFe_2O_4$. The degradation performance of three pharmaceuticals by using the photocatalyst and the recycled/spent catalysts were investigated. Besides, the knowledge on the catalyst is limited, hence a deeper study on the catalyst based on the characterization of the obtained nanoparticles will be conducted.

Based on previous studies, the reaction conditions such as light source, solution pH level, catalyst dosage and so on have a great influence on the performance of the photocatalysis process. Besides, some anions, Cl^-, F^-, SO_4^{2-}, NO_3^- and so on included, exist in the background environment and they may also affect the removal efficiency of the treatment process. Therefore, the effects of different parameters and anions were explored in this study.

Permanganate (Mn(VII); $KMnO_4$) has been widely used in water/wastewater treatment and remediation of contaminated groundwater (Ma et al. 1997, Hu et al. 2009, Jiang et al. 2009, Hu et al. 2010). The preferred characteristics of $KMnO_4$ shown in oxidation treatment include low cost, simple handling, relative stability and high efficiency over a wide pH range (Guan et al. 2010). Besides, compared to other oxidants such as chlorine and bromine, fewer harmful disinfection byproducts would be produced during the oxidation of the treated substance with permanganate (Rodriguez et al. 2007). Moreover, MnO_2, the product generated from permanganate an insoluble eco-friendly would facilitate the enhancement of coagulation and thus simultaneous adsorption of contaminants before their removal by sedimentation or filtration (Stone 1987, Ma et al. 1997, Zhang and Huang 2003, Jiang et al. 2009). Permanganate has been proven to be efficient in the degradation of multiple pharmaceuticals such as estrone, estiol, estracliol, ethylestradiol, cartamazepine, Acetaminophen (Hu et al. 2009, Guan et al. 2010, Hu et al. 2010, Wu et al. 2012, Fayad et al. 2013, Roderick et al. 2013, Zhang et al. 2013a), however, there are still a number of pharmaceuticals including caffiee, clofibrid acid, lopromid, ciprofloxacin, diclofenac, SMX, IBP are not in the list (Zhang et al. 2014a). Zhang et al. provided a clue by the combined use of catalyst Ru/TiO_2 and permanganate (Zhang et al. 2014a). Besides, the allowed inlet concentration was very low due to the unpleasant color of permanganate (Zhang et al. 2014b). Thus, catalyzing permanganate oxidation is becoming a possibility to achieve a high micropollutant removal at low permanganate dosage.

Similarly, potassium ferrate has received widespread attention and is used in coagulation, disinfection, and oxidation for multipurpose treatment of water and wastewater (Jiang et al. 2013, Jiang and Zhou 2013, Wilde et al. 2013, Barışçı et al. 2016). Compared to traditional oxidants such as chlorine, ozone, hydrogen peroxide, it has stronger oxidation ability with redox potential +2.20 V and +0.72 V, respectively, in acidic and alkaline conditions (Lee and von Gunten 2010, Ma et al. 2012, Liu et al. 2016). Besides, Fe(VI) is environmentally friendly since the by-product is the non-toxic Fe(III) (Li et al. 2005, Yang et al. 2012, Ma et al. 2015).

Apart from permanganate and ferrate, other frequently used oxidants include persulfate, oxone, hydrogen peroxide. It is assumed that the addition of the oxidants would enhance the performance of the photocatalysis process. Therefore, the information on the performance of the photocatalysis process in the presence of the commonly used oxidants /disinfectants was provided.

It was known that the partial or complete elimination of the parent compound does not necessarily indicate the reduction or the elimination of the potential adverse effects the degradation of the parent compound does not necessarily indicate of its toxicity to the environment. As already stated by several authors, some toxic degradation products may be formed during the treatments (Quero-Pastor et al. 2014, Szot 2014). Sometime, the toxicity of the treated effluent may be even higher than that of the parent compounds in the influent due to the formation of more toxic intermediates/products during the treatments. For example, a study on the toxicity of IBP and its intermediates suggests that the sub-product produced during ozonation has higher toxicity than the parent compound IBP (Quero-Pastor et al. 2014). The acute toxicity of SMX solution to *Daphnia magna* was increased after ozonation due to the formation of toxic intermediates (Abellán et al. 2007). In that case, the treatment process may not be advantageous in the treatment of the target compound. Since the aim of water treatment is to decrease or eliminate the adverse effect of the parent compounds to the environment, it is of great importance and necessary to understand the transformation products and monitor the toxicity of the pollutants during their transformation and provide basic information for the optimization of the treatment process. Therefore, assessment on whether the products still exhibit risk to life activities of aquatic organisms was conducted in this study.

The green algae *Chlorella vulgaris* is a species found worldwide and has been used in many studies on toxicity evaluation of organic pollutants (Baran et al. 2006, Qian et al. 2009, Cui and Li 2014). The brine shrimp *Artemia salina* is a microplanktonic filter feeder as well as an important aquaculture species used as live food for aquaculture organisms, including fish larvae (Kokkali et al. 2011). It is also widely used in the toxicity assessment of pollutants in aquatic environment for its cheap culture, short generation time, and high sensibility (Costello et al. 1993, Krishnakumar et al. 2007, Milhem et al. 2008, Awolola et al. 2010, da Silva et al. 2014). Utilization of aquatic organisms that can be cultured in the laboratory to assess the toxicity of pollutants can provide important clues to the underlying mechanisms of toxicity (Yan et al. 2009). In this study, the green algae *C. vulgaris* and the brine shrimps *A. salina* was used to evaluate the toxicity evolution of IBP degradation products during the process.

To fill up the above knowledge gaps, a systematic study including the synthesis and characteristic of the catalyst, the efficiency evaluation of the photocatalysis process on the removal of three pharmaceuticals, the determination of the reaction mechanism, and the toxicity assessment of the pharmaceuticals before and after the treatment were carried out.

1.2 Aims and objectives

The aim of the study is to develop an effective photocatalysis process for removal of pharmaceutical pollutants in water and wastewater. To be specific, the objectives are listed below.

(1) To synthesize a magnetic photocatalyst $CoFe_2O_4/TiO_2$ by doping commercial $CoFe_2O_4$ with TiO_2.

(2) To reveal the characteristic of the catalyst with the assistance of X-ray powder diffraction (XRD), scanning electron microscopy (SEM), transmission electron microscopy (TEM), energy dispersive X-ray analysis (EDX), diffuse reflectance infrared spectrometry (DRS), Brunauer–Emmett–Teller (BET) and zero point of charge (ZRC) measurement.

(3) To evaluate the photocatalytic efficiency of the magnetic catalyst by removing three pharmaceuticals including SMX, AP and IBP. To evaluate the magnetic property and the recyclable use of the catalyst.

(4) To give the optimal degradation conditions for the degradation performance including the light source wavelength, the catalyst dosage and the solution pH. To establish models for prediction of the reaction rate with different initial target compound concentrations.

(5) To investigate the effects of anions, oxidants on the photocatalytic process. The assessment of the possible broadened processes such as the combination of the photocatalysis process with other oxidants will be carried out.

(6) To illustrate the reaction mechanism by the detection of organic intermediates, proposal of degradation pathways, determination of inorganic ions release and measurement of total organic carbon (TOC).

(7) To determine whether the process is efficient for the toxicity elimination/reduction by the toxicity evaluation of the pharmaceuticals to planktons (*C. vulgaris* and *A. salina*) before and after the treatment.

1.3 Structures of this thesis

Based on the above work, the thesis is presented in ten chapters.

The first chapter (i.e., the present chapter) gives the background, objectives, and organization of the thesis.

The literature review is given in the second chapter, comprising of three parts. One part is the literature review of AOPs. The second part focuses on the development of titanium based on magnetic photocatalysts. The third part is the description of the target compounds, including the basic information, previous studies on their impacts on aquatic organisms, as well as the chemical treatment processes of the target compounds.

Chapter three describes the material and methods used in this study. The former one includes the chemicals, tested organism, equipment and so on. The latter one include methods of the catalyst synthesis, the characterization of the catalyst, the analysis method for concentrations of target compounds, the determination of transformation products, the mineralization evaluation and the toxicity assessment.

The characteristic and the magnetic property of the catalyst is revealed in Chapter four. Results in terms of XRD spectra, SEM image, TEM image, EDX analysis, BET surface area, DRS analysis, ZPC determination of the catalyst are listed.

Degradation of SMX, AP and IBP by UV/$CoFe_2O_4/TiO_2$ are revealed in Chapter 5, 6, 7, respectively. The best proportion in the catalyst synthesis methods is given with the SMX degradation. The separation, collection and recycling use of the catalyst is revealed. The influence of parameters including UV wavelength, catalyst dosage, initial concentrations of parent compounds, pH are determined. Reaction mechanism including the transformation products and destruction pathway is illustrated. TOC and toxicity evolution of the intermediates are measured. Besides, in Chapter seven, the impacts of anions and oxidants on IBP photodegradation are demonstrated.

Chapter 8 discuss the effect of permanganate on the photocatalysis process. In this chapter, the effect of permanganate on SMX removal under the catalytic system is explored. The optimal conditions such as permanganate dosage and pH are determined. The identification of transformation products and TOC determination are carried out. Additionally, ecotoxicity evaluation of the treated end product after SMX degradation under the treatment progress of photocatalysis with permanganate is illustrated.

The last chapter presents the conclusions of the study and recommendations for future work.

2. Chapter two Literature review

2.1 Advanced oxidation processes

Due to the sufficient quantity and strong oxidation of the radicals generated, AOPs were broadly applied in treatment of different types of pollutants in water and wastewater. The radicals utilized during the AOPs include hydroxyl radicals ($OH^\bullet$) and sulfate radicals ($SO_4^{\bullet -}$). To be specific, the processes include photolysis, photocatalysis, Fenton or Fenton-like processes, ozonation, ultrasonic irradiation and so on. In this review, the processes were classified based on the chemical agents used. The radical generation of the processes can be checked from Table 2-1.

2.1.1 Photolysis

Direct photolysis is the main destruction process for some contaminants in natural surface waters (Jin et al. 2017). Due to the cost-effectiveness, UV photolysis has been recognized as an alternative water treatment process. Compared to chlorination or ozonation, no chemical is required for the technology, and hence the taste or odor of the treated water would not be influenced (Zhang et al. 2017). Various contaminants, including some pharmaceuticals (Dong et al. 2017b, Salma et al. 2017, Santoke and Cooper 2017, Trawinski and Skibinski 2017), were reported to be effectively removed under UV irradiation (Afzal et al. 2016, Kim et al. 2016).

2.1.2 Photocatalysis

Though some pollutants can be effectively removed by direct photolysis, the wavelength applied is usually quietly limited. For organic pollutants, the most frequently used wavelength in direct photolysis is UVC. Besides, the treatment process requires a long time. To broaden the applicable light source, shorten the treatment time and save energy, various photocatalysts were developed (Chowdhury and Balasubramanian 2014, Reddy and Kim 2015, Grabowska 2016, Jiang et al. 2017).

One of the most frequently used process is UV/TiO_2 because of the environmental-friendliness (Pillai et al. 2015, Hassan et al. 2016). With the irradiation and initiation of UV, TiO_2 particles were excited, leading to the formation of positive holes and negative electrons at the conduction band (CB) and the valence band (VB), respectively. The former one has an oxidative capacity, and the latter one has a reductive capacity. Hydroxyl radicals were formed by the reaction of the holes or electrons with OH^-, H_2O, and $O_2^{\bullet -}$ at the surface of TiO_2 particles.

2.1.3 Processes based on O_3 and H_2O_2

Processes based on O_3 and H_2O_2 including ozonation, UV/O_3, UV/H_2O_2, O_3/H_2O_2, UV/O_3 /H_2O_2 are frequently applied and well investigated (Chang et al. 2014, Oh et al. 2014, Benitez et al. 2015, Ferre-Aracil et al. 2016, Hansen et al. 2016, Bourgin et al. 2017, Cheema et al. 2017, Gomes et al. 2017, Srithep and Phattarapattamawong 2017).

Radicals can be generated directly from ozonation, hence ozonation is commonly used in water/wastewater treatment (Lee et al. 2014b, Rodayan et al. 2014, Tay and Madehi 2015, Marce et al. 2016, Tekle-Rottering et al. 2016, Hopkins et al. 2017, Zhao et al. 2017). H_2O_2 can be generated from ozone initiated by the UV irradiation (Benito et al. 2017).

Radicals are generated further from H_2O_2 initiated by the UV irradiation, and UV/H_2O_2 is also an effective way for contaminants treatment (de Melo da Silva et al. 2016, Garcia-Galan et al. 2016). Radicals are also generated from the reaction between ozone and H_2O_2 (Parker et al. 2017), which is called peroxone process.

2.1.4 Processes based on Fenton

The combination of Fe^{2+} and H_2O_2 is the well-known Fenton process. In the Fenton process, H_2O_2 was activated by ferrous ions. Hydroxyl radicals are generated via hydrogen abstraction, hydrogen addition and electron transfer (Guo et al. 2014). Upon the formation of $OH^{\bullet}$, Fe(II) is turned into Fe(III) and is regenerated by $HO_2^{\bullet}$. This is known as the catalytic cycle of Fe(II)/Fe(III). UV irradiation can accelerate the regeneration of Fe(II) from Fe(III) (Yoon et al. 2017).

2.1.5 Processes based on sulfate radicals

Using persulfate ($S_2O_8^{2-}$) or oxone as oxidants to generate powerful ($SO_4^{\bullet -}$) is an alternative method for contaminants treatment (Olmez-Hanci et al. 2015). Compared to Fenton process, the sulfate radical based processes have a wide pH range (Wang and Chu 2011b).

The process includes radical generation from $S_2O_8^{2-}$, either activated by UV irradiation (Dhaka et al. 2017, Ghauch et al. 2017, Guo et al. 2017, Hou et al. 2017, Zhou et al. 2017) or ferrous and also the cycle of Fe(II)/Fe(III). During the process, $S_2O_8^{2-}$ reacts with Fe(II) and is turns into SO_4^{2-} and $SO_4^{\bullet -}$.

Oxone, known as potassium peroxymonosulfate ($2KHSO_5 \cdot KHSO_4 \cdot K_2SO_4$), is a triple salt solid compound providing HSO_5^-. The standard electrode potential of oxone is +1.82 V, which is higher than that of H_2O_2 (+1.776 V) (Betterton and Hoffmann 1990, Wang and Chu 2012). For the sulfate radical generation by activation of oxone, the reaction mechanism is rather similar to that of UV/Fe^{2+}/Persulfate. Oxone is difficult to be activated at room temperature in dark condition and the introduction of UV irradiation is therefore important (Wang and Chu 2012).

2.1.6 Ultrasonic process

Ultrasonic (US) is another process without introduction of chemicals. The efficient remove of many organic compounds by US has been reported in previous studies (Torres et al. 2008, Xu et al. 2013b, Zhou et al. 2015b, Serna-Galvis et al. 2016). In the system, the electrical energy was transform into the chemical energy and thermal energy, and then radicals are generated from various reactions (Xu et al. 2013a).

2.1.7 Combined processes

Based on the above treatment processes, multiply combined processes were developed. For example, according to Fenton, photo Fenton or Fenton like processes, novel catalysts or transition metals were used in activation of the oxidants H_2O_2 (Chen et al. 2015, Chen et al. 2017b, Chong et al. 2017, Yoon et al. 2017), persulfate (Dong et al. 2017a, Hussain et al. 2017, Li et al. 2017, Pan et al. 2017, Wang et al. 2017) or oxone (Deng et al. 2013, Hu et al. 2013, Wang et al. 2013, Liu et al. 2015b). Thermal and electronic were also used for the activation of the processes (Wang and Chu 2011a, Bu et al. 2017, Chen et al. 2017c, Yang et al. 2017, Zrinyi and Pham 2017).

Besides, other combined processes such as O_3/Photocatalysis (Biard et al. 2016), US/UV (Xu et al. 2013a), US/O_3 (Chand et al. 2009), US/Photocatalysis (Kubo et al. 2005, Wang et al. 2008), US/Fenton-like (Yehia et al. 2015, Babu et al. 2017) and so on were explored.

2.2 Photocatalysis utilizing magnetic catalysts based on TiO_2

Due to the difficulty of collection and recycling use of TiO_2, various magnetic catalysts were developed based on TiO_2 (summarized in Table 2-2). Usually, the magnetic substance was synthesized as the core, and TiO_2 was synthesized as the shell. A number of studies were reported, and most synthesized magnetic photocatalysts were highly efficient in degradation of organic contaminants.

Most of the tested target compounds were dyes, few studies focused on the destruction of pharmaceutical molecular with magnetic photocatalysts. As reported in many studies, the photocatalysts coated with magnetic substances were easily separated from the treated solutions and still efficient in removal of probe compounds even after several times of recycle use.

2.2.1 Magnetic catalysts based on ferrite and TiO_2

In the research by Gao et al. (Gao et al. 2016), TiO_2 was synthesized with hydrothermal method, and was modified by various ferrites (MFe_2O_4, M = Ni, Co, Zn, and Sr). Among all the ferrites coated TiO_2, $NiFe_2O_4/TiO_2$ modification was claimed to show the most enhancement in photocatalytic activity of TiO_2. Another attempt made by utilizing Ni-Cu-Zn ferrite/TiO_2 was to study the degradation of methylene blue (MB) under UV illumination (Fu et al. 2011).

Sol-gel method was employed for Ag loaded Ni-Cu-Zn ferrite/SiO_2/TiO_2 composite. The photocatalytic activity of the catalyst of was proven by the significant destruction of MB solutions under a 35-W Xe arc lamp and color temperature of 6000 K (Chen et al. 2017a).

2.2.1.1 Catalysts based on $NiFe_2O_4/TiO_2$

Mechanochemical method from a mixture of and P25 was performed to obtain the catalysts $NiFe_2O_4/TiO_2$. In the composite, $NiFe_2O_4/TiO_2$ provides fast and efficient heating under radiofrequency field, and P25 plays the role of an active catalyst. The sulfated composite catalysts show high catalytic activity according to the yield of amide in the condensation of aniline and 3-phenylbutyric acid (Houlding et al. 2015).

As was reported by Xu et al. (Xu et al. 2007, Xu et al. 2008), the egg-like $NiFe_2O_4/SiO_2/TiO_2$ was synthesized employing chemical precipitation means, reverse micelle technique and a liquid catalytic phase transformation method. Compared to $NiFe_2O_4/TiO_2$, the additional SiO_2 layer between the magnetic core and the TiO_2 shell enhanced the photocatalytic activity of methyl orange (MO) under UV irradiation, since it played the role of barrier for the injection of charges from TiO_2 particles to $NiFe_2O_4$. Another try is the degradation of Violet 5B with $NiFe_2O_4/SiO_2/TiO_2$ under UV light (Yuan et al. 2010).

2.2.1.2 Catalysts based on $CoFe_2O_4/TiO_2$

For the magnetic nanocatalyst $CoFe_2O_4/TiO_2$, co-precipitation method and sol–gel technology was employed for synthesis of the core $CoFe_2O_4$ nanoparticles and the shell TiO_2 nanocrystals, respectively (Sathishkumar et al. 2013). It was reported that rutile phase of TiO2, which was more thermodynamically stable, was formed with the induction of $CoFe_2O_4$ (Sathishkumar et al. 2013). Reactive Red 120 as the target compound was removed with the photocatalysts under a tungsten halogen lamp (wavelength > 400 nm). Another try of pollutants degradation making use of $CoFe_2O_4/TiO_2$ is the degradation of the dye Procion Red MX-5B (Procion) under UV wavelength of 365 nm (Fu et al. 2005). Co-precipitation method and sol–gel technology was performed for the synthesis of the core $CoFe_2O_4$ and the shell TiO_2 nanocrystals, respectively, and the catalyst was obtained finally by heat-treatment at 450 °C. The synthesis of $CoFe_2O_4/TiO_2$ was also achieved by the sol–gel method combined with solvent-thermal technique, the photocatalytic activity was proven by the degradation of MB under UV illumination (Li et al. 2009a).

Core-shell magnetic nanoparticles $CoFe_2O_4/SiO_2/TiO_2$ have been prepared using metallorganic precursors and sintering at 600 °C. Under UV light, the obtained catalysts can be used in photodegradation of MB (Greene et al. 2014).

2.2.1.3 Catalysts based on $ZnFe_2O_4/TiO_2$

The quasi-cube nanocrystals $ZnFe_2O_4$ were firstly obtained by a facile hydrothermal method. Then the physically grind of approach $ZnFe_2O_4$ with P25 results in the nanocomposite. Mineralization of Rhodamine B (RhB) was well achieved with the treatment process of UV/$ZnFe_2O_4$/P25 (Zhang et al. 2010b). Sol-gel method was also utilized for synthesis of $ZnFe_2O_4/TiO_2$ and the obtained catalysts were efficient in degradation of RhB (Zhang et al. 2008). $ZnFe_2O_4/TiO_2$ was also developed by coprecipitation/hydrolysis route, the obtained composites were active in the degradation of phenol from UV to visible wavelengths (> 400 nm) (Srinivasan et al. 2006). It was reported that the $ZnFe_2O_4/TiO_2$ nanotube arrays prepared via electrochemical process with a novel cathodic electrodeposition method showed photocatalytic active in the degradation of 4-chlorophenol under UV irradiation. The photoelectrocatalytic ability of the cataysts can be enhanced to visible light if annealing was followed during the catalyst synthesis (Hou et al. 2010a, b). The nanocomposite material $ZnFe_2O_4/TiO_2$ prepared by a colloid chemistry method exhibited photocatalytic activity under sunlight irradiation by phenol photodegradation (Yuan and Zhang 2001). The electrochemical anodization method and facile hydrothermal route were employed for TiO_2 preparation and deposition of $ZnFe_2O_4$ on TiO_2 nanoparticles. The modified nanoparticles extended the photo response in the visible light region by the destruction of acid orange II (Wang et al. 2013). The wet method was also performed in the synthesis of $ZnFe_2O_4/TiO_2$ and the photocatalytic activity was proven by the MO degradation under UV-VIS irradiation (Moreira et al. 2012).

$ZnFe_2O_4/TiO_2$/Granular activated carbon was developed and employed as the photocatalyst. The catalysts calcined at 500 °C showed significantly photocatalytic activity in degradation of acid dye under visible light irradiation (Wang et al. 2009b).

2.2.1.4 Catalysts based on $CuFe_2O_4/TiO_2$

For the preparation of $CuFe_2O_4/TiO_2$, the microwave-assisted method and sol–gel method were employed. The photocatalysts showed good behavior on the degradation of four various azo dyes under UV irradiation (Masoumi et al. 2016a).

The photocatalytic activity was promoted visible light region by the incorporation of the silver nanoparticles with simple precipitation method (Masoumi et al. 2016b). Graphene was also employed and implanted into the magnetic catalysts, $CuFe_2O_4/TiO_2$/Graphene nanocomposites prepared via a one-step hydrothermal method was reported to show photocatalytic activity in terms of MB destruction under visible light radiation (Yu and Zhang 2016).

2.2.1.5 Catalysts based on $BaFe_2O_4/TiO_2$

For the barium ferrite coated TiO_2 nanoparticles, hydrolysis and condensation of titanium bis-ammonium lactato dihydroxide or titanium n-butoxide were performed (Lee et al. 2004). Under the irradiation of UV lamps at wavelength of 365 nm, the catalysts showed photocatalytic activity in degradation of procion.

Wet-chemical methods were employed for the synthesis of $BaFe_2O_4/SiO_2/TiO_2$ (Lee et al. 2006). The catalysts contribute for the photodegradation of procion under UV illumination at wavelength of 302 nm. The as-prepared composite particles were reported to be more photoactive after the heat-treatment at 500 ˚C for 1 h (Lee et al. 2006).

2.2.1.6 Catalysts based on $MgFe_2O_4/TiO_2$

Information on $MgFe_2O_4/TiO_2$ application in pollutants treatment in aqueous phase is still limited. The mixing-annealing method was successfully used in synthesis of $MgFe_2O_4/TiO_2$. Photocatalytic activity of the composite photocatalysts was proven by the photodegradation of RhB under UV and visible light irradiation (Zhang et al. 2011).

2.2.2 Magnetic catalysts based on iron oxides and TiO_2

Another group of commonly used magnetic material is the iron oxides. For example, by wet-chemical processing and ultrasound irradiation, a photocatalyst $Fe_2O_3/Fe_3O_4/TiO_2/C$ was developed and used for the degradation of organic dyes reactive black 5 and Rh B exposed to visible-light (Lee et al. 2014a). The photocatalytic activity of the $Fe_xO_y/TiO_2/Ag$ nanoparticles showed a significant increase in under visible light compared to P25 owing to the presence of Ag. The antibiotic compound, nalidixic acid, was removed efficiently with the treatment process $VIS/Fe_xO_y/TiO_2/Ag$ (Petronella et al. 2017). Hereby the magnetic catalyst based on Fe_2O_3 or Fe_3O_4 coated with TiO_2 were reviewed.

2.2.2.1 Catalysts based on Fe_2O_3/TiO_2

In the preparation process of α-Fe_2O_3/TiO_2, hydrothermal treatment was frequently employed. Liu and Gao found that even visible light irradiation was able to active the photocatalysis of MB with the obtained α-Fe_2O_3/TiO_2 (Liu and Gao 2006). Magnetic γ-Fe_2O_3/TiO_2 was developed with an asymmetric shrinkage approach and was able to degrade RhB with visible light (Mou et al. 2012). A solvent-free mechanochemical process was reported for the synthesis of Fe_2O_3/TiO_2. The treatment efficiency of Fe_2O_3/TiO_2 was even higher than the P25 for the treatment of paper mill effluent indicated by COD (Subramonian et al. 2017). Another study illustrated that synthesized Fe_2O_3/TiO_2 was efficient in treatment of Orange II under visible light (Peng et al. 2010).

An easy chemical route was employed for the synthesis of (γ-Fe_2O_3/SiO_2)$_n$/TiO_2, the photocatalytic activity of the hybrid nanoparticles was proven by the degradation of MB under UV light (Wang et al. 2009a).

A metal organic chemical vapor deposition method was reported to be convenient and efficient in preparation of Fe_2O_3/TiO_2/Activated carbon. The obtained catalysts showed photocatalytic activity in the photodegradation or decoloration of MO under visible light irradiation (Zhang and Lei 2008).

2.2.2.2 Catalysts based on Fe_3O_4/TiO_2

To obtain the amorphous Fe_3O_4/TiO_2, a single sonochemical approach was employed through hydrolysis and condensation of titanium isopropoxide and iron sulfate heptahydrate (Abbas et al. 2014). The catalyst showed an excellent performance on the destruction of MB under UV irradiation, and the reaction was accelerated significantly with the introduction of H_2O_2 without UV. The sol-gel method was also explored for the synthesis of Fe_3O_4/TiO_2, and the catalyst showed good response in the decomposition of tartrazina dye (Heredia et al. 2015) and bromamine acid (Fei. et al. 2010). Hollow spherical Fe_3O_4/TiO_2 hybrid photocatalysts were successfully prepared through a poly (styrene-acrylic acid) template method and exhibited good photocatalytic activity on degradation of RhB under UV light irradiation (Sa et al. 2009). Besides, attempts on application of the core-shell nanocrystal Fe_3O_4/TiO_2 in the treatment of endocrine disrupting chemical (bisphenol A and dibutyl phthalate) under UV illumination (Chalasani and Vasudevan 2013) were made. The facile liquid phase deposition route was utilized for the fabrication of Fe_3O_4/TiO_2 core-shell microspheres and the photocatalytic decomposition of MB was investigated under visible light (Zheng et al. 2016).

A great many studies also focus on the photocatalytic application of $Fe_3O_4/SiO_2/TiO_2$. The magnetic photocatalyst were synthesized with solution method, and was employed in the treatment of textile wastewater which contains various dyes and chemicals under UV irradiation (Ahangara et al. 2016). Additionally, $Fe_3O_4/SiO_2/TiO_2$ was developed and applied to degrade diclofenac by photoelectron-catalytic treatment process (Hu et al. 2011). The core–shell nanomaterial $Fe_3O_4/SiO_2/TiO_2$ can also be prepared by co-precipitation method, under UV illumination, reactive black 5 can be removed with the photocatalysts (Lucas et al. 2013). In a study on photocatalytic degradation of RhB, solvothermal reaction, the typical Stböer process and sol–gel method was performed for synthesis of Fe_3O_4 particles, Fe_3O_4/SiO_2 particles, and the core-shell $Fe_3O_4/SiO_2/TiO_2$ (Liu et al. 2011). Another study utilizing solvothermal and sol-gel method to obtain the nanoparticles $Fe_3O_4/SiO_2/TiO_2$ revealed the excellent performance of the catalysts for the degradation and decoloration of MO and MB dyes under UV irradiation (Liu et al. 2013b). Additionally, degradation of P-Nitrophenol was carried out by photocatalytic process using the catalyst $Fe_3O_4/SiO_2/TiO_2$ under UVC light source (Rezaei-Vahidian et al. 2017).

The composites $Fe_3O_4/SiO_2/TiO_2$/Graphene were obtained by combining sol–gel method and assembling processes. The introduction of graphene led to the strong light absorption in the visible region. The typical herbicide 2,4-dichlorophenoxyacetic acid (2,4-D) was removed completely from water under simulated solar light irradiation, and the removal efficiency is even higher than commercial P25 (Tang et al. 2013).

Similarly, due to the strong absorption and scattering properties of Ag nanoparticles, the photocatalytic activity of $Fe_3O_4/TiO_2/Ag$ was greatly promoted in visible light region, which was verified by the degradation of MB solution. The study also suggested the SiO_2 interlayer between the core Fe_3O_4 and the shell TiO_2 be employed for the prevention of Fe_3O_4 photodissolution during photocatalysis (Zhan et al. 2014).

Solvothermal and sol–gel methods were performed to form $Fe_3O_4/SiO_2/TiO_2/AgBr$. The photocatalyst exhibited high photocatalytic activity in the degradation of MB under visible light (Liu et al. 2013c).

Apart from the above materials, iodine was also doped in the magnetic nanoparticles to promote the phocatalytic activity of the catalysts to visible light region. The nanoparticles $Fe_3O_4/SiO_2/TiO_2/I$ were efficient in degradation of phenol from the aqueous solution under visible-light illumination (He et al. 2012).

2.2.3 Other magnetic cores

In a study by Gaikwad et al., three types of maganetic catalysts, Fe/TiO_2, FeN/TiO_2, $CoFe_2O_4/FeN/TiO_2$, were demonstrated. Through the decomposition of MO under both UV and visible light, the photocatalytic activity of the nanocomposites, was determined in the order $FeN/TiO_2 > Fe/TiO_2 > CoFe_2O_4/FeN/TiO_2$ (Gaikwad et al. 2016).

The hydrothermal method combined in situ reduction route were performed for synthesis of Fe/TiO_2. Its photoactivity under UV light irradiation was even higher than that of P25 by photocatalytic degradation of acetic acid and formaldehyde (Li et al. 2009b).

The photocatalyst, Ni/TiO_2 composite, has been successfully synthesized. The TiO_2 films were by coated onto one-dimensional magnetic Ni nanostructures. The photocatalytic activity of the catalysts was demonstrated by the destruction of MO under UV light (Pang et al. 2011).

Modified sepiolite was also investigated as the magnetic source, and the catalyst Modified sepiolite/TiO_2 was synthesized by a sol–gel method. The adsorption ability and photocatalytic activity of the obtained composites were significantly enhanced compared to neat TiO_2, which was proven by the 2,4-dichlorophenol removal with UV irradiation. (Li et al. 2015).

2.3 Target compounds

The basic information of the target compounds in this study is shown in Table 2-3.

2.3.1 Sulfamethoxazole

2.3.1.1 Basic information

Sulfamethoxazole (SMX, 4-amino-N-(5-methyl-3-isoxazolyl) benzenesulfon-amide), a white, odorless, and tasteless antimicrobial agent, is commonly used as the human and veterinary medicine. As human medicine, SMX is used to treat diseases such as middle ear infection, conjunctivitis, bronchitis, urinary tract infection, malaria, toxoplasmosis, and traveler's diarrhea (Damschen and Lundgren 2009). As veterinary medicine, SMX is used as feed additives to promote growth and weight gain of food animals apart from the application in treating diseases and infections (Pereira and Cass 2005).

Because of the industrial and domestic activities, SMX may end up in the waterbody through various routes such as pharmaceutical effluents, toilet flushing, and excretes with or without proper treatment (Heberer 2002). For examples, the livestock excretions, including the metabolized residues, may penetrate the soil and reach the groundwater or be washed off from the soil as a surface runoff after a rainfall storm.

Traces of SMX have been identified in almost all kinds of surface water and in the effluents of municipal sewage treatment plant (Gobel et al. 2004, Gobel et al. 2005, Pereira and Cass 2005, Brown et al. 2006, Miege et al. 2009). In a survey conducted by the United States, SMX was listed as one of the top six most frequently detected compounds (Koplin et al. 2002). SMX was detected at 47 ng/L, 193 ng/L, and 480 ng/L, in Victoria Harbor (Minh et al. 2009), Pearl River (Yang et al. 2013), and Germany (Hirsch et al. 1999), respectively. In the effluent of STPs, SMX was detected at 52.6 ng/L and 2000 ng/L in Hong Kong (Gulkowska et al. 2008) and Germany (Loos et al. 2013), respectively.

2.3.1.2 Adverse effect of SMX on aquatic organisms

Owing to the low biodegradability, SMX can persist in the environment for a long time and thus was categorized as a persistent antibiotic (Dirany et al. 2011). It has been proved that even low concentration levels of SMX would pose a serious environmental risk by altering microbial community structure via the yielding of antibiotic resistance (Underwood et al. 2011). Due to its similar structure to PABA (para-aminobenzoic acid, an intermediate in the synthesis of folate by bacteria, plants, and fungi), SMX can prevent normal bacteria from binding PABA with folic acid enzyme and interfere the synthesis of folic acid, a critical metabolite in DNA synthesis (Hida et al. 2005, Nguyen and Clarke 2012). Since the bacterial resistance to this antibiotic owing to its prolonged presence in environments has been well demonstrated, human health may be threatened if antibiotics fail in clinical application (Sanderson et al. 2004, Kemper 2008, Lin and Huang 2008, Zhang et al. 2010a).

The existence of SMX in the environment may induce the mutations of some bacteria, thus yield antibiotic resistance (Iliades et al. 2004). In addition, SMX can affect the aquatic ecosystem by inhibiting the life activity of aquatic organisms. The summary of effects of SMX on aquatic organisms was listed in Table 2-4. From the table, SMX has adverse effect on various groups of aquatic organisms. Growth inhibition to bacterial, phytoplankton, and zooplankton were detected. In addition, acute toxicity to zooplanktons exposed to 50-100 μM SMX was reported. For instance, the growth of zooplankton *Ceriodaphnia dubia* and algae *Pinnularia subcapitata* was inhibited when the concentration of SMX reached 0.21 mg/L (0.83 μM) (Isidori et al. 2005) and 0.52 mg/L (2.06 μM) (Isidori et al. 2005), respectively. Due to its toxicological effects to the environment and thus the potential risk to human health, it is crucial to study an efficient way for the degradation of SMX.

2.3.1.3 Previous studies on SMX degradation by chemical treatment processes

Numerous studies have been conducted in terms of the treatment progress of SMX (Table 2-5). As is shown in the table, processes based on photolysis, photocatalysis, Fenton, ozonation, sulfate radicals based processes, ultrasonic process have been widely explored.

The studies prove that no significant degradation was observed under UVA irradiation while UVC and vaccum-UV showed high reactivity, and vaccum-UV is the most effective light source for the photolysis (Kim et al. 2015). Even under the sunlight for one week, SMX showed 50% destruction (Gmurek et al. 2015). Six transformation products were determined during the photolysis and the growth inhibition of treated SMX solution to *Vibrio fischeri* was slightly reduced (Niu et al. 2013, Gmurek et al. 2015).

In the photocatalysis treatment processes, the most used catalysts are based on TiO_2, and the processes are mostly combined with UV. In the process UV/TiO_2, eight intermediates were detected (Abellán et al. 2007, Fukahori and Fujiwara 2015). The growth inhibition of SMX solution to *C. vulgaris* was decreased after the photocatalytic treatment (Baran et al. 2006). Another study showed that the toxicity to *V. fischeri* was increased after the treatment process UV/TiO_2 but decreased if the salinity was elevated (Yang et al. 2015). The catalysts used in SMX degradation include TiO_2/Activated carbon fiber, TiO_2-

expanded perlite, granular activated carbon supported TiO_2, TiO_2/Cu, TiO_2 Millennium PC500 immobilized on glass plates, Ti-doped β-Bi_2O_3, MnO_2. For the process UV/Ti-doped β-Bi_2O_3, no toxicity decrease was found (Niu et al. 2013). And for the process with MnO_2, the reaction is rather slow, with only 60% removal efficiency in 24 hours (Wan et al. 2015).

Electro-Fenton, solar photo-Fenton, photoelectro-Fenton and other Fenton-like processes such as UV/H_2O_2 and $LaFeO_3$/H_2O_2 were developed. The treated SMX solution showed 20-40% higher inhibitory effect to *Vibrio qinghaiensis* after the treatment process UV/H_2O_2 in synthetic fresh and hydrolyzed urine (Zhang et al. 2015c). The study of solar photo-Fenton showed that the toxicity evolution of the treated SMX solution is different between the reaction system of distilled water and seawater (Trovo et al. 2009a). The toxicity to *Daphnia magna* was decreased from 85% to 20% in the reaction system of distilled water. In contrary, in the reaction system of seawater, the toxicity to *V. fischeri* increased from 16% to 86% (Trovo et al. 2009a).

Persulfate can be activated by ferrous, iron or heat and produce radicals to remove SMX molecular. However, the treated SMX was reported to be more toxic for heat activated persulfate process (Gao et al. 2014b). And there is still limited information on new process such as Peroxymonosulfate/Benzoquinone in terms of transformation products and toxicity evolution.

SMX can be totally removed by direct oxidation of ozone or ferrate (VI) (Martins et al.

2015a, Zhou and Jiang 2015). However, the direct oxidation potential of chlorine is limited in SMX removal, for only about 20% removal efficiency was achieved in presence of 2 mg/L chlorine to treat 5 mg/L SMX. The introduction of ultrasound to ozone or ferrate (VI) can significantly improve the removal efficiency, especially the former one, can well promote the cleavage of S-N bond (Guo et al. 2015, Zhang et al. 2015a). Other hybrid process such as Ru/TiO_2-catalyzed permanganate was also proven to be highly efficient in SMX removal.

2.3.2 Antipyrine

2.3.2.1 Basic information

Antipyrine (AP, also known as phenazone, 2,3-dimethyl-1-phenyl-3-pyrazolin-5-one), a powerful analgesic, antipyretic and anti-inflammatory drug (Miao et al. 2015), is selected as the target compound owing to its wide use, removal resistance, frequent detection and the insufficient toxicity information (Monteagudo et al. 2016).

AP is applied extensively and largely consumed in many countries (Pieper et al. 2010). For example, about 0.35 g/capita AP was consumed in Germany every year (Tan et al. 2013b). AP is very polar, highly environmental persistent and hardly degradable (Tan et al. 2013a). According to Zuehlke et al., only about 30% AP was removed in traditional sewage treatment plant (STP) (Zuehlke et al. 2006). Owing to the incomplete removal, AP is frequently detected in STP effluents, rivers, ground water and even drinking water (Tan et al. 2013a). For instance, the concentration of AP was determined to be 2.5–0.05 µg/L in drinking water from Germany (Rodil et al. 2012).

The data on toxicity of AP was scarce. To humans, long term exposure to AP may cause lungs and mucosas damages (Cai et al. 2013). An inhibition value of 8% was detected on *V. fischeri*, however the concentration of AP was not given (Calza et al. 2011). Besides, the information on the toxicity of AP to phytoplanktons and zooplanktons is still limited.

2.3.2.2 Previous studies on AP degradation by chemical treatment processes

Compared to the abundant studies of SMX degradation, the information on AP degradation provided by previous studies is rather scarce (Table 2-6). For the photolysis study of AP, only the light source of UVC was investigated (Tan et al. 2013b). The catalyst applied to AP removal is limited to TiO_2 (P25) (Calza et al. 2011). The thirteen intermediates were indicated to be easily degraded and non-toxic to *V. fischeri*. The used oxidants include H_2O_2 (Tan et al. 2013b), persulfate (Tan et al. 2013a), ozone (Miao et al. 2015), chlorine (Rodil et al. 2012). AP can be directly removed with oxidants ozone and chlorination. However, most of the then products during ozonation treatment were reported to be more toxic (Miao et al. 2015). The application of UV to H_2O_2 or persulfate would enhance the destruction rate of AP significantly. As recommended by Tan et. al., given the energy and chemical costs, the priority for treatment process selection should be UVC/Persulfate > UVC > UVC/H_2O_2 (Tan et al. 2013b).

2.3.3 Ibuprofen

2.3.3.1 Basic information

Ibuprofen (IBP, a-methyl-4-[isobutyl] phenylacetic acid), is a widely used drug to mitigate fever, migraine, muscle pain, toothaches and arthritis in the world (Georgaki et al. 2014). Due to its various applications, huge amount of IBP is manufactured. Then IBP can enter the water body through various human and/or industrial activities, such as human excreta, the disposal of surplus household drugs, and emissions from production lines (Quero-Pastor et al. 2014). For example, 0.025-0.475 μg/L IBP was detected in surface water and drinking water in England and Wales, respectively (Boxall et al. 2014).

2.3.3.2 Adverse effect of IBP on aquatic organisms

The effects of IBP on aquatic organisms are summarized in Table 2-7. Even at these levels, IBP can pose adverse effects on the aquatic ecosystem. For instance, the survival of *Oryzias latipes* was threatened when exposed to 0.0001 mg/L IBP (0.0485 nM) (Han et al. 2010). It is interesting to note that IBP showed different effect on different algae. For *C. vulgaris*, IBP has a significant inhibition effect on its growth (Geiger et al. 2016). While for *Synechocystis* sp., IBP can even promote its growth at 10 μg/L (0.0485 μM).

2.3.3.3 Previous studies on IBP degradation by chemical treatment processes

Different methods have been examined on the treatment of IBP, including photolysis, photocatalysis, electro-peroxone, ozonation, and photo-Fenton and so on (Table 2-8).

Among the UV irradiation sources, UVC was reported to be efficient in IBP removal (da Silva et al. 2014), and only about 10% of IBP was destructed in 120 mins for UVA. During the photolysis process with UV-VIS, six transformation products were determined and two of them were demonstrated to be toxic to fibroblasts and erythrocyte (Castell et al. 1987). In the reaction systems of direct photolysis (UVA and UVC radiation) and photocatalysis (UVA/TiO_2 and UVC/TiO_2), totally eleven transformation products were detected by LC-HRMS, and no higher eco-toxicity was found to *A. salina*. Apart from TiO_2, ZnO and $BiVO_4$ are also employed in IBP degradation, the former one is efficiently activated by UVA and the latter one can make use of solar light.

The comparison study of IBP degradation under UVC and UVC/H_2O_2 illustrated that H_2O_2 even hindered the photolysis process (Yuan et al. 2009). Though IBP can be directly oxidized by ozone, with 99% removal efficiency in 20 mins, the toxicity of the treated solution to *Selenastrum capricornium* was actually increased since some transformation products with higher toxicity were formed (Quero-Pastor et al. 2014). The new process peroxone, as a combination of ozone and hydrogen peroxide, showed a better performance than UV/H_2O_2, with 85% removal efficiency compared to 59%. Electro-peroxone was also studied and it was proven to be more efficient in IBP destruction than ozone, electrolysis. The effluent from the treatment process was reported to be less toxic to *V. fischeri*, and the toxic products can be completely mineralized in the electro-peroxone process (Li et al. 2014).

Compared to the hydroxylated-IBP byproducts without mineralization in solar photolysis cleavage of H_2O_2, Fenton reaction improved 10% mineralization and solar photo-Fenton further promoted the decarboxylation of IBP and 40% mineralization was achieved (Mendez-Arriaga et al. 2010). Additionally, comparison study of electro-Fenton UVA photoelectro-Fenton, and solar photoelectro-Fenton was carried out (Skoumal et al. 2009). Solar photoelectro-Fenton was indicated to be the most potent method by giving 92% mineralization. Aromatics and carboxylic acids were detected as the transformation products and oxalic acid was defined to be the ultimate product. Direct oxidation by H_2O_2, $KMnO_4$, $K_2Cr_2O_7$ were also studied, however, the treatment processes usually took a long time (3 hours-30 days) (Caviglioli et al. 2002). Hybrid processes such as UV/US/Fe^{3+}, UV/US/TiO_2, and UV/O_3/TiO_2 showed a synergy effects and high removal efficiencies (Giri et al. 2010) (Madhavan et al. 2010).

Though some methods were reported to be effective, there are drawbacks in application, such as the high energy cost for the electro-peroxone process (Li et al. 2014); limited solubility of ozone gas and slow reaction/high production cost in the ozonation process (Quero-Pastor et al. 2014); and low applicable pH range for the photo Fenton (Mendez-Arriaga et al. 2010).

Table 2-1 Reaction mechanism of frequently used advanced oxidation processes

Process	Reactions	
Heterogeneous phtocatalysis	Catalyst + $hv \rightarrow e^{-}_{cb} + hv^{+}_{vb}$	(Equation 2-1)
	$hv^{+}_{vb} + OH^{-} \rightarrow OH^{\bullet}$	(Equation 2-2)
	$hv^{+}_{vb} + H_2O \rightarrow OH^{\bullet} + H^{+}$	(Equation 2-3)
	$e^{-}_{cb} + O_2 \rightarrow O_2^{\bullet}$	(Equation 2-4)
$UV/O_3/H_2O_2$ $(O_3/H_2O_2$ UV/H_2O_2 $UV/O_3)$	$3\ O_3 + H_2O \rightarrow 2OH^{\bullet} + 4O_2$	(Equation 2-5)
	$O_3 + H_2O \xrightarrow{hv} H_2O_2 + O_2$	(Equation 2-6)
	$H_2O_2 \xrightarrow{hv} 2OH^{\bullet}$	(Equation 2-7)
	$H_2O_2 \rightarrow HO_2^{-} + H^{+}$	(Equation 2-8)
	$O_3 + H_2O_2 \rightarrow OH^{\bullet} + O_2 + HO_2^{\bullet}$	(Equation 2-9)
	$O_3 + HO_2^{-} \rightarrow OH^{\bullet} + O_2^{-} + O_2$	(Equation 2-10)
	$O_3 + O_2^{-} \rightarrow O_3^{-} + O_2$	(Equation 2-11)
	$O_3^{-} + H_2O \rightarrow OH^{\bullet} + OH^{-} + O_2$	(Equation 2-12)
$UV/Fe^{2+}/H_2O_2$ $(UV/Fe^{2+}$ UV/H_2O_2 Fe^{2+}/H_2O_2 (Fenton))	$H_2O_2 \xrightarrow{hv} 2OH^{\bullet}$	(Equation 2-7)
	$Fe^{2+} + H_2O_2 \rightarrow Fe^{3+} + OH^{\bullet} + OH^{-}$	(Equation 2-13)
	$H_2O_2 + OH^{\bullet} \rightarrow HO_2^{\bullet} + H_2O$	(Equation 2-14)
	$Fe^{3+} + H_2O_2 \rightarrow Fe^{2+} + HO_2^{\bullet} + H^{+}$	(Equation 2-15)
	$Fe^{3+} + HO_2^{\bullet} \rightarrow Fe^{2+} + O_2 + H^{+}$	(Equation 2-16)
	$Fe^{2+} + HO_2^{\bullet} \rightarrow Fe^{3+} + OH^{-}$	(Equation 2-17)
	$Fe^{2+} + OH^{\bullet} \rightarrow Fe^{3+} + OH^{-}$	(Equation 2-18)
UV/Fe^{2+}/Persulfate	$Fe^{2+} \xrightarrow{hv} Fe^{3+} + e^{-}$	(Equation 2-19)

(UV/Fe^{2+} UV/Persulfate Fe^{2+}/Persulfate)	$Fe^{3+} + H_2O \rightarrow [Fe(OH)]^{2+} + H^+$	(Equation 2-20)
	$[Fe(OH)]^{2+} \xrightarrow{hv} Fe^{2+} + OH^{\bullet}$	(Equation 2-21)
	$Fe^{2+} + S_2O_8^{\ 2-} \rightarrow SO_4^{\bullet -} + Fe^{3+} + SO_4^{2-}$	(Equation 2-22)
	$Fe^{2+} + SO_4^{\ \bullet -} \rightarrow Fe^{3+} + SO_4^{2-}$	(Equation 2-23)
	$S_2O_8^{\ 2-} \xrightarrow{hv} 2SO_4^{\bullet -}$ (Equation 2-1)	(Equation 2-24)
UV/Fe^{2+}/Oxone (UV/Fe^{2+} UV/Oxone Fe^{2+}/Oxone)	$Fe^{2+} \xrightarrow{hv} Fe^{3+} + e^-$	(Equation 2-19)
	$Fe^{3+} + H_2O \rightarrow [Fe(OH)]^{2+} + H^+$	(Equation 2-20)
	$[Fe(OH)]^{2+} \xrightarrow{hv} Fe^{2+} + OH^{\bullet}$	(Equation 2-21)
	$Fe^{2+} + HSO_5^- \rightarrow SO_4^{\bullet -} + Fe^{3+} + OH^-$	(Equation 2-25)
	$Fe^{2+} + SO_4^{\ \bullet -} \rightarrow Fe^{3+} + SO_4^{2-}$	(Equation 2-23)
	$HSO_5^- \xrightarrow{hv} SO_4^{\bullet -} + OH^{\bullet}$	(Equation 2-26)
US	$H_2O \rightarrow H^{\bullet} + OH^{\bullet}$	(Equation 2-27)
	$H^{\bullet} + O_2 \rightarrow HO_2^{\bullet}$	(Equation 2-28)
	$H^{\bullet} + HO_2^{\bullet} \rightarrow H_2O_2$	(Equation 2-29)
	$H^{\bullet} + H_2O_2 \rightarrow H_2 + HO_2^{\bullet}$	(Equation 2-30)
	$H^{\bullet} + O_2 \rightarrow OH^{\bullet} + O^{\bullet}$ (or $HO_2^{\bullet}$)	(Equation 2-31)
	$O^{\bullet} + H_2O \rightarrow 2\ OH^{\bullet}$ (or H_2O_2)	(Equation 2-32)
	$O^{\bullet} + H_2O_2 \rightarrow OH^{\bullet} + HO_2^{\bullet}$	(Equation 2-33)
	$O^{\bullet} + H_2 \rightarrow OH^{\bullet} + H^{\bullet}$	(Equation 2-34)
	$O^{\bullet} + HO_2^{\bullet} \rightarrow OH^{\bullet} + O_2$	(Equation 2-35)

Table 2-2 Magnetic catalysts based on TiO_2 for degradation of organic pollutants

Catalyst	Target compound	Light source	Reference
Ni-Cu-Zn ferrite/TiO_2	MB	UV	(Fu et al. 2011)
Ni-Cu-Zn ferrite/SiO_2/TiO_2/Ag	MB	UV-VIS	(Chen et al. 2017a)
$NiFe_2O_4/TiO_2$	Aniline 3-phenylbutyric acid	UV	(Houlding et al. 2015)
$NiFe_2O_4/SiO_2/TiO_2$	MO	UV	(Xu et al. 2007, Xu et al. 2008)
	Violet 5B	UV	(Yuan et al. 2010)
	Reactive Red 120	VIS	(Sathishkumar et al. 2013)
$CoFe_2O_4/TiO_2$	Procion	UV	(Fu et al. 2005)
	MB	UV	(Li et al. 2009a)
$CoFe_2O_4/SiO_2/TiO_2$	MB	UV	(Greene et al. 2014)
$ZnFe_2O_4/TiO_2$	RhB	UV	(Zhang et al. 2010b)
	RhB	UV	(Zhang et al. 2008)
	Phenol	UV-VIS	(Srinivasan et al. 2006)
	4-chlorophenol	UV-VIS	(Hou et al. 2010a, b)
	Phenol	Sunlight	(Yuan and Zhang 2001)
	Acid orange II	VIS	(Wang et al. 2013)
	MO	UV-VIS	(Moreira et al. 2012)
$ZnFe_2O_4/TiO_2$/Granular activated carbon	Acid dye	VIS	(Wang et al. 2009b)
$CuFe_2O_4/TiO_2$	Azo dyes	UV	(Masoumi et al. 2016a)
$CuFe_2O_4/TiO_2$/Ag	Azo dyes	VIS	(Masoumi et al. 2016b)
$CuFe_2O_4/TiO_2$/Graphene	MB	VIS	(Yu and Zhang 2016)
$BaFe_2O_4/TiO_2$	Procion	UV	(Lee et al. 2004)
$BaFe_2O_4/SiO_2/TiO_2$	Procion	UV	(Lee et al. 2006)
$MgFe_2O_4/TiO_2$	RhB	UV-VIS	(Zhang et al. 2011)
$Fe_2O_3/Fe_3O_4/TiO_2/C$	Reactive black 5 Rh B	VIS	(Lee et al. 2014a)
Fe_xO_y/TiO_2/Ag	Nalidixic acid	VIS	(Petronella et al. 2017)

α-Fe_2O_3/TiO_2	MB	VIS	(Liu and Gao 2006)
γ-Fe_2O_3/TiO_2	RhB	VIS	(Mou et al. 2012)
Fe_2O_3/TiO_2	Paper mill effluent	UV	(Subramonian et al. 2017)
Fe_2O_3/TiO_2	Orange II	VIS	(Peng et al. 2010)
$(\gamma\text{-}Fe_2O_3/SiO_2)_n/TiO_2$	MB	UV	(Wang et al. 2009a)
Fe_2O_3/TiO_2/Activated carbon	MO	VIS	(Zhang and Lei 2008)
Fe_3O_4/TiO_2	MB	UV	(Abbas et al. 2014)
	Tartrazina	UV-VIS	(Heredia et al. 2015)
	Bromamine acid	UV	(Fei. et al. 2010)
	RhB	UV	(Sa et al. 2009)
	Bisphenol A Dibutyl phthalate	UV	(Chalasani and Vasudevan 2013)
	MB	VIS	(Zheng et al. 2016)
$Fe_3O_4/SiO_2/TiO_2$	Textile wastewater	UV	(Ahangara et al. 2016)
	Diclofenac	UV	(Hu et al. 2011)
	Reactive black 5	UV	(Lucas et al. 2013)
	RhB	UV	(Liu et al. 2011)
	MO, MB	UV	(Liu et al. 2013b)
	P-Nitrophenol	UVC	(Rezaei-Vahidian et al. 2017)
Fe_3O_4/ SiO_2/TiO_2/Graphene	2,4-D	Solar light	(Tang et al. 2013)
Fe_3O_4/TiO_2/Ag	MB	VIS	(Zhan et al. 2014)
$Fe_3O_4/SiO_2/TiO_2$/AgBr	MB	VIS	(Liu et al. 2013c)
$Fe_3O_4/SiO_2/TiO_2$/I	Phenol	VIS	(He et al. 2012)

Fe/TiO_2, FeN/TiO_2, $CoFe_2O_4$/FeN/TiO_2	MO	UV-VIS	(Gaikwad et al. 2016)
Fe/TiO_2	Acetic acid Formaldehyde	UV	(Li et al. 2009b)
Ni/TiO_2	MO	UV	(Pang et al. 2011)
Modified sepiolite/TiO_2	2,4-dichlorophenol	UV	(Li et al. 2015)

Table 2-3 Basic information of the target compounds in this study

Parameters	SMX	AP	IBP
Chemical Structure	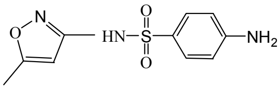	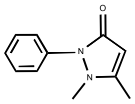	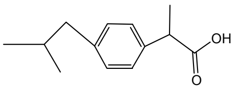
Formula	$C_{10}H_{12}N_3O_3S$	$C_{11}H_{12}N_2O$	$C_{13}H_{18}O_2$
Molecular Weight	253.28	188.23	206.29
CAS No.	723-46-6	60-80-0	15687-27-1
Melting Point	169 °C	110-113 °C	75-77 °C
Solubility (25 °C, in water, mg/L)	281	51,900	21
pK_a	1.7, 5.6	1.4	4.91

Table 2-4 Effects of sulfamethoxazole on aquatic organisms

Groups	Species	Test-type	Data (μM)	Reference
Bacteria	*Escherichia coli*	EC50 (growth)	12.3	(Wammer et al. 2006)
	Vibrio fischeri	EC50 (growth)	0.83	(Isidori et al. 2005)
		EC50 (luminescence)	7	(Majewsky et al. 2014)
Phyto-plankton	*Pinnularia subcapitata*	EC50 (growth)	2.06	(Isidori et al. 2005)
	Chlorella vulgaris	EC50 (growth)	6	(Borecka et al. 2016)
Zoo-plankton	*Ceriodaphnia dubia*	LC50	61.30	(Isidori et al. 2005)
		EC50 (growth)	0.83	(Isidori et al. 2005)
	Brachionus calyciflorus	LC50	103.83	(Isidori et al. 2005)
		EC50	38.06	(Isidori et al. 2005)
	Daphnia magna	LC50	99.60	(Isidori et al. 2005)
	Thamnocephalus platyurus	LC50	139.76	(Isidori et al. 2005)

Table 2-5 Chemical treatment processes for sulfamethoxazole degradation

Process		Reference
Photolysis	UVA, UVC, VUV	(Kim et al. 2015)
	Sunlight	(Gmurek et al. 2015)
Photocatalysis	UV/TiO_2	(Abellán et al. 2007, Hu et al. 2012, Fukahori and Fujiwara 2015, Huang et al. 2015, Yang et al. 2015)
	UV/Ti-doped ß-Bi_2O_3	(Niu et al. 2013)
	UV/TiO_2/Activated carbon	(Huang et al. 2015)
	UV/TiO_2-expanded perlite	(Dlugosz et al. 2015)
	TiO_2 Millennium PC500	(Ahmed et al. 2014)
	VIS /TiO_2/Cu	(Chiang and Doong 2015)
	UV/TiO_2/$ZnFe_2O_4$	(Liu et al. 2015a)
	Ru/TiO_2/Permanganate	(Zhang et al. 2014a)
	Ti/$Ru_{0.3}Ti_{0.7}O_2$	(Hussain et al. 2015)
	MnO_2	(Wan et al. 2015)
H_2O_2 based	UV/H_2O_2	(Yu et al. 2015, Zhang et al. 2016)
	Solar photo-Fenton	(Trovo et al. 2009a)
	$LaFeO_3$/H_2O_2	(Nie et al. 2015)
	Electro-Fenton	(Dirany et al. 2011)
	Photoelectro-Fenton: UVA/ Activated carbon fiber	(Wang et al. 2011)
Sulfate radical based	UV/Peroxydisulfate	(Zhang et al. 2016)
	Ferrous/Persulfate	(Ji et al. 2014)
	Fe/Persulfate	(Ghauch et al. 2013)
	Thermo/Persulfate	(Gao et al. 2014b, Ji et al. 2015)
	Fe(II)/HSO_5^-/Hydroxylamine	(Liu et al. 2017)
	Peroxymonosulfate/ Benzoquinone	(Zhou et al. 2015a)
O_3 based	Ozonation	(Abellan et al. 2008, Gao et al. 2014a, Dai et al. 2015, Martins et al. 2015a)
	O_3/US	(Guo et al. 2015, Naddeo et al. 2015)
	O_3/H_2O_2	(Martins et al. 2015b)
	O_3/Fe^{2+}	(Shahidi et al. 2015)
US based	Fe(VI)-US	(Zhang et al. 2015a)
Others	Chlorination	(Gao et al. 2014a, Gaffney Vde et al. 2016)
	Ferrate(VI)	(Sharma et al. 2006, Zhou and Jiang 2015)

Table 2-6 Chemical treatment processes for antipyrine degradation

Process	Reference
UVC	(Tan et al. 2013b)
UV/TiO_2 (P25)	(Calza et al. 2011)
UV/H_2O_2	(Yuan et al. 2009, Tan et al. 2013b)
UVC/Persulfate	(Tan et al. 2013b)
Heat/Persulfate	(Tan et al. 2013a)
UVC/US/Persulfate	(Monteagudo et al. 2016)
Ozonation	(Miao et al. 2015)
Chlorination	(Rodil et al. 2012)

Table 2-7 Effects of ibuprofen on aquatic organisms

Groups	Species	Test-type	Data (µM)	Reference
Bacteria	*Vibrio fischeri*	EC50 (15 min/ Bioluminescence	92.72	(Farre et al. 2001)
Phyto-plankton	*Skeletonema costatum*	EC50 (96 h/Growth)	34.47	(Knoll/BASF 1995, Webb 2003)
	Desmodesmus subspicatus	EC50 (72 h/Growth)	1661.17	(Cleuvers 2004)
	Lemna gibba	EC50 (7 d/Wet weight)	4.85	(Pietrini et al. 2015)
	Lemna minor	EC50 (7 d/Growth)	19.42	(Pomati et al. 2004)
	Chlorella vulgaris	L(E)C50	399.27	(Geiger et al. 2016)
	Synechocystis sp.	72% increase	0.0485	(Pomati et al. 2004)
Zoo-plankton	*Daphnia magna*	LC50 (48 h)	643.69	(Heckmann et al. 2007)
		NOEC (21 d/Reproduction)	5.97	(Han et al. 2010)
	Moina macrocopa	EC50 (48 h/Immobilization)	352.43	(Han et al. 2010)
	Daphnia	L(E)C50	491.26	(Cleuvers 2004)
Nekton	*Lepomis macrochirus*	LC50 (96 h)	839.81	(Knoll/BASF 1995, Webb 2003)
	Oryzias latipes	NOEC (120 d/Survival)	0.000485	(Han et al. 2010)
		LOEC (6 weeks/Reproduction)	0.485	(Flippin et al. 2007)
Zoo-benthos	*Hydra vulgaris*	NOEC (7 d/Survival)	4.85	(Pascoe et al. 2003)
	Hydra attenuate	LC50 (96 h)	108.54	(Quinn et al. 2008)
		EC50 (96 h/Feeding)	18.69	(Quinn et al. 2008)

Table 2-8 Chemical treatment processes for ibuprofen degradation

	Process	Reference
Potolysis	UV	(da Silva et al. 2014, Iovino et al. 2016)
	UV-VIS	(Castell et al. 1987)
Photocatalysis	UV/TiO_2	(da Silva et al. 2014)
	UV/VIS/TiO_2 & ZnO	(Georgaki et al. 2014)
	Solar light/$BiVO_4$	(Li et al. 2016)
H_2O_2 based	UV/H_2O_2	(Yuan et al. 2009, Scheideler et al. 2011)
	Photo-Fenton	(Mendez-Arriaga et al. 2010)
	(UVA or Solar)/Electro-Fenton	(Skoumal et al. 2009)
O_3 based	Electro-peroxone	(Li et al. 2014)
	Ozonation	(Quero-Pastor et al. 2014)
	O_3/H_2O_2	(Scheideler et al. 2011)
	O_3/UV/TiO_2	(Giri et al. 2010)
Sulfate radical based	UV/Fe(III)/Oxone	(Rao et al. 2016)
US based	US/UV/TiO_2, US/UV/Fe^{3+}	(Madhavan et al. 2010)
Others	$KMnO_4$, H_2O_2	(Caviglioli et al. 2002)

3. Chapter three Materials and methods

3.1 Materials

All chemicals used in this study are summarized in Table 3-1. The chemicals used in reactions were of at least analytical standard, solvents employed in HPLC and LC/MS analysis were of HPLC grade and LC/MS grade, respectively. All solutions were prepared in ultrapure water from a Bamstead NANO pure water system (Thermo Fisher Scientific Inc., USA).

The green algae *C. vulgaris* and the brine shrimps *A. salina* were selected as the test organism for phytoplankton and zooplankton, respectively, because of their wide distribution, cheap/easy culture and high sensitivity to toxicants (Banister and Campbell 1985, Smith 2001, Barhoumi and Dewez 2013, Rajabi et al. 2015). The algae *Isochrysis galbana* was used as the diets of *A. salina.*

The algae *C. vulgaris*, *I. galbana* and dehydrated cysts of the brine shrimp *A. salina* were purchased from Biotech Company of Jiangmen, China. The algae were cultured in f/2 medium (Guillard 1975) at temperature 22 ± 1°C, with a 12 h light/12 h dark photoperiod. The water used in the culture of *C. vulgaris* was ultrapure water. The water used in the culture of *I. galbana* was artificial seawater, prepared by the method modified from Kester et al. (Kester et al. 1967). Prior to each use, the water was subjected to filtration with a 0.22 µm mixed cellulose esters (MCE) membrane filter and sterilization. The cysts of the brine shrimp were suspended in sterile seawater at 28 ºC with continuous aeration and illumination. Instar I stage larvae i.e. nauplii hatched in 24 hours were separated and used for the toxicity test.

3.2 Methods

All experiments were conducted at 22 ± 1 °C without special claim.

3.2.1 Catalyst synthesis and characterization

The catalyst $CoFe_2O_4/TiO_2$ was synthesized by heterjunction commercial $CoFe_2O_4$ and P25 with coprecipitation method. The synthesis process was modified from the method reported by Gao et al. (Gao et al. 2009). Firstly, 2.1 g $CoFe_2O_4$ and a certain dosage of $TiCl_4$ were introduced in 200 ml ultrapure water. The pH value of the solution was adjusted to 9-10 with ammonia under mechanical stirring at 15 ºC for l h, during which P25 was added into the solution stepwise. Then, the obtained particles were washed with ultrapure water three times, and the obtained particles were dried in vacuum drying oven at 80 ˚C for 48 h.

The phase of magnetic photocatalysts $CoFe_2O_4/TiO_2$ was characterized by the X-ray diffraction technique. The XRD analysis was carried out on an X-ray diffractometer (Smartlab) with Cu-Kα radiation (A = 0.1540 nm) employing a scan rate (2θ) of 5º/min ranging from 20° to 80°. The accelerating voltage and the applied current were 15 kV and 20 mA, respectively.

The SEM (scanning electron microscopy) images with EDX (Energy Dispersive X-ray spectroscopy) analysis were obtained from a field-emission scanning electron microscopy (FE-SEM; JEOL Model JSM-6700F, Tokyo, Japan). The TEM (transmission electron microscopy) images were obtained with a JEOL JEM-2100HR electron microscopy instrument (JEOL Model JEM-2100HR).

The diffuse reflectance spectra (DRS) of the catalysts was obtained using a Varian Cary 100 Scan Ultraviolet-visible (UV–VIS) spectrophotometer equipped with a labsphere diffuse reflectance accessory over a range of 200–800 nm. Labsphere USRS-99-010 was used as the reflectance standard. Kubelka–Munk method was employed for the conversion from reflection to absorbance (He et al. 2008).

The BET surface area of the catalyst was obtained from N_2 adsorption/desorption isotherms at 77 K with an ASAP 2020 automatic analyzer (Micromeritics Instrument Corp., Norcross, GA, USA).

The zero point of charge (ZPC) was determined by batch equilibrium technique (Ibrahim et al. 2016). A certain amount (0.1 g in this study) of the catalyst were introduced into 100 mL of 0.1 mol/L NaCl solution. Initial pH values (pH_0) of NaCl solutions were adjusted from 5 to 9 via addition of 0.1 mol/L HCl or NaOH solutions. The solutions suspended with the catalysts were stirred with mechanical stirrer for 24 hours. After filtration, the pH values of the suspensions were measured again and marked as pH_t. The pH levels were monitored by a digital pH meter (model: HANNA instrument, B417).

3.2.2 Photodegradation of the target compounds

The UV-induced photocatalytic reaction was carried out in a Rayonet^{TM} RPR-200 photochemical reactor containing twelve phosphor-coated low-pressure mercury lamps (illustrated in Figure 3-1) at room temperature (air-conditioned) i.e. 23 ± 1 °C. The photo-reactor and all lamps were purchased from The Southern New England Ultraviolate Co., Branford, Connecticut, USA. The relative energy of the lamps under different wavelength is shown in Figure 3-2.

To ensure a thorough mixing, 150 mL of solution was dispensed into a 300 mL quartz cylinder and mixed with a non-metal mechanical stirrer before and during the illumination. To exclude the effect of adsorption on the degradation, the predetermined amount of $CoFe_2O_4/TiO_2$ was added into 150 mL SMX solution and stirred mechanically in darkness for 30 minutes to achieve adsorption equilibrium. Then, the reaction was started by turning on the lamps. At preset intervals, 1 mL sample was withdrawn and filtered through a 0.22 μm membrane filter (ADVANTEC HP020AN, Japan, with recovery rate of 100%) for further analysis. All experiments were conducted in duplicate, and the error is less than 5%.

3.2.3 Concentration determination of target compounds

A High-Performance Liquid Chromatograph (HPLC) system, equipped with a Waters 515 HPLC pump, a Waters 717 plus autosampler, a Restek C18 column (5 µm, 4.6×250 mm) and a Waters 2489 Dual absorbance detector was performed for the measurement of target compounds' concentration.

The UV absorption spectra of the target compounds were obtained from a spectrophotometer (biochrom, Libra S12). The detection wavelength was determined from the UV absorption spectra (Figure 3-3), and the wavelength of 263 nm, 261 nm and 220 nm was selected for SMX, AP, IBP, respectively. The flow rate was 1 mL/min and the injection volume was 10 µL. For SMX concentration determination, the mobile phase was a mixture of 50% acetonitrile (ACN) and 50% of 5 mM KH_2PO_4, with pH level adjusted to 3.0 by introduction of H_3PO_4. For AP concentration determination, the mobile phase was a mixture of 25% acetonitrile and 75% of ultrapure water. For IBP concentration determination, the mobile phase was a mixture of 75% ACN and 25% ultrapure water with 0.001% acetic acid. Methanol (50%) was used as the wash solvent. Standard lines for peak area of target compounds in terms of the concentration are shown in Figure 3-4.

3.2.4 Intermediates detection

An Ultrapure Liquid Chromatograph/Electrospray Ionization-Mass Spectrometry (UPLC/ESI-MS) system was employed for the intermediates determination. The system is controlled by the LC/MSD ChemStation software version A.09.03 and consists of a quaternary pump, a vacuum degasser, an autosampler, a diode array detector (DAD), an ion trap mass spectrometer detector (MSD), and a thermostated column compartment with a Thermo Hypersil GOLD column (1.9 µm, 50 × 2.1 mm, maintained at 30ºC during analysis). Chromatography was conducted with a Dionex UltiMate 3000 Ultra-high Performance Liquid Chromatography (UPLC). Mass analysis was performed with a Bruker amaZon SL ion trap mass analyzer in positive ion mode with a mass range of 50–400 m/z. The system was controlled by the LC/MSD ChemStation software version A.09.03. The flow rate and injection volume were 0.15 mL/min and 10 µL, respectively.

Formic acid (0.1%) and isopropyl alcohol were used as the wash solvent. Nitrogen was employed as both drying and nebulizer gas. ACN and 0.1% formic acid were used as the mobile phases indicated as A and B, respectively. For the LC/MS method in Chapter 5 and 8, a linear gradient progressed from 10% A (0-2 min) to 70% A in 2-15 min, maintained at 70% A for 3 min, and finally went back to the initial mobile-phase. For the LC/MS method in Chapter 6, a linear gradient progressed from 5% A (0-2 min) to 30% A in 2-20 min, maintained at 30% A for 3 min, and finally back to the initial mobile-phase.

3.2.5 Measurement of TOC and inorganic ions

The mineralization was determined as a ratio of final to initial content of TOC (C/C_0) in the solution. A TOC analyzer which consists of an autosampler (shimadzu, ASI-L) and a CO_2 conductivity detector was used to measure the content of TOC.

The inorganic ion release during SMX and AP degradation was expressed as a ratio of final to the total mass of nitrogen (C/C_t). A potable colorimeter (Hach, DR/890) was performed to monitor concentrations of nitrate (NO_3^-), nitrite (NO_2^-), ammonium (NH_4^+), sulfate (SO_4^{2-}).

The concentration of Fe^{2+} was determined with a UV-VIS spectrophotometer (biochrom, Libra S12) at 510 nm using 1,10-phenanthroline as the indicator. The concentration of permanganate in Chapter eight was measured at 526 nm with the spectrophotometer.

3.2.6 Toxicity test

The toxicity of SMX and degradation products was evaluated on samples collected at different reaction/degradation time. All experiments were performed in triplicate at temperature 20 ± 0.5°C, and pH 7.0 ± 0.2.

3.2.6.1 Toxicity assessment on the algae C. vulgaris

Experiments were carried out in 20 mL glass tubes with 10 mL test liquid. Exact 1 mL algae *C. vulgaris* at exponential growth phase was transferred to the test solutions. The culture conditions, including the medium and illumination were the same as those mentioned above in 3.1. The density of the algae was determined by microscope examination every other day. The obtained growth curves were correlated by Logistic growth model. The governing equation of Logistic Equation is as follows (Pearl and Reed 1920):

$$dN / dt = r N (K - N) / K \qquad \text{(Equation 3-1)}$$

where t is the time; N is the number of a population at time t; r is the growth rate; K is the carrying capacity.

After integration, a working model is available as (McKendricka and Pai 1912):

$$N = K / (1 + e^{(a - r t)}) \qquad \text{(Equation 3-2)}$$

where a is a constant related to N_0 (the initial number of the population), $N_0 = K / (1 + e^{a})$. The above integral form of Logistic Equation was used to analyze the data, and the values of a, r and K were determined by Origin 8.0.

3.2.6.2 Toxicity assessment on the brine shrimp A. salina

Toxicity assessment utilizing mortality of *A. salina* was firstly performed. The acute toxicity test of *A. salina* was performed in a 24-well polystyrene plate with 1 mL test solution. The test solution was diluted with an equal amount of double concentrated seawater to guarantee the suitable salinity environment for the brine shrimp. Ten healthy and vivacious larvae were introduced randomly to each well of the plate. The algae *I. galbana* were added as diets. The number of alive larvae in each well was determined under a stereomicroscope and dead brine shrimps (completely motionless) were removed. The percentages of survival were then calculated.

In Chapter 5, toxicity assessment utilizing clearance rate of *A. salina* was conducted according to the followed procedures. Feeding of the brine shrimp was carried out in 30 mL glass tubes with 10 mL test liquid and 10 mL double concentrated seawater. The brine shrimps were concentrated with an 80 μm mesh, and then re-suspended in ultrapure water in a 5 ml sterilized centrifuge tube as stock for the tests. After a homogenous distribution with gentle mixture, three samples were taken and fixed with Lugol's Iodine Solution, then the density of the brine shrimps was determined under a dissecting microscope. Brine shrimps and the algae *I. galbana* (as diets) were transferred to the tubes successively. Diets were collected and the biomass was determined before and after the tests respectively. The diet biomass was represented by cell density of the algae monitored by a microscope.

Control groups without brine shrimps were set to eliminate the algae density change caused by the algae growth during the experiments. Clearance rate (CR, $\mu L \cdot ind^{-1} \cdot min^{-1}$) was calculated as follows (Frost 1972):

$$CR = V \times (\ln(E_0 / E_t) / \ln(C_0 / C_t)) / (t \times N) \qquad \text{(Equation 3-3)}$$

where CR, Clearance rate ($\mu L \cdot ind^{-1} \cdot min^{-1}$), indicates the water volume filtered by each feeder every minute; V is the volume of solution; E_0 and E_t are the particle biomass of experiment group at time 0 and t, respectively; C_0 and C_t are the particle biomass of control group at time 0 and t, respectively; t is the feeding time (24 hours in this study); and N is the number of brine shrimps.

In Chapter 8, toxicity assessment employing ingestion of *A. salina was carried out.* Feeding experiment on *A. salina* was then conducted in glass tubes with 10 ml experimental volume. Before exposed to the algae, the brine shrimps were concentrated and the density was determined. The tested solution, the concentrated shrimps and the algae at exponential growth phase were transferred to the tubes. After five hours, the brine shrimps were transferred to 80 μm meshes and washed with artificial seawater for several times. Then the brine shrimps were transferred to 5 mL acetone at -20 °C for 24 h. UV-VIS spectrometer was performed to determine the Chlorophyll *a* content in the guts of the brine shrimps, which reflect the feeding of brine shrimps. The Chlorophyll *a* content was calculated by the following equation (Lichtenthaler and Buschmann 2001).

$$\text{Chlorophyll } a \text{ (ng/ind)} = (11.24\ A_{662} - 2.04\ A_{645}) \times 10^{6} / N \qquad \text{(Equation 3-4)}$$

where A_{662} and A_{645} is the absorbance at wavelength of 662 and 645 nm, respectively. N is the number of the brine shrimps.

One-way ANOVA was performed with SPSS 13.0 to compare effects of different samples collected at different time on the algae growth, mortality, clearance rate and ingestion of the brine shrimps.

Table 3-1 Information of chemicals used in this study

Name	CAS No.	Molecular Weight	Formula	Manufacturer
Target compounds				
SMX	131-11-3	194.18	$C_{10}H_{11}N_3O_3S$	Sigma Aldrich Inc.
IBP	84-74-2	278.34	$C_{13}H_{18}O_2$	Sigma Aldrich Inc.
AP	84-66-2	222.24	$C_{12}H_{14}O_4$	Sigma Aldrich Inc.
Compounds used in catalyst synthesis				
Titanium tetrachloride	7550-45-0	189.71	$TiCl_4$	Sigma Aldrich Inc.
Titanium oxide	13463-67-7	79.87	TiO_2	Sigma Aldrich Inc., Degussa
Cobalt ferrite	12052-28-7	234.62	$CoFe_2O_4$	US Research Nanomaterials Inc.
Ammonia	1336-21-6	35.04	$NH_3 \cdot H_2O$	Sigma Aldrich Inc.
Compounds used in HPLC and LC/MS				
Potassium phosphate monobasic	7778-77-0	136.09	KH_2PO_4	Sigma Aldrich Inc.
Orthophosphoric acid	7664-38-2	97.994	H_3PO_4	Sigma Aldrich Inc.
Acetonitrile	75-05-8	41.05	C_2H_3N	Sigma Aldrich Inc., Tedia Company
Acetic acid	64-19-7	60.05		Sigma Aldrich Inc.
Formic acid	64-18-6	46.03	CH_2O_2	Tedia Company
Methanol	67-56-1	32.04	CH_4O	Tedia Company
Isopropyl alcohol	67-63-0	60.10	C_3H_8O	Tedia Company
Compounds used in photoreactions				
Hydrochloric acid	7647-01-0	36.46	HCl	Sigma Aldrich Inc.

Sodium hydroxide	1310-73-2	40.00	$NaOH$	Sigma Aldrich Inc.
Potassium ferrate(VI)	39469-86-8	198.04	K_2FeO_4	Sigma Aldrich Inc.
Potassium permanganate	7722-64-7	158.04	$KMnO_4$	Sigma Aldrich Inc.
Hydrogen peroxide	7722-84-1	34.01	H_2O_2	Sigma Aldrich Inc.
Potassium persulfate	7727-21-1	270.33	$K_2S_2O_8$	Sigma Aldrich Inc.
Oxone	37222-66-5	152.17	$KHSO_5\cdot 0.5KHSO_4\cdot 0.5K_2SO_4$	Sigma Aldrich Inc.
Sodium thiosulfate	7772-98-7	158.11	$Na_2S_2O_3$	Sigma Aldrich Inc.
Sodium nitrate	7631-99-4	84.99	$NaNO_3$	Sigma Aldrich Inc.
Sodium fluoride	7681-49-4	41.99	NaF	Sigma Aldrich Inc.
Sodium chloride	7647-14-5	58.44	$NaCl$	Sigma Aldrich Inc.
Sodium sulfate	7757-82-6	142.04	Na_2SO_4	Sigma Aldrich Inc.
Ferrous sulfate heptahydrate	7720-78-7	278.05	$FeSO_4\cdot 7H_2O$	Sigma Aldrich Inc.
1, 10-phenanthroline	5144-89-8	198.22	$C_{12}H_{10}N_2O$	Riedel-de Haën
Methanol	67-56-1	32.04	CH_4O	Tedia Company
Tert-Butanol	75-65-0	74.12	$C_4H_{10}O$	Sigma Aldrich Inc.
Trichloromethane	67-66-3	119.38	$CHCl_3$	Sigma Aldrich Inc.
Standard of intermediates				
3-Amino-5-methylisoxazole	1072-67-9	98.10	$C_4H_6ON_2$	Sigma Aldrich Inc.
SFL	63-74-1	172.20	$C_6H_8O_2N_2S$	Sigma Aldrich Inc.

Figure 3-1 Apparatus used for the photoreactions.

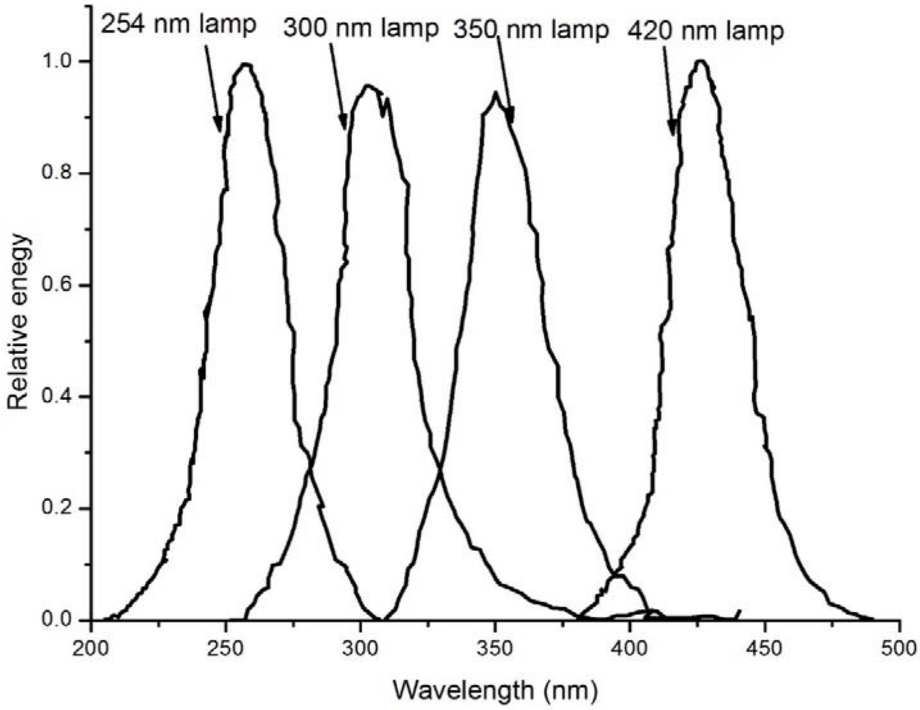

Figure 3-2 Relative energy of lamps under different wavelengths.

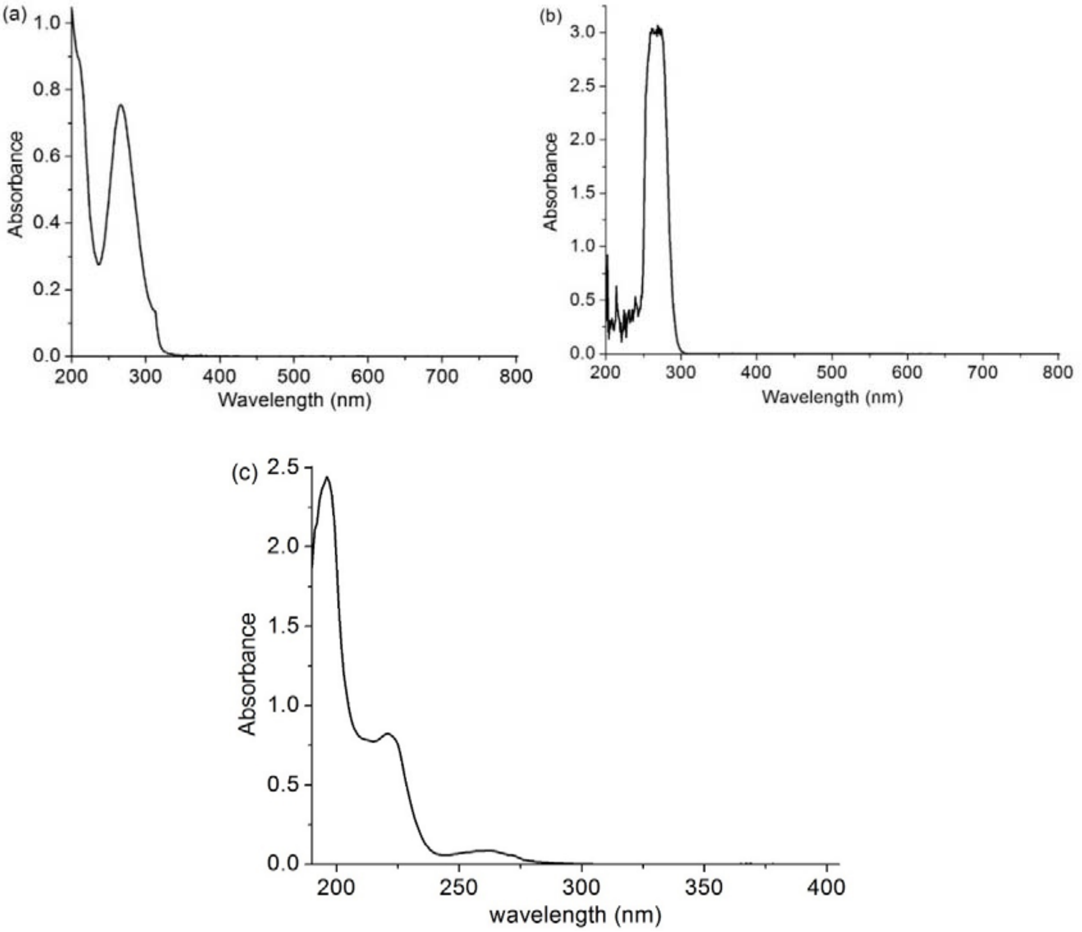

Figure 3-3 Absorbance of target compounds. (a) Absorbance of sulfamethoxazole. (b) Absorbance of antipyrine. (c) Absorbance of ibuprofen.

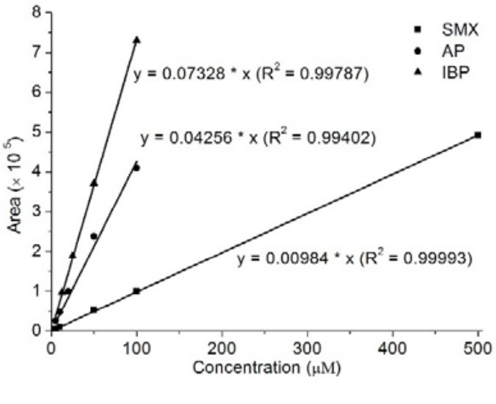

Figure 3-4 Standard line for peak area of target compounds in terms of the concentration.

4. Chapter four Characteristics and magnetic property of the catalyst

4.1 Introduction

According to Chapter three, different proportions of $TiCl_4$ and TiO_2 (P25) particles were introduced during the photocatalyst synthesis. The four groups of photocatalysts were firstly employed in SMX degradation (the data are shown in Chapter five). Then the group of the photocatalyst which shows the best performance in SMX destruction was utilized for the characterization, magnetic property test and other detailed studies. This chapter reveals the characterization including XRD, SEM, TEM, EDS, BET, DRS, ZPC and magnetic property test of the photocatalyst.

4.2 Results and discussion

4.2.1 XRD pattern of the catalyst

To verify the components of the synthesized catalyst, the X-ray Diffraction pattern of the prepared composite is shown in Figure 4-1. The peaks of $CoFe_2O_4$, TiO_2 anatase phase and rutile phase in the $CoFe_2O_4/TiO_2$ composite were clearly observed.

According to the standard diffraction pattern of Joint Committee on Powder Diffraction

Standards (JCPDS), the main characteristic peaks of $CoFe_2O_4$ (JCPDF File no. 22-1086) (Standards 1995c) observed at $2\theta = 29.9^{\circ}$, 35.2°, 36.2°, 42.8°, 56.6° and 62.3° are well indexed to the crystal plane of $CoFe_2O_4$ at (220), (311), (222), (400), (511) and (440), respectively. Besides, the peaks appeared at 25.2°, 37.8°, 48.1°, 54.8°, 62.6° corresponding to anatase TiO_2 (JCPDF File no. 21-1272) (Standards 1995a) at (101), (004), (200), (105) and (204) and the peaks at 27.4° for the characteristic reflection of rutile TiO_2 (JCPDF file no. 21-1276) (Standards 1995b) can also be observed in Figure 4-1.

The crystal structure of $CoFe_2O_4$, anatase TiO_2 and rutile TiO_2 in the new composite is as same as their original structure. No other peak except the peaks of $CoFe_2O_4$, TiO_2 anatase phase and rutile phase was found. Therefore, no phase change of the crystal structure was caused, and no new substance formed in the preparation process. The introduction of Cl^- and NH_4^+ due to the addition of $TiCl_4$ and $NH_3 \cdot H_2O$ was apparently washed away during the preparation, which guarantees the purity of the material and excludes the effect of inorganic ions on the degradation.

4.2.2 Morphology of the catalyst

The formation of homogeneous spherical aggregates is observed in SEM images of the synthesized catalyst $CoFe_2O_4/TiO_2$ (Figure 4-2). The TEM image was demonstrated in Figure 4-3 (a). The particle size distribution from TEM images with the software ImageJ was obtained in Figure 4-3 (b). The particle size ranges from 20 to 50 nm. The average particle size is around 30 nm, as defined by the size corresponding to the peak of the

Gaussian fitting curve. Fig. 4-3 (c) shows that the particle size distribution of the catalyst in aqueous phase. The particle size ranges from 100 to 250 nm, and the average particle size is 164 nm. The result is quite different from that measured in TEM image due to the aggregates property of the catalyst in aqueous phase. The particle size distribution in aqueous phase indicates actual performance of the catalyst in the water treatment.

The attached EDX (Figure 4-4) exhibits the elemental analysis of the $CoFe_2O_4/TiO_2$ nanocatalysts. The peaks of Co, Fe, Ti and O and the atomic ratios are well justified. For example, the mole ratio of Ti/Fe is approximately 7/1, which agrees with the estimation calculated from the catalyst synthesis. The unexpected presence of a small fraction of element carbon (C) was possibly ascribed to the polymer adhesive which attached the sample on the testing plate.

4.2.3 UV-VIS DRS

The UV–VIS DRS data shown in Figure 4-5 indicate that the light absorption of TiO_2 (no matter common TiO_2 or Degussa P25) has a clear cut off above 400 nm, while high absorption was observed for the full visible region for $CoFe_2O_4$ and the synthesized $CoFe_2O_4/TiO_2$. The Tauc plot graph approach was applied for the calculation of the band gap energy by using (Police et al. 2014):

$$E_g\ (\text{eV}) = 1239.8 / \lambda\ (\text{nm}) \qquad \text{(Equation 4-1)}$$

where E_g is the band gap of the catalyst and λ is the absorption wavelength. Corresponding to the enhanced absorption intensity in visible light region, the band gap of $CoFe_2O_4/TiO_2$ (~1.4 eV) is significantly reduced compared to that of TiO_2 (~3.1 eV).

The decrease of the band gap after doping with the magnetic material is possibly ascribed to the presence of impurity energy level or defect energy level. Owing to the approximate ionic radius of Fe^{3+} (0.64 A°), Co^{2+} (0.65 A°) and Ti^{4+} (0.68 A°), TiO_2 lattice is accessible to the doping ion (i.e. Fe^{3+} and Co^{2+}) (Hu et al. 2012). The replacement of Ti^{4+} by Fe^{3+} and/or Co^{2+} in crystal structure of TiO_2, or the incorporation into the crystal intervals may result in the formation of crystal defect (Hu et al. 2012). A new impurity level is introduced to the CB of TiO_2, and the electrons can be promoted from the VB to these impurity levels, leading to the reduction of band gap energy (Hu et al. 2012).

Reduced band gap energy between the CB and VB may result in lower excitation photon energy, thus more photogenerated electrons and holes can be introduced to participate in the photocatalytic reactions, leading to the improvement of the photocatalytic activity. The response region of $CoFe_2O_4/TiO_2$ composite catalyst may be broadened from UV to visible light; including the green energy source, solar light, for the degradation of pollutants in water.

4.2.4 Surface area of the catalyst

The BET results showed that the specific surface area is enhanced after doping (Figure 4-6). The slight increase of the specific surface area can also be explained by the substitution of Ti^{4+} by Fe^{3+} or/and Co^{2+} (Zhong et al. 2013). The surface of the catalyst is the site where the reaction occurs, and higher value of surface area may indicate higher activity of the catalyst (Zhang and Wang 2014). Therefore, the result indicates that the composite material may have a higher activity than the sole catalyst $CoFe_2O_4$ or TiO_2.

4.2.5 ZPC of the catalyst

The ZPC of catalyst was calculated from the interval point of the measured initial-final pH curve with the zero pH difference line (Figure 4-7). The ZPC value was determined as around 8.0.

4.2.6 Magnetic property of the catalyst

The magnetic activity was evaluated with result shown in Figure 4-8, where the photos show the $CoFe_2O_4/TiO_2$ photocatalyst suspended in the SMX solution with and without the magnetic field. The separation process is thorough and fast, it only takes 1-2 seconds to collect almost all the spent photocatalyst.

4.3 Summary

In this chapter, the characteristic and magnetic property of the obtained catalyst were revealed. The average particle size was determined to be around 20-50 nm and 100-250 nm, in solid and aqueous phase, respectively. The catalyst was demonstrated to be homogenous spherical aggregates from SEM image. The phases of $CoFe_2O_4$, anatase TiO_2

and rutile TiO_2 in the $CoFe_2O_4/TiO_2$ composite were clearly observed. The presence and atomic ratios of Co, Fe, Ti and O from the catalyst were well justified. Reduced band gap energy and increased specific surface area compared to TiO_2 was found for the obtained catalyst. The ZPC value of the catalyst was determined to be around 8.0. The catalyst can be easily separated from the solution with external magnetic field, indicating the magnetic property of the catalyst.

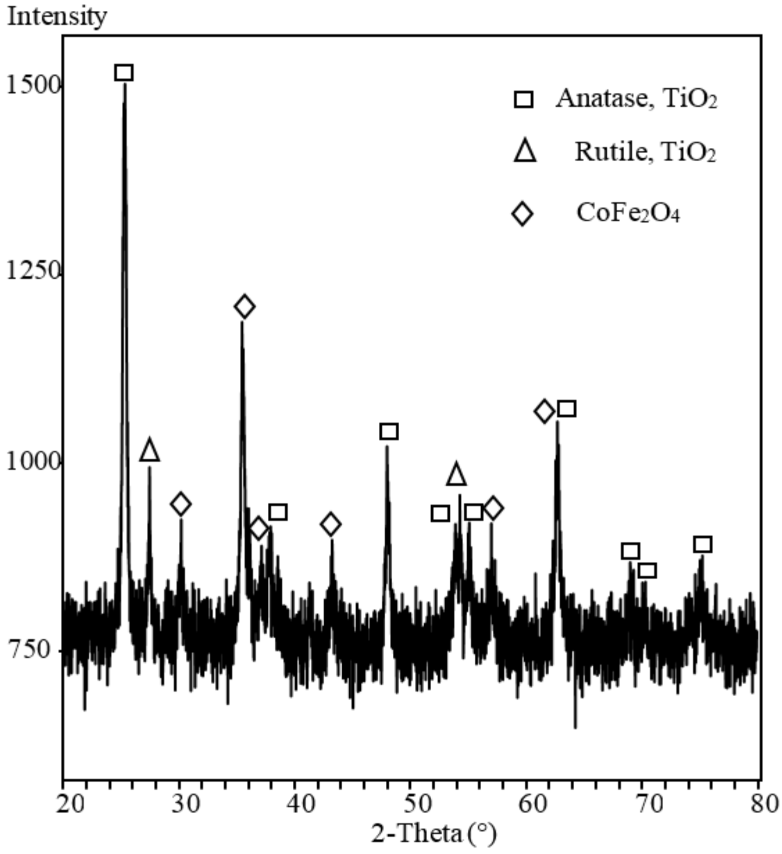

Figure 4-1 XRD pattern of the obtained catalyst.

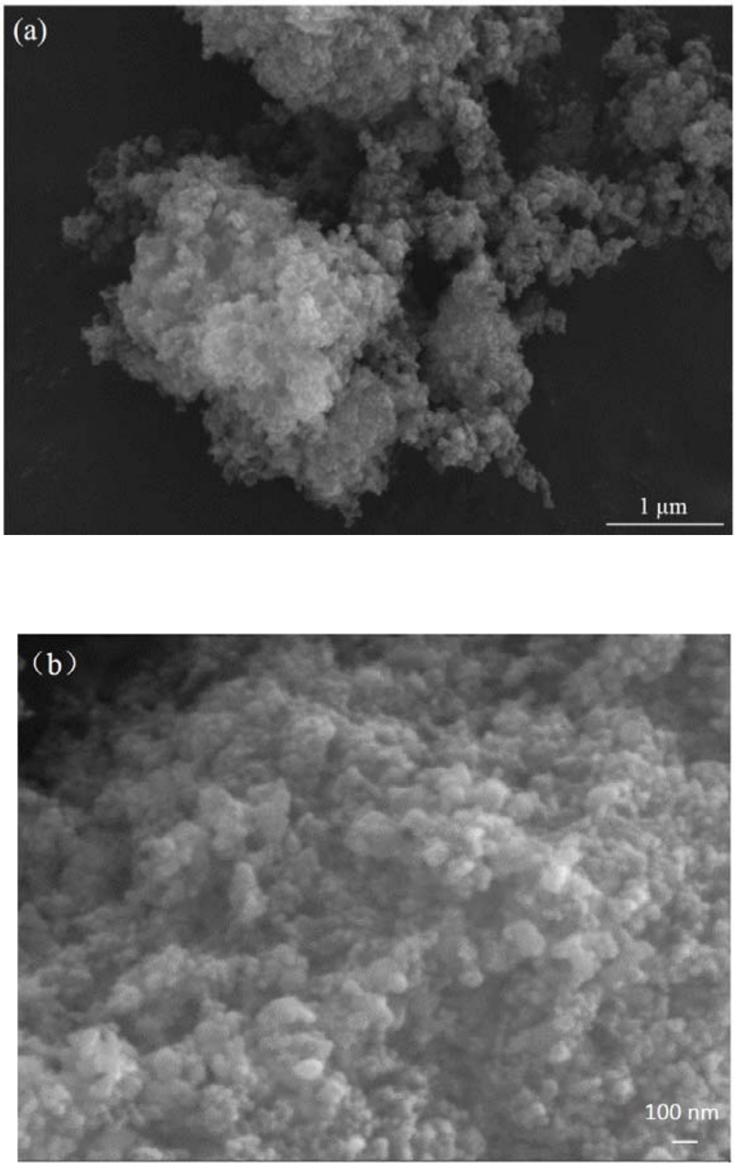

Figure 4-2 SEM image of the obtained catalyst.

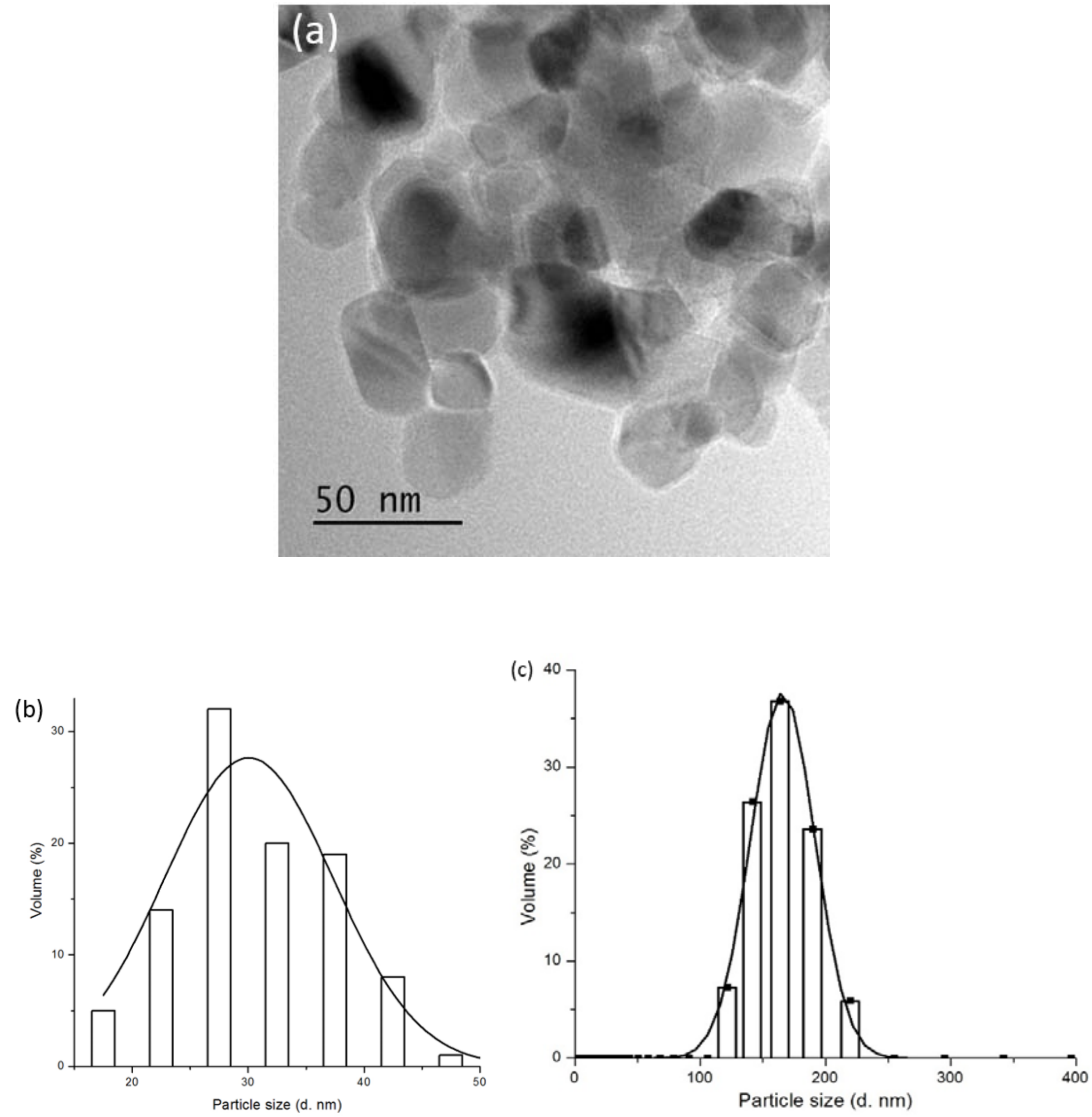

Figure 4-3 TEM image and particle size distribution of the obtained catalyst. (a) TEM image (b) Particle size distribution in solid phase. (c) Particle size distribution in aqueous phase.

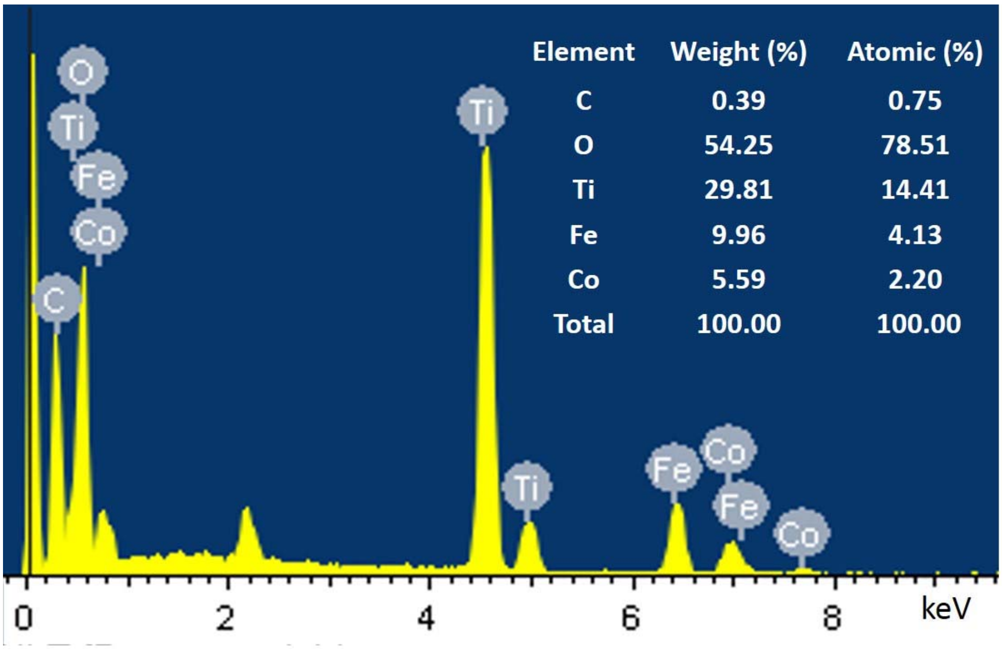

Element	Weight (%)	Atomic (%)
C	0.39	0.75
O	54.25	78.51
Ti	29.81	14.41
Fe	9.96	4.13
Co	5.59	2.20
Total	100.00	100.00

Figure 4-4 EDX spectra of the obtained catalyst.

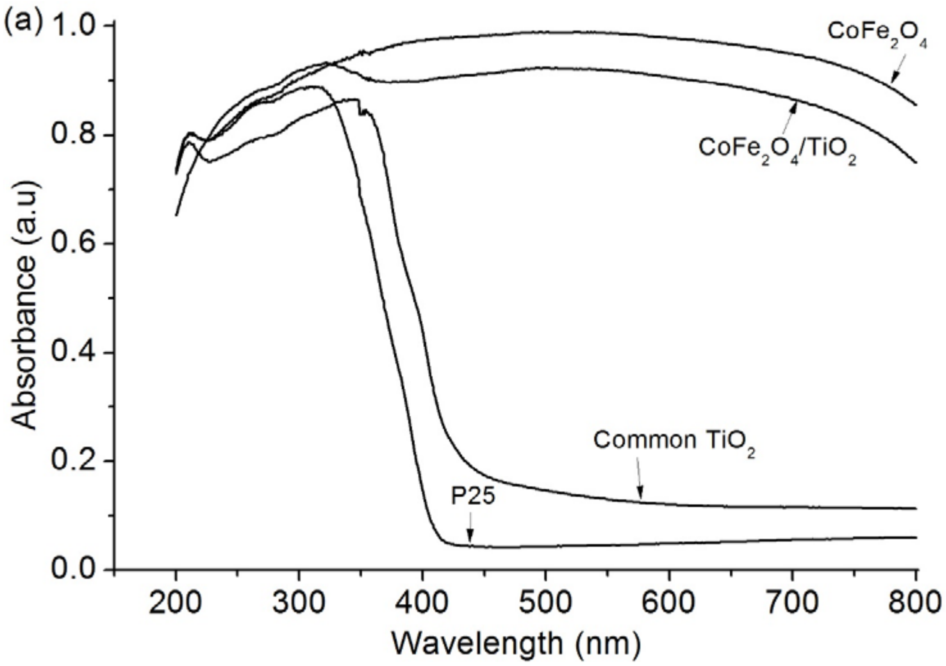

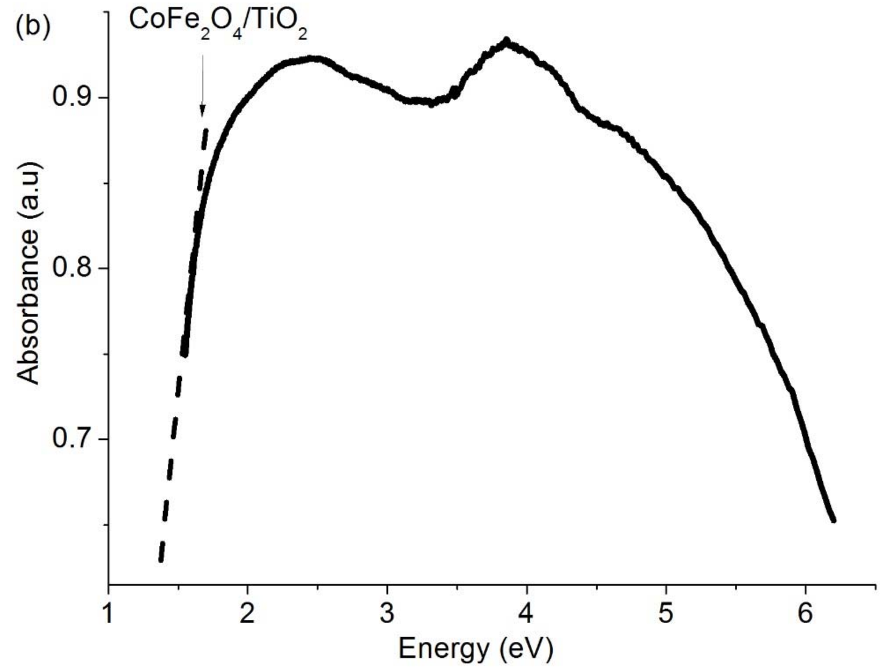

Figure 4-5 Kubelka-Munk absorbance spectra of the obtained catalyst.

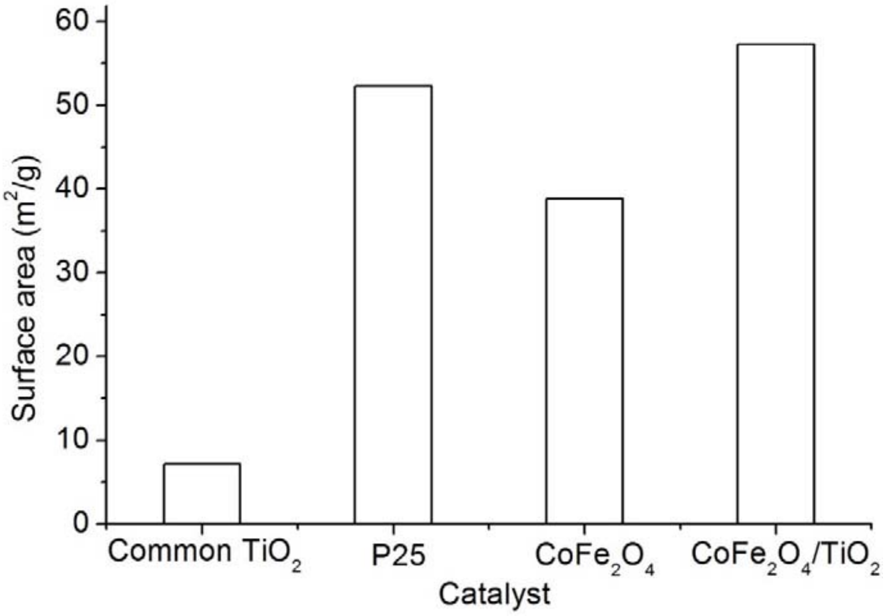

Figure 4-6 BET surface area of the obtained catalyst.

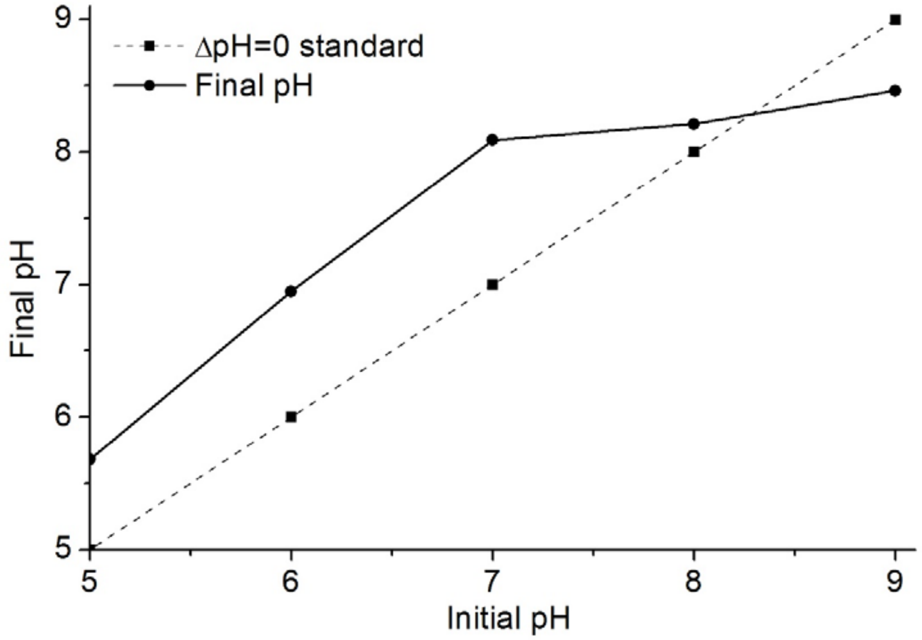

Figure 4-7 ZPC measurement of the obtained catalyst.

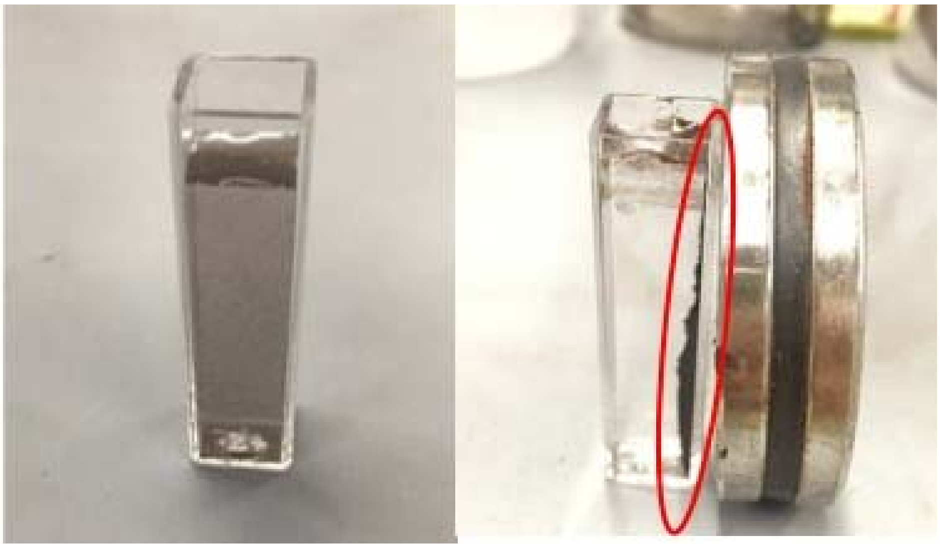

Figure 4-8 Separation of $CoFe_2O_4/TiO_2$ from the treated sulfamethoxazole solution.

5. Chapter five Photodegradation of sulfamethoxazole with the magnetic catalyst

5.1 Introduction

As is demonstrated in chapter two, SMX is one of the most frequently antibiotics over the worldwide. The adverse effects of SMX on the aquatic organisms have been well studied. The decomposition of SMX receives great concern and a great number of attempts have been made on the SMX degradation by chemical treatment processes. In this chapter, the photocatalytic activity evaluation on the four groups of photocatalysts synthesized with different P25 addition dosage was carried out by the SMX degradation under UV irradiation. The group of the photocatalyst which gives the highest SMX removal efficiency is employed in the next detailed studies.

The effect of reaction parameters including UV wavelength, catalyst dosage, SMX initial concentration, pH value and the introduction of ferrate on the reaction was investigated. The reaction mechanism during the treatment including the detection of organic intermediates, the reaction pathway proposal, the TOC reduction, and the inorganic ions release was explored. The toxicity evolution of the degradation intermediates to aquatic organisms, including the green alga *C. vulgaris* and the brine shrimp *A. salina* was studied.

5.2 Results and discussion

5.2.1 The photocatalytic activity of catalysts obtained from different processes

Processes with different dosages of $TiCl_4$ were carried out to investigate the best dosages of $TiCl_4$ and P25. The photocatalytic activity of the synthesized catalysts, sole-$CoFe_2O_4$, and P25 is shown in Figure 5-1. It was found that all the destruction curves followed pseudo first-order kinetics. The reaction constant was calculated by Equation 5-1.

$$k = \ln (C_0 / C) / t \qquad \text{(Equation 5-1)}$$

In the equation, k and t is the reaction rate constant and the reaction time, respectively. C_0 and C are the SMX initial concentration and SMX concentration at time t, respectively.

It was a surprise to note, only about 10% SMX was removed by the $CoFe_2O_4$ (in the presence of UV) at the end of the reaction, which is even lower than that by using sole-UV (about 40% removal). This is because the $CoFe_2O_4$ has a lower photocatalytic activity in the degradation of SMX and the particle of the $CoFe_2O_4$ blocks the photons' path, which inhibits the direct photolysis of the UV (the transmission of the solution with $CoFe_2O_4$ is 48.2% lower than that without the catalyst). When $TiCl_4$ was added, however, the removal efficiency was significantly improved comparing to that of sole-$CoFe_2O_4$. These observations suggest that both direct photolysis and photocatalysis coexist in the process.

The accelerated reaction compared to that with sole-$CoFe_2O_4$ is attributed to the formation of TiO_2 via the hydrolysis of $TiCl_4$, as follows:

$$TiCl_4 + 2H_2O \rightarrow TiO_2 + 4HCl \qquad \text{(Equation 5-2)}$$

The TiO_2 formed on the surface of $CoFe_2O_4$ core can be calculated stoichiometrically according to the Equation 5-2. The required P25 (added separately) to make up the difference and ensure a same overall TiO_2 in the composite photocatalyst can then be estimated. The result shows that the photocatalytic activity of the synthesized catalysts increases largely with the addition of P25. About 75% SMX was removed at the end of the reaction with the catalyst synthesized by the mixture of 3 mL $TiCl_4$ and 2.2 g P25, i.e. 34% P25 in the composite. Higher the percentage of P25, faster the reaction rate as shown in Figure 5-1 (b). At 62% P25, the SMX was completely removed in 120 minutes, indicating that P25 played the main role in the photocatalysis. This can be evident by the good degradation efficiency with pure P25, where all the SMX was removed in 20 minutes, however, it should be noted that this is not a fair test, since the pure P25 has much smaller particle size than that of synthesized magnetic catalyst at the same dosage. As was defined in Chapter 4, the average particle size of the synthesized catalyst in aqueous phase is around 160 nm, while the size of TiO_2 (P25) is 21-26 nm (Raj and Viswanathan, Ohno et al. 2001). In addition, the newly synthesized TiO_2 via hydrolysis is mainly functioned as an adhesive to bond the $CoFe_2O_4$ core and the P25 together. It's reasonable for the synthesized TiO_2 having less active sites or surface area for the reaction.

It is well known that phase structures have great influence on the photocatalytic activity of catalysts (Zhou et al. 2012). There are mainly two phases for TiO_2, i.e. anatase and rutile phases. The former has been confirmed to play the main part in photocatalytic activity owing to its low recombination rate of photogenerated electrons and holes (Kontos et al. 2005, Deiana et al. 2010). Besides, it was found that the composite of two phases of titania performed better (Yu and Wang 2008). Therefore, a high ratio of anatase/rutile would be beneficial for the photocatalytic activity.

There are different ways to synthesize $CoFe_2O_4/TiO_2$, and titania was mostly synthesized via the hydrolysis of titanium butoxide or titanium tetrachloride. The phase structure of synthesized titania and thus the photocatalytic activity can be changed by calcination (Wang et al. 2012). Though the catalysts synthesized based on the above process was proved to be efficient in the degradation of some dye such as MB (Hu et al. 2012). Unfortunately, the same process was tested and proved to be inefficient in the degradation of SMX in this study (data not shown). By doping P25 to $CoFe_2O_4$, in the assistance of forming fresh TiO_2 during the synthesis was therefore investigated.

Though the reaction rate looks increase continually with the increase of P25 dosage, the further increase of the P25 percentage will make the free dispersion of P25 to the core surface difficult, likely due to the deficiency of the adhesive (i.e. fresh TiO_2) as discussed before. Alternatively, if the dosage of $TiCl_4$ and P25 were increased simultaneously and kept the dosage of $CoFe_2O_4$ unchanged, the resulted catalyst will no longer be magnetic. Therefore, the catalyst used in the following study was synthesized with 2.1 g $CoFe_2O_4$, 0.5 mL TiO_2 and 4.0 g P25, at its optimal condition.

5.2.2 Effect of reaction parameters on the photodegradation process

5.2.2.1 Photodegradation under different UV wavelength

During photodegradation, direct-photolysis and photocatalysis may occur at the same time since both the parent compound SMX and the catalyst absorb light. To determine the role of the catalyst and the optimal light source, photolysis (i.e. without catalyst) and photocatalysis (i.e. with catalyst) of SMX under different light sources (UV wavelengths) were examined.

From Figure 5-2, the catalyst played a positive role at the wavelength of 350 nm. For the direct photolysis of SMX solution exposed to UV lamps at 350 nm, and about 20% SMX was removed with UV illumination in 50 mins. Previous studies reported that photolysis of SMX only occurred under UV in the wavelength below 310 nm (Abellán et al. 2007). The results suggested that photolysis of SMX at UV 350 nm observed in this study may be due to the insignificant but non-zero molar absorptivity of SMX at 350 nm and/or the board-band nature of UV 350 nm lamp, which have a small tailing reaching the wavelength around 310 nm.

At wavelength of 254 and 300 nm, however, the presence of catalyst slowed down the reaction compared to the process without the catalyst. The result is mainly attributed to the weaker excitation of the catalyst by UVC and UVB at 254 and 300 nm, respectively (see the DRS data in Chapter 4). The process performance is further deteriorated by the light shielding effect since the transmission of the solution dropped dramatically from 100% to about 80% after introducing the catalysts at dosage of 0.5 g/L.

Though photolysis of SMX is fast, unfortunately the mineralization of SMX (i.e. TOC elimination) by photolysis is inefficient comparing to that of photocatalysis. Therefore, the wavelength of 350 nm was selected exclusively as the light source for the remaining study.

5.2.2.2 Photodegradation with different SMX initial concentrations

The effect of initial concentrations of SMX ($[SMX]_0$) was examined in the photocatalytic process. It is indicated that lower initial concentration results in higher removal efficiency. The final removal efficiency at 100 min increased from 40% to 99% as the $[SMX]_0$ decreased from 200 to 5 μM (Figure 5-3 a). In this study, since the UV intensity is a constant, the increase of $[SMX]_0$ will make the solution property changed from optical dilute to optical dense. The deficiency of photons of the latter cases is the reason contributed to its lower degradation efficiency. A linear correlation between k and ln $[SMX]_0$ can be established as shown in Figure 5-3 (b).

5.2.2.3 SMX destruction with different catalyst dosages

In Figure 5-4, the SMX destruction performance was investigated as the catalyst dosage varying from 0 to 2.0 g/L. Only about 20% SMX was removed under the irradiation of UV without using the photocatalyst. After introducing the photocalyst the reaction rate enhanced significantly. The final removal increased from about 20% to 94% as the dosage of catalyst increased from 0 g/L to 0.5 g/L. After the optimal dosage at 0.5 g/L, the further increment of the dosage will retard the reaction. This is likely ascribed to the reduction in the light penetration resulting from the abundance of catalyst particles. This light attenuation effect was justified in Figure 5-4 (c), in which the transmission decreased significantly with the increase of the catalyst dosage. It is also interesting to note that in the dosage range of 0.5–2.0 g/L, two linear correlations between k and catalyst dosage, and transmission and catalyst dosage were identified. Therefore, a liner correlation between the k and transmission is established and well justifies the light attenuation assumption. The catalyst dosage at 0.5 g/L was determined as the optimum dosage for the catalyst in this process, in which SMX was completely degraded in 50 min.

According to the linear correlations of k and $[SMX]_0$ (Figure 5-3 b), as well as k and catalyst dosage (Figure 5-4 b in the range of 0.5-2.0 g/L), the pseudo first-order rate constant (k, min^{-1}) of SMX destruction becomes predictable in terms of $[SMX]_0$ and catalyst dosage. By using multi-regression technique, a prediction model is shown in the following equation which only works for the experimental systems used in this study.

$$k = 7.94\times10^{-2} - 1.39\times10^{-2}\,[\text{Catalyst}] - 1.14\times10^{-2}\,\ln[\text{SMX}]_0 \quad (R^2=0.9979) \qquad \text{(Equation 5-3)}$$

5.2.2.4 Photodegradation under different levels of pH

Since the pH level plays an important role in the degradation process, six pH levels ranging from 2.2 to 10.8 were investigated in this study. As the pK_{a1} and pK_{a2} is 1.85 ± 0.30 and

5.60 ± 0.04, respectively (Babić et al. 2007), the test was conducted in

1) pH 2.2, a point in which pH ≈ pK_{a1};

2) pH 3.6 and 5.2, two points between pK_{a1} and pK_{a2};

3) pH 6.8, 8.8, and 10.8, three points above pK_{a2}.

The results are shown in Figure 5-5, in which the fastest reaction occurred at pH 2.2, 96% of SMX was removed in 5 minutes, and followed by pH 3.6, and pH 10.8. However, it was observed that the catalyst became unstable at these extreme pH levels. That is, at the pH levels of 2.2, 3.6 and 10.8, some white/milky substance leached out to the solution. To understand the mechanism of the fast reactions at these extreme pH levels, a series of tests was conducted.

The possible adsorption and hydrolysis contributed to the degradation of SMX at extreme pH levels were examined first. The results were shown in Figure 5-6 (a), where the "-30 to 0 minutes" is the pre-adsorption for equilibrium as mentioned in the methodology. It was found that the process of adsorption and hydrolysis are insignificant. The result of insignificant hydrolysis agrees with the results from a previous study (Trovo et al. 2009a). Therefore, the fast reaction at pH levels 2.2, 3.6 and 10.8 was not due to the additional adsorption nor hydrolysis.

The white substance that leached out to the solution was examined next. After the adsorption reached the equilibrium, the catalyst was removed by a magnet, and the milky solution was used to react with the SMX under the UV. The result shown in Figure 5-6 (b) indicated that the degradation curve was similar to that shown in Figure 5-5 (a). This suggests that the fast reaction at extreme pH levels was mainly due to the leaching of TiO_2/P25 from the catalyst surface.

The mass of leached TiO_2 was determined by paper filtration, after drying, the percentage of leached TiO_2 was shown in Figure 5-6 (c). It was found that, about 35% and 20% of TiO_2 leached from the catalyst at pH 2.2 and 10.8, respectively. Higher the leaching of TiO_2, higher the removal efficiency, this leaching pattern (Figure 5-6 c) is even similar to that of the reaction rate (Figure 5-5 b), thus this similarity of pattern reconfirms the contribution of leached TiO_2 to the enhanced reaction rate at extreme pH levels. However, it should be noted that very low (2%-3%) or no TiO_2 leached was observed at pH levels ranged from 5.2 to 8.8. In fact, the observed low level mass loss in Figure 5-6 (a) may be due to the imperfect filtration and drying process. Therefore, the synthesized catalyst is considered to be very stable at neutral pH range for real application.

Within the pH range of 5.2 and 8.8, the best pH for the process is at pH 5.2. Increase of pH from 5.2 to 8.8 causes a small drop in removal efficiency. At pH 5.2, most of the SMX exists in the neutral state (Radke et al. 2009, Trovo et al. 2009b) and has stronger light absorption (Niu et al. 2013), resulting in a higher degradation efficiency. When the pH level is higher than pK_{a2} (5.6), most of the SMX becomes negatively charged conjugate base, and strong oxidants like hydroxyl radical generally has lower affinity to react with the negatively charged compound (Boreen et al. 2004, Radke et al. 2009, Trovo et al. 2009b), leading to a lower degradation efficiency.

The pH change during the process of adsorption (time before 0) and photocatalytic reaction (time after 0) is shown in Figure 5-7. In the process of adsorption, pH dropped when the initial pH level is 8.8 and above, while the pH increased slightly and had no significant change at neutral (6.8-5.2) and acidic (3.6-2.2) conditions, respectively. It suggests that the surface of $CoFe_2O_4/TiO_2$ is close to neutral. During the photocatalytic reaction, a significant pH drop occurred when the initial pH level is high. The pH drop is likely due to the formation of CO_2 and low molecular organic acids from the destruction of SMX. Given to the fact that H_2CO_3 is a weak acid, with the value of pK_a at 6.3 and 10.3, the H^+ released to the solution was not sufficient to change the solution pH when the initial pH level was in the neutral to acidic range, therefore, a relatively stable pH was observed.

In practice, the removal of SMX at extremely low or high pH is not recommended. Therefore, pH of 5.2 was selected for further study, and no pH adjustment is required in SMX removal.

5.2.3 Effect of ferrate on the reaction

Ferrate has a strong oxidation capacity, however, the SMX destruction occurred only at the initial period time of the introduction (Figure 5-8 a). About 65% of SMX was removed within five minutes with sole 100 μM ferrate. The destruction curve leveled off in the next twenty minutes, indicating no SMX decomposition occurred any more. The removal efficiency was enhanced to about 75% with further introduction of UV (i.e., UV/100 μM ferrate). It should be noticed that the enhancement is much higher than that of SMX photolysis within twenty minutes. The reason for the increased SMX removal efficiency also includes the generation of $OH^{\bullet}$ originated from the ferrate indirectly. The Fe^{3+} generated from hydroxylation of ferrate (Equation 5-4) can further result in $[Fe(OH)]^{2+}$ (Equation 2-20), which can lead to the formation of Fe^{3+} and $OH^{\bullet}$ (Equation 2-21). About 80% SMX was removed under the treatment process UV/Catalyst/100 μM ferrate in twenty-five minutes, indicating only 5% SMX destruction was attributed to the catalyst.

$$FeO_4^{2-} + 5\,H_2O \rightarrow Fe^{3+} + 3/2\,O_2 + 10\,OH^- \qquad \text{(Equation 5-4)}$$

Figure 5-8 (b) shows the SMX degradation under UV/Catalyst reaction system with different concentrations of ferrate. The reaction was significantly accelerated due to the introduction of ferrate. Complete removal of SMX under UV/Catalyst/250 μM ferrate can be shortened to 120 minutes, and the time was a half if the concentration of ferrate doubled (UV/Catalyst/500 μM ferrate). In the reaction system UV/Catalyst/Ferrate, the SMX removal was mainly due to the oxidation of ferrate. And the oxidation of ferrate occurred at the moment that ferrate was introduced, then the reaction slowed down. The reaction was more efficient by the stepwise addition of ferrate, where 50 μM ferrate was introduced every time and it takes sixty minutes to remove SMX completely with total 250 μM ferrate. With low concentration of ferrate (50 or 125 μM), the reaction was faster than that without ferrate before 60 or 70 minutes, while the removal efficiency was actually lower than that under the reaction system without ferrate at the end of the reaction (i.e., 120 mins). During the reaction, some brick red deposits were formed and may blocked the photon path. Therefore, to play a positive role, the concentration of the ferrate should be high enough and the stepwise addition was suggested.

5.2.4 Photocatalytic activity of recycled catalyst

Since the advantage by using the composite photocatalyst is the association of magnetic and photocatalytic properties, it is necessary to evaluate the recycling efficiency of the catalyst, including the mass loss during the separation or collection and whether the recycled catalyst can maintain its performance in reaction after several runs of usage.

After each photocatalytic reaction, the catalyst was separated, collected and washed with ultrapure water, then dried at 80 ºC. The weight loss during the tests was determined to be less than 5%. It should be noted that the washing and drying of spent catalyst are not necessary in real applications, so that the mass loss in practice should be much lower than 5%. After five times of recycling, the performance of the reused catalyst in degrading SMX was shown in Figure 5-9, in which the photocatalytic activity of the recycled catalyst is similar to the fresh catalyst without noticeable degradation. This demonstrates that the photocatalytic activity of synthesized $CoFe_2O_4/TiO_2$ is very stable. Given the magnetic and stable photocatalytic properties, the $CoFe_2O_4/TiO_2$ catalyst should have good application prospects in water/wastewater treatment.

5.2.5 Mineralization and destruction mechanism of SMX

5.2.5.1 TOC reduction

The ability of the photocatalyst in the SMX mineralization was also tested by measuring the TOC variation during the degradation process. The initial SMX concentration was adjusted to 100 μM to increase the accuracy of TOC analysis. In the proposed process, the involvement of UV direct photolysis and the photocatalysis was well taken into account. Figure 5-10 shows the separate contribution of UV direct photolysis and the photocatalysis for the overall SMX decomposition and TOC removal.

In spite of the obvious destruction of SMX by photolysis (about 50% removal efficiency), its corresponding TOC destruction is low (about 5% removal efficiency) during the reaction. The reaction was accelerated when the catalyst was introduced. The reaction rate constant of using UV/$CoFe_2O_4/TiO_2$ (0.88 h^{-1}) was five times of that using sole UV (0.16 h^{-1}). The considerable enhancement by the combined use of the UV radiation with the catalyst (i.e. UV/$CoFe_2O_4/TiO_2$) was observed at 100% and 50% removal of SMX and TOC, respectively, in 5 hours.

It is interesting to note that there is no lag phase of TOC destruction at the early stage of the process. This suggests the intermediates generated in the process can easily be decomposed by the direct photolysis and/or photocatalysis in the UV/$CoFe_2O_4/TiO_2$ process. Judging from the TOC destruction curves at Figure 5-10, the fraction of TOC/SMX removal (i.e. TOC removal per unit of SMX destruction) at 5 hour of the direct photolysis and photocatalysis was 0.07 and 0.59, respectively, indicating that photocatalysis plays a much more important role in the removal of TOC than that of direct photolysis.

5.2.5.2 Proposed pathways of SMX degradation

The corresponding chemical structures of the degradation intermediates and pathways in UV/$CoFe_2O_4$/TiO_2 are proposed. A total of sixteen intermediates were identified in the LC-ESI-MS chromatogram. Four of them (C1, C2, C4 and C14), asterisked in Figure 5-11, were newly reported in the study of SMX product determination. The proposed degradation pathway and the information of the detected intermediates (formula and experimental mass) are shown in Figure 5-11. There are mainly four possible destruction pathways, i.e. hydroxylation, cleavage of S-N bond, nitration of amino group, and isomerization.

The hydroxylation may occur by hydroxyl radical ($OH^•$) attack to the benzene ring, the isoxazole ring, and the amino group on the benzene ring. Three mono-hydroxylation (C11, C13, C14) and two di-hydroxylation products (C8, C12) were detected. Further oxidation of the isoxazole ring in C11 resulted in ring opening and the formation of C3 and C16. The intermediate C9 was generated by the oxidation process after the opening of the isoxazole ring in C13, and C8. The cleavage of the bond between isoxazole ring and the amine group of SMX, C13, C8 and C9 led to the formation of C5. The cleavage of the bond between isoxazole ring and the amine group of C12 and C14 led to the formation of C4. The C4 can also be generated by the hydroxylation process with hydroxyl radical attacking to the amino group on the benzene ring of C5. The loss of amino group or hydroxyl group led to the formation of C2. Hydroxylation was also reported in other studies (Abellán et al. 2007, Abellan et al. 2008, Trovo et al. 2009a, Trovo et al. 2009b, Niu et al. 2013) and is possibly the dominant destruction pathway due to the largest peak areas of the intermediates.

The C1 and C7 were resulted from the cleavage of S-N bond between sulfonyl group and the amine group in the sulfonamide group, the C7 was also reported in the photo-Fenton and photolysis process (Trovo et al. 2009a, Niu et al. 2013). Simultaneously, the C1 was formed by a carboxyl bonding (sourced from a formic acid in the solution) to the amine group.

Another possible pathway took place by the electrophilic attack at the amino group in the benzene ring. The amino group was oxidized to nitro group; hence nitro-sulfamethoxazole i.e. C15 was formed. The conversion of C15 to C6 was the result of addition of the OH-group to the benzene ring. This pathway was also observed in SMX degradation by the ozonation (Abellan et al. 2008).

The conversion of SMX to C10 was possible via the isomerization of O-N bond at the isoxazole ring, similar observation was also reported in the photo-Fenton process (Trovo et al. 2009a). C10 was also the only intermediate detected in the photolysis process, indicating that photocatalysis was conducive to the bond cleavage of the parent compound. This result also explains the low TOC removal efficiency in photolysis process.

5.2.5.3 Transformation of sulfur and nitrogen

To better understand further the degradation pathway of SMX and formation of inorganic intermediates, the concentrations of sulfate (SO_4^{2-}), ammonium (NH_4^+), nitrate (NO_3^-) and nitrite (NO_2^-) were determined, as shown in Figure 5-12.

Gradual increase of SO_4^{2-} was observed in the reaction. About 20 μM SO_4^{2-} was released during the degradation of the first hour, accounting for about 20% of the total mass of sulfate. At the end of the reaction (i.e. 5 hours), about 45% of the total sulfur was released, when 100% of SMX and 50% of TOC was removed. This result is superior than the observation form Abellán et al. (Abellán et al. 2007), where only 40%, 80%, and 17% of SO_4^{2-}, SMX and TOC generation/destruction were observed, respectively, in a UV/TiO_2 process after 6 hours.

In the UV/$CoFe_2O_4$/TiO_2 process, a large amount of ammonium (100 μM or about 33% of total nitrogen mass) was generated, while only trace levels of [NO_3^-] and [NO_2^-] at 2.7 μM (or 1% mass), and 0.7 μM (or 0.25% mass), respectively, were detected. There are three nitrogen moieties in SMX; two exist in amine groups, and the other one is at the 2-position in the isoxazole ring. Nitrogen in amine groups is susceptible to originate NH_4^+, and nitrogen in the isoxazole ring might be converted to NH_4^+, NO_2^-, and NO_3^- (Nohara et al. 1996). NH_4^+ comes principally from the amino group, and also may come from the nitrogen in the isoxazole ring. Once the NH_4^+ is formed in the solution, it generally has lower priority to be oxidized (into NO_2^-, and then NO_3^-) comparing to that of the organics. A good example is that the NH_4^+ is the end product of COD test by using dichromate, rather than NO_2^-, nor NO_3^-. This is the reason of high [NH_4^+] acclamation, and low [NO_3^-] and [NO_2^-] levels in the solution.

In addition, it is interesting to note (from Figure 5-12) that the generation curves of [SO_4^{2-}], [NH_4^+], and [NO_3^-] are all linear and increase with time (after 1 hour), while the [NO_2^-] maintains at a constant. This is a good evidence to show that the TOC destruction is still in progress and the formation/destruction of [NO_2^-] has reached a steady state (between NH_4^+ and NO_3^-) in the studied period.

5.2.6 Toxicity evolution during SMX degradation

5.2.6.1 Effect of SMX and the degradation products on C. vulgaris

The effect of the SMX solutions before and after the photocatalytic treatment on the growth of *C. vulgaris* is presented in Figure 5-13. The growth curves of the algae exposed to samples collected at different degradation time are displayed in Figure 5-13 (a). All the algae growth curves conformed to the typical S-curve. The calculated values of K and r based on the logistic growth model are shown in Figure 5-13 (b).

It was found that the toxicity of the solution to *C. vulgaris* was significantly reduced during the degradation of SMX. Before the treatment, the growth of the algae was significantly inhibited by SMX with the lowest K (9.26×10^6 cells/mL) and r (0.31 d^{-1}). During the first two-hour of treatment, SMX quickly transformed into intermediates and the toxicity of the solution significantly reduced (with higher values of K and r, $p < 0.05$).

At the later stage of the treatment, the K and r values were even higher than those of pure water ($K = 2.33\times10^{7}$ cells/mL and $r = 0.42\ d^{-1}$), suggesting the SMX has been transformed from a toxicant into nutrients. This may be attributed to the increased concentration of inorganic salts released from the SMX decomposition (including NH_4^+, NO_3^-, NO_2^- and SO_4^{2-}) which can serve as nutrients for the growth of the algae. The destructed organics after losing their toxicity may become an extra carbon source for promoting the growth of algae. It was reported that low molecular organic acid (i.e. the end products of this process) can also be used as the carbon source for the algae (Liu et al. 2013a) other than CO_2. In addition, ferrous ion (Fe^{2+}) released from the catalyst during the reaction can also provide as promotion factor for the algae growth owing to the weak acid environment. The detected concentration of Fe^{2+} is shown in Figure 5-13 (c).

However, at the later stage of the reaction, the increment of K and r values gradually leveled off (but still higher than water). This is possibly because the accumulation of inorganic salts has reached their plateaus (Figure 5-12) in the solution, which became the limiting factor for the further growth of algae; during which, the CO_2 is abundant in the solution (Figure 5-13 c) and cannot be the limiting factor.

By taking a closer look at the Figure 5-13 (b), it was found that the growth of the algae apparently had a drop at 4 h. One possibility is that some toxic intermediates may be generated at that time. After cross-checking the intermediate data from the reaction mechanism, the inhibited growth may be attributed to the accumulation of C5, i.e. sulfanilamide (SFL), which could be an effective sulfonamide antibacterial.

To verify this, the effect of SFL (at a similar initial level of SMX) on the growth of the algae was studied. As is shown in Figure 5-14, the growth of the algae exposed to SFL (with K value of 1.20×10^7 cells/mL and r value of 0.24 d^{-1}) was significantly lower than that of water (with K value of 2.87×10^7 cells/mL and r value of 0.34 d^{-1}), indicating that the SFL has a similar adverse effect on the algae growth as SMX. In addition, the introduction of SFL to SMX-3 h led to reduction of the algae growth, with K value falling from 3.53×10^7 cells/mL to 2.82×10^7 cells/mL and r value from 0.72 d^{-1} to 0.33 d^{-1}, respectively.

Since the SFL can be further degraded in the process, the sink of K and r only last for a short period, then they resume the up-rising pattern again as shown in Figure 5-13 (b). The result also elucidates that the degradation of SMX by UV/$CoFe_2O_4$/TiO_2 is efficient in the reduction of toxicity to the algae.

5.2.6.2 Effect of SMX and the degradation products on A. salina

Contaminants in the water environment may also induce the adverse effects on the activities of zooplanktons such as survival, feeding, and growth. The effect of SMX degradation products on the survival of *A. salina* was studied, and it was found that no mortality was observed when exposing *A. salina* to the untreated and treated solutions for

24 h (data not shown). Therefore, the effect of SMX degradation products on the feeding of *A. salina* was further studied.

The result shows that the feeding of *A. salina* was significantly inhibited upon exposed to untreated SMX, where the clearance rate (CR) was about 2.3 $\mu L \cdot ind^{-1} \cdot min^{-1}$, i.e. about 18% of the control group (Figure 5-15). During the UV/$CoFe_2O_4$/TiO_2 process, the CR gradually increased, and the CR of *A. salina* went up to 6.1 $\mu L \cdot ind^{-1} \cdot min^{-1}$, i.e. about half of the control group after 5 hour of treatment. The inhibition was apparently reduced but not eliminated likely due to the existence of organic intermediates. It was expected that the toxicity of SMX solution would be totally eliminated when all the intermediates were mineralized to inorganic substances at an extended reaction time. The adverse effect of SMX and its degradation products on the feeding of the brine shrimp may lead to the growth inhibition of aquatic organisms at higher tropic level, and then the whole ecosystem through the food chain or food web. The result suggests that low level pollutants that escaped from the wastewater treatment are capable of affecting the balance of ecosystem. Therefore, comprehensive toxicity assessments of those contaminants are necessary to ensure an acceptable toxicity of the chemical residues in the effluent.

5.3 Summary

In this chapter, the photocatalytic activity of the obtained catalyst was evaluated by the degradation of SMX. The optimal conditions during the catalyst synthesis and SMX degradation were explored.

The SMX degradation was found to be a pseudo first-order kinetics. The optimal formula for the catalyst synthesis 2.1 g $CoFe_2O_4$, 0.5 mL TiO_2 and 4.0 g P25. The catalyst was determined to play a positive role in 350 nm while a negative role in 300 and 254 nm, so UV wavelength 350 nm was recommended for the reaction system. The observed rate constant (k, min^{-1}) is predictable by a proposed model in terms of the [$CoFe_2O_4/TiO_2$] and $[SMX]_0$, where the working catalyst dosage was 0.5-2.0 g/L, with the optimal pH at 5.2. The photocatalyst was found stable within the pH range of 5.2 and 8.8, while TiO_2 leaching would only occur at extreme acidic or alkali environment. SMX was almost completely removed in 50 minutes at 0.5 g/L $CoFe_2O_4/TiO_2$ at pH 5.2. The recycling tests proved that the photocatalytic activity of the recycled catalyst remains intact even after 5 times of reuse, suggesting the $CoFe_2O_4/TiO_2$ catalyst has good performance in real applications. The removal efficiency of SMX under the photocatalysis system was enhanced with high concentration of ferrate, while reduced in the presence of the low concentration of ferrate. And the stepwise addition of ferrate was suggested for higher reaction rate.

Photocatalysis plays a much more important role in the removal of TOC than that of direct photolysis, judging from the higher fraction of TOC/SMX removal by photocatalysis than that by the direct photolysis. Sixteen intermediates were detected, and four of them were newly reported in the degradation of SMX. There are four main pathways during the degradation, i.e. hydroxylation, cleavage of S-N bond, nitration of amino group, and isomerization. About 45% of the total sulfur was released as SO_4^{2-}, and 33%, 1% and 0.25% of the total nitro was released as NH_4^+, NO_3^- and NO_2^-, respectively.

The toxicity of the treated solution was significantly reduced compared to that of the parent compound SMX. For the effect of the treated solution on the algae growth, the K and r values of the algae growth curve increased after the treatment. At the later stage of treatment, the K an r values were even higher those of pure water, suggesting the SMX has been transformed from a toxicant into nutrients. The algae growth due to the release of inorganic substances and carbon source, serving as nutrients, was detected in the process. During which, a small offset to the growth was observed likely due to the generation of a toxic intermediate, sulfanilamide, which fortunately can be quickly destructed in the process. For the effect on the brine shrimp, no mortality was found, but the feeding of the brine shrimp was inhibited by the SMX and its intermediates. The clearance rate increased from 2.3 to 6.1 $\mu L \cdot ind^{-1} \cdot min^{-1}$ during the process but it's still lower than that of the control group. This suggests the adverse effect was gradually reduced but not eliminated. Therefore, longer degradation time may be needed for the total toxicity removal.

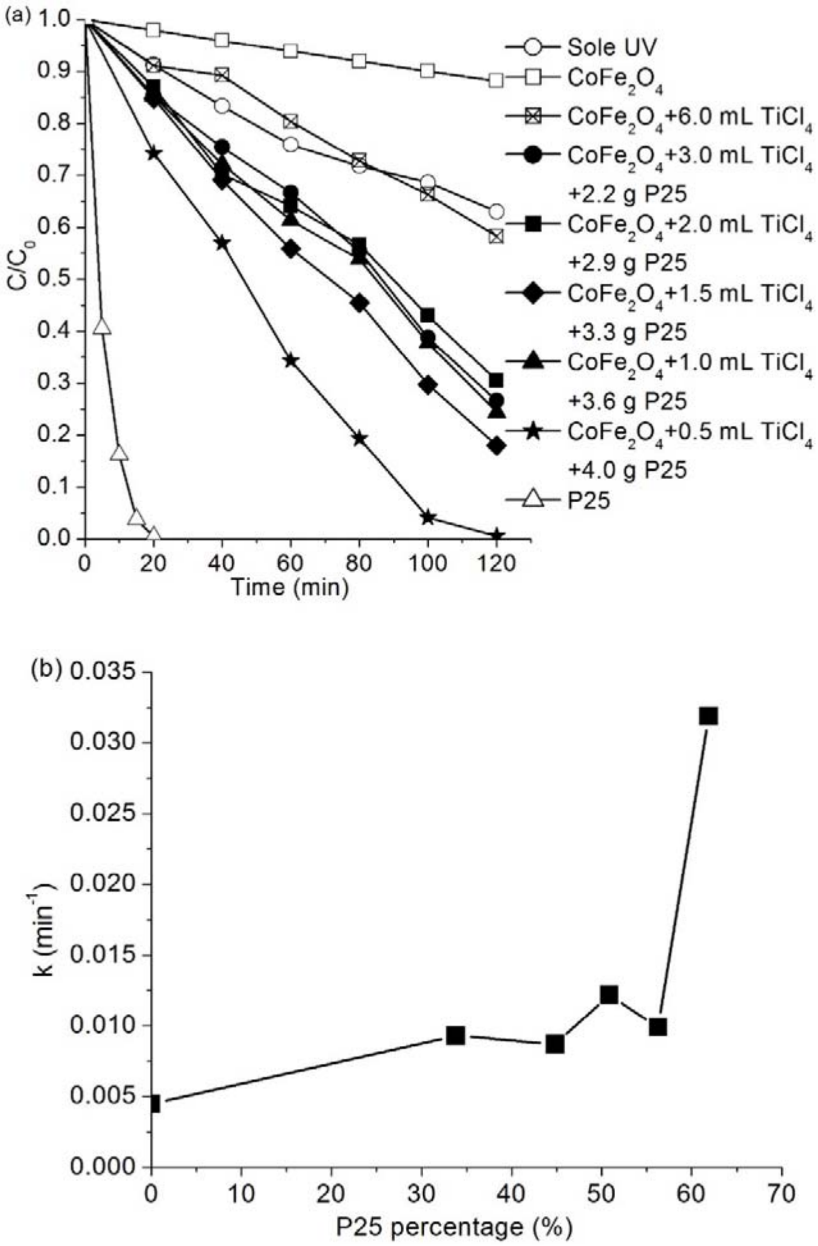

Figure 5-1 Photocatalytic activity of catalysts with different processes. (a) Sulfamethoxazole destruction curves with catalysts obtained from different processes. (b) Destruction rate constant as a function of P25 percentage. *Experimental condition:* $[\mathrm{SMX}]_0$ = 20 μM, catalyst dosage = 1.0 g/L, twelve 350 nm UV lamps were employed.

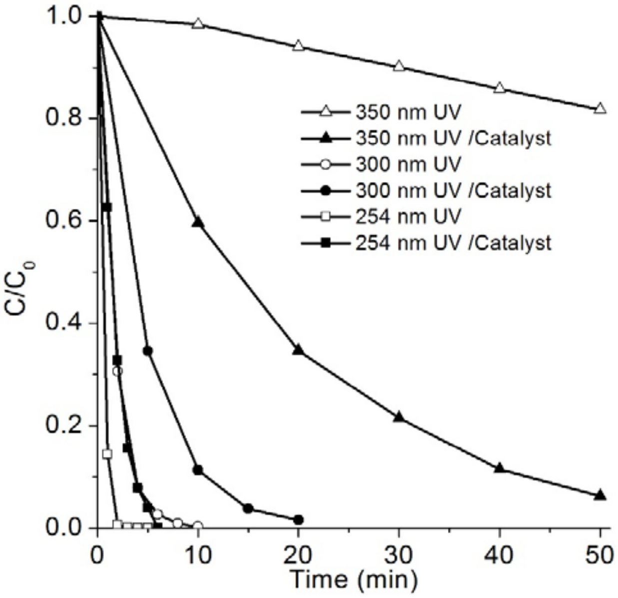

Figure 5-2 Effect of UV wavelength on sulfamethoxazole degradation. *Experimental condition:* [SMX]$_0$ = 5 μM, catalyst dosage = 0.5 g/L (if any), twelve UV lamps were employed.

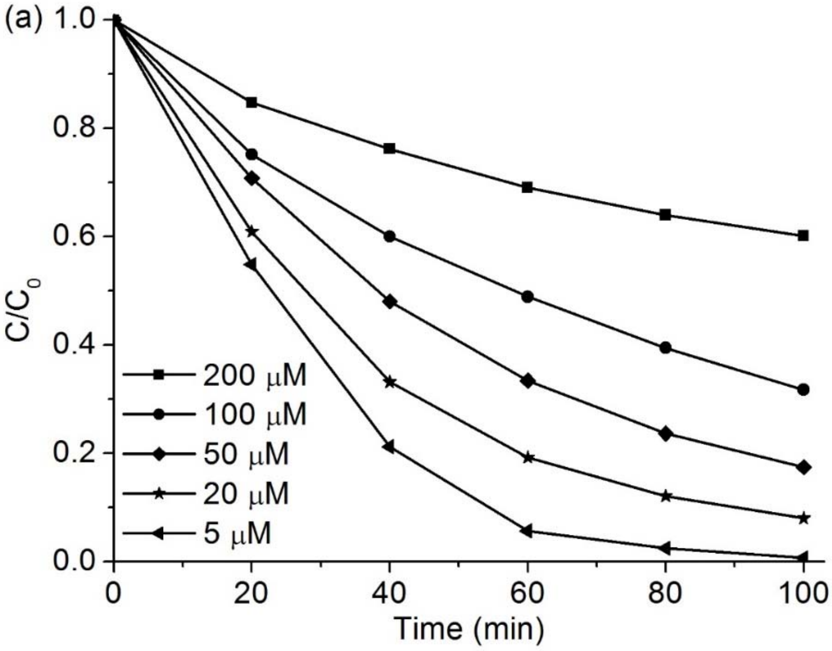

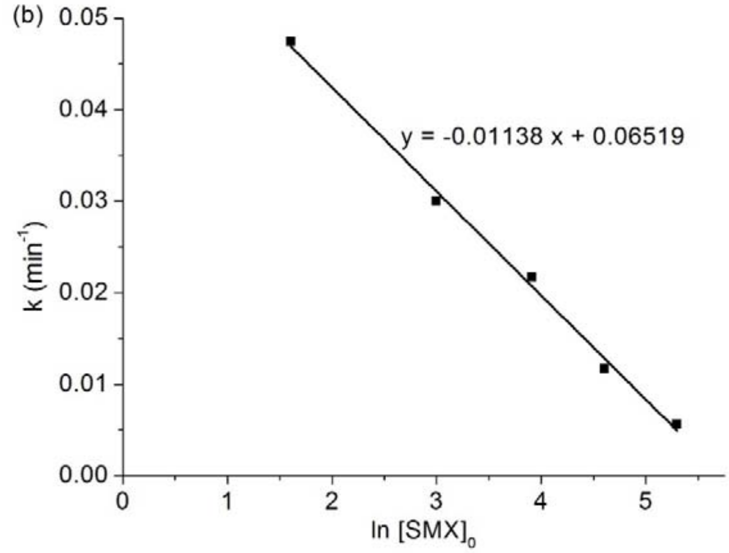

Figure 5-3 Effect of initial concentration of sulfamethoxazole on the photodegradation. (a) Sulfamethoxazole destruction curves with varied initial concentration. (b) Destruction rate constant as a function of initial concentration of sulfamethoxazole. *Experimental condition:* catalyst dosage = 1.0 g/L, twelve 350 nm UV lamps were employed.

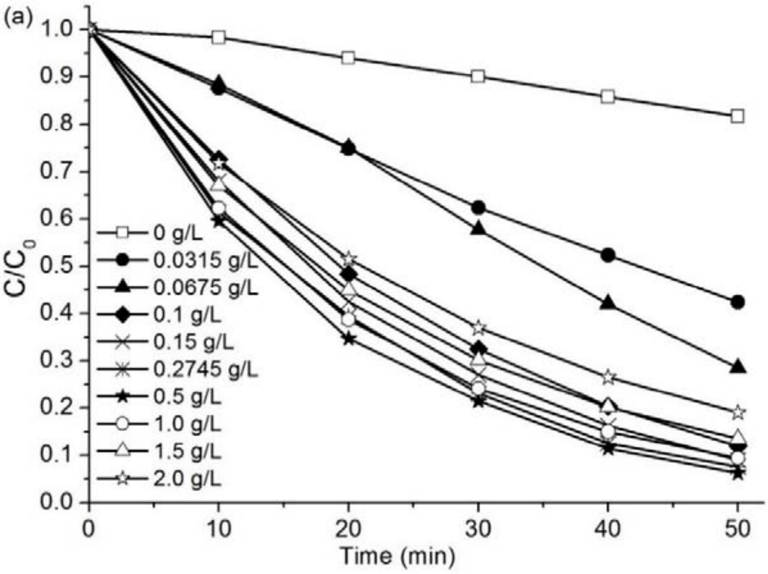

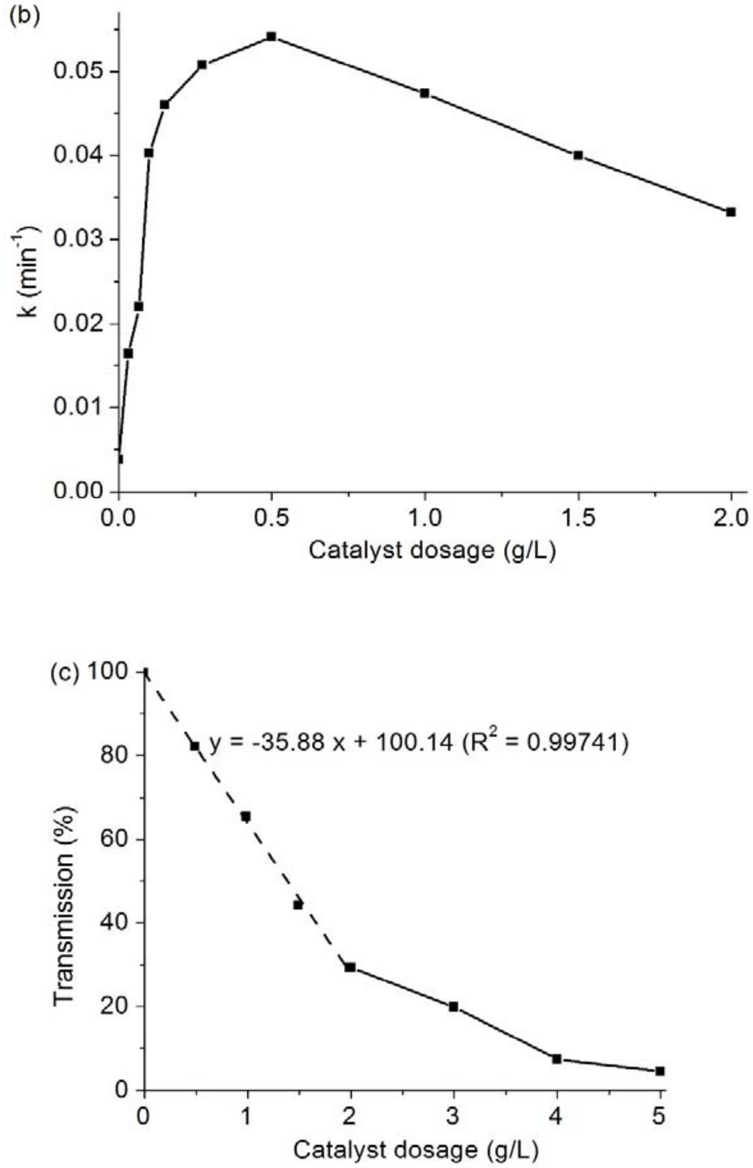

Figure 5-4 Effect of catalyst dosage on the photodegradation. (a) Sulfamethoxazole destruction curves with varied catalyst dosages. (b) Destruction rate constant as a function of catalyst dosage. (c) Transmission as a function of catalyst dosage. *Experimental condition:* $[SMX]_0$ = 5 µM, twelve 350 nm UV lamps were employed.

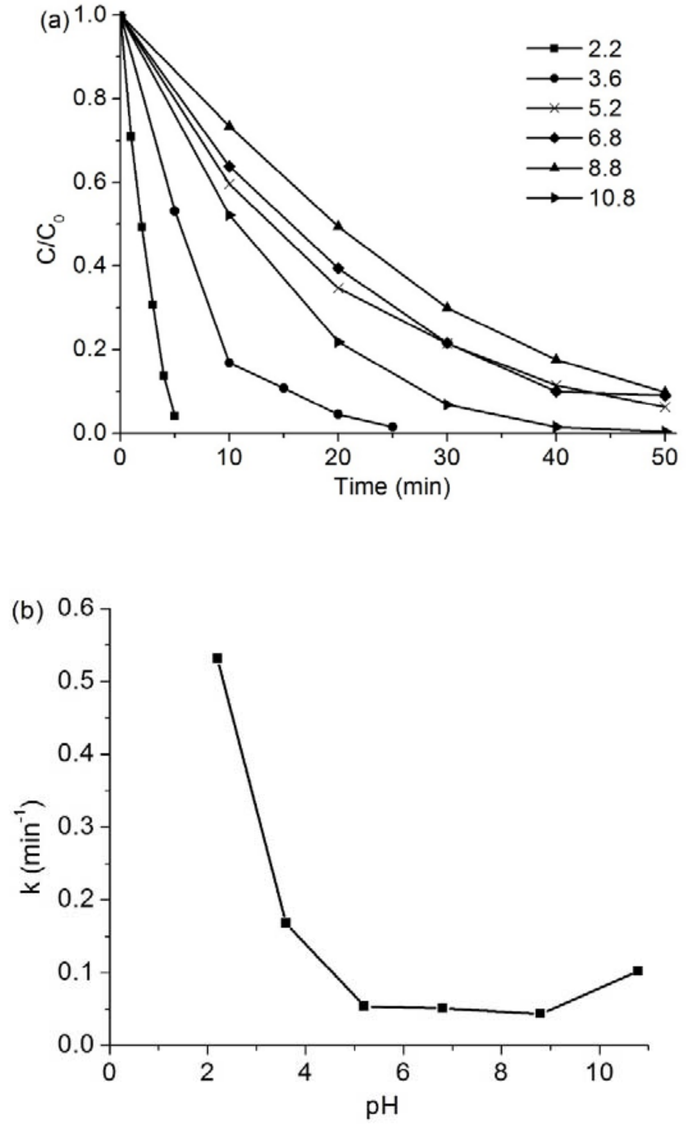

Figure 5-5 Effect of pH value on the photodegradation. (a) Sulfamethoxazole destruction curves with varied solution pH. (b) Destruction rate constant as a function of pH levels. *Experimental condition:* $[SMX]_0$ = 5 μM, catalyst dosage = 0.5 g/L, twelve 350 nm UV lamps were employed.

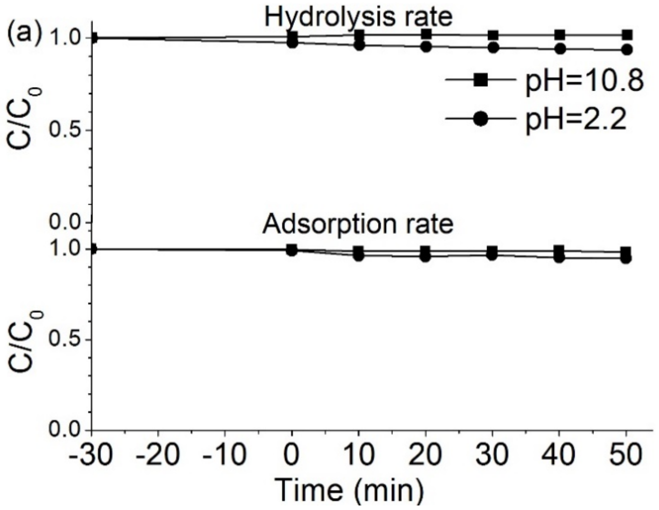
(a)
Hydrolysis rate
Adsorption rate
C/C$_0$
1.0
0.5
0.0
pH=10.8
pH=2.2
-30
-20
-10
0
10
20
30
40
50
Time (min)

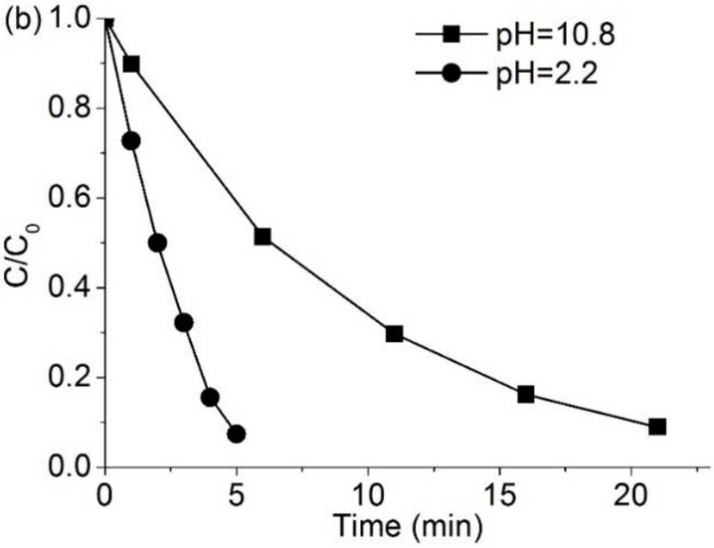
(b)
C/C$_0$
1.0
0.8
0.6
0.4
0.2
0.0
pH=10.8
pH=2.2
0
5
10
15
20
Time (min)

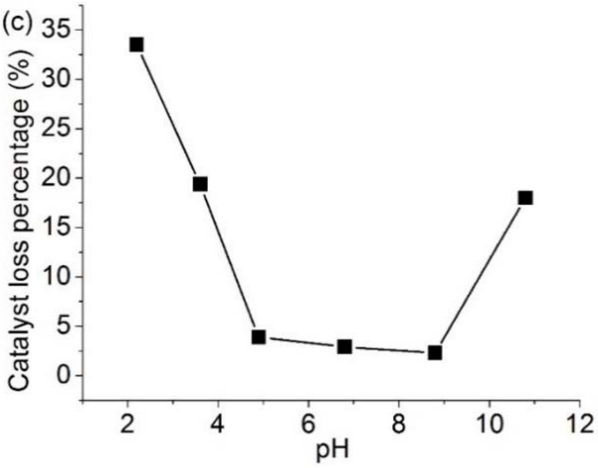

Figure 5-6 Tests on catalyst stability and leaching. (a) Hydrolysis rate and adsorption rate during the photodegradation. (b) Degradation of sulfamethoxazole under leaching TiO_2. (c) Catalyst leaching dosage. *Experimental condition:* $[SMX]_0$ = 5 μM, catalyst dosage = 0.5 g/L, twelve 350 nm UV lamps were employed.

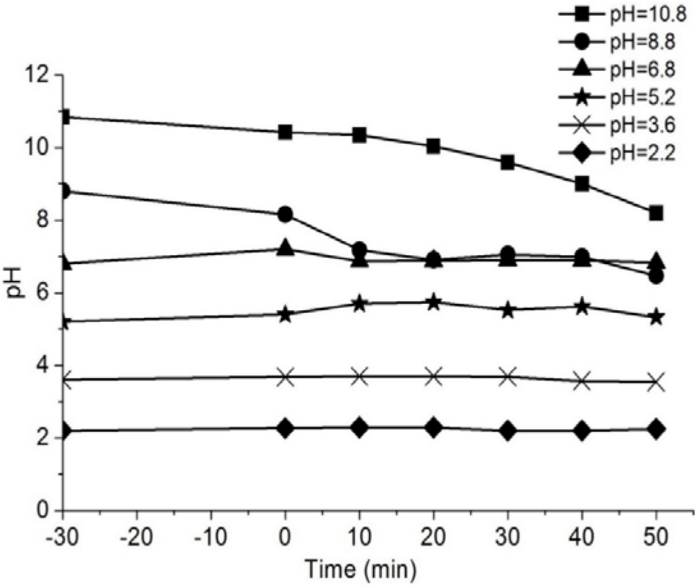

Figure 5-7 The change of pH values during the sulfamethoxazole photodegradation. *Experimental condition*: $[SMX]_0$ = 5 μM, catalyst dosage = 0.5 g/L, twelve 350 nm UV lamps were employed.

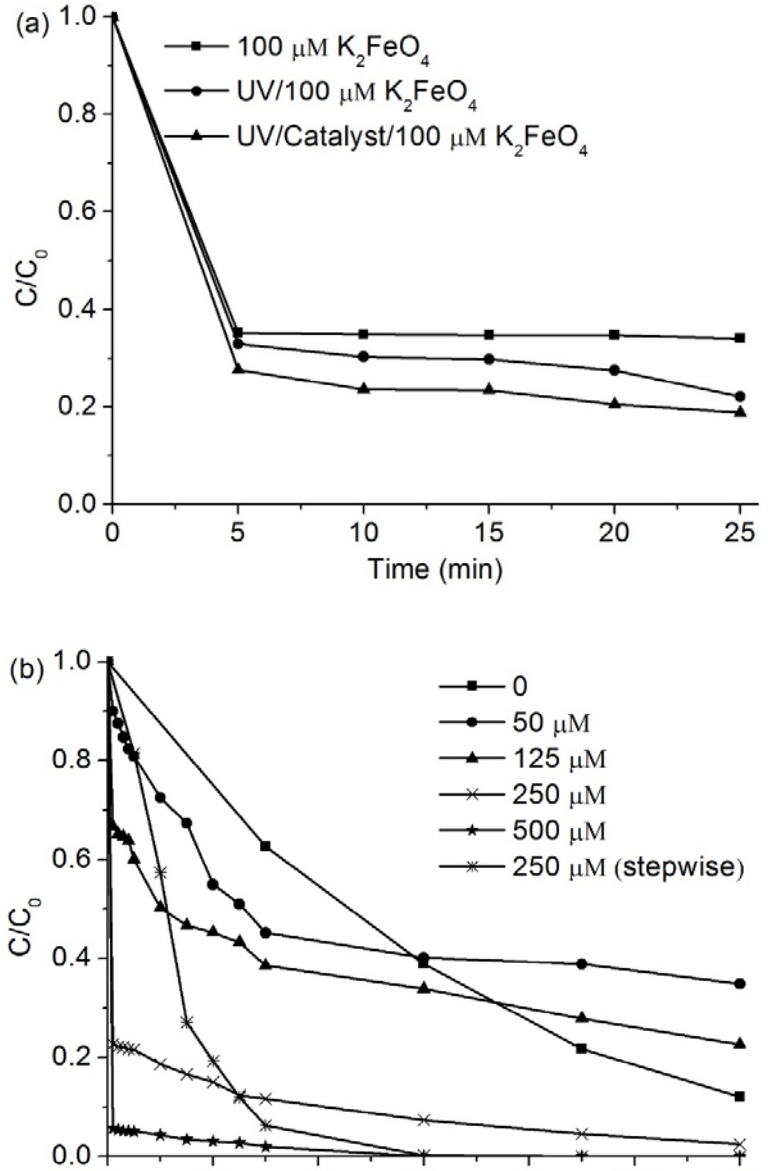

Figure 5-8 Sulfamethoxazole photodegradation with the introduction of K_2FeO_4. (a) Sulfamethoxazole destruction with different processes by ferrate. (b) Effect of ferrate at different concentrations on the photodegradation. *Experimental condition:* $[SMX]_0 = 5$ μM, catalyst dosage = 0.5 g/L, twelve 350 nm UV lamps were employed.

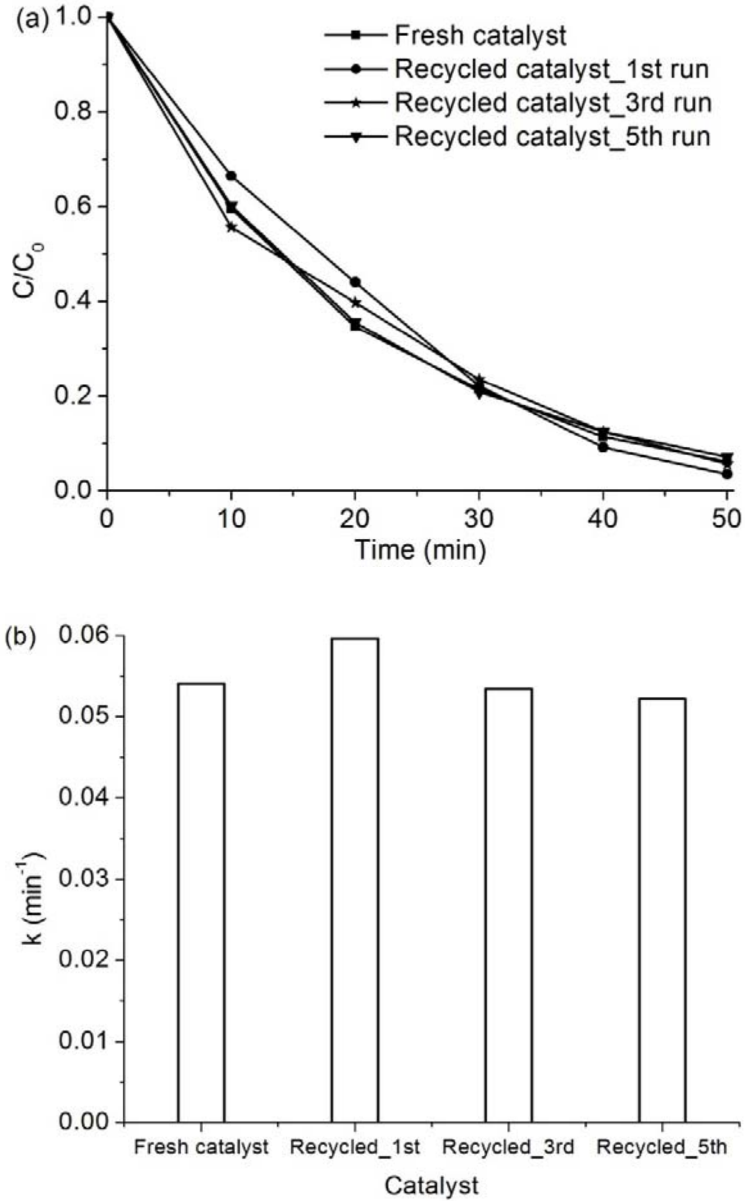

Figure 5-9 Recycle use of the catalyst. (a) Sulfamethoxazole destruction curves with recycled catalysts. (b) Destruction rate constant of photodegradation with recycled catalysts. *Experimental condition:* $[SMX]_0$ = 5 μM, catalyst dosage = 0.5 g/L, twelve 350 nm UV lamps were employed.

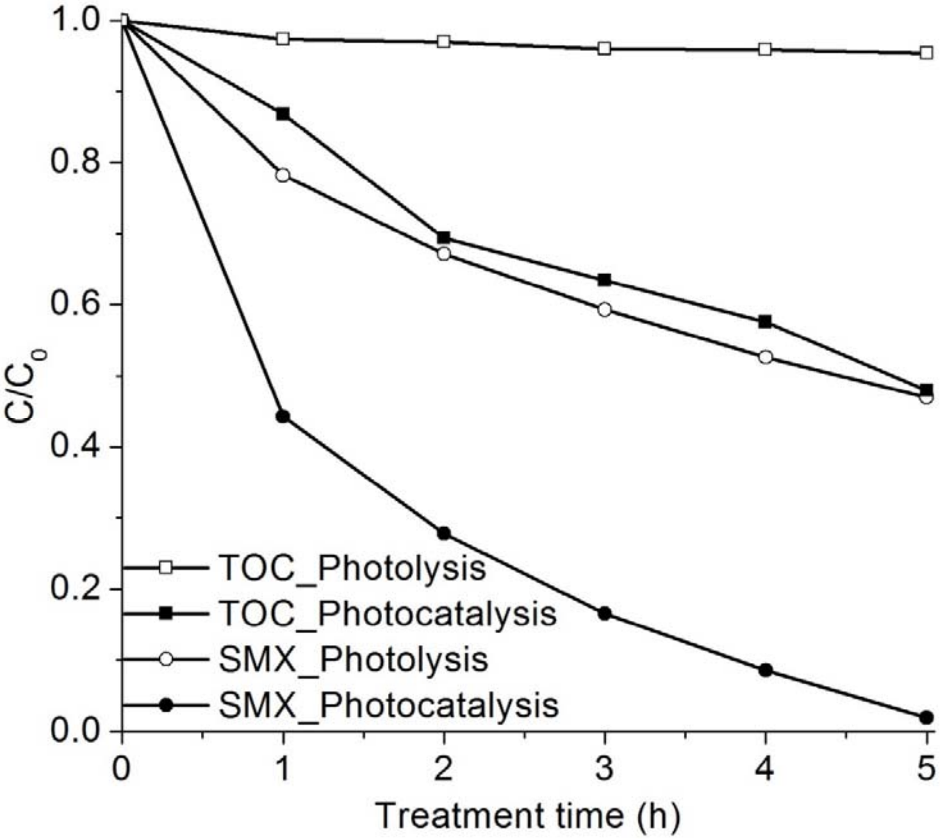

Figure 5-10 Sulfamethoxazole destruction and TOC reduction by photolysis and photocatalysis. *Experimental condition:* $[SMX]_0$ = 100 μM, catalyst dosage = 0.5 g/L, twelve 350 nm UV lamps were employed.

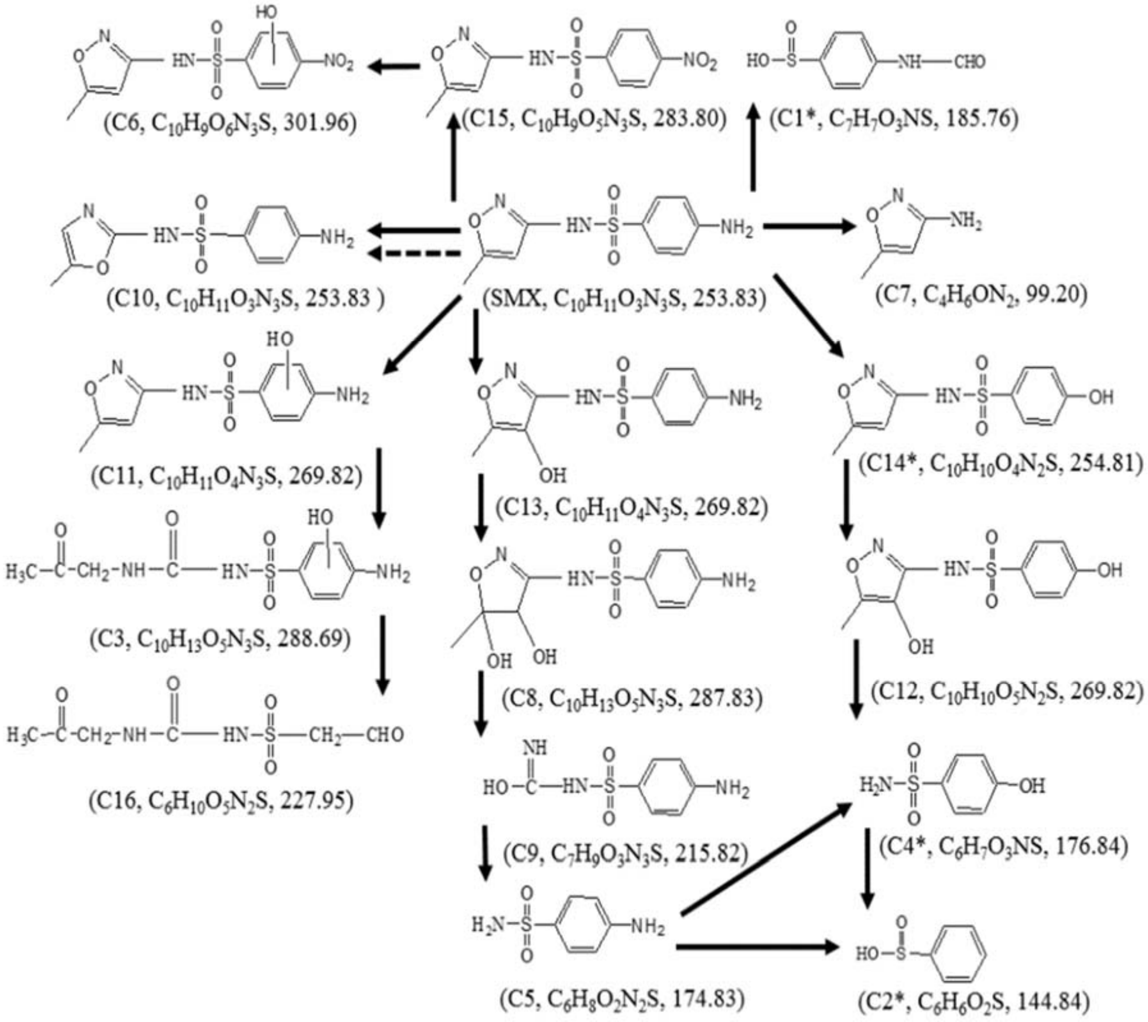

Figure 5-11 Proposed pathways of sulfamethoxazole degradation under UV/$CoFe_2O_4/TiO_2$. (The dash line indicates the pathway detected in the photolysis process, * indicates the newly reported intermediates).

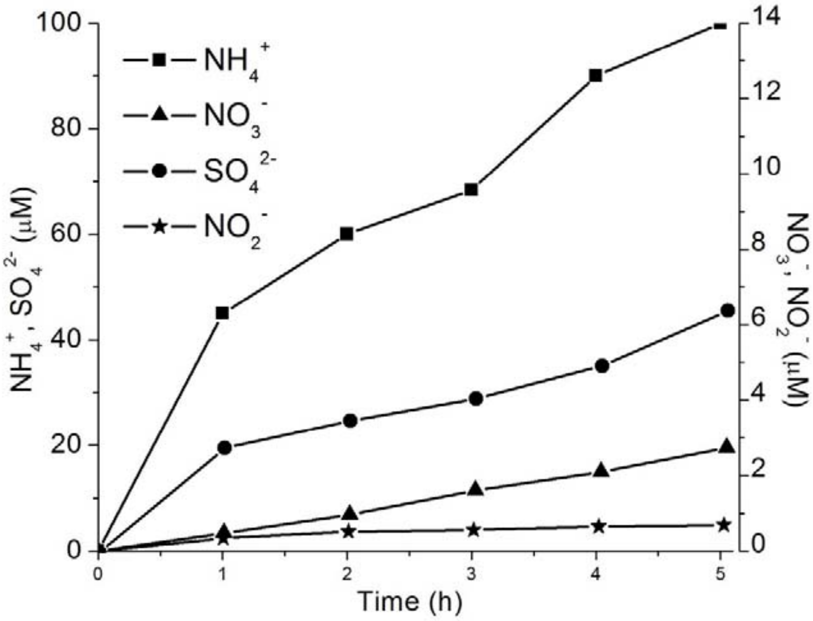

Figure 5-12 Formation of inorganic ions during UV/$CoFe_2O_4$/TiO_2 treatment.

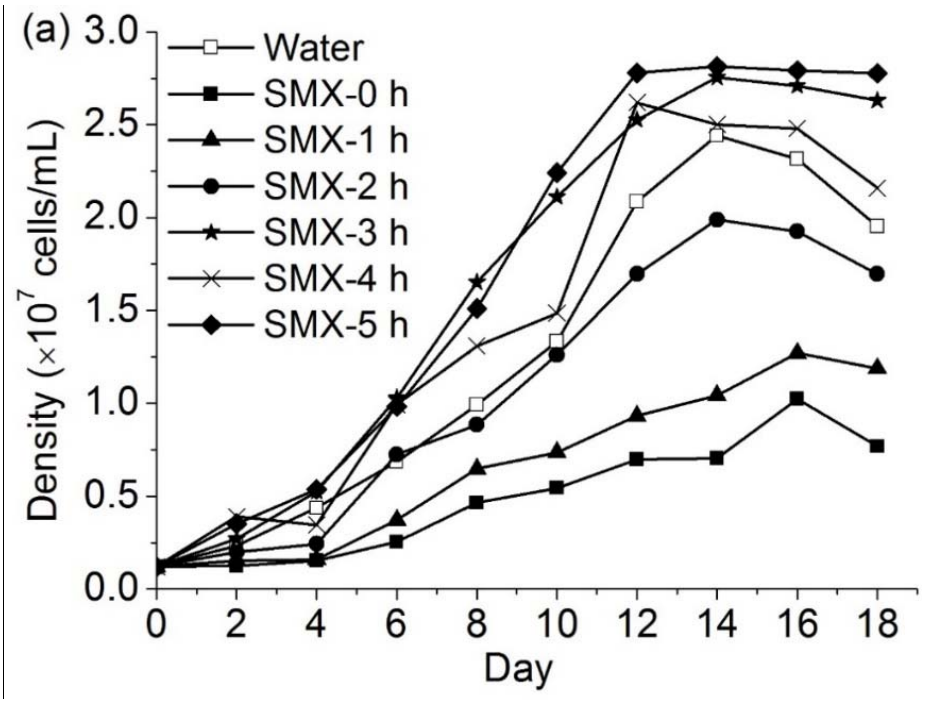

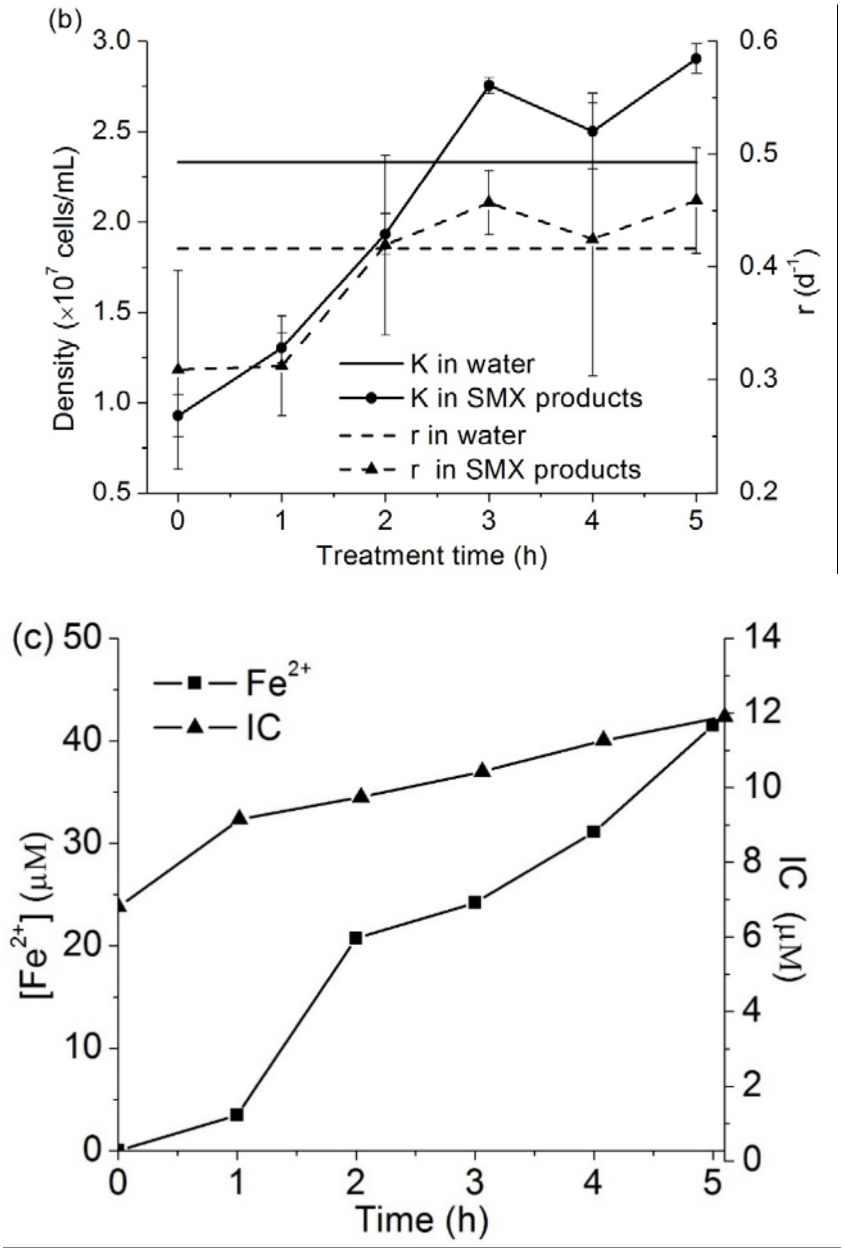

Figure 5-13 Effect of sulfamethoxazole and the degradation products on the growth of *Chlorella vulgaris*. (a) Growth curve of *C. vulgaris* in different culture media. (b) K and r of *C. vulgaris* population growth. (c) Change of inorganic carbon (IC) content and ferrous ion (Fe^{2+}) concentration of the reaction system during UV/$CoFe_2O_4$/TiO_2 treatment.

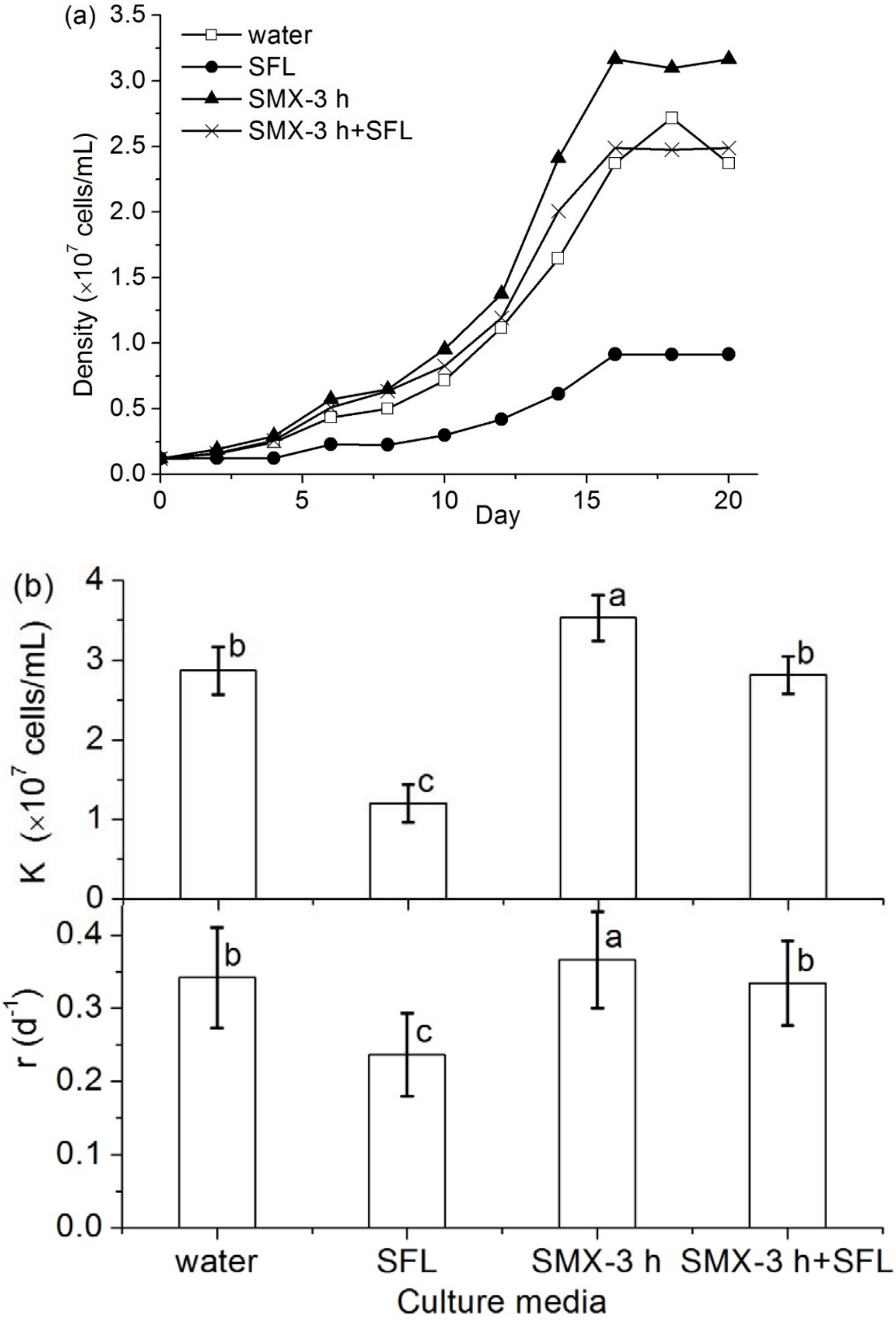

Figure 5-14 Effect of sulfanilamide on the growth of *Chlorella vulgaris*. (a) Growth curve of *C. vulgaris* in different culture media. (b) K and r of *C. vulgaris* population growth.

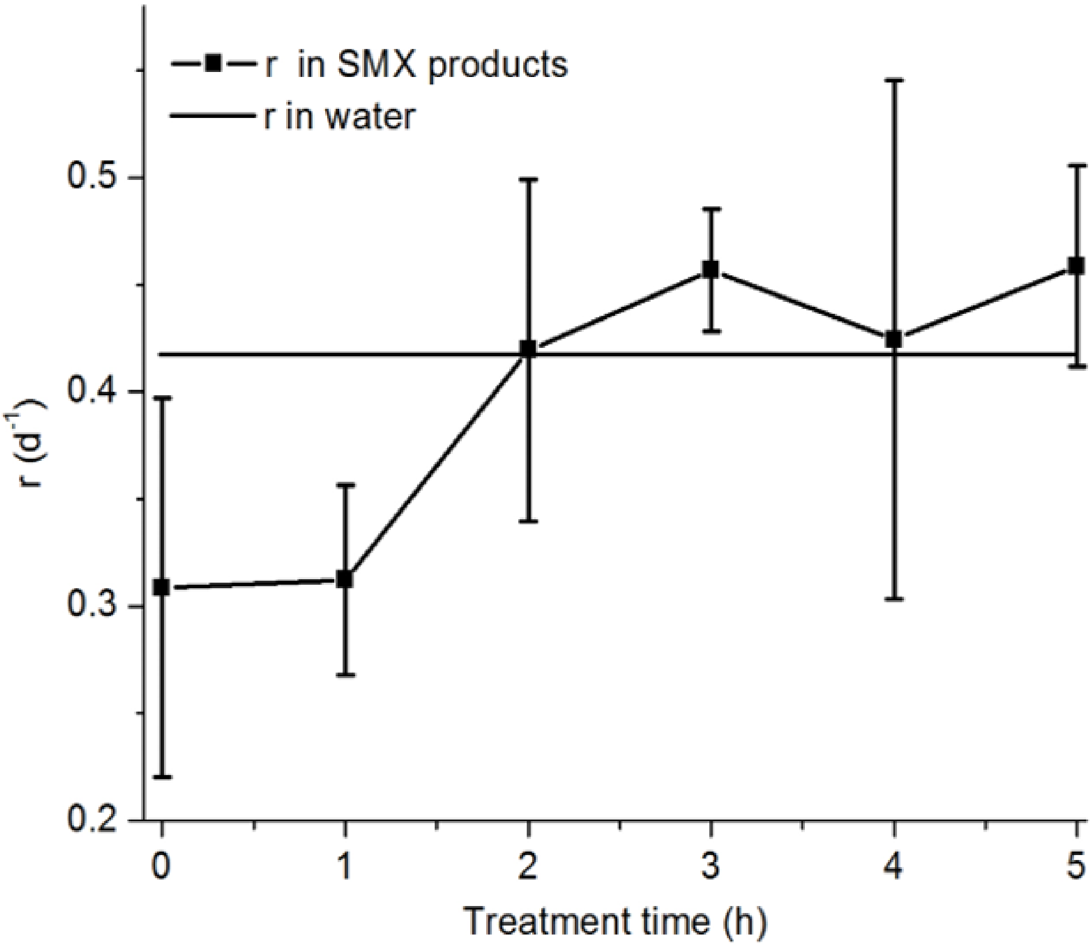

Figure 5-15 Effect of sulfamethoxazole and the degradation products on the feeding of *Artemia salina.*

6. Chapter six Photodegradation of antipyrine with the magnetic catalyst

6.1 Introduction

In Chapter five, the catalyst was proven to be efficient on degradation of antibiotic SMX, while whether it is widely applicable in degradation of other pharmaceutical molecule is unknown. In this chapter, the target compound AP from another pharmaceutical group was selected. The optimal reaction conditions, including the light source, catalyst dosage, initial concentration of parent compound, solution pH level were determined. The destruction mechanism, including organic intermediates, TOC reduction, inorganic ions release was investigated. The effects of AP on the growth of and the survival of were explored to fill up the knowledge gap on the scarce data in terms of the toxicity of AP to aquatic organisms. The toxicity evolution of the generated AP degradation products was explored to assess the safety of the treatment process.

6.2 Results and discussion

6.2.1 Effect of reaction conditions on the photocatalysis process

6.2.1.1 Wavelength of light source

Degradation of AP under different light sources (wavelengths) was examined to determine the optimal light source. In addition, the possible involvement of hydrolysis, adsorption and direct photolysis during the reaction was also evaluated. The hydrolysis and adsorption were found insignificant (data not shown), while the direct photolysis varied at different wavelengths from Figure 6-1. For direct-photolysis (i.e. no catalyst), the fastest AP destruction occurs at 254 nm, where AP was completely removed in 5 minutes. The removal efficiency reduces to about 40% (at 20 min) as UV wavelength increases to 300 nm, and no direct-photolysis was observed at 350 nm or 420 nm. The result is consistent with the AP's absorption spectrum, where no significant absorption is observed for wavelength higher than 300 nm.

It is interesting to note that though the removal efficiency of direct-photolysis at 254 nm is the highest, the presence of catalyst in fact will slow down the reaction slightly, because of the light shielding effect revealed in chapter five. However, the catalyst plays a positive and promising role at 300 nm, where the removal efficiency was enhanced from 40% to 100% at the end of the reaction after the catalyst was introduced. That is, the removal fraction of AP by direct-photolysis and photocatalysis is about 0.4 to 0.6 at 300 nm. At 350 nm, after using catalyst, the removal of AP was enhanced from 0 to 70%, which is solely attributed to photocatalysis since there is no direct-photolysis at this wavelength. By examining the absorption spectra of AP and catalyst, in the range of 200-300 nm, both the target compound AP and the catalyst can compete for the photons. The above test results reveal that AP and the catalyst prevails in the photon absorption at wavelength of 254 nm and 300 nm (and above), respectively.

Based on information from Chapter 4, the nanocatalyst $CoFe_2O_4/TiO_2$ is active in the visible region given the strong absorption intensity in the range of 200-800 nm. However, the degradation of AP under 420 nm or/above (data on AP degradation under wavelength above 420 nm is not shown) was insignificant. The red shift (i.e. the extension of absorption wavelength threshold) of composite catalyst $CoFe_2O_4/TiO_2$ to the visible region is apparently due to the introduction of $CoFe_2O_4$, while the TiO_2 has very low absorption in these wavelengths. For one thing, it is the VB of $CoFe_2O_4$ that can be excited to generate electrons under visible light. While the low mass ratio of $CoFe_2O_4$ in the composite catalyst and its main role as a catalyst core rather than shell may lead to lower photogenerated electrons, and thus limited radicals ($OH^•$). For another, the chemical bonding between $CoFe_2O_4$ and TiO_2 is not strong. The two parts of the composite catalyst (i. e. $CoFe_2O_4$ and TiO_2) can only perform their roles separately. Energy level coupling including the transfer of electron from CB of $CoFe_2O_4$ to CB of TiO_2 and the transfer of holes from VB of TiO_2 to VB of $CoFe_2O_4$ is not effective (Shi et al. 2014). Without a useful energy level coupling, separation of photogenerated electrons and holes, and extension of the lifetime of the excited electrons (e^-) and holes (h^+) would be difficult, and finally no or very few electrons can transfer to the catalyst surface and take part in the photo-reaction.

The UV 350 nm was chosen as the exclusive light source for the detail study, for its potential applications in the environment by using the sunlight.

6.2.1.2 Catalyst dosage

In Figure 6-2, the effect of catalyst dosage on AP destruction was investigated. It was found that the reaction rate was elevated with the increase of the catalyst dosage from 0 g/L to 0.5 g/L. The photodegradation however slow down above the optimal dosage at 0.5 g/L, likely owing to the reduction in the transmission of photons with redundant catalyst particles revealed in Chapter five. The catalyst dosage at 0.5 g/L was therefore used as the catalyst dosage in the remaining tests.

6.2.1.3 Value of pH

The pH levels above the pK_a of AP (1.4) (Staiger et al. 1980) were tested. From Figure 6-3, the lower pH results in higher removal efficiency.

When the pH level is higher than 6.4 (pK_{a1} of H_2CO_3), the dissolved carbon dioxide (CO_2) in the reaction system (from the air and mineralization of AP destruction) is transformed into bicarbonate (HCO_3^-) ions. The latter may compete with AP for hydroxyl radicals (Rao and Chu 2013) and further lead to the retardation of AP degradation (Equation 6-1).

$$HCO_3^- + OH^{\bullet} \rightarrow CO_3^{\bullet -} + H_2O \qquad \text{(Equation 6-1)}$$

Another possible reason accounting for the faster destruction at low pH is the larger surface area of the catalyst. As was demonstrated in previous study, the effective diameter of the catalysts is the largest at pH of ZPC (around 8.0 in this study) (Chen and Chu 2012). The smaller size of the catalyst at lower pH offers larger surface area, more opportunities to contact with the target molecules and absorb the UV light. In this case, the degradation of AP would be enhanced. In addition, the lower pH may induce mild leaching of metals out of the catalyst (Chapter five), which promotes the catalysis via a faster homogeneous phase reaction.

During the reaction, the change of pH level was monitored. The increase and decrease of solution pH in acidic and the alkalic conditions were detected, respectively. The change may be due to the interaction between the catalyst, the proton and hydroxyl ions in the solution, and its balance with the generation of low-molecular organic acids as end products. Since extremely low pH is not practical in water treatment processes, pH of 5.5 was recommended based on the fundamental study.

6.2.1.4 Initial AP concentration

The effect of initial concentrations of AP ($[AP]_0$) on the photocatalytic process is shown in Figure 6-4. Generally, higher the $[AP]_0$, (i.e. lower the photon / $[AP]_0$ ratio), lower the reaction rate, because the UV intensity and likely the $[OH^\bullet]$ are constants. A linear correlation between k and ln $[AP]_0$ was derived as shown in Equation 6-1 for the prediction of the pseudo first-order rate constant (k, min^{-1}) in AP destruction by the process under the optimal reaction conditions.:

$$k = -8.05 \times 10^{-3} \ln [AP]_0 + 5.11 \times 10^{-2} \ (R^2 = 0.98) \qquad \text{(Equation 6-2)}$$

6.2.2 Mechanism of the photodegradation

During the reaction, AP was firstly decomposed to its daughter compounds, then eventually mineralized by generating inorganic molecules (CO_2, H_2O, NH_4^+, NO_3^-, and NO_2^-). To reveal the reaction mechanism, the organic intermediates, the TOC content, and the inorganic ions were monitored.

Totally ten organic intermediates were identified in the LC-ESI-MS chromatogram. Five of them (C3, C5, C6, C8 and C9), asterisked in Figure 6-5, are the first time being reported in the study of AP degradation. Information of the detected intermediates including formula, mass, chemical structures, and the degradation pathways are proposed in Figure 6-5.

Mono-hydroxylated-AP derivatives, generated by hydroxyl radical ($OH^•$) attack were identified. They are proposed as the dominant products in the whole reaction as seen from the comparatively high peak areas (Figure 6-6 a). It's interesting to note that, in this study, no di- or tri-hydroxylation products were found, which were observed in other AOPs (Calza et al. 2011). This is likely due to the formation of excess [$OH^•$] dosage in the beginning of many AOPs, which can easily create an environment for multi-hydroxylation on AP molecules. In this study however, the generation of [$OH^•$] is under controlled and limited to the surface of catalyst, so the chance for generating di- and tri- hydroxylation intermediates is low. From the application point of view, the former is good for quick reaction of parent compound, but many hydroxyl radicals are wasted for generating futile intermediates with larger molecules. The latter though has a slower degradation of the parent compound, but it's a cleaner process, in which the hydroxyl radicals are used more effectively and less intermediates are generated. This is especially useful if mineralization is the process design target, because the elimination of multi-hydroxylation will minimize the unnecessary energy and chemical consumption. In addition, the hydroxyl group tends to be combined with the formic acid (a common end product in the AOP), which can be verified from the presence of C5. The hydroxymethyl group -CH_2OH can be further oxidized to aldehyde group –CHO, forming the products of C6 and C7.

Demethylation is another dominant pathway in this process, leading to the formation of C8. The radical attack at the pentacyclic ring results in the cleavage of C-N and N-N bonds, the result is the scission of C8 into the open-ring intermediates C9 and C10 (N-phenylpropinamide).

The peak areas of the intermediates as a function of treatment time are shown in Figure 6-6. During the first hour of treatment, only mono-hydroxylated derivatives were detected. However, the TOC reduction and ammonia release at the first hour (Figure 6-7) suggest that pentacyclic ring opening actually occurred. It is therefore believed that all the proposed intermediates have been formed, though they were too low to be detected yet.

This is further confirmed by the decrease trend of the benzene ring balance assuming that all the intermediates have the same molar absorption. However, there is a crest at 2 h, in which the levels of all the mono-hydroxylated derivatives elevated to their peaks and the aldehyde C6 and C7 just became detectable. The crest is apparently due to the overestimation of the molar absorptivity of the mono-hydroxylated derivatives. Fortunately, such an overestimation becomes insignificant at the later stage as indicated in the tailing of Figure 6-7. At the end of the treatment, approximately 45% of AP was mineralized according to the TOC measurement as also shown in Figure 6-7.

Both nitrogen moieties in AP come from the pentacyclic ring, and the result indicates that most of the nitrogen in pentacyclic ring transfers to ammonia (NH_4^+). Approximately 60 μM (60% of total nitrogen mass) was generated at the end of the reaction (i.e. 5 h) from Figure 6-7, indicating that the pentacyclic ring has been opened and separated from the benzene ring. Nitrate (NO_3^-) and nitrite (NO_2^-) were also being detected but in trace level (0.55%, 0.13% of total nitrogen mass for NO_3^-, NO_2^-, respectively) after 24 h of reaction. The formation of NO_3^- and NO_2^- may come directly from the pentacyclic ring or be transformed from oxidation of NH_4^+. The late presence of nitrate and nitrite reveals that the radicals have a priority to oxidize the organic intermediates than the inorganic ammonia. This is likely because the solution pH has a lower pH level than ZPC. The surface of the catalyst is positively charged, and the NH_4^+ is repelled away from the catalyst surface and thus has less opportunity to be oxidized.

6.2.3 Toxicity evolution during AP degradation

6.2.3.1 Effect of AP and the degradation products on C. vulgaris

The effect of the parent compound AP on the algae *C. vulgaris* was firstly examined.

Judging from the calculated growth rate r given in Figure 6-8, it was interesting to note that no adverse effect of AP was detected and the growth of *C. vulgaris* in AP solutions was even better than that in water. The result was possibly due to the adverse effect of AP on some bacteria in the algae culture media (Aiad et al. 2017). The result also reveals that pharmaceuticals have diverse effects on the growth of algae since some other pharmaceuticals e.g. SMX were found to be harmful to the algae growth (Baran et al. 2006).

For the degradation products, similarly, no adverse effect was observed, the growth rate r exposed to intermediates were higher than those of algae exposed to untreated solution. The nutrient source of the algae is mainly composed of inorganic substances (e.g. inorganic nitrogen, phosphorus and sulfate), trace metal, and vitamin (f/2 culture media can be referred (Guillard 1975)). Some studies have shown that low organic molecules are also beneficial to algae growth (Liu et al. 2013a). Therefore, the acceleration of algae growth exposed to treated solutions is possibly attributed to the transformation of AP to nutrients including small organic molecules, inorganic carbon, and ammonia.

6.2.3.2 Toxicity of AP and the degradation products on A. salina

Survival of *A. salina* exposed to different concentrations of AP was determined, and the result was shown in Figure 6-9 (a). The survival of shrimps was significantly reduced after 48 h or 72 h of exposure to low concentrations of AP. Median lethal doses (LD50) at different time and concentration were calculated and indicated in Figure 6-9 (a).

The survival was not significantly reduced at 24 h, while it was observed that their swimming ability has been significantly inhibited; about 60% of the alive brine shrimps can only swing with their antennas rather than swim freely after the exposure at 50 μM AP. It is assumed that the feeding activity of *A. salina* would be further inhibited, since the brine shrimps obtain food by either using spines on the legs as they swim or quick movements of appendages (Larsen et al. 2008). It is predicted that the survival of shrimps will be further reduced after longer exposure due to both acute toxicity (lethal, inhibition of swimming) and chronic toxicity (inhibition of the feeding) of AP.

After the treatment of AP by photodegradation (i.e. UV/$CoFe_2O_4/TiO_2$), the survival of shrimps rises to the level of control group. It is interesting to note that, for the treated solution sample collected at 1 h, the toxicity was close to the control even if the sample actually contains about 20 μM AP (Figure 6-9 b). This is inconsistent to the data as shown in Figure 6-9 (a), where the survival rate exposed to pure AP at 20 μM was significantly lower than the control group. Besides, survival of shrimps presents a linear trend corresponding to the treatment time in the first hour. By comparing the above observations with the LC/MS data, the dominant byproducts during the first hour were the mono-hydroxylated AP. Despite of the few information available for the hydroxylated compounds of AP, it was reported that the Kow of aromatics are generally reduced after hydroxylation. For instance, the log Kow value of phenol (1.5) (Schultz et al. 1996) is lower than that of benzene (2.13) (Veith et al. 1979), the log Kow values of 3-Methylphenol (1.98) (Schultz et al. 1996), Benzyl alcohol (1.10) (Martin 1996) are lower than that of methylbenzene (2.72) (EPA 2005), the log Kow values of ethylphenol (2.50) (Schultz et al. 1996) and phenethyl alcohol (1.57) (Marsili 2011) are lower than that of ethylbenzene (3.15) (Chiou 1985). As has been illustrated, compounds with lower Kow are generally less toxic due to their poor accessibility to the inner mitochondria membrane (Mcfarland 1970). The generation of the hydroxylated compounds may cover the biological membranes of brine shrimps, and hinder the entry of AP to the inner mitochondria membrane.

As is seen from the experiment results, the mortality caused by AP was apparently hindered by the byproducts via the antagonism effect. This is an advantage of treatment processes based on hydroxyl radical, since hydroxylated compounds are commonly generated in such processes and the toxicity is possibly reduced via this mechanism.

6.3 Summary

A systematic study based on AP toxicity reduction during the photocatalytic degradation was conducted. The UV wavelength of 350 nm, the catalyst dosage of 0.5 g/L, and acidic condition were favorable for AP destruction by photocatalysis. Ten organic intermediates, 45% TOC reduction and 60% ammonia release were identified during the process. The parent compound AP and the treated solutions show positive effect on the growth of *C. vulgaris*. Moreover, acute toxicity of AP to brine shrimps *A. salina* was eliminated with the destruction of AP. The results suggest that the process UV/$CoFe_2O_4$/TiO_2 can be an effective way on removal and toxicity reduction of some refractory pharmaceuticals.

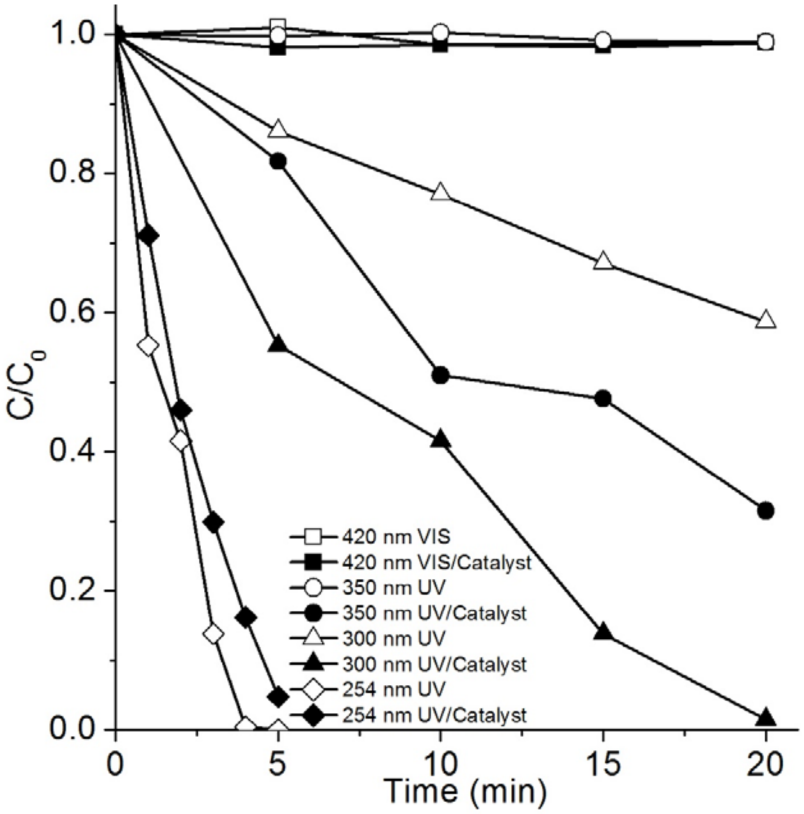

Figure 6-1 Antipyrine photodegradation with varied light sources. *Experimental condition:* $[AP]_0$ = 0.5 μM, catalyst dosage = 0.5 g/L, pH =8.5, twelve lamps were used.

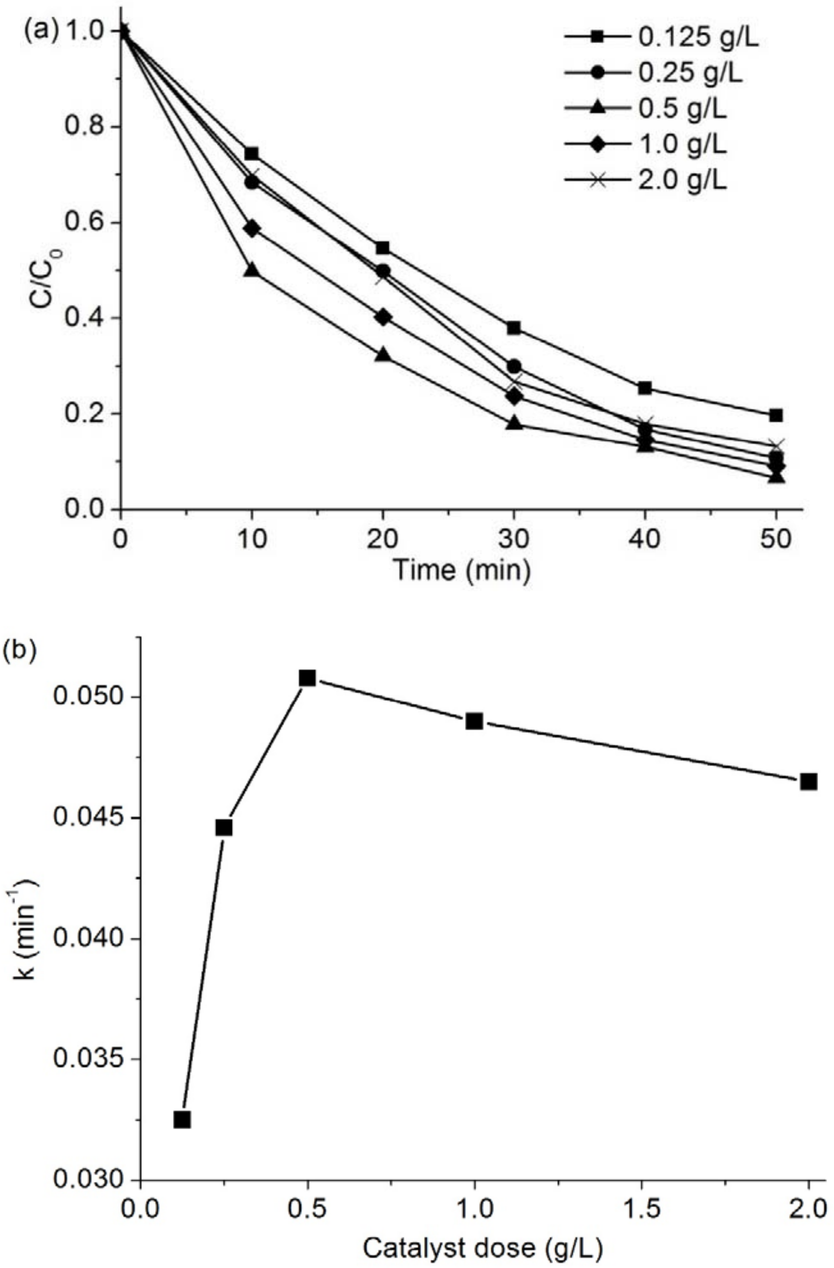

Figure 6-2 Antipyrine photodegradation with varied catalyst dosages. (a) Antipyrine destruction curves with different dosages of catalyst. (b) Reaction rate of antipyrine destruction in terms of catalyst dosage. *Experimental condition:* $[AP]_0$ = 0.5 µM, pH =8.5, twelve lamps at 350 nm were used.

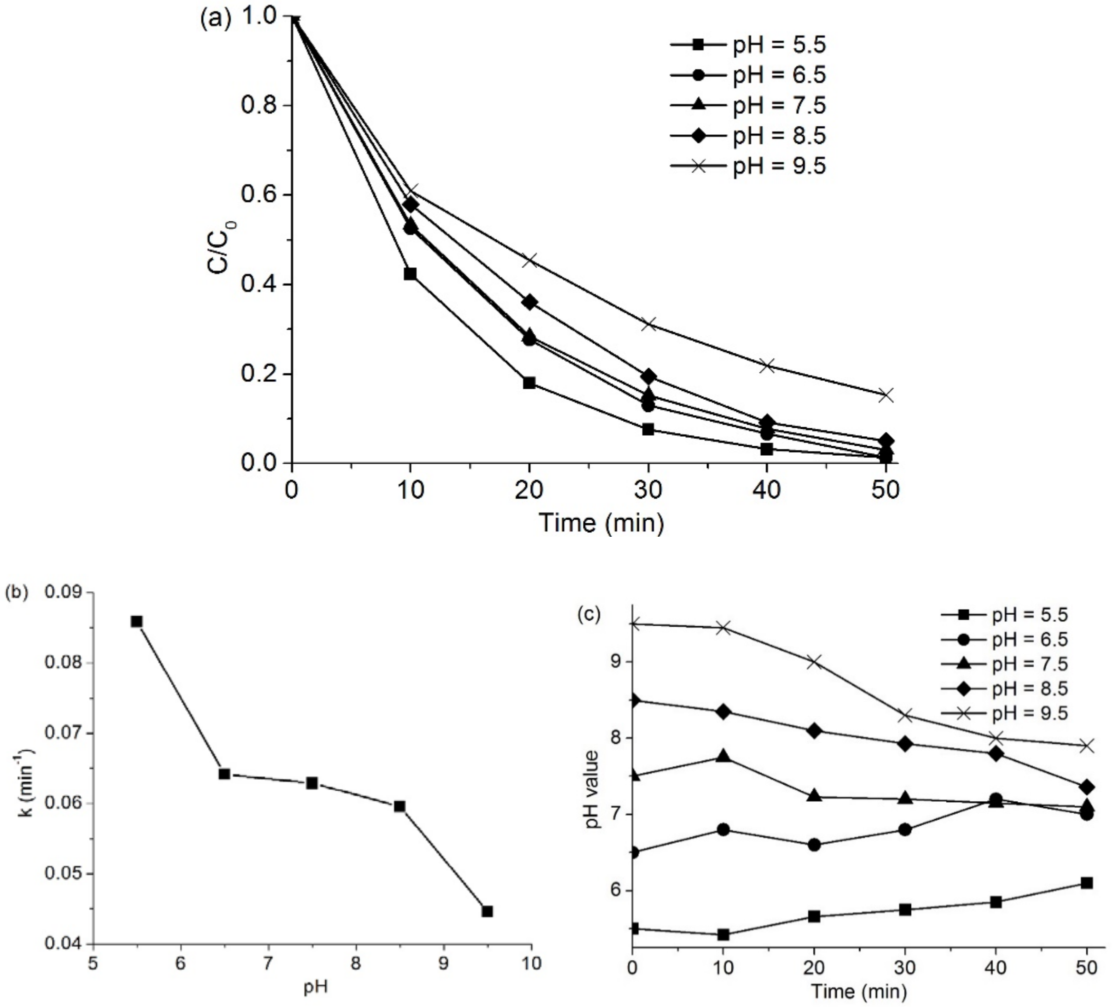

Figure 6-3 Antipyrine photodegradation with varied initial pH value. (a) Antipyrine destruction curves under different initial pH values. (b) Reaction rate of antipyrine photodegradation in terms of initial pH value. (c) The pH change during antipyrine destruction. *Experimental condition:* $[AP]_0$ = 0.5 μM, catalyst dosage = 0.5 g/L, twelve lamps at 350 nm were used.

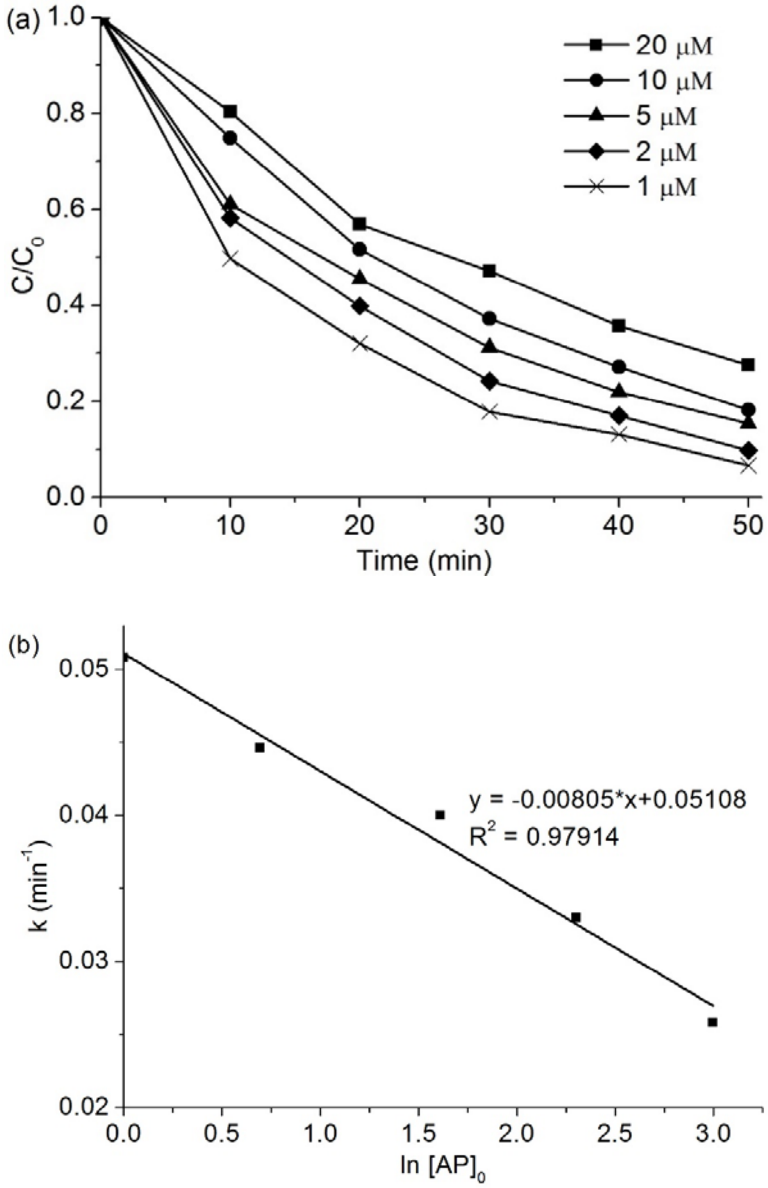

Figure 6-4 Photodegradation under varied initial concentrations of antipyrine. (a) Antipyrine destruction curves at different initial concentrations of antipyrine. (b) Reaction rate of antipyrine photodegradation in terms of initial concentration. *Experimental condition:* catalyst dosage = 0.5 g/L, pH =5.5, twelve lamps at 350 nm were used.

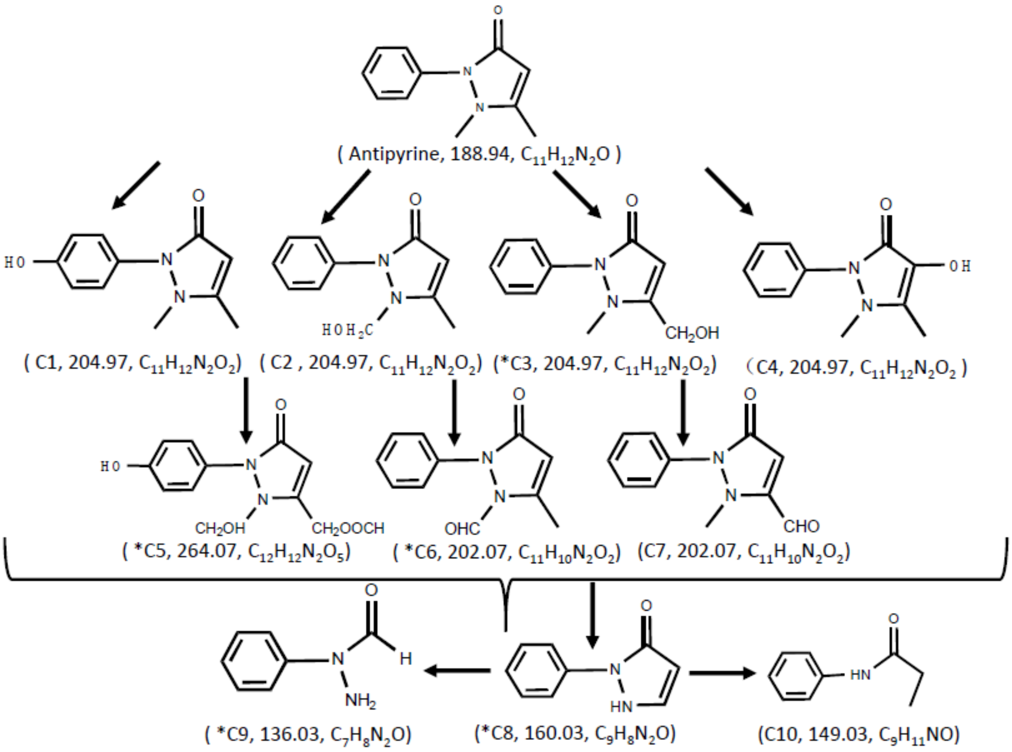

Figure 6-5 Proposed pathway of antipyrine degradation. (The asterisks indicate newly reported products.)

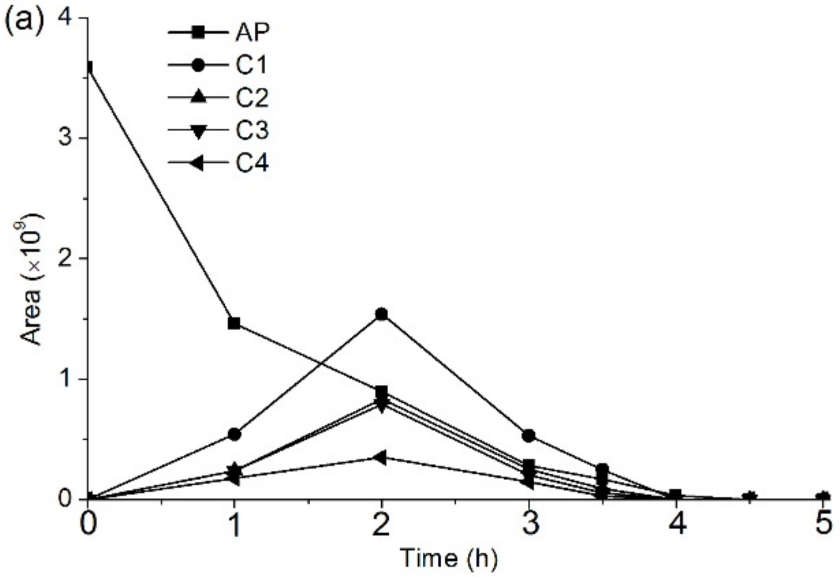

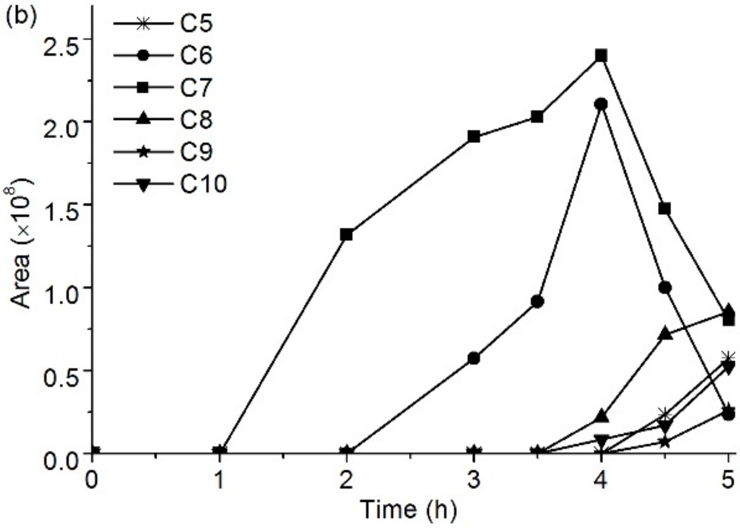

Figure 6-6 Peak areas of antipyrine and products generated during antipyrine degradation.

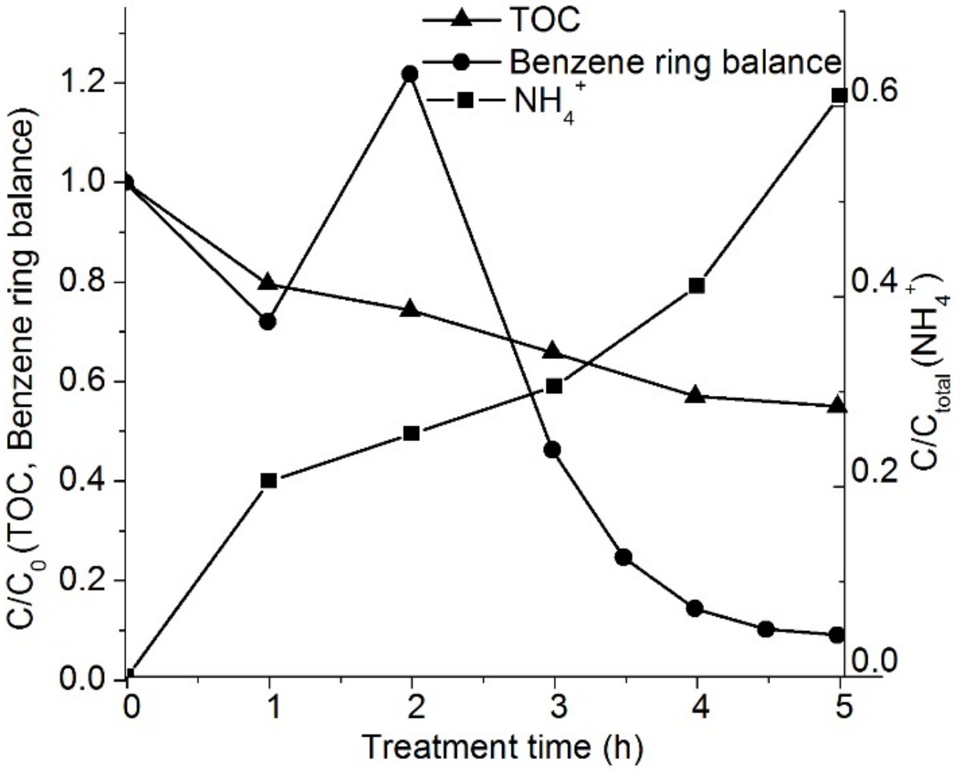

Figure 6-7 TOC reduction, benzene ring balance and ammonia release during antipyrine degradation. *Experimental condition:* $[AP]_0$ = 55 μM, catalyst dosage = 0.5 g/L, pH =5.5.

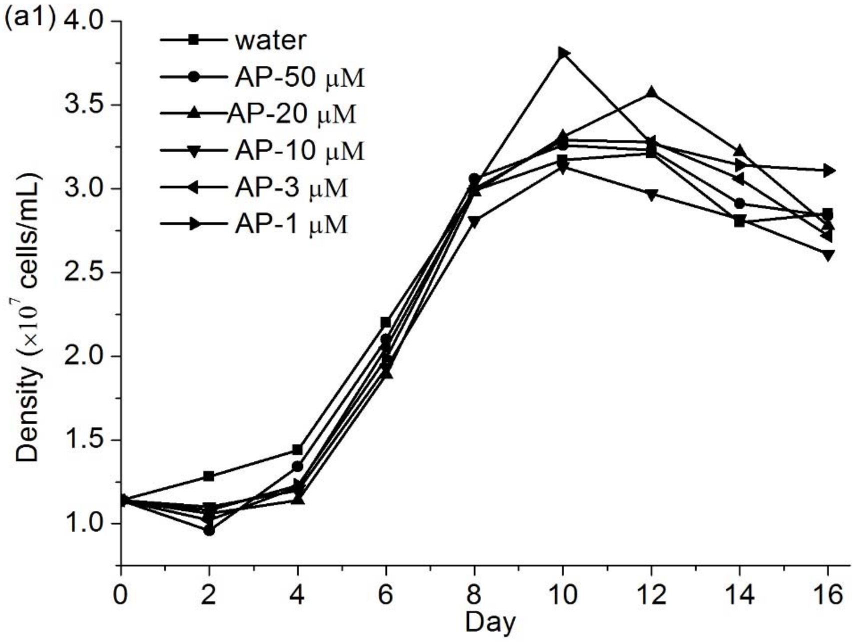
(a1)
water
AP-50 μM
AP-20 μM
AP-10 μM
AP-3 μM
AP-1 μM
Density (×10^7 cells/mL)
4.0
3.5
3.0
2.5
2.0
1.5
1.0
0
2
4
6
8
10
12
14
16
Day

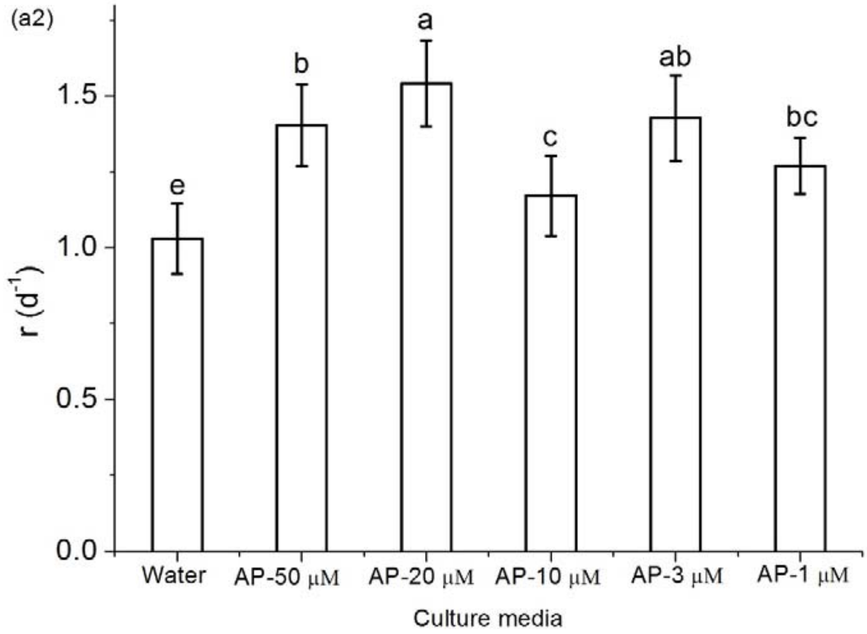
(a2)
r (d^-1)
1.5
1.0
0.5
0.0
e
b
a
c
ab
bc
Water
AP-50 μM
AP-20 μM
AP-10 μM
AP-3 μM
AP-1 μM
Culture media

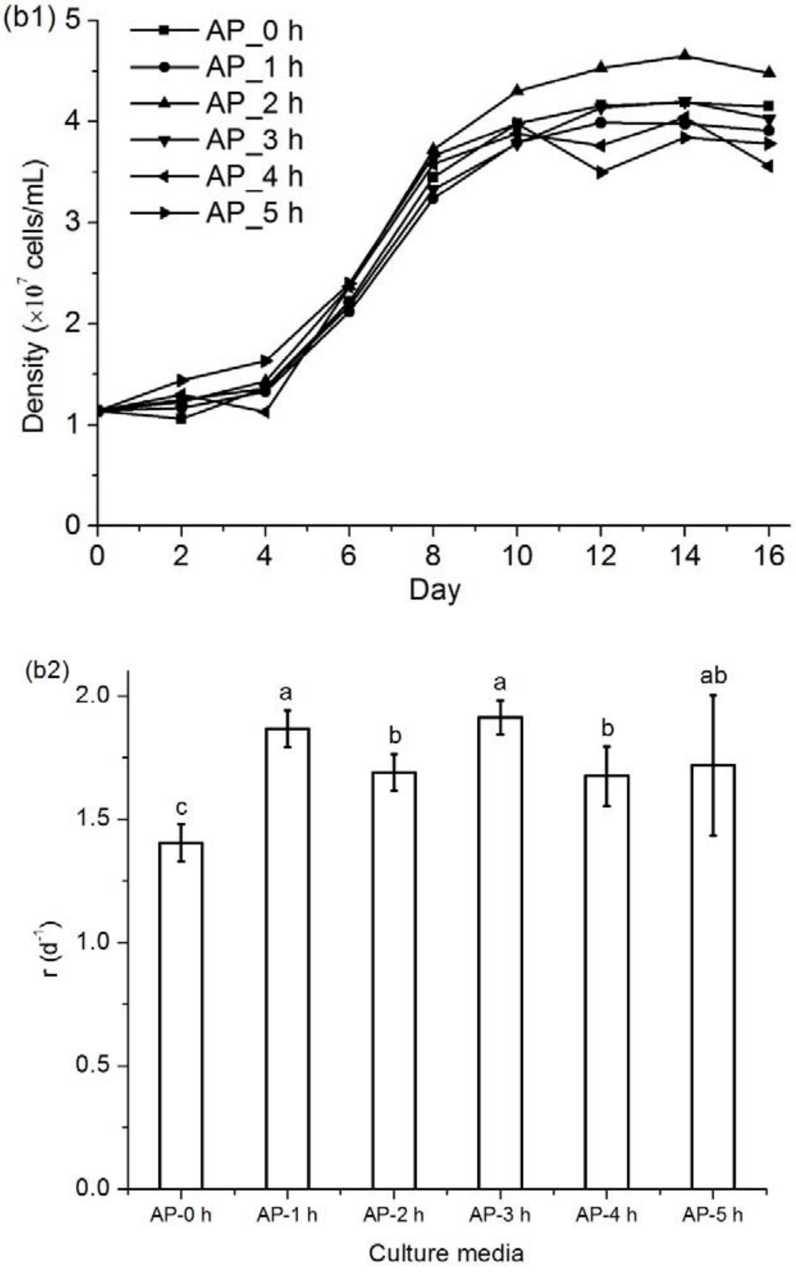

Figure 6-8 Effect of antipyrine and the degradation products on the growth of *Chlorella vulgaris*. (a) Growth of *C. vulgaris* exposed to different concentrations of antipyrine. (b) Growth of *C. vulgaris* exposed to degradation products collected at different treatment time.

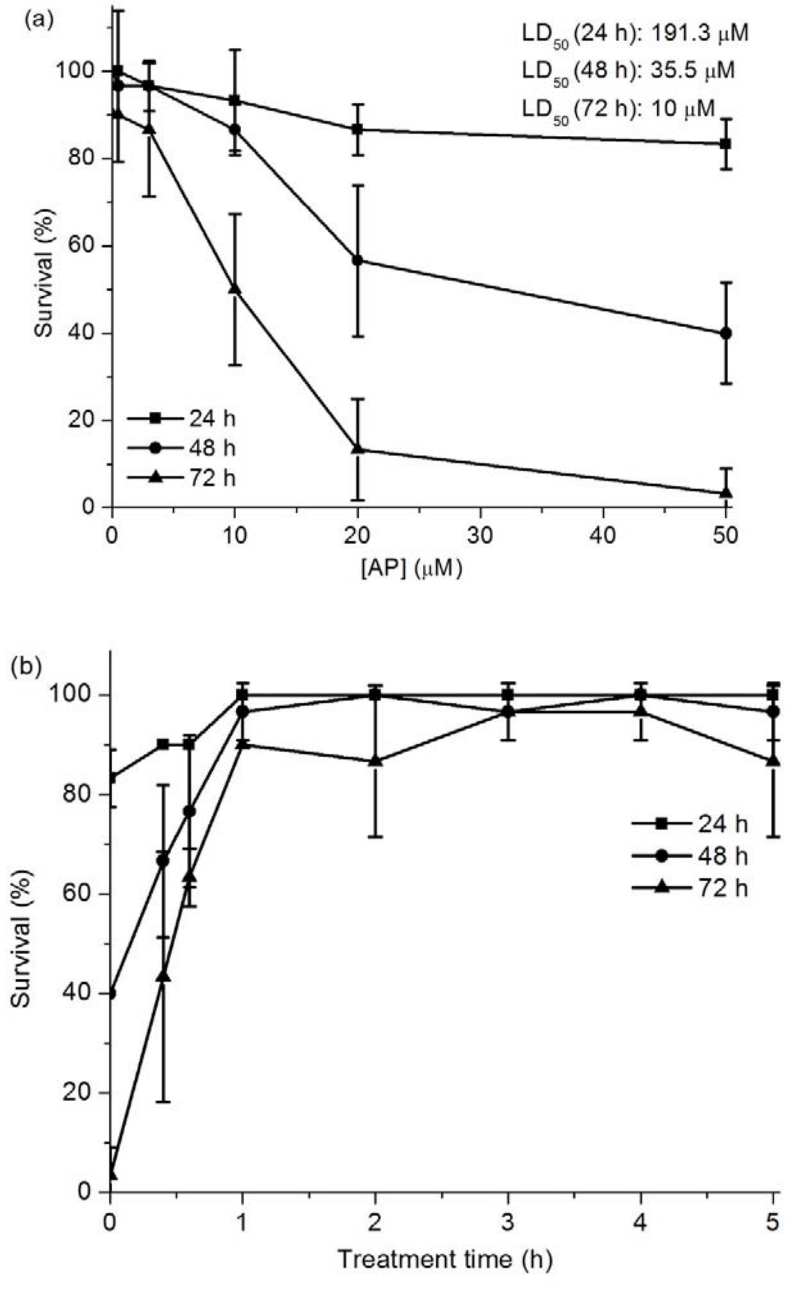

Figure 6-9 Survival of *Artemia salina* exposed to antipyrine and the degradation products. (a) Survival of *A. salina* exposed to different concentrations of antipyrine. (b) Survival of *A. salina* exposed to degradation products collected at different treatment time. *Experimental condition:* [AP]$_0$ = 55 μM, catalyst dosage = 0.5 g/L, pH =5.5.

7 Chapter seven Photodegradation of ibuprofen with the magnetic catalyst

7.1 Introduction

In the last chapter, antipyrine was selected as a representative compound of NSAID group. It is difficult to identify the effect of treatment process on the toxicity evolution to algae since AP was proven to have positive effect on the algae growth. Therefore, another NSAID, IBP was selected as IBP was proven to inhibit the growth of *C. vulgaris*. In this chapter, IBP degradation under the reaction system UV/$CoFe_2O_4/TiO_2$ was evaluated. Apart from the optimization of the reaction conditions, the effects of common anions (NO_3^-, Cl^-, F^- and CO_3^{2-}) and oxidants (oxone, persulfate and perhydrol) on IBP photodegradation were investigated. In addition, the TOC reduction and toxicity evolution during the treatment process was evaluated.

7.2 Results and discussion

7.2.1 Effect of the reaction conditions on the photodegradation

7.2.1.1 Effect of UV wavelength

Before the tests, the hydrolysis and adsorption of IBP were determined. The IBP solution was placed in the darkness with mechanical stirring to determine the possible hydrolysis, which was found to be insignificant. The catalyst was then introduced to the solution and the adsorption effect was also found to be insignificant. The adsorption loss of the probe compound to the catalyst was therefore ignored in this study.

The study in previous chapters indicates that 350 nm is the optimal wavelength that the photocatalyst $CoFe_2O_4/TiO_2$ plays its role. In the photodegradation of IBP, however, it is found that 300 nm is the optimal condition. From Figure 7-1, IBP experienced significant direct photolysis under the wavelength of 254 nm, where about 50% IBP was removed in 10 mins. However, the introduction of the catalyst hindered the decomposition of IBP under the wavelength of 254 nm because of the photo-shielding effect. The situation was reversed with the wavelength elevated to 300 nm. Under the wavelength of 300 nm and 350 nm, no significant direct photolysis was detected. The removal efficiency of IBP was raised to 70% and 80% under the wavelength of 300 nm and 350 nm, respectively due to the addition of the photocatalyst to the reaction system. Since the removal efficiency under 300 nm was much higher than that under 350 nm, 300 nm was determined to be the optimal wavelength and would be used in the detailed study of IBP photocatalyst by UV/$CoFe_2O_4/TiO_2$. This result is quite different from that of the other previous two target compounds, where 350 nm was the optimal wavelength.

7.2.1.2 Effect of UV intensity

It was proposed that the higher UV intensity would result in the higher reaction rate (Xu et al. 2013a). In this study, the UV intensity was represented by the lamps number. The experiment result gave a strong evidence that the reaction rate was enhanced from 0.10 min^{-1} to 0.28 min^{-1} with the increase of lamps number from 6 to 14. A linear correlation was established between the lamps number with the reaction rate (Figure 7-2).

7.2.1.3 Effect of catalyst dosage

To determine the optimal catalyst dosage, the effect of catalyst dosage ranged from 0.25 g/L to 2.0 g/L on the IBP destruction was explored (Figure 7-3). It was observed that the increment of the catalyst dosage resulted in the increase of the IBP removal efficiency before the breakpoint of 0.5 g/L. After the breakpoint, reaction rate of IBP photodegradation reduced with the increase of the catalyst dosage because of the reduction in the light penetration illustrated in Chapter five.

7.2.1.4 Effect of pH value

To determine the effect of pH value on the removal efficiency of IBP by the photocatalysis process, IBP photodegradtion under five levels of pH was measured with other conditions staying constant. The result in Figure 7-4 indicated that IBP photodegradation under UV/$CoFe_2O_4$/TiO_2 was strongly dependent on the pH value. With the increment of pH level, the reaction rate decreased from 0.21 min^{-1} to 0.15 min^{-1}.

There are four reasons accounting for the favorable reaction under acidic environment. Firstly, IBP molecular exhibit neutral and negatively charged state under and above the pH level of 4.91 (pK_a value of IBP), respectively. It has been well proven that molecular under neutral state are much more susceptibly attacked by radicals compared to those under negatively charged state (Niu et al. 2013). Therefore, the pH level of 4.5 is much more favorable than 5.5 in terms of radical attack.

Secondly, during the reaction, carbon dioxide (CO_2) was generated continuously from the mineralization of IBP molecular. Also, there were CO_2 dissolved from the air. In alkalic environment, CO_2 exists in the form of HCO_3^- in the reaction system. The dissolved HCO_3^- may compete for radicals with the IBP molecular. In this condition, less radicals were used for decomposition of IBP and thus lower reaction rate was obtained.

Thirdly, the repulsion between the catalyst and the target compounds IBP would hinder destruction of IBP in alkalic condition. The catalyst was also negatively charged when the pH level was above 8.1 (ZPC of the catalyst). In this case, the target IBP compounds were repelled away from the surface of the catalyst. As a result, the reaction was slowed down significantly.

Lastly, it was reported that at pH values that were near ZPC of the catalyst, the surface area of the catalyst was getting smaller (Chen and Chu 2012). Consequently, the catalyst has a larger surface area and thus a higher photocatalytic efficiency, leading to higher reaction rate in acidic environment.

7.2.1.5 Effect of IBP initial concentration

In the above experiments, high initial concentration of IBP ($[IBP]_0$) was employed given the detection limit of HPLC. In the practice of water/wastewater treatment, $[IBP]_0$ may vary in a large scale in real water/wastewater. To obtain the possible correlation of $[IBP]_0$ with the reaction rate, IBP photodegradation experiments were carried out in the conditions that $[IBP]_0$ was varied in the range of 5 μM to 100 μM and other parameters were kept constant. The result was shown in Figure 7-5. It was found that the higher the initial concentration of IBP resulted in the lower reaction rate of IBP photodegradation. This can be ascribed to the fact that the generated photon was constant. The higher the initial concentration of IBP, the lower photon dosage was shared for each IBP molecular and thus the lower reaction rate. The linear relationship between $[IBP]_0$ and the reaction rate was established and can be employed for the prediction of the reaction rate constants in IBP photodegradation by the process UV/$CoFe_2O_4$/TiO_2.

7.2.2 Effect of anions on IBP photodegradation

The effect of different anions on the photocatalysis process is shown in Figure 7-6, where all the tested anions show the negative effect except NO_3^-. As is mentioned above in 7.2.1.4, HCO_3^- would react with $OH^•$, and the generated radical $CO_3^{•-}$ is much less active than $OH^•$. Apart from the scavenging effect, another reason may be the slight increase of pH value after the introduction of HCO_3^-. As is reported, the introduction of 10 mM HCO_3^- resulted in the increase of pH value from near neutral to weak alkaline (Chen and Chu 2015).

Similarly, for the negative effect of Cl^- on the photocatalysis process, it can be attributed to the reaction of Cl^- with $OH^\bullet$ (Equation 7-1 to Equation 7-4) (Truong et al. 2004). As is illustrated in the equations, the directly generated radical $ClOH^{\bullet -}$ can further result in the formation of radicals $HClOH^\bullet$, $Cl^\bullet$, and $Cl_2^{\bullet -}$, which are all less active than $OH^\bullet$ (Truong et al. 2004). As was demonstrated by Truong et al. (Truong et al. 2004), $Cl_2^{\bullet -}$ is the dominant radical among the four radicals generated. Since the redox potential of $Cl_2^{\bullet -}$ (around 1.36 eV) is far lower than that of $OH^\bullet$ (up to 2.9 eV) (Truong et al. 2004), the reaction was slowed down accordingly.

$$Cl^- + OH^\bullet \rightarrow ClOH^{\bullet -} \qquad \text{(Equation 7-1)}$$

$$ClOH^{\bullet -} + H^+ \rightarrow HClOH^\bullet \qquad \text{(Equation 7-2)}$$

$$HClOH^\bullet \rightarrow Cl^\bullet + H_2O \qquad \text{(Equation 7-3)}$$

$$Cl^\bullet + Cl^- \rightarrow Cl_2^{\bullet -} \qquad \text{(Equation 7-4)}$$

The destruction of IBP was also slightly hindered in the presence of F^-. As is suggested in previous study, introduction of F^- may inhibit the approach of target compound to the surface of the catalyst (Chen and Chu 2012). The exclusive hydrogen bond (O-H···F) may be formed around the surface of the catalyst. In this case, the hydroxyl ions would be tied up and bided. Consequently, the surface property of the catalyst is possibly changed and thus the radical formation may be hindered.

The positive impact of NO_3^- was significant by the increase of reaction rate from about 0.1 min^{-1} to about 0.15 min^{-1}. The significant elevation is probably resulted from the additional formation of radicals including $NO_2^•$, $O^{•-}$, $OH^•$ (Keen et al. 2012). As is shown in Equations, one reaction pathway is the release of NO_3^- to NO_2^-. Another transformation pathway is the release of NO_3^- to $NO_2^•$ and $O^{•-}$. The released $O^{•-}$ can lead to the formation of $OH^•$, which can further react with NO_2^- and result in $NO_2^•$. The generated radicals in these processes, $OH^•$ and $NO_2^•$ included, contribute to the enhancement of the removal efficiency in the presence of NO_3^-.

$$NO_3^- \rightarrow NO_2^- + \frac{1}{2} O_2 \quad \text{(Equation 7-5)}$$

$$NO_3^- \rightarrow NO_2^• + O^{•-} \quad \text{(Equation 7-6)}$$

$$O^{•-} + H_2O \rightarrow OH^• + OH^- \quad \text{(Equation 7-7)}$$

$$OH^• + NO_2^- \rightarrow NO_2^• + OH^- \quad \text{(Equation 7-8)}$$

7.2.3 Effect of oxidants on IBP photodegradation

From Figure 7-7, it can be seen that the reaction rate was significantly increased with the addition of oxone or persulfate, while the reaction was significantly slowed down with the introduction of H_2O_2. Approximately 9 μM IBP was removed in 2 mins under the process UV/$CoFe_2O_4$/TiO_2 with the assistance of 0.25 mM oxone, and the reaction rate is about ten times of that under the photocatalysis without oxidants. The sharp elevation is owing to the formation of a great amount of radicals $SO_4^{\bullet -}$ and $OH^{\bullet}$ after the introduction of oxone (Equation 2-26).

For the process UV/Catalyst/Persulfate, it takes 8 mins to remove 90% of IBP molecular, and the reaction rate is around 3 times of that under the process UV/$CoFe_2O_4$/TiO_2. The accelerated reaction rate is due to the generation of radical $SO_4^{\bullet -}$ with the addition of persulfate (Equation 2-24).

The slower reaction under UV/Catalyst/Persulfate compared to UV/Catalyst/Oxone can be contributed to two reasons. As is shown in the equations, 1 M $SO_4^{\bullet -}$ and 1 M $OH^{\bullet}$ can be generated for the case with 1 M oxone, and 2 M $SO_4^{\bullet -}$ can be generated as a result of the addition of 1 M persulfate. The number of radicals generated has no difference from the same concentration of oxone and persulfate. However, the radical $OH^{\bullet}$ has a much higher redox potential than $SO_4^{\bullet -}$. Therefore, the addition of oxone raised the removal efficiency to a much higher level than persulfate. Another important reason is that the pH value of the solution would be significant reduced due to the addition of oxone, while the opposite was the case for persulfate. As is mentioned above, acidic environment is much more favorable for IBP degradation. As a consequence, oxone is much more beneficial for the reaction.

The addition of H_2O_2, however, slowed down the reaction slightly. It was reported that at low concentrations, H_2O_2 can enhance the performance of the photocatalysis by generating $OH^{\bullet}$ (Equation 2-7). However, the increase in H_2O_2 level would inhibit the destruction of target organic compounds beyond an optimal concentration. The excessive amount of H_2O_2

may react with $OH^\bullet$ and $OH^\bullet$ would lead to the formation or generation of hydroperoxyl radical $HO_2^\bullet$ (Equation 2-14). Since the radical has a much lower oxidation capability than $OH^\bullet$, the reaction was retarded. Therefore, for the purpose of enhancement of removal efficiency with the assistant of H_2O_2, it is suggested that the introduced dosage of H_2O_2 should be controlled in a certain range.

7.2.4 TOC change during IBP photodegradation

The initial concentration of IBP was enhanced to 100 μM because of the detection limit of TOC analyzer. IBP can be removed completely in 120 mins, however, the mineralization is only 35% (Figure 7-8). The low mineralization indicates the presence of a large amount of organic intermediates. To achieve the complete mineralization, longer time of degradation is needed.

7.2.5 Toxicity evolution during IBP destruction

7.2.5.1 Effect of IBP and the products on the growth of C. vulgaris

The growth curves of *C. vulgaris* exposed to the IBP solutions before and after the treatment process is illustrated in Figure 7-9 (a). The values of environment capacity K and growth rate r were calculated according to the Logistic growth model and were demonstrated in Figure 7-9 (b).

The adverse effect of the parent compound IBP to *C. vulgaris* was gradually eliminated with the decomposition of IBP. As it can be seen, the growth of the algae was significantly inhibited exposed to 100 μM IBP solution, with K (1.55×10^7 cells/mL) and r ($0.36\ d^{-1}$) significantly lower than that obtained from the growth curve of algae exposed to water (with K value at 2.06×10^7 cells/mL and r value at $0.42\ d^{-1}$, respectively, $p < 0.05$ in all cases).

The inhibition effect was less significant when the algae was exposed to the solution treated for 40 minutes (IBP-40 min), where the concentration of IBP declined to 40 μM and the K and r values of the algae growth increased to 1.98×10^7 cells/mL, $0.39\ d^{-1}$, respectively.

After the IBP solution was treated for 80 minutes and the IBP concentration dropped to 20 μM, the adverse effect of the solution was not significant, where values of K (2.09×10^7 cells/mL) and r ($0.43\ d^{-1}$) had no significant difference with those observed from the growth curve of algae exposed to water.

The final product of the treatment process showed a positive effect on the algae growth, where the value of r ($0.47\ d^{-1}$) are even higher than that in water, indicating that the destruction process is safe for growth of *C. vulgaris*.

7.2.5.2 Effect of IBP and the products on A. salina

In this study, the initial IBP concentration was 100 μM, and no adverse effect on the survival or the feeding *A. salina* was detected. As was reported in previous studies, the

NOECs of IBP on zooplanktons were rather high, usually higher than 300 μM (Knoll/BASF 1995, Cleuvers 2004, Heckmann et al. 2007, Han et al. 2010). Besides, the survival and the feeding of *A. salina* exposed to the degradation products showed no significant difference compared to that in control group. Therefore, it was believed that no product that is more toxic to *A. salina* was generated during the IBP destruction.

7.3 Summary

IBP degradation under the reaction system UV/$CoFe_2O_4$/TiO_2 including the optimization of the reaction conditions, the effects of common anions and oxidants, the TOC reduction and toxicity evolution were investigated.

The UV wavelength of 300 nm, the catalyst dosage of 0.5 g/L, and acidic condition were favorable for IBP destruction by photocatalysis. The removal efficiency was significantly elevated with the addition of oxone or persulfate, and the reaction was faster in the presence of oxone than the same concentration of persulfate. However, the reaction was significantly slowed down with the introduction of H_2O_2. Except NO_3^-, all the tested anions, Cl^-, F^- and CO_3^{2-} included, showed adverse effects on the reaction. Approximately 35% TOC reduction was detected when the parent compound IBP was totally removed. The adverse effect of the parent compound IBP to *C. vulgaris* was gradually eliminated with the decomposition of IBP. No adverse effect was detected for the survival and the feeding of *A. salina* exposed to IBP and the degradation products.

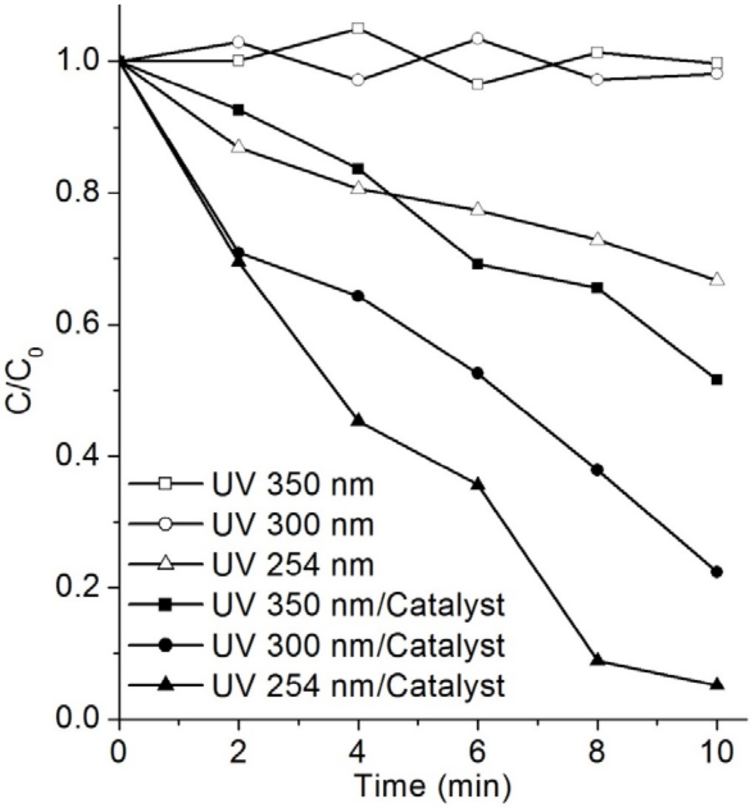

Figure 7-1 Ibuprofen degradation under different UV wavelength. *Experimental condition:* $[IBP]_0$ = 5 μM, catalyst dosage = 0.5 g/L, twelve UV lamps were employed.

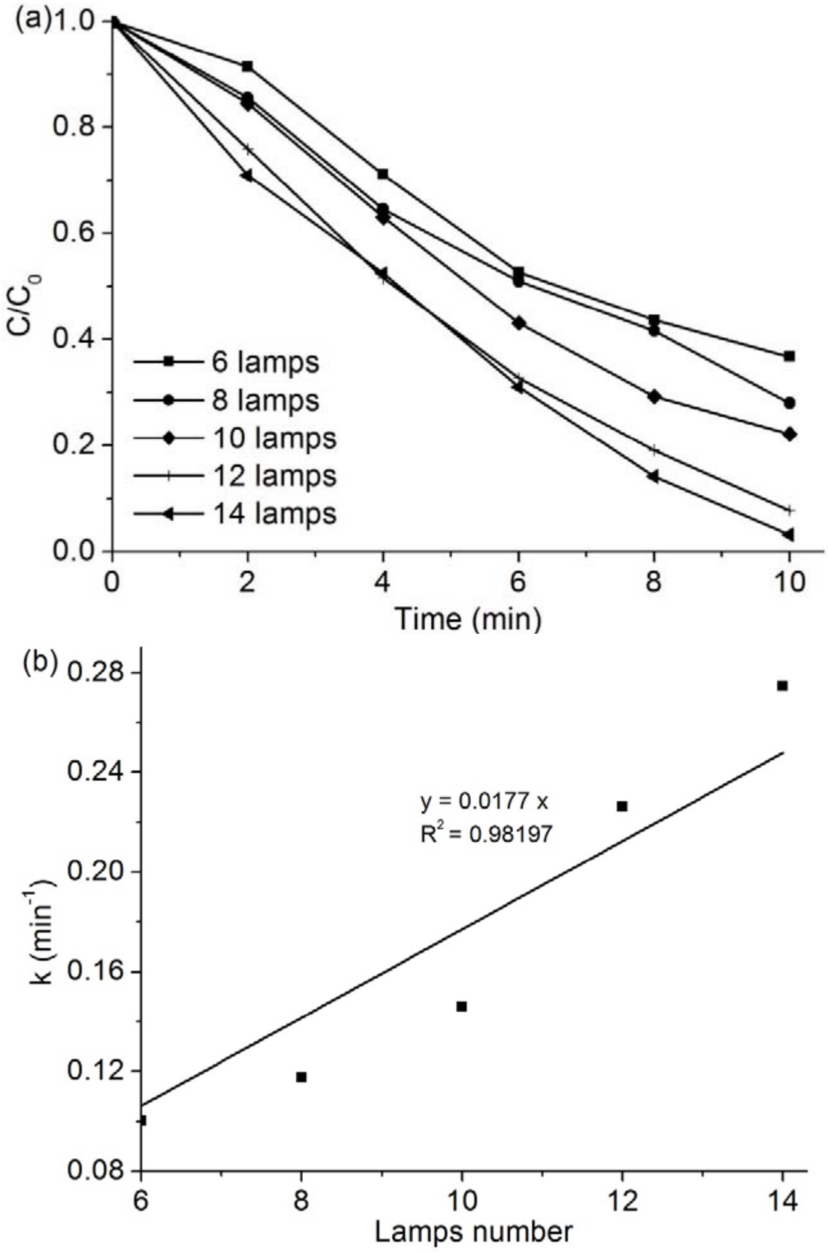

Figure 7-2 Ibuprofen photodegradation with varied UV intensity. (a) Ibuprofen destruction curves with different UV intensity (lamps number). (b) Destruction rate constant as a function of lamps number. *Experimental condition:* $[IBP]_0$ = 5 μM, Catalyst dosage = 0.5 g/L, UV lamps at 300 nm were employed.

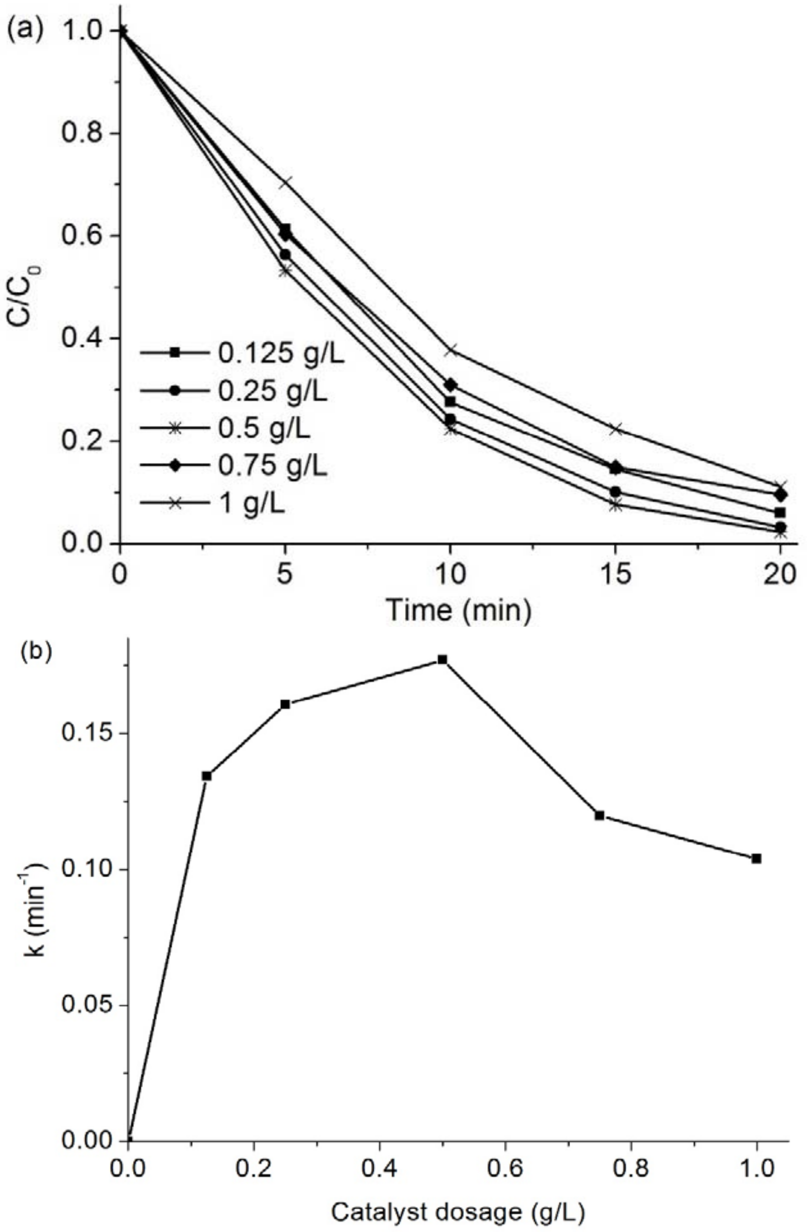

Figure 7-3 Ibuprofen photodegradation with varied catalyst dosages. (a) Ibuprofen degradation curves of ibuprofen under different catalyst dosages. (b) Destruction rate constant as a function of catalyst dosage. *Experimental condition:* [IBP]$_0$ = 5 µM, twelve 300 nm UV lamps were employed.

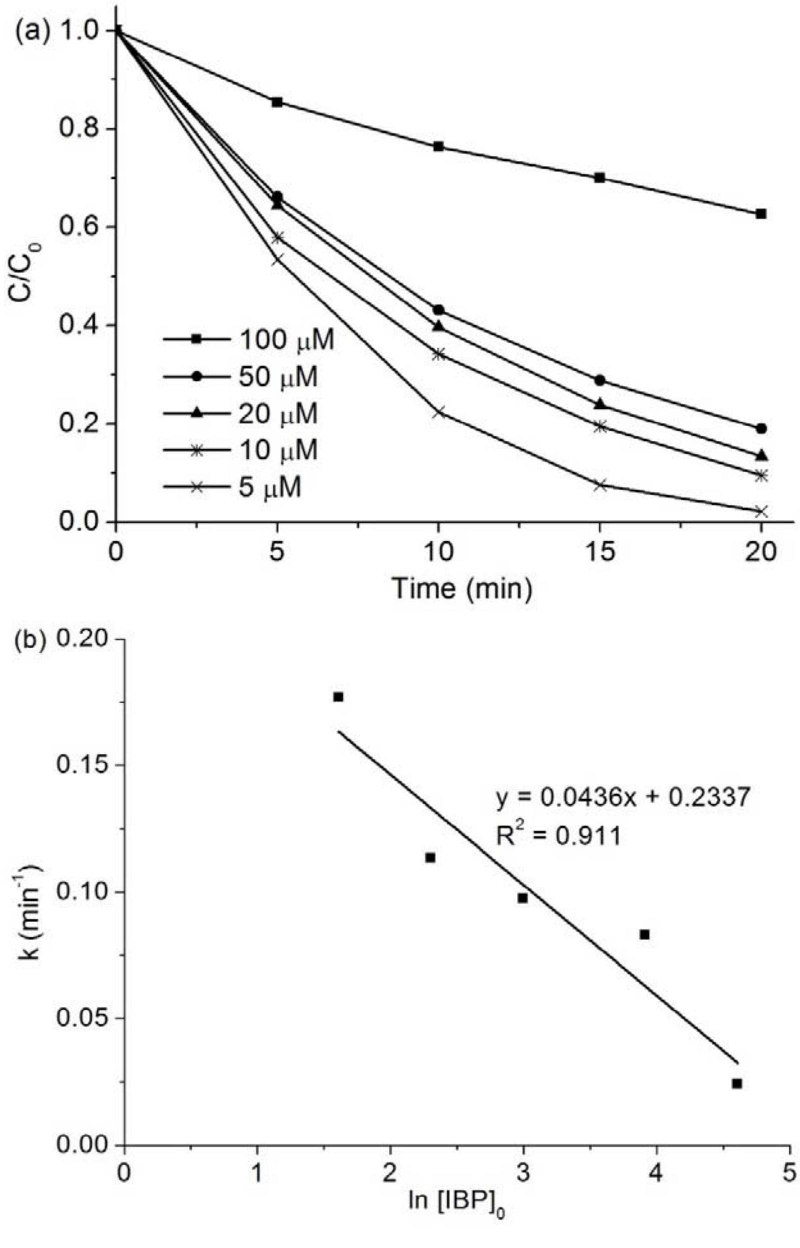

Figure 7-4 Photodegradation of ibuprofen at different initial concentrations. (a) Destruction curves of ibuprofen at different initial concentration ([IBP]$_0$). (b) Destruction rate constant as a function of [IBP]$_0$. Experimental condition: Catalyst dosage = 0.5 g/L, twelve 300 nm UV lamps were employed.

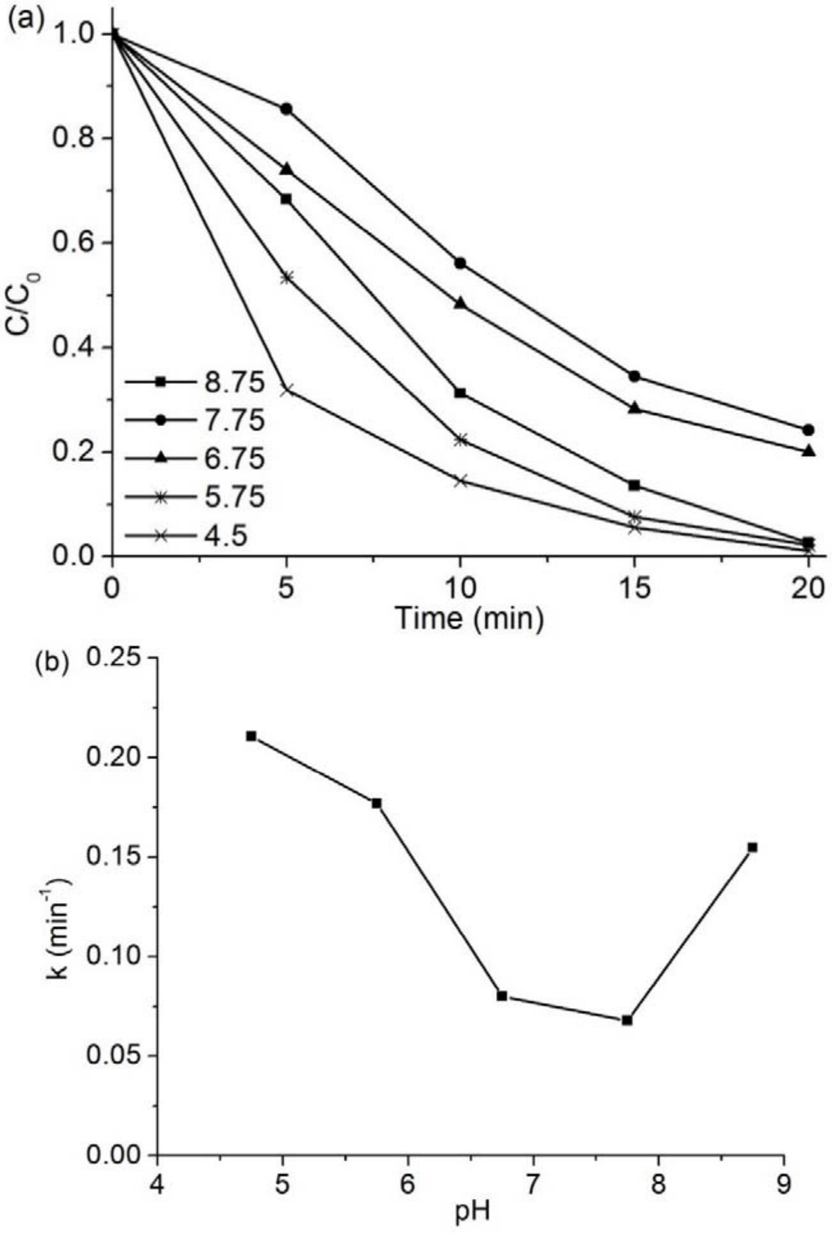

Figure 7-5 Ibuprofen degradation under varied initial pH values. (a) Destruction curves of ibuprofen under different initial pH values. (b) Destruction rate constant as a function of initial pH value. *Experimental condition*: $[IBP]_0$ = 5 µM, catalyst dosage = 0.5 g/L, twelve 300 nm UV lamps were employed.

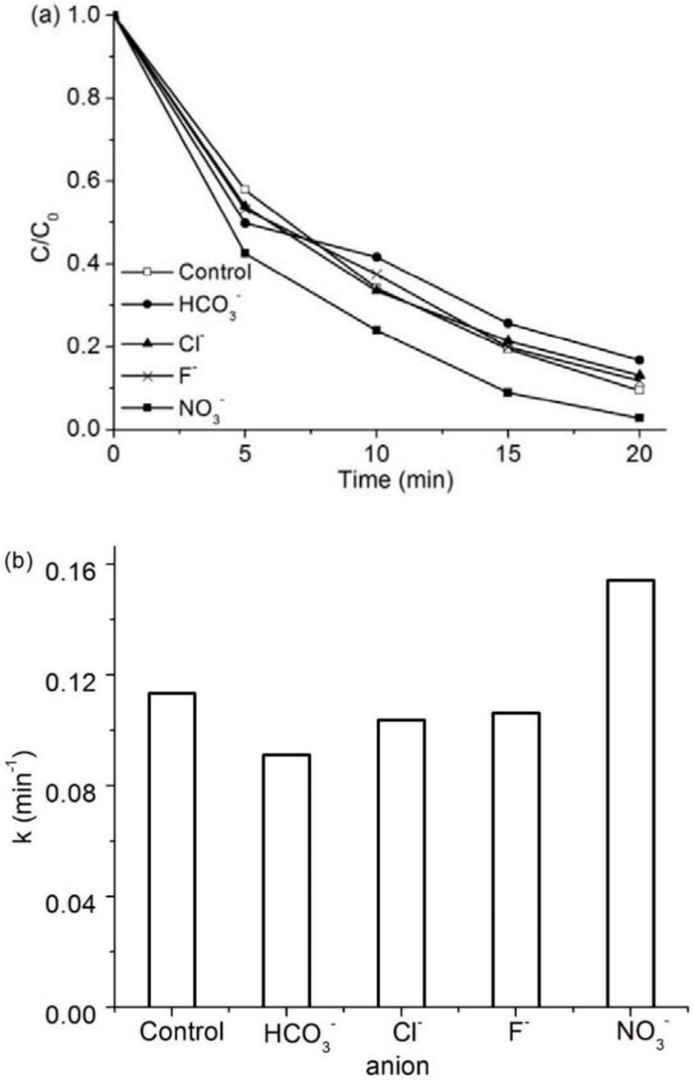

Figure 7-6 Effect of anions on the ibuprofen photodegradation. (a) Ibuprofen destruction curves with various anions. (b) Reaction rate constant with different anions. *Experimental condition:* [IBP]$_0$ = 10 μM, catalyst dosage = 0.5 g/L, [anion]$_0$ = 250 μM twelve UV lamps at 300 nm were employed.

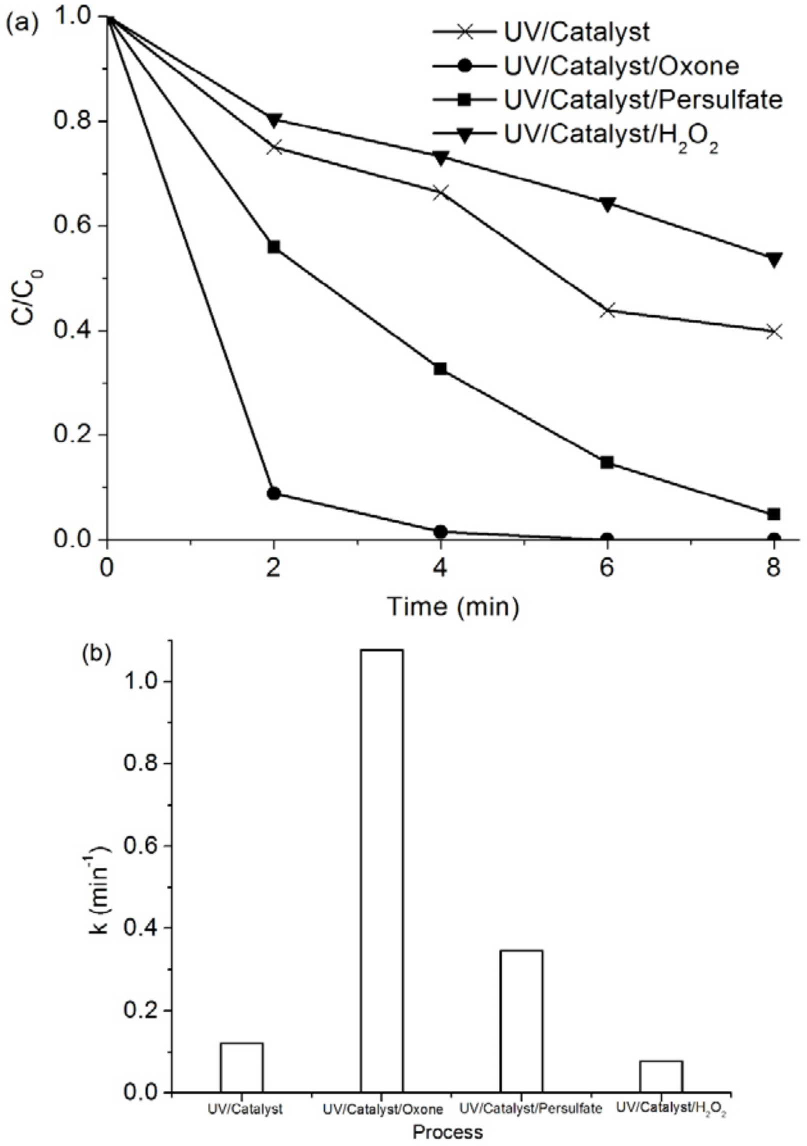

Figure 7-7 Effect of oxidants on the ibuprofen photodegradation. (a) Ibuprofen destruction curves with various oxidants. (b) Destruction rate constant under different treatment processes. *Experimental condition:* $[IBP]_0$ = 10 µM, catalyst dosage = 0.5 g/L, twelve UV lamps at 300 nm were employed.

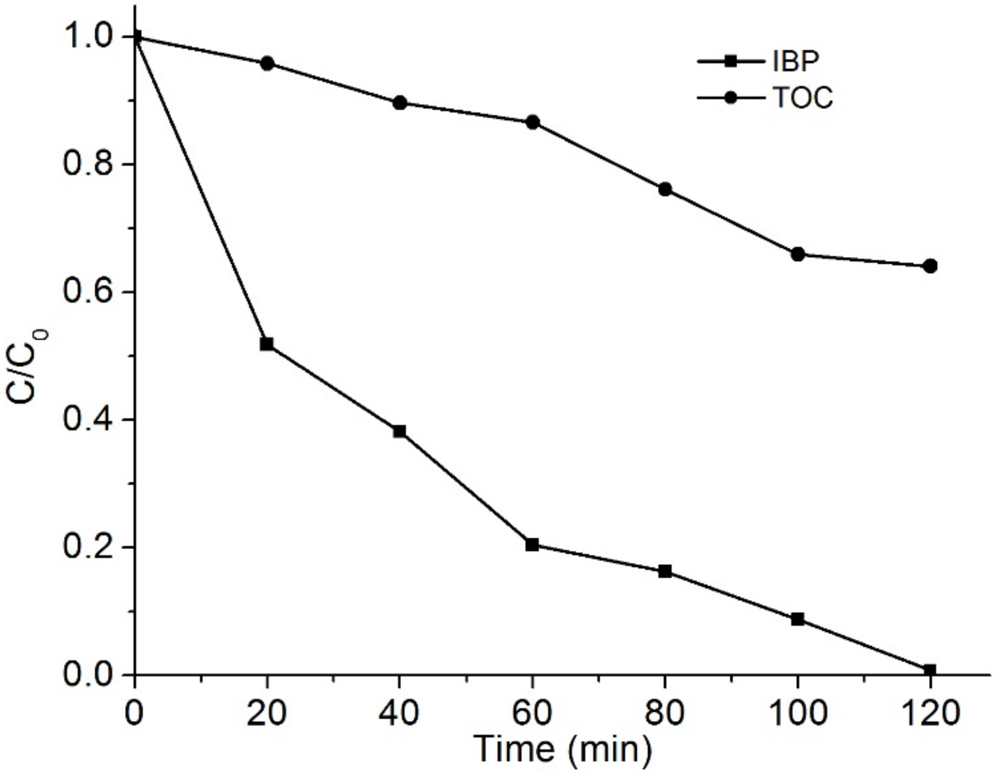

Figure 7-8 Ibuprofen destruction and TOC reduction under optimal conditions. *Experimental condition:* $[IBP]_0$ = 100 µM, catalyst dosage = 0.5 g/L, twelve 300 nm UV lamps were employed.

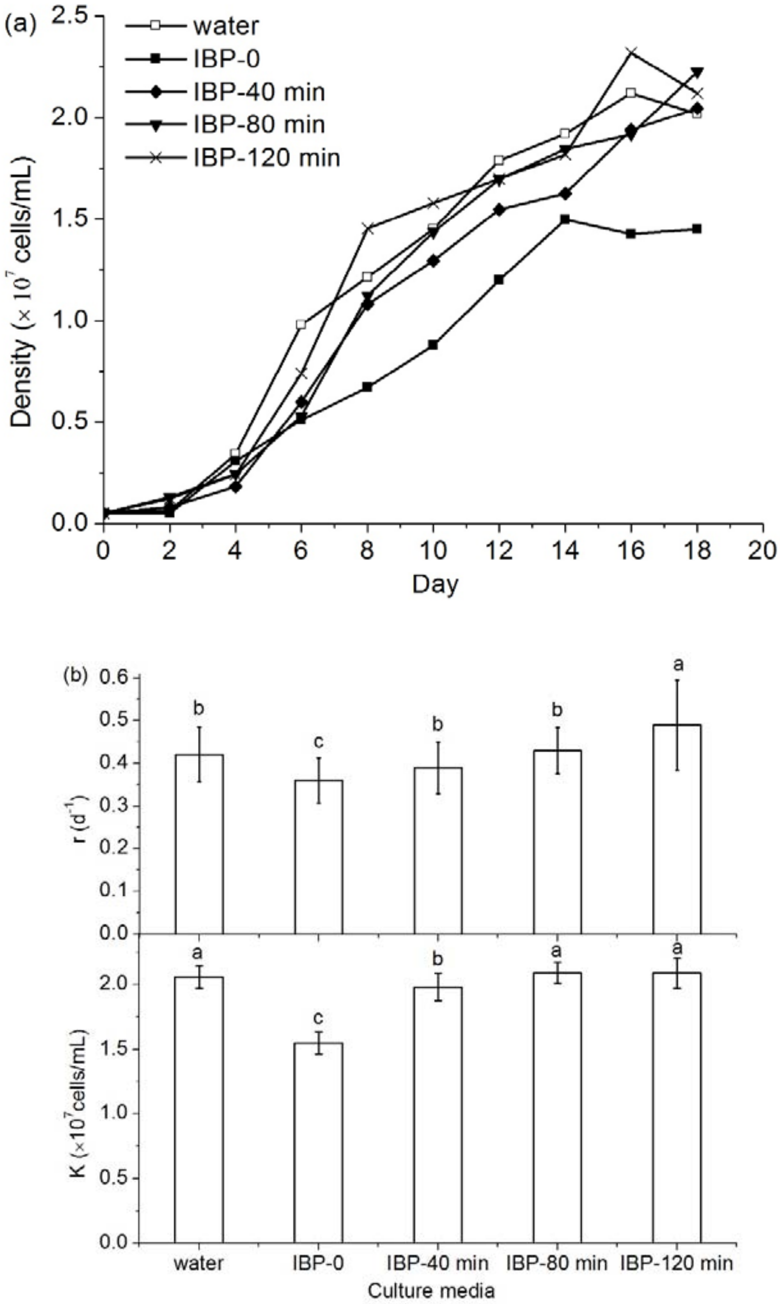

Figure 7-9 Effect of ibuprofen and the treated solutions obtained at different time on the growth of *Chlorella vulgaris*. (a) Growth curves of *C. vulgaris* in different culture media. (b) K and r values of *C. vulgaris* population growth.

8 Chapter eight Effect of permanganate on sulfamethoxazole degradation

8.1 Introduction

In Chapter five, it is proven that the photocatalysis process was efficient in SMX removal. In Chapter five and seven, the photodegradation process with the addition of the commonly used oxidant including ferrous, persulfate, oxone and hydrogen peroxide was studied. To date, scarce information was provided in previous studies on the transformation of SMX in the presence of permanganate. Moreover, whether the products still exhibit risk to life activities of aquatic organisms requires assessment. In this chapter, the effect of permanganate in SMX removal under the catalytic system was studied. Additionally, the identification and ecotoxicity evaluation of transformation products during SMX degradation under the treatment progress of photocatalysis with permanganate were carried out.

8.2 Results and discussion

8.2.1 Effect of reaction parameters on the photocatalytic performance

8.2.1.1 Role of permanganate in SMX degradation

From Figure 8-1, no significant SMX destruction was detected with sole permanganate, neither the combination of catalyst with permanganate. Further increase of the permanganate dosage ([Permanganate] : $[SMX]_0 = 20:1$) gave no significant improvement at all (data not shown), suggesting the limitation of sole permanganate application in water treatment.

However, as UV is used, the improvement of SMX degradation was identified. The removal efficiency of UV/Permanganate is higher than that of photolysis process, in which the UV has the potential to initiate the transformation of permanganate to lower valence state; SMX can be oxidized by the transformed permanganate and photolysis, simultaneously. The fastest SMX destruction occurred when UV, catalyst and permanganate coexist, this process will then be studied in details.

8.2.1.2 Effect of permanganate dosage on the photocatalytic performance

In Figure 8-2, the effect of permanganate dosage on SMX destruction in UV/Catalyst/Permanganate process was investigated. It is interesting to find that the reaction rate was not always continuously elevated with the increase of the permanganate dosage.

Compared to the photocatalysis process without permanganate, the reaction rate was increased as permanganate dosage increased from 0 to 5 μM. However, the reaction rate then showed a sudden drop at the permanganate dosage between 5-10 μM. Above 10 μM, the reaction rate showed a linear increase again and maximized at 100 μM. The further increase of the permanganate will retard the reaction.

From Figure 8-2 (b), the permanganate induced a fast SMX degradation at the first 20 mins, and then followed by a slower reaction, indicating that some byproducts (sourcing from permanganate) formed at later stage might hinder the reaction. To verify this, XRD analysis of the spent catalyst was conducted, and byproduct MnO_2 was identified on the surface of catalyst (Figure 8-2 d) (McMurdie and Golovato 1948).

It is believed that the MnO_2 can play both positive and negative roles in this process. As reported previously, MnO_2 generated from permanganate has the potential to catalyze the degradation of triclosan, 2-chloroplenol, 4-chloroplenol (pH 4-5) in-situ or ex-situ (Jiang et al. 2009). However, the catalytic ability is rather limited by pH levels. Increment of pH value would decrease the catalytic ability of MnO_2 significantly. Above pH value of 7, no significant catalytic effect was detected. The adherence of MnO_2 onto the catalyst may prohibit the contact of the target compound with the catalyst.

This assumption was confirmed by a separated test, where the decrease of removal efficiency with the recycled catalyst was observed (Figure 8-2 e). To make a fair test, the catalyst separated and dealt with the same procure from the reaction system after SMX degradation under the process UV/Catalyst was used as the control group. The two recycled catalyst was introduced to SMX solution respectively, and then SMX removal efficiency under the treatment process UV/Catalyst was examined. The result showed that the former catalyst showed a much poorer performance compared to the latter one because of the adhered MnO_2. The result explains the drop of the reaction rate at certain [permanganate], where the adverse effect of MnO_2 surpassed the oxidation process. Similar result has been reported in the butylparaben decomposition by Ru/CeO_2 with the assistance of permanganate, where MnO_2 was detected by TEM image on the surface of the catalyst and the removal efficiency was decreased owing to MnO_2 (Zhang et al. 2013b).

It should be noted that the formation of MnO_2 on the surface of catalyst is likely limited to a thin layer of maybe few molecules, which will not significant hinder the photocatalytic process and therefore, the reaction rate increased again when the [Permanganate] is higher than 10 μM.

During the process, the dosage of consumed permanganate is constant in spite of initial permanganate dosage. For instance, around 40 μM and 10 μM permanganate were used during the first 20 mins and the second 20 mins, and the total consumption was about 100 μM in 50 mins. Therefore, the shortage of permanganate contributes to the other reason for the adverse effect of processes with permanganate below 100 μM.

For SMX treatment under the process UV/Catalyst/200 μM [permanganate], the removal efficiency was higher than that with 10 or 20 μM permanganate because of the sufficient permanganate. However, the removal efficiency was lower than that with 50 μM permanganate at the first 20 mins but the value surpassed then after 40 mins. As mentioned above, a maximum of approximately 100 μM permanganate can be made used of during the reaction even the permanganate dosage higher than 100 μM. The overdosed permanganate played negative role due to the light attenuation, and that is possibly the reason accounting for the drop of reaction rate. After reaction time of 40 mins, the oxidation by permanganate may cover part of adverse effect by light attenuation.

Therefore, in the reaction system, sufficient permanganate played positive role, while byproduct MnO_2 and overdosed permanganate played negative roles. There is an optimal dosage for permanganate for the balance of positive and negative effect. From the above results, permanganate dosage of 100 μM was determined as the optimal condition in terms of reaction rate. However, permanganate dosage of 5 μM may be the other selection considering the recycled use of the catalyst.

Therefore, in a real application, proper selection of permanganate level is critical to maximize its performance, minimize the possible MnO_2 interference, and avoid causing the unwanted light attenuation effect.

8.2.1.3 Effect of pH value on the photocatalytic performance

The reaction rate in the pH range of 5-9 was evaluated to determine the optimal pH value. From Figure 8-3, apparently acidic environment gives higher removal efficiency, and the reasons are complicated as discussed below. At pH 5, SMX (with pK_{a1} and pK_{a2} at 1.8 and 5.6, respectively, Equation 8-1) is mainly in the neutral state, which has higher affinity to react with the hydroxyl radical compared to its negatively charged state at pH higher than 5.6.

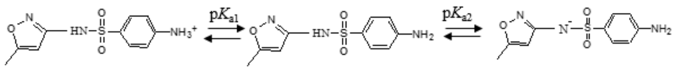

(Equation 8-1)

When the pH level went up to levels higher than 6.4 (pK_{a1} of H_2CO_3), the competition of hydroxyl radical between SMX and HCO_3^- ions (dissolved CO_2 in the reaction system) would retard SMX degradation (Rao and Chu 2013).

The continuous drop of reaction rate above pH level of 8 may be attributed to the ZPC of the catalyst (8.1) (Chen and Chu 2012). When the pH level is higher than 8.1, both the catalyst and SMX molecule are negatively charged. Approaching of SMX to the surface of the catalyst would be inhibited because of the repulsion force built between the same electric charged catalyst and SMX molecules. In this case, the degradation of SMX would be suppressed.

From the point of permanganate, another reason is that in acidic environment, permanganate has a higher oxidation potential (Fayad et al. 2013, Zhang and Guan 2013). As was reported previously, the oxidation potential of permanganate decreased from 1.30 V to 0.99 V from pH level of 5 to 9 (Zhang et al. 2014b). Therefore, lower the solution pH, faster the Redox process. It is also because of the quick consumption of proton in acidic medium (Equation 8-2), the bulk solution pH gradually approaches the neutral during the process. In basic environment, however, the proton consumption is no longer an issue, so the solution pH gradually dropped to neutral likely due to the formation and accumulation of low-molecular organic acids (e.g., formic acid).

$MnO_4^- + 4H^+ + 3e^- \longrightarrow MnO_2 + 2H_2O$ (Equation 8-2)

Another mechanism is that in acidic environment, the metal element (Co^{2+}/Fe^{2+}) in the catalyst may be transformed to its oxidized form (Co^{3+}/Fe^{3+}), which have good potential to initiate an indirect oxidation route (Equations 8-3 to 8-6) that further accelerate the SMX oxidation.

$Fe^{2+} + MnO_4^- \longrightarrow Fe^{3+} + MnO_2$ (Equation 8-3)

$SMX + Fe^{3+} \longrightarrow SMX\ (oxidized) + Fe^{2+}$ (Equation 8-4)

$Co^{2+} + MnO_4^- \longrightarrow Co^{3+} + MnO_2$ (Equation 8-5)

$SMX + Co^{3+} \longrightarrow SMX\ (oxidized) + Co^{2+}$ (Equation 8-6)

8.2.1.4 Effect of initial SMX concentration on the photocatalytic performance

Degradation of SMX at various initial concentration ($[SMX]_0$) under the process UV/ Catalyst/100 μM permanganate is shown in Figure 8-4. It was no surprise to find that the lower $[SMX]_0$, the higher the reaction rate. It is easy to understand that for solutions in lower $[SMX]_0$, more photon, radical and permanganate dosage are available for per SMX molecular. The pseudo first-order rate constant (k, min^{-1}) was found to be inversely proportional to $[SMX]_0$, which contributes to a good linear prediction of SMX photodegradation under different $[SMX]_0$ (Equation 8-7).

$$k = 3.34 / [SMX]_0 \ (R^2 = 0.99) \qquad \text{(Equation 8-7)}$$

8.2.2 Reaction mechanism of the photodegradation with permanganate

To reveal the reaction mechanism, LC/MS was performed to identify the transformation products and the possible destruction pathway. From the nine byproducts detected, four of them (C2, C6, C7 and C9), asterisked in Figure 8-5, are the first time being reported in the study of SMX degradation. Information of the detected intermediates including formula, mass, chemical structures, and the degradation pathways are proposed in Figure 8-5.

The parent compound SMX showed a molecular ion $[M+H]^+$ at 253.83 in MS spectrum. Among the organic intermediates detected, the molecular ion $[M+H]^+$ at 253.83 identified was supposed to be the isomer of SMX, resulting from the isomerization of O-N bond at the isoxazole ring. The other pair of isomers C2 and C3, with the molecular ion $[M+H]^+$ of 178.84 and at retention time of 15.7 and 18.5 min, were supposed to be originated from the cleavage of S-C bond of C1 and the parent compound (SMX), respectively. For C4 (*m/z* = 99.34 for $[M+H]^+$), a transformation product frequently detected in SMX degradation (Trovo et al. 2009a, Niu et al. 2013, Gao et al. 2014a, Guo et al. 2015), is proposed to be 3-Amino-5-methylisoxazole. It comes from the cleavage of S-N bond between sulfonyl group and the amine group in the sulfonamide group. The product C5 (*m/z* = 269.82 for $[M+H]^+$) suggested typical introduction of hydroxyl group and was therefore identified to be the monohydroxylated derivative of SMX. From the ion fragments of *m/z* at 114.03 and 157.85 (1+), it can be proposed that the attack of the hydroxyl radical occurred on the isoxazole ring. It is also commonly identified in SMX degradation with processes dominated by $OH^•$ radical (Abellán et al. 2007, Trovo et al. 2009a, Niu et al. 2013). The formation of C6 (*m/z* = 316.08 for $[M+H]^+$) consists of two mechanisms, i.e., hydroxylation and nitration of amino group in the benzene ring. The ion fragment of *m/z* at 186.85 (1+) demonstrated the transformation from $–NH_2$ to $–NO_2$. Dihydroxylated and nitrated derivatives of SMX possibly escaped from detection in this study since they were reported in previous studies (Trovo et al. 2009a, Gao et al. 2014a). Further oxidation of the isoxazole ring and dihydroxylation of C6 lead to the formation of C7, which was previously detected in SMX degradation by ultrasound/ozone oxidation process (Guo et al. 2015). Denitration of C7 results in the generation of C8, which may also come from oxidation of the isoxazole ring and deamination of SMX. Finally, the intermediate C9 was generated by oxidation of the isoxazole ring in SMX molecular.

Possible radicals contribute to the degradation are $OH^•$ and $O_2^{•-}$. To determine whether there is any change on dominant radicals after the introduction of permanganate, quenchers were introduced to the processes. Tert-butanol and trichloromethane are the effective scavenger for $OH^•$ and $O_2^{•-}$ with rate constants of $3.8\text{-}7.6 \times 10^8$ M^{-1} s^{-1} (Zhao et al. 2010) and 3×10^{10} M^{-1} s^{-1} (Watts et al. 1999, Teel and J.Watts 2002, Bae et al. 2013), respectively. Overdosed tert-butanol and trichloromethane (the mole ratio of quencher to oxidants is

1000:1) were introduced to the reaction, respectively. As is shown in Figure 8-6, for the two processes, quench of $OH^{\bullet}$ would result in significant reduction of reaction rate, while $O_2^{\bullet -}$ would not. This suggests $OH^{\bullet}$ dominates he SMX degradation.

To understand the mineralization of SMX and its daughter compounds, the concentrations of sulfate (SO_4^{2-}), ammonium (NH_4^+), nitrate (NO_3^-) and nitrite (NO_2^-) and TOC were determined. From the end product, about 27.3 μM sulfate was detected, accounting for approximately 55% of total sulfur mass. For the nitro generation, NH_4^+ can be released from the two amino groups, as well as the isoxazole ring, while NO_2^- and NO_3^- come from the isoxazole ring and the further oxidation of NH_4^+. The result shows that 62.8 μM i.e., about 42% of total nitrogen mass resulted in ammonium, while only 0.484 μM (or 0.3% mass), and 0.283 μM (or 0.19% mass) of nitrogen ended up as $[NO_3^-]$ and $[NO_2^-]$, respectively. The higher inorganic ions release in this study compared to that in UV/Catalyst process is consistent with the higher TOC reduction (67%, Figure 8-7), suggesting that a larger extent of SMX mineralization occurred. This is possibly due to the oxidation of small organic substance with the assistance of permanganate. Therefore, the use of permanganate can not only accelerate the reaction rate but also facilitate mineralization of SMX.

8.2.3 Toxicity evaluation of the end product of the treated SMX solution

In water treatment, the potential adverse effects of parent compounds, transformation products and the introduced reagents on the aquatic organisms should be considered; the toxicity variation of the treated effluent in the process is therefore accessed.

8.2.3.1 Effect of the end product on C. vulgaris

The effect of SMX and the degradation products on the algae *C. vulgaris* was examined. Judging from the calculated growth rate r given in Figure 8-8, the adverse/toxic effect of SMX on the growth of *C. vulgaris* was significantly decreased.

Compared to the toxicity evolution result from process without permanganate, the remaining toxicity may be caused by the residual permanganate. As reported previously, about 90% of algae cells died in four hours by 10 μM permanganate (Chen and Yeh 2005).

To examine the safe level of residual permanganate, the effect of permanganate at different concentrations was studied. The result showed that the observed non-effective concentration is around 1 μM (Figure 8-8 b), where the permanganate can even promote the algae growth, since trace concentrations of manganese can serve as nutrition for algae growth (Provasoli 1958). Inhibition was observed as the concentration higher than 2 μM. Though permanganate can be transformed to MnO_2 under solar light, the transformation product MnO_2 was suggested to have adverse effect on the algae growth (Chen and Yeh 2005). That could be the possible reason accounting for the residual toxicity even after the permanganate is consumed. This may be a potential threat to the aquatic organisms applying permanganate to the water treatment. Permanganate over the concentration of 10 μM is colorable and can be detected. However, for permanganate below the detectable limit, the concentration should be determined by other methods. The toxicity test reveals that it is necessary to detect the permanganate concentration in the effluent water in application of permanganate in water treatment. On the other hand, this may be an advantage in case of eutrophic wastewater, where permanganate can play the roles of oxidizing organic pollutants and inhibiting the algae bloom.

It should be noted that apart from the permanganate, the intermediates may partly contribute to the overall adverse effect. However, as the separate standard chemicals of these intermediates are unavailable, no fair test can be done. Besides, some intermediates may escape from our detection. Therefore, the adverse effect of the final product on algae growth may attribute to more than one reason.

8.2.3.2 Effect of the end products on A. salina

In Chapter four, it has been reported that 50 μM of SMX gave no threat to the survival of *A. salina*, while the toxic effect due to the end products to the test organisms is yet unknown. Two frequently intermediates 4-NO_2 and –OH-SMX were reported to have inhibitions on the growth of bacteria *V. fischeri* (Majewsky et al. 2014). However, in this study, no mortality was observed in terms of the end product (data not shown). The ingestion of *A. salina* is significantly better than that of end product from the photocatalysis treatment without permanganate (i.e., UV/$CoFe_2O_4/TiO_2$, Figure 8-8 c), indicating the presence of permanganate in the photocatalysis process contributes the elimination of some toxic products. This is coincident with the higher TOC reduction obtained. For the good sake of both algae growth and ingestion of *A. salina*, longer treatment time may be needed for a thorough mineralization and elimination of possible toxic byproducts.

8.3 Summary

SMX decomposition under the photocatalysis system combined with permanganate was explored in this paper. SMX degradation was negligible by sole permanganate but can be accelerated in the photocatalysis system with the assistance of permanganate. However, permanganate may also slow down the photocatalytic degradation at a small range of dosages owing to the formation of thin layers of MnO_2 at the catalyst surface, and/or light attenuation when permanganate is overdosed. Acidic environment is favorable for SMX degradation. Reaction rate of SMX at different initial concentration was predicable by a proposed equation $k = 3.34 / [SMX]_0$ ($R^2 = 0.99$). Nine intermediates and four pathways were proposed for SMX degradation. About 55% of total sulfur was released as sulfate, and 42%, 0.3%, 0.19% of total nitrogen mass resulted in ammonium, nitrate and nitrite, respectively. Approximately 67% TOC reduction was achieved in 50 min, a more thorough mineralization is possible at longer reaction time. The toxicity of SMX to the algae growth and the feeding of *A. salina* was significantly reduced after the treatment. The concentration of residual permanganate is suggested to be monitored and controlled for its possible threat to the algae growth.

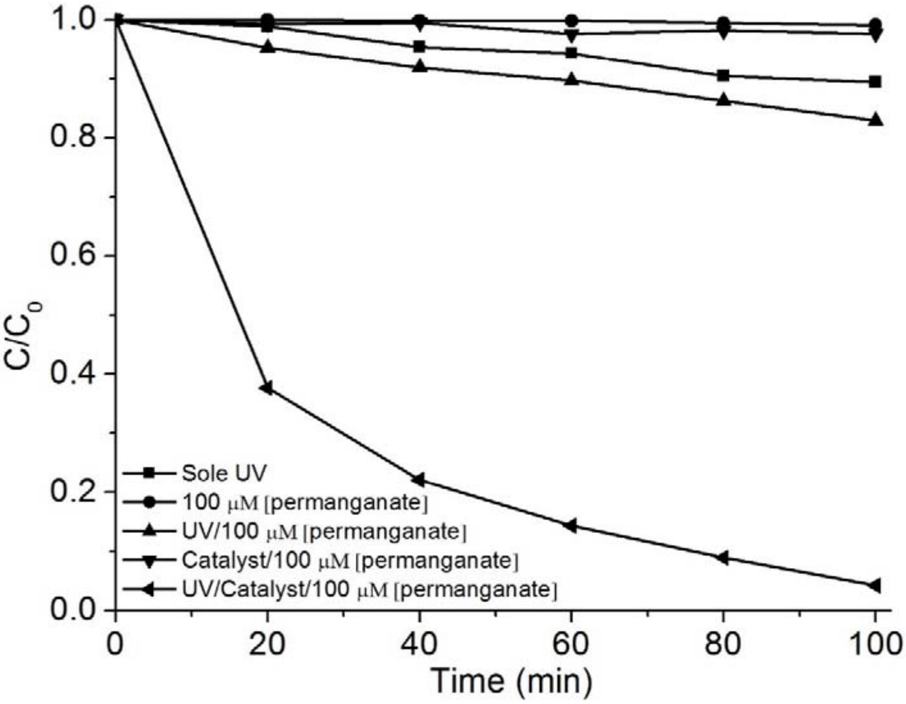

Figure 8-1 Role of permanganate in the reaction. *Experimental condition:* $[SMX]_0$ = 50 μM, catalyst dosage = 0.5 g/L, twelve UV lamps were employed.

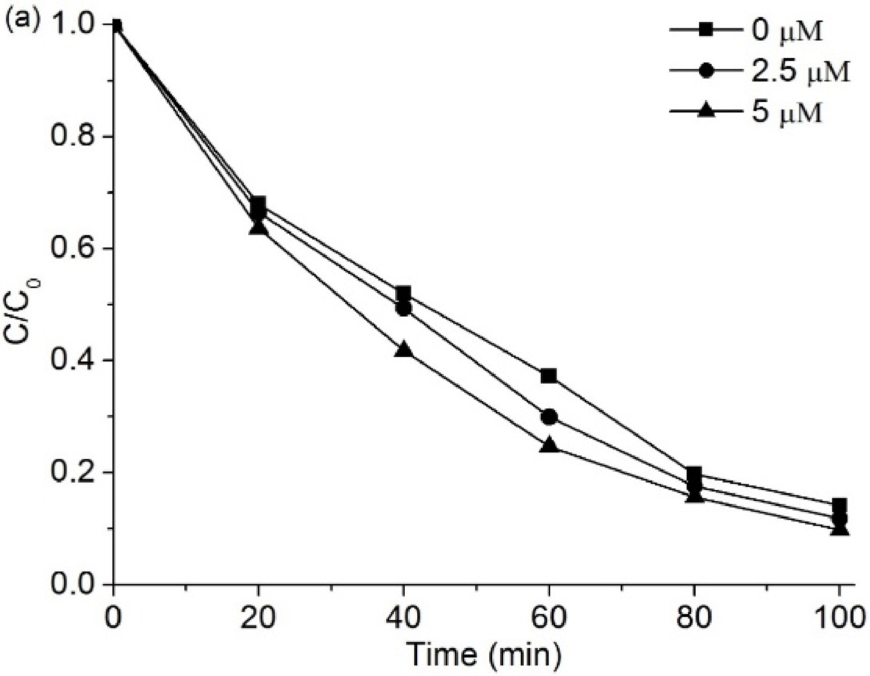

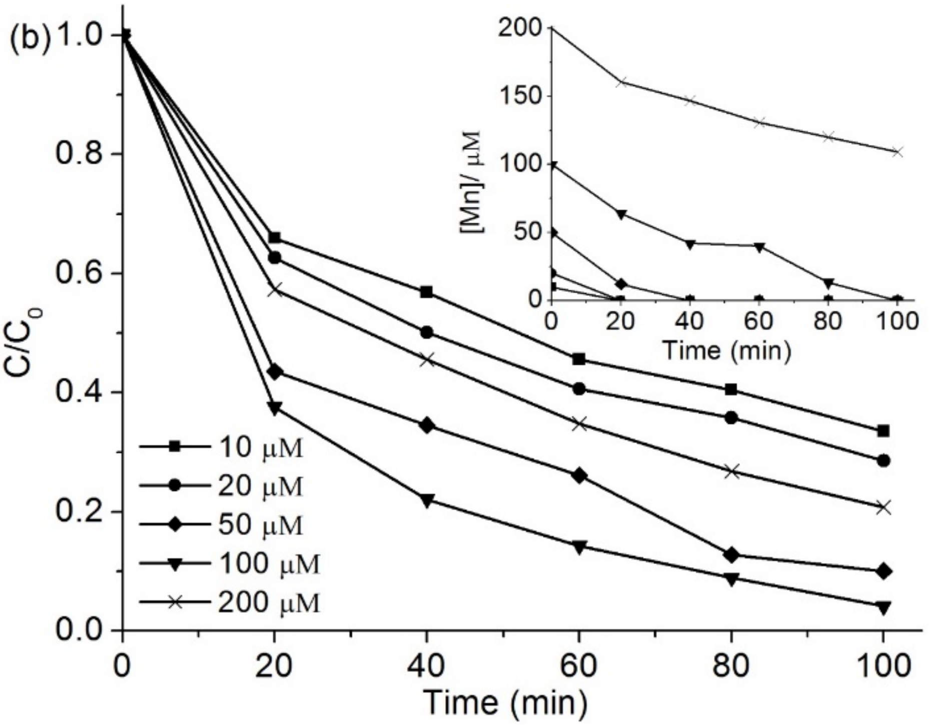
(b)
1.0
0.8
0.6
0.4
0.2
0.0
C/C$_0$
0
20
40
60
80
100
Time (min)
10 μM
20 μM
50 μM
100 μM
200 μM
200
150
100
50
0
[Mn]/ μM
0
20
40
60
80
100
Time (min)

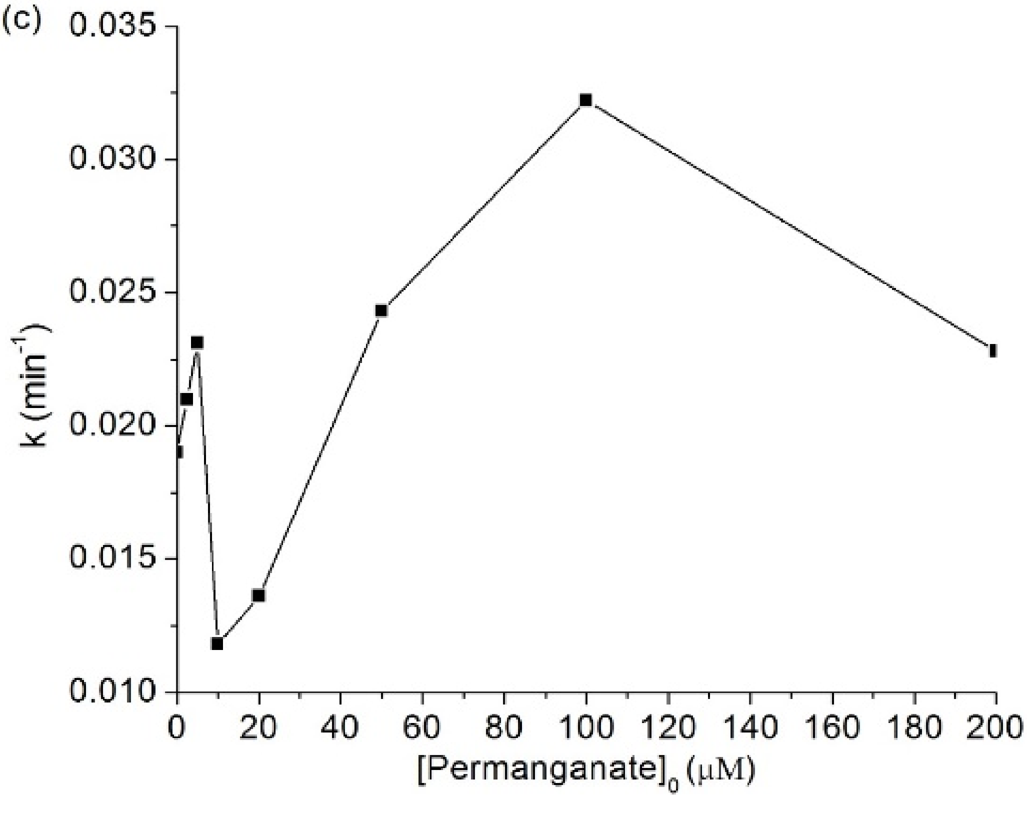
(c)
0.035
0.030
0.025
0.020
0.015
0.010
k (min^{-1})
0
20
40
60
80
100
120
140
160
180
200
[Permanganate]$_0$ (μM)

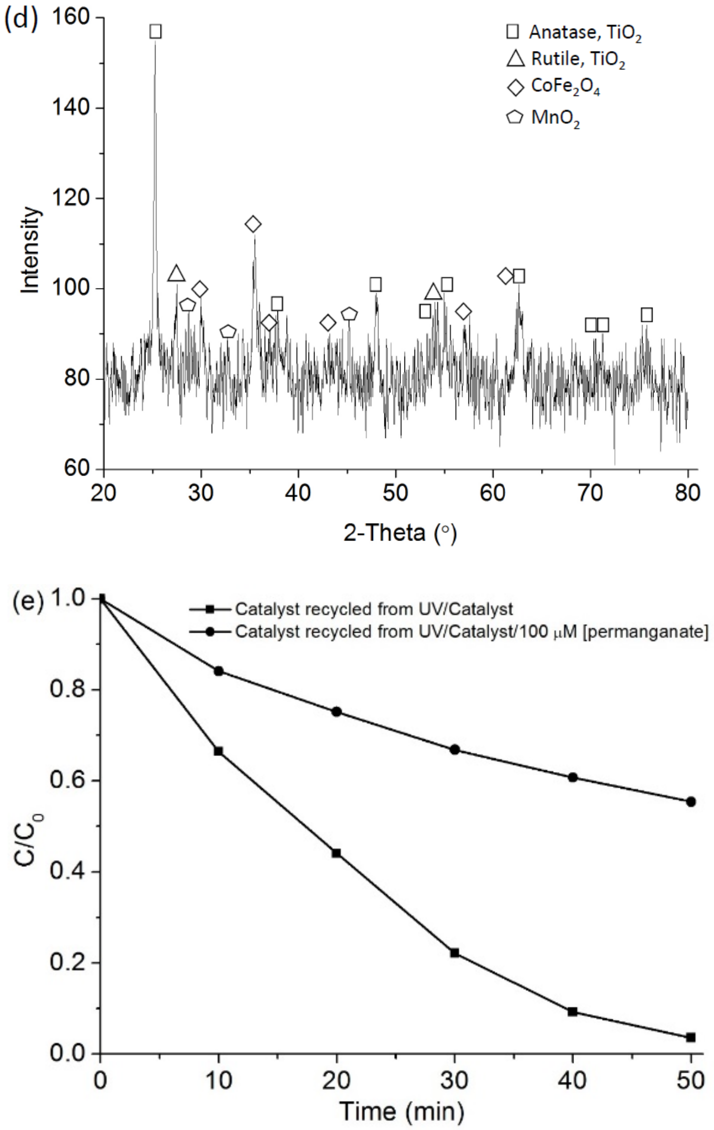

Figure 8-2 Effect of permanganate dosage on the reaction rate. (a, b, c) Sulfamethoxazole degradation under UV/Catalyst/Permanganate process with different permanganate dosage. (d) XRD spectra of recycled catalyst. (e) Sulfamethoxazole degradation under UV/Catalyst with recycled catalyst from UV/Catalyst/100 μM [permanganate]. *Experimental condition:* catalyst dosage = 0.5 g/L, twelve UV lamps were employed. (a, b, c) $[SMX]_0$ = 50 μM, (e) $[SMX]_0$ = 5 μM.

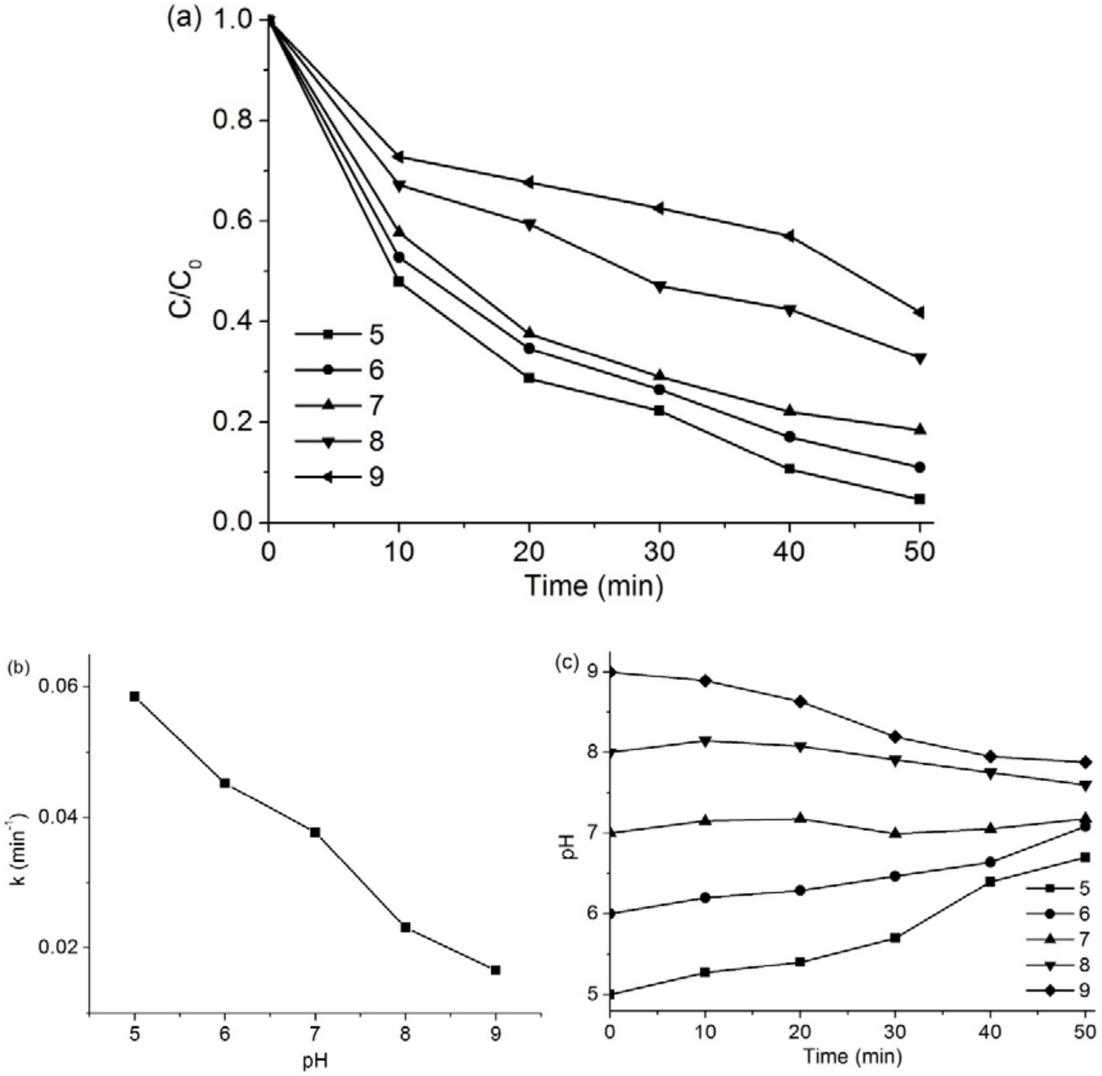

Figure 8-3 Sulfamethoxazole destruction by the process UV/Catalyst/Permanganate with varied pH values. (a) Sulfamethoxazole destruction curves with varied pH values. (b) Sulfamethoxazole destruction rates in terms of pH value. (c) The change of pH value during the treatment process. *Experimental condition:* $[SMX]_0$ = 50 μM, catalyst dosage = 0.5 g/L, [permanganate] = 100 μM, twelve UV lamps were employed.

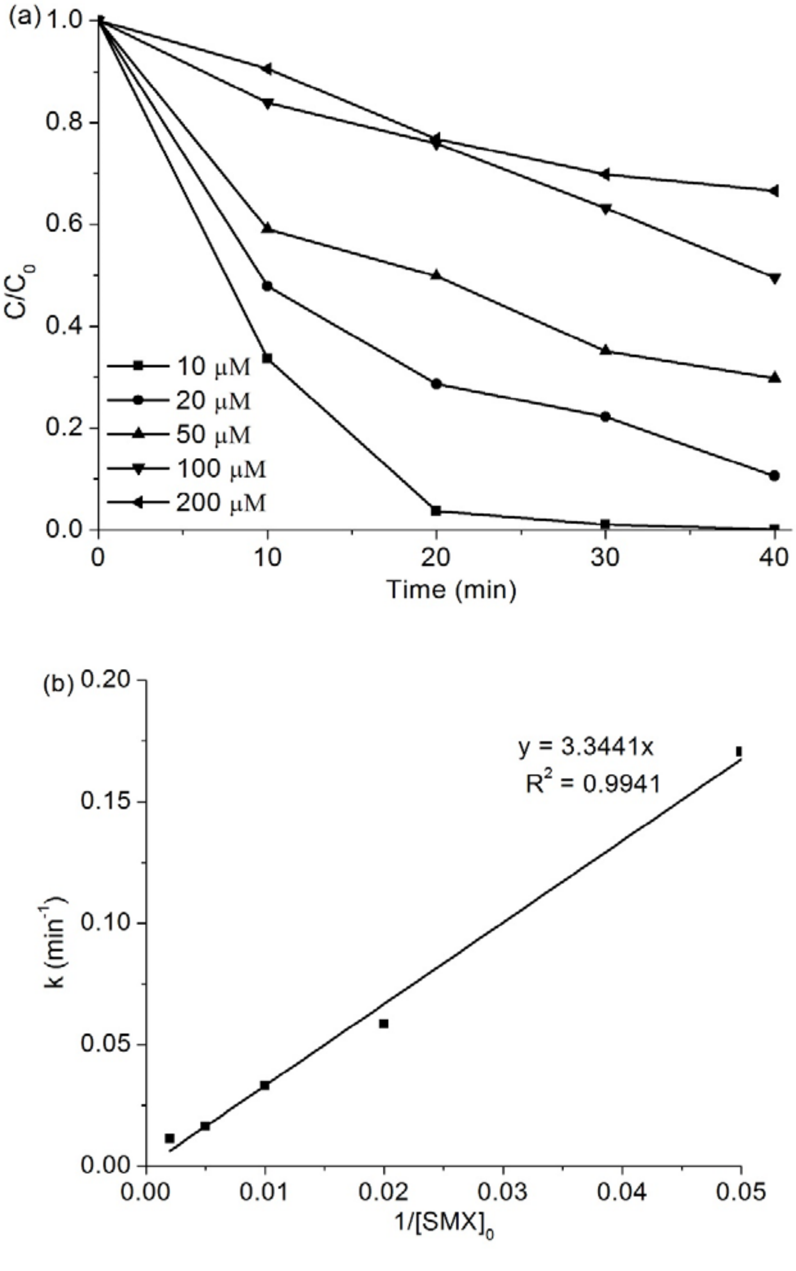

Figure 8-4 Destruction of sulfamethoxazole at varied initial concentrations by the process UV/Catalyst/Permanganate. (a) Destruction curves of sulfamethoxazole at different concentrations. (b) Destruction rates in terms of sulfamethoxazole initial concentration. *Experimental condition*: catalyst dosage = 0.5 g/L, pH = 5, twelve UV lamps were employed.

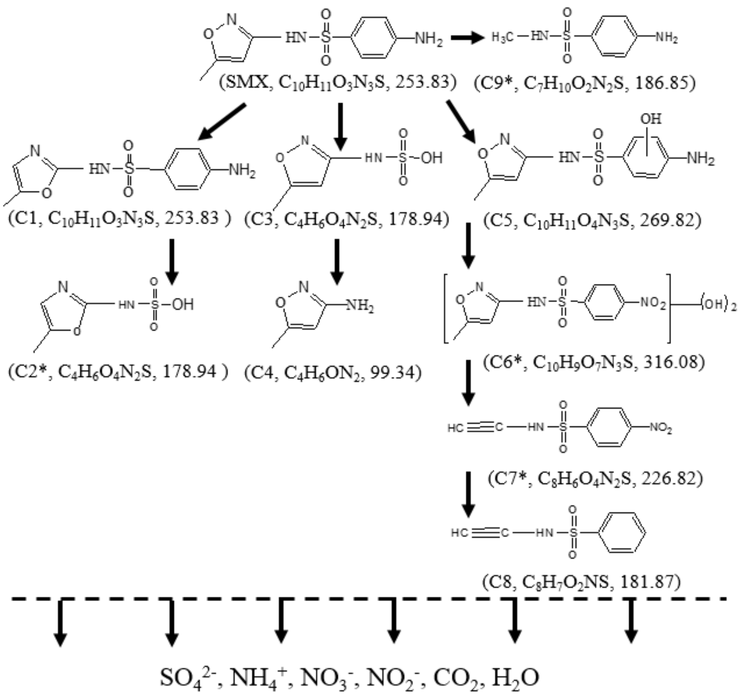

Figure 8-5 Destruction pathway during the process UV/Catalyst/Permanganate. (* indicates newly reported intermediates during sulfamethoxazole degradation.)

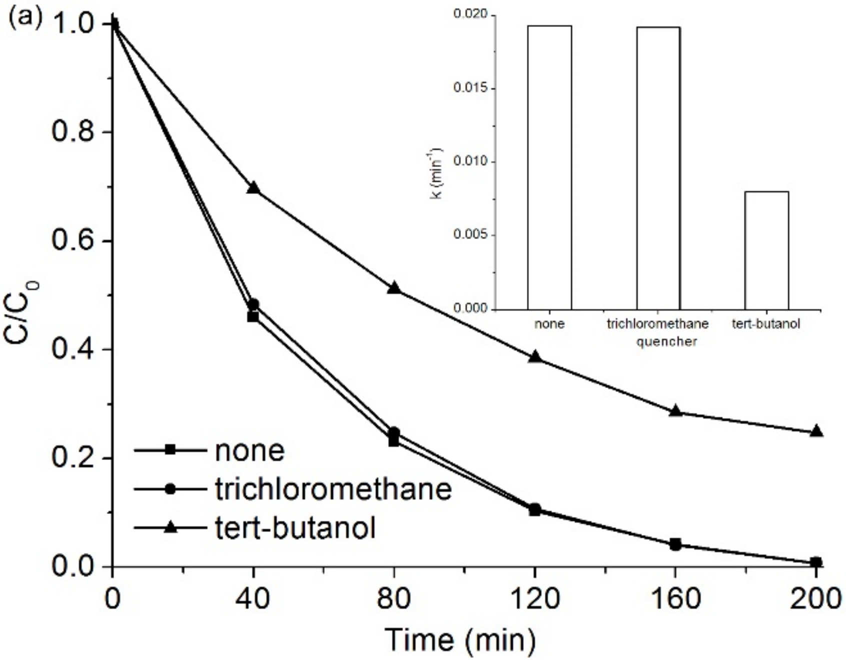

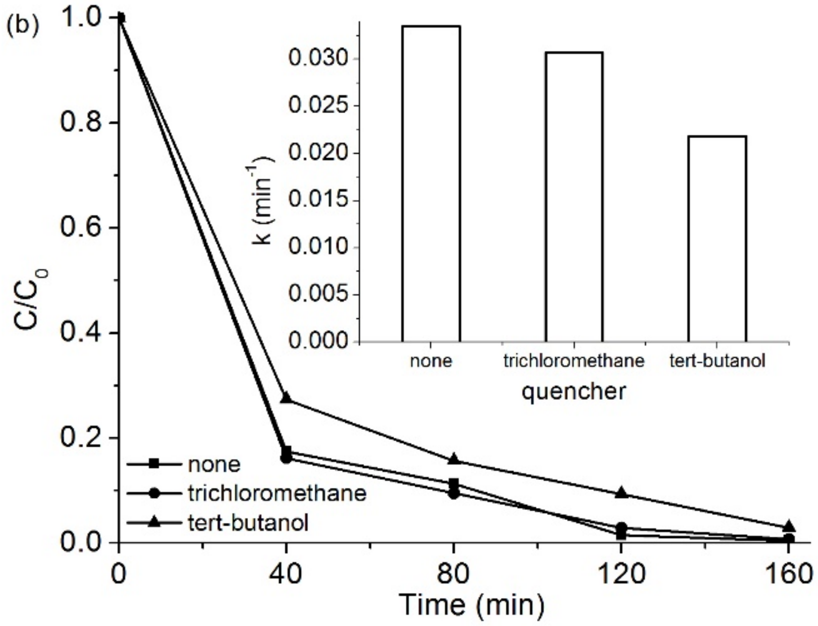

Figure 8-6 Determination of the dominant radical in the reaction. (a) Quench test of process UV/Catalyst. (b) Quench test of process UV/Catalyst/100 μM [permanganate]. Experimental condition: twelve UV lamps were employed. $[SMX]_0$ = 50 μM, catalyst dosage = 0.5 g/L.

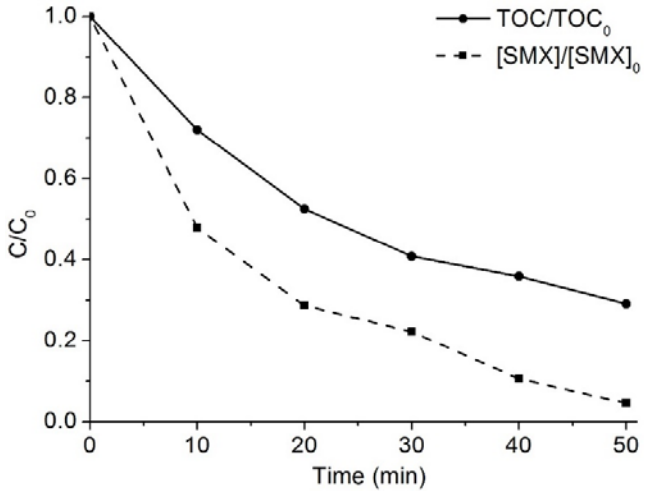

Figure 8-7 TOC reduction during the reaction. *Experimental condition:* $[SMX]_0$ = 50 μM, catalyst dosage = 0.5 g/L, [Permanganate] = 100 μM, twelve UV lamps were employed.

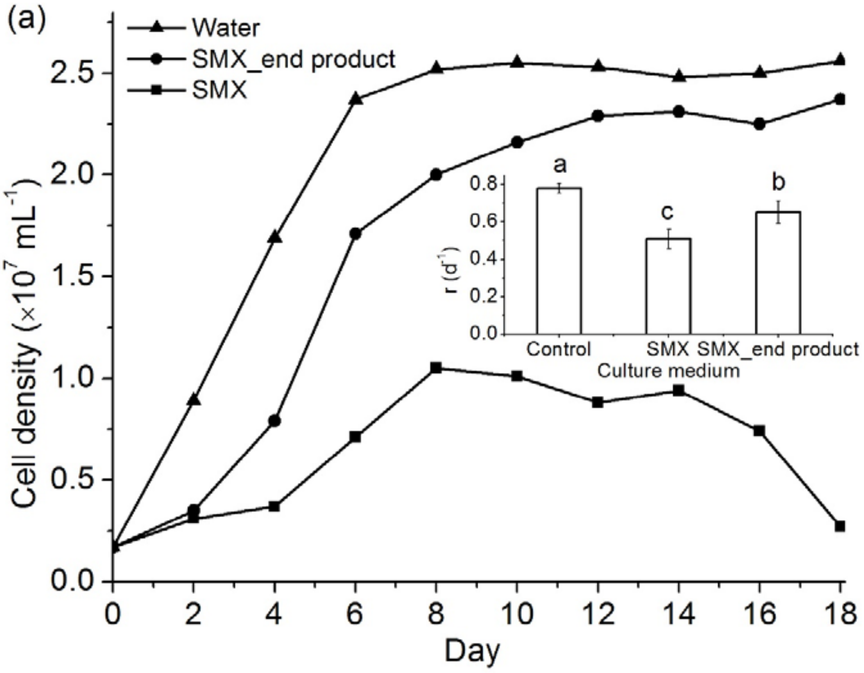
(a)
Water
SMX_end product
SMX
Cell density (×10^7 mL^-1)
0.0
0.5
1.0
1.5
2.0
2.5
0
2
4
6
8
10
12
14
16
18
Day
r (d^-1)
0.0
0.2
0.4
0.6
0.8
a
c
b
Control
SMX
SMX_end product
Culture medium

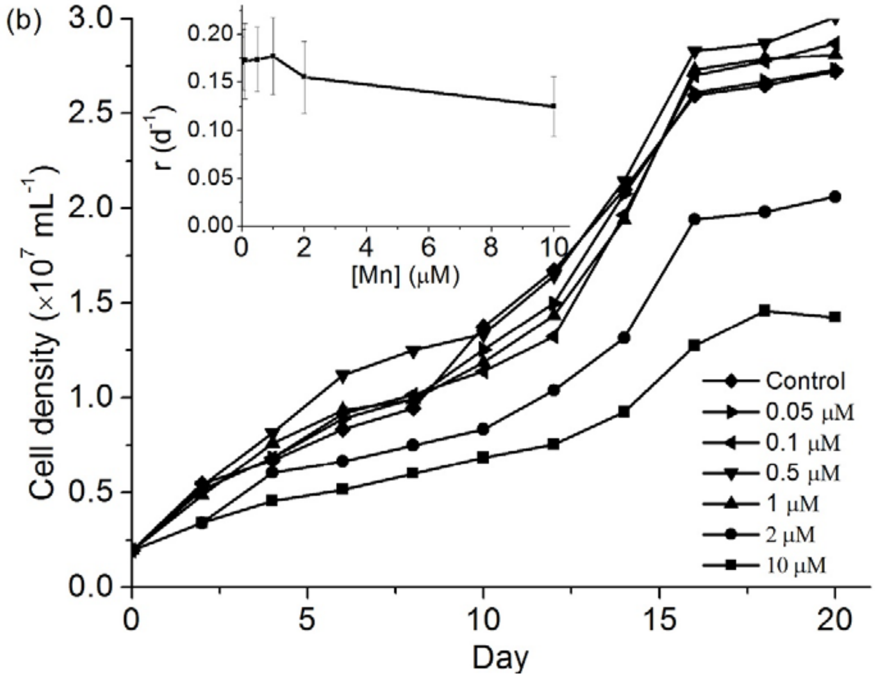
(b)
Cell density (×10^7 mL^-1)
0.0
0.5
1.0
1.5
2.0
2.5
3.0
0
5
10
15
20
Day
r (d^-1)
0.00
0.05
0.10
0.15
0.20
0
2
4
6
8
10
[Mn] (μM)
Control
0.05 μM
0.1 μM
0.5 μM
1 μM
2 μM
10 μM

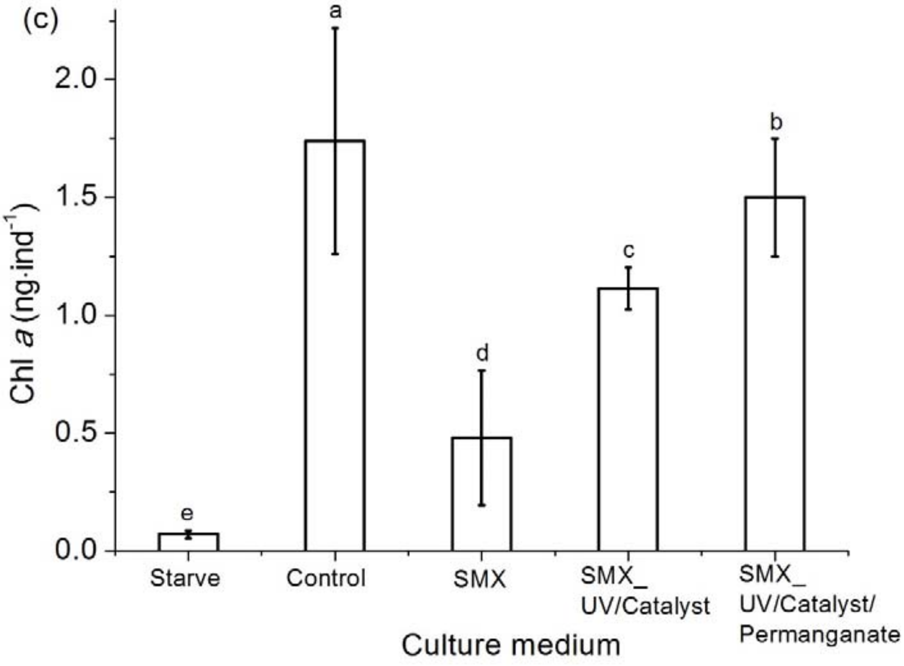

Figure 8-8 Effect of the obtained final product on *Chlorella vulgaris* and *Artemia salina*. (a) Algae growth exposed to the end product of the treated sulfamethoxazole. (b) Algae growth exposed to different concentrations of permanganate. (c) Feeding of *A. salina* exposed to different culture media.

9. Chapter nine Conclusions and recommendations

9.1 Conclusions

In this study, the removal efficiency, TOC reduction and toxicity evolution of pharmaceuticals during the photodegradation by UV/$CoFe_2O_4$/TiO_2 was investigated. To be specific, the effect of reactions parameters (light source, light intensity, catalyst dosage, solution pH and initial concentration of the target compounds), the effect of anions, the effect of oxidants, the reaction mechanisms (organic intermediates detection, TOC reduction, inorganic ions release) and the toxicity of the treatment products to *C. vulgaris* and *A. salina* were determined.

9.1.1 Properties of the catalyst

The catalyst was demonstrated to be homogenous spherical aggregates. The phases of $CoFe_2O_4$, anatase TiO_2 and rutile TiO_2, and the atomic ratios of Co, Fe, Ti and O from the catalyst were well justified. Reduced band gap energy and increased specific surface area compared to TiO_2 was found for the obtained catalyst. The average particle size and the ZPC value was determined to be around 30 nm and 8.0, respectively.

The photocatalyst was easily to be separated from the solution, indicating good magnetic property. The recycling tests proved that the photocatalytic activity of the recycled catalyst remains intact even after 5 times of reuse.

The photocatalyst was found stable within the pH range of 5.2 and 8.8, while TiO_2 leaching would only occur at extreme acidic or alkali environment.

9.1.2 The effect of reactions parameters and anions on the photodegradation

The photodegradation of the pharmaceuticals was found to be a pseudo first-order kinetics. The reaction conditions at UV wavelength of 300-350 nm, the catalyst dosage of 0.5 g/L and acidic pH level were favorable for the photodegradation of the pharmaceuticals. Besides, higher light intensity or lower initial concentration of the parent compounds result in higher removal efficiency. The observed rate constants are predictable by a proposed model in terms of the initial concentration of the target compounds.

The tested anions, Cl^-, F^- and CO_3^{2-} included, showed adverse effects on the removal efficiency of IBP, while NO_3^- accelerated the photodegradation significantly.

9.1.3 The effect of oxidants on the photodegradation

The removal efficiency of IBP was significantly elevated with the addition of oxone or persulfate, and the reaction was faster in the presence of oxone than the same concentration of persulfate. However, the reaction was significantly slowed down with the introduction of H_2O_2.

Photodegradation was accelerated in the photocatalysis system with the assistance of ferrate and permanganate. However, ferrate and permanganate also slowed down the photocatalytic degradation at certain dosages.

The presence of permanganate contributes for a more thorough mineralization according to the detected intermediates, the higher inorganic ions release, the higher TOC reduction and the better ingestion of *A. salina*. The toxicity of SMX to the algae growth was significantly reduced but not totally eliminated due to the residual permanganate.

9.1.4 Reaction mechanisms during the photocatalysis process

About 50%, 45% and 35% TOC was eliminated as the target compounds SMX, AP and IBP were removed completely by the photocatalysis process, respectively. The radical OH· and hydroxylated products are the dominant radical and transformation intermediates during the photodegradation.

For SMX destruction, sixteen intermediates were detected, and four of them were newly reported in the degradation of SMX. About 45% of the total mass sulfur source transformed to sulfate ion, and around 25%, 1%, and 0.25% of the total nitrogen transformed to ammonium, nitrogen, and nitrite ions. Four main pathways during the degradation, i.e. hydroxylation, cleavage of S-N bond, nitration of amino group, and isomerization were proposed.

Upon the photodegradation of AP, ten organic intermediates were identified, and five of them were newly reported in AP treatment process. 60% ammonia release were identified during the process. Hydroxylation, demethylation and the cleavage of the pentacyclic ring were included in the decomposition pathways.

9.1.5 Toxicity evolution of the treated pharmaceuticals

Generally, the toxicity of the treated solution was significantly reduced compared to that of the parent compounds.

For the effect of the treated SMX solution on the algae growth, the SMX was transformed from a toxicant into nutrients gradually during the photodegradation. At the later stage of treatment, the K and r values were even higher those of pure water because of the release of inorganic substances and carbon source serving as nutrients. A small offset to the growth was observed likely due to the generation of a toxic intermediate, sulfanilamide, which fortunately can be quickly destructed in the process. The parent compound AP and its degradation products show positive effects on the growth of the algae. The adverse effect of the parent compound IBP to *C. vulgaris* was gradually eliminated with the decomposition of IBP.

For the effect on the brine shrimp, no mortality was found, but the feeding of the brine shrimp was inhibited by the SMX and its intermediates. The clearance rate increased during the process but was still lower than that of the control group, suggesting the adverse effect was gradually reduced but not eliminated. Therefore, longer degradation time may be needed for the total toxicity removal. Moreover, acute toxicity of AP to brine shrimps *A. salina* was eliminated with the destruction of AP. No adverse effect was detected for the survival and the feeding of *A. salina* exposed to IBP and the degradation products.

The results suggest that the process UV/$CoFe_2O_4/TiO_2$ can be an effective way on removal and toxicity reduction of refractory pharmaceuticals.

9.2 Limitations of this study and recommendations for future work

Firstly, experiments in this study were carried out under idealized conditions in lab-scale batch reactors. In real application, there are various chemicals or microorganisms in the background water or wastewater. In future work, the effects of more elements on the degradation efficiency should be taken into account. Therefore, experiments based on real wastewater in pilot-scale are recommended.

Secondly, though the red shift of the catalyst was observed based on DRS data, the degradation of the tested pharmaceuticals under 420 nm or/above was insignificant. Therefore, the catalyst can be further improved to shift the effective wavelength to the visible region. For example, incorporation of visible-activated material such as graphene can be tried.

Thirdly, in this study, most of the proposed intermediates are not available from the market. Most of the structures were obtained based on the LC/MS data, which may not be precise. Besides, the toxicity of the products was only limited to the overall treated solution but seldom referred to the separate toxicity of each intermediate. To obtain the accurate structures of the intermediates and the separate toxicity of each intermediate, attempts on intermediates synthesis in labs are recommended to be made. Additionally, the data of intermediates from IBP photodegradation is unavailable from LC/MS. Other method e.g., GC/MS is recommended to be tried.

Lastly, for the toxicity part, only growth of *C. vulgaris*, survival and feeding of *A. salina* were tested. Since organisms have variable sensitivity to different pharmaceuticals, it is advisable to conduct tests on more aquatic organisms at various tropic levels and more indicators of life activities (e.g., reproduction) to collect abundant data. Besides, the information on the impacts of common pharmaceuticals on aquatic organisms is still limited. It is suggested that the data of this part should be filled up and toxicity database be established.

References

Abbas, M., B. P. Rao, V. Reddy, and C. Kim. 2014. Fe_3O_4/TiO_2 core/shell nanocubes: single-batch surfactantless synthesis, characterization and efficient catalysts for methylene blue degradation. Ceram. Int. **40**:11177-11186.

Abellán, M. N., B. Bayarri, J. Giménez, and J. Costa. 2007. Photocatalytic degradation of sulfamethoxazole in aqueous suspension of TiO_2. Appl. Catal. B-Environ. **74**:233-241.

Abellan, M. N., W. Gebhardt, and H. F. Schroder. 2008. Detection and identification of degradation products of sulfamethoxazole by means of LC/MS and -MSn after ozone treatment. Water Sci. Technol. **58**:1803-1812.

Afzal, A., J. Kang, B.-M. Choi, and H.-J. Lim. 2016. Degradation and fate of N-nitrosamines in water by UV photolysis. Int. J. Greenh. Gas Con. **52**:44-51.

Ahangara, L. E., K. Movassaghia, M. Emadib, and F. Yaghoobia. 2016. Photocatalytic application of TiO_2/SiO_2-based magnetic nanocomposite ($Fe_3O_4@SiO_2/TiO_2$) for reusing of textile wastewater. Nano. Chem. Res. **1**:33-39.

Ahmed, O., M.-N. Pons, H. Lachheb, A. Houas, and O. Zahraa. 2014. Degradation of sulfamethoxazole by photocatalysis using supported TiO_2. Sustain. Environ. Res. **24**:381-387.

Aiad, I., M. I. Marzouk, S. A. Shaker, N. E. Ebrahim, A. A. Abd-Elaal, and S. M. Tawfik. 2017. Antipyrine cationic surfactants capping silver nanoparticles as potent antimicrobial agents against pathogenic bacteria and fungi. J. Mol. Liq. **243**:572-583.

Arora, A., V. Jaswal, K. Singh, and R. Singh. 2016. Applications of metal/mixed metal oxides as photocatalyst: a review. Ori. J. Chem. **32**:2035-2042.

Awolola, G. V., O. O. Oluwaniyi, A. Solanke, O. O. Dosumu, and A. O. Shuiab. 2010. Toxicity assessment of natural and chemical coagulants using brine shrimp (*Artemia salina*) bioassay. Int. J. Biol. Chem. Sci. **4**:633-641.

Babić, S., A. J. M. Horvat, M. P. Dragana, and M. Kaštelan-Macan. 2007. Determination of pK_a values of active pharmaceutical ingredients. TrAC Trend. Anal. Chem. **26**:1043-1061.

Babu, S. G., P. Aparna, G. Satishkumar, M. Ashokkumar, and B. Neppolian. 2017. Ultrasound-assisted mineralization of organic contaminants using a recyclable $LaFeO_3$ and Fe^{3+}/persulfate Fenton-like system. Ultrason. Sonochem. **34**:924-930.

Bae, S., D. Kim, and W. Lee. 2013. Degradation of diclofenac by pyrite catalyzed Fenton oxidation. Appl. Catal. B-Environ. **134-135**:93-102.

Bagheri, S., and N. M. Julkapli. 2016. Magnetite hybrid photocatalysis: advance environmental remediation. Rev. Inorg. Chem. **36**:135-151.

Bagheria, H., A. Afkhamib, and N. A. 2016. Removal of pharmaceutical compounds from hospital wastewaters using nanomaterials: a review. Anal. Bioanal. Chem. Res. **3**:1-18.

Banister, K. E., and A. Campbell. 1985. The encyclopedia of aquatic life. 1st U.S. Ed edition (November 1985) edition. Checkmark Books, New York.

Baran, W., J. Sochacka, and W. Wardas. 2006. Toxicity and biodegradability of sulfonamides and products of their photocatalytic degradation in aqueous solutions. Chemosphere **65**:1295-1299.

Barhoumi, L., and D. Dewez. 2013. Toxicity of superparamagnetic iron oxide nanoparticles on green alga *Chlorella vulgaris*. BioMed Res. Int. **2013**:1-11.

Barışçı, S., F. Ulu, M. Sillanpää, and A. Dimoglo. 2016. The usage of different forms of ferrate (VI) ion for amoxicillin and ciprofloxacin removal: density functional theory based modelling of redox decomposition. J. Chem. Technol. Biot. **91**:257-266.

Barnes, K. K., D. W. Kolpin, E. T. Furlong, S. D. Zaugg, M. T. Meyer, and L. B. Barber. 2008. A national reconnaissance of pharmaceuticals and other organic wastewater contaminants in the United States groundwater. Sci. Total Environ. **402**:192-200.

Benitez, F. J., J. L. Acero, F. J. Real, G. Roldan, and E. Rodriguez. 2015. Ozonation of benzotriazole and methylindole: kinetic modeling, identification of intermediates and reaction mechanisms. J. Hazard. Mater. **282**:224-232.

Benito, A., A. Penades, J. L. Lliberia, and R. Gonzalez-Olmos. 2017. Degradation pathways of aniline in aqueous solutions during electro-oxidation with BDD electrodes and UV/H_2O_2 treatment. Chemosphere **166**:230-237.

Biard, P.-F., B. Werghi, I. Soutrel, R. Orhand, A. Couvert, A. Denicourt-Nowicki, and A. Roucoux. 2016. Efficient catalytic ozonation by ruthenium nanoparticles supported on SiO_2 or TiO_2 : towards the use of a non-woven fiber paper as original support. Chem. Eng. J. **289**:374-381.

Borecka, M., A. Bialk-Bielinska, L. P. Halinski, K. Pazdro, P. Stepnowski, and S. Stolte. 2016. The influence of salinity on the toxicity of selected sulfonamides and trimethoprim towards the green algae *Chlorella vulgaris*. J. Hazard. Mater. **308**:179-186.

Boreen, A. L., W. A. Arnold, and K. McNeill. 2004. Photochemical fate of sulfa drugs in the aquatic environment: sulfa drugs containing five-membered heterocyclic groups. Environ. Sci. Technol. **38**:3933-3940.

Bourgin, M., E. Borowska, J. Helbing, J. Hollender, H. P. Kaiser, C. Kienle, C. S. McArdell, E. Simon, and U. von Gunten. 2017. Effect of operational and water quality parameters on conventional ozonation and the advanced oxidation process O_3/H_2O_2: Kinetics of micropollutant abatement, transformation product and bromate formation in a surface water. Water Res. **122**:234-245.

Boxall, A. B., V. D. Keller, J. O. Straub, S. C. Monteiro, R. Fussell, and R. J. Williams. 2014. Exploiting monitoring data in environmental exposure modelling and risk assessment of pharmaceuticals. Environ. Int. **73**:176-185.

Brown, K. D., J. Kulis, B. Thomson, T. H. Chapman, and D. B. Mawhinney. 2006. Occurrence of antibiotics in hospital, residential, and dairy effluent, municipal wastewater, and the Rio Grande in New Mexico. Sci. Total Environ. **366**:772-783.

Bu, L., S. Zhou, Z. Shi, L. Deng, and N. Gao. 2017. Removal of 2-MIB and geosmin by electrogenerated persulfate: performance, mechanism and pathways. Chemosphere **168**:1309-1316.

Cai, M., L. Zhang, F. Qi, and L. Feng. 2013. Influencing factors and degradation products of antipyrine chlorination in water with free chlorine. J. Environ. Sci. **25**:77-84.

Calza, P., C. Medana, E. Raso, V. Giancotti, and C. Minero. 2011. Characterization of phenazone transformation products on light-activated TiO_2 surface by high-resolution mass spectrometry. Rapid Commun. Mass Sp. **25**:2923-2932.

Carlsson, C., A. K. Johansson, G. Alvan, K. Bergman, and T. Kuhler. 2006. Are pharmaceuticals potent environmental pollutants? Part I: environmental risk assessments of selected active pharmaceutical ingredients. Sci. Total Environ. **364**:67-87.

Casbeer, E., V. K. Sharma, and X.-Z. Li. 2012. Synthesis and photocatalytic activity of ferrites under visible light: A review. Sep. Purif. Technol. **87**:1-14.

Castell, J. V., M. J. Gomezl, M. A. Miranda, and I. M. Morera. 1987. Photolytic degradation of ibuprofen, toxicity of the isolated photoproducts on fibroblasts and erythrocytes. Photochem. Photobio. **46**:991-996.

Caviglioli, G., P. Valeria, P. Brunella, C. Sergio, A. Attilia, and B. Gaetano. 2002. Identification of degradation products of ibuprofen arising from oxidative and thermal treatments. J. Pharmaceut. Biomed. Anal. **30**:499-509.

Chalasani, R., and S. Vasudevan. 2013. Cyclodextrin-functionalized Fe_3O_4@TiO_2: reusable, magnetic nanoparticles for photocatalytic degradation of endocrine-disrupting chemicals in water supplies. Nano **7**:4093-4104.

Chand, R., N. H. Ince, P. R. Gogate, and D. H. Bremner. 2009. Phenol degradation using 20, 300 and 520 kHz ultrasonic reactors with hydrogen peroxide, ozone and zero valent metals. Sep. Purif. Technol. **67**:103-109.

Chang, J., Z. L. Chen, Z. Wang, J. M. Shen, Q. Chen, J. Kang, L. Yang, X. W. Liu, and C. X. Nie. 2014. Ozonation degradation of microcystin-LR in aqueous solution: intermediates, byproducts and pathways. Water Res. **63**:52-61.

Cheema, W. A., K. M. Kaarsholm, and H. R. Andersen. 2017. Combined UV treatment and ozonation for the removal of by-product precursors in swimming pool water. Water Res. **110**:141-149.

Chen, C.-C., D. Jaihindh, S.-H. Hu, and Y.-P. Fu. 2017a. Magnetic recyclable photocatalysts of Ni-Cu-Zn ferrite@SiO_2@TiO_2@Ag and their photocatalytic activities. J. Photochem. Photobio. A-Chem. **334**:74-85.

Chen, F., S. Xie, X. Huang, and X. Qiu. 2017b. Ionothermal synthesis of Fe_3O_4 magnetic nanoparticles as efficient heterogeneous Fenton-like catalysts for degradation of organic pollutants with H_2O_2. J. Hazard. Mater. **322**:152-162.

Chen, J. J., and H. H. Yeh. 2005. The mechanisms of potassium permanganate on algae removal. Water Res. **39**:4420-4428.

Chen, M., and W. Chu. 2012. Degradation of antibiotic norfloxacin in aqueous solution by visible-light-mediated C-TiO_2 photocatalysis. J. Hazard. Mater. **219-220**:183-189.

Chen, M., and W. Chu. 2015. Photocatalytic degradation and decomposition mechanism of fluoroquinolones norfloxacin over bismuth tungstate: experiment and mathematic model. Appl. Catal. B-Environ. **168-169**:175-182.

Chen, Y., P. Deng, P. Xie, R. Shang, Z. Wang, and S. Wang. 2017c. Heat-activated persulfate oxidation of methyl- and ethyl-parabens: effect, kinetics, and mechanism. Chemosphere **168**:1628-1636.

Chen, Y., J. Fang, S. Lu, Y. Wu, D. Chen, L. Huang, C. Cheng, L. Ren, X. Zhu, and Z. Fang. 2015. Plasmonic Ag-pillared rectorite as catalyst for degradation of 2,4-DCP in the H_2O_2-containing system under visible light irradiation. J. Hazard. Mater. **297**:278-285.

Chiang, L.-F., and R.-a. Doong. 2015. Enhanced photocatalytic degradation of sulfamethoxazole by visible-light-sensitive TiO_2 with low Cu addition. Sep. Purif. Technol. **156**:1003-1010.

Chiou, C. T. 1985. Partition coefficients of organic compounds in lipid-water systems and correlations with fish bioconcentration factors. Environ. Sci. Technol. **19**:57-62.

Chong, S., G. Zhang, N. Zhang, Y. Liu, T. Huang, and H. Chang. 2017. Diclofenac degradation in water by $FeCeO_x$ catalyzed H_2O_2: influencing factors, mechanism and pathways. J. Hazard. Mater. **334**:150-159.

Chowdhury, S., and R. Balasubramanian. 2014. Graphene/semiconductor nanocomposites (GSNs) for heterogeneous photocatalytic decolorization of wastewaters contaminated with synthetic dyes: a review. Appl. Catal. B-Environ. **160-161**:307-324.

Christofersen, K., B. Rieman, A. Klysner, and M. Scwdergaard. 1993. Potential role of fish predation and natural populations zooplankton in structuring a plankton community in eutrophic lake water. Limnol. Oceanogr. **38**:561-573.

Cleuvers, M. 2004. Mixture toxicity of the anti-inflammatory drugs diclofenac, ibuprofen, naproxen, and acetylsalicylic acid. Ecotox. Environ. Safe. **59**:309-315.

Cooper, E. R., T. C. Siewicki, and K. Phillips. 2008. Preliminary risk assessment database and risk ranking of pharmaceuticals in the environment. Sci. Total Environ. **398**:26-33.

Costello, M. J., K. Fretwell, and P. Read. 1993. Toxicity of sewage sludge to *Crangon crangon* and *Artemia salina*, with reference to other marine Crustacea. Aquat. Living Resour. **6**:351-356.

Cui, Y., and D. Li. 2014. Effects of six pesticides on the growth of *Chlorella vulgaris*. Pages 106-109. 2014 IEEE Workshop on Advanced Research and Technology in Industry Applications (WARTIA). IEEE, Canada.

da Silva, J. C., J. A. Teodoro, R. J. Afonso, S. F. Aquino, and R. Augusti. 2014. Photolysis and photocatalysis of ibuprofen in aqueous medium: characterization of by-products via liquid chromatography coupled to high-resolution mass spectrometry and assessment of their toxicities against *Artemia salina*. J. Mass Spectrom. **49**:145-153.

Dai, Q., L. Chen, S. Zhou, and J. Chen. 2015. Kinetics and mechanism study of direct ozonation organics in aqueous solution. RSC Adv. **5**:24649-24654.

Damschen, W. C., and R. F. Lundgren. 2009. Occurrence of emerging contaminants in water and bed material in the Missouri River, North Dakota, 2007.

Dana W. Kolpin, Edward T. Furlong, Michael T. Meyer, E. Michael Thurman, Steven D. Zaugg, Larry B. Barber, and H. T. Buxton. 2002. Pharmaceuticals, hormones, and other organic wastewater contaminants in U.S. streams, 1999-2000: a national reconnaissance. Environ. Sci. Technol. **36**:1202-1211.

de Melo da Silva, L., R. Pereira Cavalcante, R. Fabbro Cunha, F. Gozzi, R. Falcao Dantas, S. C. de Oliveira, and A. J. Machulek. 2016. Tolfenamic acid degradation by direct photolysis and the UV-ABC/H_2O_2 process: factorial design, kinetics, identification of intermediates, and toxicity evaluation. Sci. Total. Environ. **573**:518-531.

Deiana, C., E. Fois, S. Coluccia, and G. Martra. 2010. Surface structure of TiO_2 P25 nanoparticles: infrared study of hydroxy groups on coordinative defect sites. J. Phys. Chem. C **114**:21531–21538.

Deng, J., Y. Shao, N. Gao, C. Tan, S. Zhou, and X. Hu. 2013. $CoFe_2O_4$ magnetic nanoparticles as a highly active heterogeneous catalyst of oxone for the degradation of diclofenac in water. J. Hazard. Mater. **262**:836-844.

Dhaka, S., R. Kumar, M. A. Khan, K.-J. Paeng, M. B. Kurade, S.-J. Kim, and B.-H. Jeon. 2017. Aqueous phase degradation of methyl paraben using UV-activated persulfate method. Chem. Eng. J. **321**:11-19.

Dirany, A., S. Efremova Aaron, N. Oturan, I. Sires, M. A. Oturan, and J. J. Aaron. 2011. Study of the toxicity of sulfamethoxazole and its degradation products in water by a bioluminescence method during application of the electro-Fenton treatment. Anal. Bioanal. Chem. **400**:353-360.

Dlugosz, M., P. Zmudzki, A. Kwiecien, K. Szczubialka, J. Krzek, and M. Nowakowska. 2015. Photocatalytic degradation of sulfamethoxazole in aqueous solution using a floating TiO_2-expanded perlite photocatalyst. J. Hazard. Mater. **298**:146-153.

Dong, H., Q. He, G. Zeng, L. Tang, L. Zhang, Y. Xie, Y. Zeng, and F. Zhao. 2017a. Degradation of trichloroethene by nanoscale zero-valent iron (nZVI) and nZVI activated persulfate in the absence and presence of EDTA. Chem. Eng. J. **316**:410-418.

Dong, H., Z. Qiang, J. Lian, and J. Qu. 2017b. Degradation of nitro-based pharmaceuticals by UV photolysis: kinetics and simultaneous reduction on halonitromethanes formation potential. Water Res. **119**:83-90.

Du, B., S. P. Haddad, A. Luek, W. C. Scott, G. N. Saari, L. A. Kristofco, K. A. Connors, C. Rash, J. B. Rasmussen, C. K. Chambliss, and B. W. Brooks. 2014. Bioaccumulation and trophic dilution of human pharmaceuticals across trophic positions of an effluent-dependent wadeable stream. Philos. Trans. R. Soc. Lond. B. Biol. Sci. **369**.

Edwards, A. M., and A. Yool. 2000. The role of higher predation in plankton population models. J. Plankton Res. **22** 1085-1112.

Ellis, J. B. 2006. Pharmaceutical and personal care products (PPCPs) in urban receiving waters. Environ. Pollut. **144**:184-189.

EPA, U. S. E. P. A. U. S. 2005. Toxicological review of toluene (CAS no 108-88-3) EPA/635/R-05/004, Washington, DC.

Eric A. Betterton, and M. R. Hoffmann. 1990. Kinetics and mechanism of the oxidation of aqueous hydrogen sulfide by peroxymonosulfate Environ. Sci. Technol. **24**:1819-1824.

Falkowski, P. 2012. The power of plankton. Nature **483**:17-20.

Farré, M. l., S. Pérez, L. Kantiani, and D. Barceló. 2008. Fate and toxicity of emerging pollutants, their metabolites and transformation products in the aquatic environment. TrAC Trend. Anal. Chem. **27**:991-1007.

Farre, M. l., I. Ferrer, A. Ginebreda, M. Figueras, L. Olivella, L. Tirapu, M. Vilanova, and D. Barcelo. 2001. Determination of drugs in surface water and wastewater samples by liquid chromatography–mass spectrometry: methods and preliminary results including toxicity studies with Vibrio fischeri. J. Chromatogr. A **938**:187–197.

Fayad, P. B., A. Zamyadi, R. Broseus, M. Prevost, and S. Sauve. 2013. Degradation of progestagens by oxidation with potassium permanganate in wastewater effluents. Chem. Cent. J. **7**:84.

Fei., X., X. Xu., G. Jia., and Q. Li. 2010. Preparation and photocatalytic activity of magnetic Fe_3O_4/TiO_2 photocatalyst. 2010 2nd Conference on Environmental Science and Information Application Technology.

Ferre-Aracil, J., Y. Valcarcel, N. Negreira, M. L. de Alda, D. Barcelo, S. C. Cardona, and J. Navarro-Laboulais. 2016. Ozonation of hospital raw wastewaters for cytostatic compounds removal. Kinetic modelling and economic assessment of the process. Sci. Total Environ. **556**:70-79.

Flippin, J. L., D. Huggett, and C. M. Foran. 2007. Changes in the timing of reproduction following chronic exposure to ibuprofen in Japanese medaka, *Oryzias latipes*. Aquat. Toxicol. **81**:73-78.

Focazio, M. J., D. W. Kolpin, K. K. Barnes, E. T. Furlong, M. T. Meyer, S. D. Zaugg, L. B. Barber, and M. E. Thurman. 2008. A national reconnaissance for pharmaceuticals and other organic wastewater contaminants in the United States untreated drinking water sources. Sci. Total Environ. **402**:201-216.

Frost, B. W. 1972. Effects of size and concentration of food particles on the feeding behavior of the marine planktonic copepod *Calanus pacificus*. Limnol. Oceanogr. **17**:805-815.

Fu, W., H. Yang, M. Li, M. Li, N. Yang, and G. Zou. 2005. Anatase TiO_2 nanolayer coating on cobalt ferrite nanoparticles for magnetic photocatalyst. Mater. Lett. **59**:3530-3534.

Fu, Y.-P., W.-K. Chang, H.-C. Wang, C.-W. Liu, and C.-H. Lin. 2011. Synthesis and characterization of anatase TiO_2 nanolayer coating on Ni–Cu–Zn ferrite powders for magnetic photocatalyst. J. Mater. Res. **25**:134-140.

Fukahori, S., and T. Fujiwara. 2015. Photocatalytic decomposition behavior and reaction pathway of sulfamethazine antibiotic using TiO_2. J. Environ. Manage **157**:103-110.

Gaffney Vde, J., V. V. Cardoso, M. J. Benoliel, and C. M. Almeida. 2016. Chlorination and oxidation of sulfonamides by free chlorine: Identification and behaviour of reaction products by UPLC-MS/MS. J. Environ. Manage **166**:466-477.

Gaikwad, P. N., P. P. Hankare, T. M. Wandre, K. M. Garadkar, and R. Sasikala. 2016. Photocatalytic performance of magnetically separable Fe, N co-doped TiO_2-cobalt ferrite nanocomposite. Mater. Sci. Eng. B **205**:40-45.

Gao, S., Z. Y. Li, and X. L. Zhang. 2009. Preparation and characterization of a novel core shell structure $CoFe_2O_4/TiO_2$ magnetic nano-photocatalyst. J. Funct. Mater. Dev. **15**:201-205.

Gao, S., Z. Zhao, Y. Xu, J. Tian, H. Qi, W. Lin, and F. Cui. 2014a. Oxidation of sulfamethoxazole (SMX) by chlorine, ozone and permanganate--a comparative study. J. Hazard. Mater. **274**:258-269.

Gao, X., X. Liu, Z. Zhu, X. Wang, and Z. Xie. 2016. Enhanced photoelectrochemical and photocatalytic behaviors of MFe_2O_4 (M = Ni, Co, Zn and Sr) modified TiO_2 nanorod arrays. Sci. Rep. **6**:30543.

Gao, Y.-q., N.-y. Gao, Y. Deng, D.-q. Yin, Y.-s. Zhang, W.-l. Rong, and S.-d. Zhou. 2014b. Heat-activated persulfate oxidation of sulfamethoxazole in water. Desalin. Water Treat. **56**:2225-2233.

Garcia-Galan, M. J., A. Anfruns, R. Gonzalez-Olmos, S. Rodriguez-Mozaz, and J. Comas. 2016. Advanced oxidation of the antibiotic sulfapyridine by UV/H_2O_2:

Characterization of its transformation products and ecotoxicological implications. Chemosphere **147**:451-459.

Garcon, V. C., A. Oschlies, S. C. Doney, D. McGillicuddy, and J. Waniek. 2001. The role of mesoscale variability on plankton dynamics in the North Atlantic. Deep-Sea Res. II **48**:2199-2226.

Georgaki, I., E. Vasilaki, and N. Katsarakis. 2014. A Study on the degradation of carbamazepine and ibuprofen by TiO_2& ZnO photocatalysis upon UV/Visible-light irradiation. Am. J. Anal. Chem. **05**:518-534.

Ghauch, A., G. Ayoub, and S. Naim. 2013. Degradation of sulfamethoxazole by persulfate assisted micrometric Fe^0 in aqueous solution. Chem. Eng. J. **228**:1168-1181.

Ghauch, A., A. Baalbaki, M. Amasha, R. El Asmar, and O. Tantawi. 2017. Contribution of persulfate in UV-254 nm activated systems for complete degradation of chloramphenicol antibiotic in water. Chem. Eng. J. **317**:1012-1025.

Giri, R. R., H. Ozaki, S. Ota, R. Takanami, and S. Taniguchi. 2010. Degradation of common pharmaceuticals and personal care products in mixed solutions by advanced oxidation techniques. Int. J. Environ. Sci. Tech. **7**:251-260.

Gmurek, M., H. Horn, and M. Majewsky. 2015. Phototransformation of sulfamethoxazole under simulated sunlight: Transformation products and their antibacterial activity toward Vibrio fischeri. Sci. Total Environ. **538**:58-63.

Gobel, A., C. S. McArdell, M. J.-F. Suter, and W. Giger. 2004. Trace determination of macrolide and sulfonamide antimicrobials, a human sulfonamide metabolite, and trimethoprim in wastewater using liquid chromatography coupled to electrospray tandem mass spectrometry. Anal. Chem. **76**:4756-4764.

Gobel, A., A. Thomsen, C. S. Mcardell, A. Joss, and W. Giger. 2005. Occurrence and sorption behavior of sulfonamides, macrolides, and trimethoprim in activated sludge treatment. Environ. Sci. Technol. **39**:3981-3989.

Gomes, J., R. Costa, R. M. Quinta-Ferreira, and R. C. Martins. 2017. Application of ozonation for pharmaceuticals and personal care products removal from water. Sci. Total Environ. **586**:265-283.

Grabowska, E. 2016. Selected perovskite oxides: characterization, preparation and photocatalytic properties—a review. Appl. Catal. B-Environ. **186**:97-126.

Greene, D., R. Serrano-Garcia, J. Govan, and Y. K. Gun'ko. 2014. Synthesis characterization and photocatalytic studies of cobalt ferrite-silica-titania nanocomposites. Nanomaterials (Basel) **4**:331-343.

Gros, M., M. Petrovic, A. Ginebreda, and D. Barcelo. 2010. Removal of pharmaceuticals during wastewater treatment and environmental risk assessment using hazard indexes. Environ. Int. **36**:15-26.

Guan, X., D. He, J. Ma, and G. Chen. 2010. Application of permanganate in the oxidation of micropollutants: a mini review. Front. Environ. Sci. Engin. China **4**:405-413.

Guillard, R. R. 1975. Culture of phytoplankton for feeding marine invertebrates. Pages 29-60 *in* Walter L. Smith and M. H. Chanley, editors. Culture of marine invertebrate animals. Springer.

Gulkowska, A., H. W. Leung, M. K. So, S. Taniyasu, N. Yamashita, L. W. Yeung, B. J. Richardson, A. P. Lei, J. P. Giesy, and P. K. Lam. 2008. Removal of antibiotics from wastewater by sewage treatment facilities in Hong Kong and Shenzhen, China. Water Res. **42**:395-403.

Guo, H., T. Ke, N. Gao, Y. Liu, and X. Cheng. 2017. Enhanced degradation of aqueous norfloxacin and enrofloxacin by UV-activated persulfate: kinetics, pathways and deactivation. Chem. Eng. J. **316**:471-480.

Guo, S., G. Zhang, and J. Wang. 2014. Photo-Fenton degradation of rhodamine B using Fe_2O_3-Kaolin as heterogeneous catalyst: characterization, process optimization and mechanism. J. Colloid Interface Sci. **433**:1-8.

Guo, W. Q., R. L. Yin, X. J. Zhou, J. S. Du, H. O. Cao, S. S. Yang, and N. Q. Ren. 2015. Sulfamethoxazole degradation by ultrasound/ozone oxidation process in water: kinetics, mechanisms, and pathways. Ultrason. Sonochem. **22**:182-187.

Gupta, S. M., and M. Tripathi. 2011. A review of TiO_2 nanoparticles. Chinese Sci. Bull. **56**:1639-1657.

Han, S., K. Choi, J. Kim, K. Ji, S. Kim, B. Ahn, J. Yun, K. Choi, J. S. Khim, X. Zhang, and J. P. Giesy. 2010. Endocrine disruption and consequences of chronic exposure to ibuprofen in Japanese medaka (*Oryzias latipes*) and freshwater cladocerans *Daphnia magna* and *Moina macrocopa*. Aquat. Toxicol. **98**:256-264.

Hansen, K. M. S., A. Spiliotopoulou, R. K. Chhetri, M. Escolà Casas, K. Bester, and H. R. Andersen. 2016. Ozonation for source treatment of pharmaceuticals in hospital wastewater – ozone lifetime and required ozone dose. Chem. Eng. J. **290**:507-514.

Hassan, M., Y. Zhao, and B. Xie. 2016. Employing TiO_2 photocatalysis to deal with landfill leachate: current status and development. Chem. Eng. J. **285**:264-275.

He, Q., Z. Zhang, J. Xiong, Y. Xiong, and H. Xiao. 2008. A novel biomaterial — Fe_3O_4:TiO_2 core-shell nano particle with magnetic performance and high visible light photocatalytic activity. Opt. Mater. **31**:380-384.

He, Z., T. Hong, J. Chen, and S. Song. 2012. A magnetic TiO_2 photocatalyst doped with iodine for organic pollutant degradation. Sep. Purif. Technol. **96**:50-57.

Heberer, T. 2002. Occurrence, fate, and removal of pharmaceutical residues in the aquatic environment: a review of recent research data. Toxicol. Lett. **131**:5-17.

Heckmann, L. H., A. Callaghan, H. L. Hooper, R. Connon, T. H. Hutchinson, S. J. Maund, and R. M. Sibly. 2007. Chronic toxicity of ibuprofen to *Daphnia magna*: Effects on life history traits and population dynamics. Toxicol. Lett. **172**:137-145.

Heredia, C. L., E. L. Sham, and E. M. Farfán-Torres. 2015. Tartrazine degradation by supported TiO_2 on magnetic particles. Revista Materia **20**:668-675.

Herndl, G. J., and T. Reinthaler. 2013. Microbial control of the dark end of the biological pump. Nature Geosci. **6**:718-724.

Hida, S., M. Yoshida, I. Nakabayashi, N. N. Miura, Y. Adachi, and N. Ohno. 2005. Anti-fungal activity of sulfamethoxazole toward Aspergillus Species. Biol. Pharm. Bull **28**:773-778

Hirsch, R., T. Ternes, K. Haberer, and K. L. Kratz. 1999. Occurrence of antibiotics in the aquatic environment. Sci. Total Environ. **225**:109–118.

Hopkins, Z. R., S. Snowberger, and L. Blaney. 2017. Ozonation of the oxybenzone, octinoxate, and octocrylene UV-filters: reaction kinetics, absorbance characteristics, and transformation products. J. Hazard. Mater. **338**:23-32.

Hou, S., L. Ling, C. Shang, Y. Guan, and J. Fang. 2017. Degradation kinetics and pathways of haloacetonitriles by the UV/persulfate process. Chem. Eng. J. **320**:478-484.

Hou, Y., X.-Y. Li, Q.-D. Zhao, X. Quan, and G.-H. Chen. 2010a. Electrochemical method for synthesis of a $ZnFe_2O_4/TiO_2$ composite nanotube array modified electrode with enhanced photoelectrochemical activity. Adv. Funct. Mater. **20**:2165-2174.

Hou, Y., X.-Y. Li, Q.-D. Zhao, X. Quan, and G.-H. Chen. 2010b. Electrochemically assisted photocatalytic degradation of 4-Chlorophenol by $ZnFe_2O_4$-modified TiO_2 nanotube array electrode under visible light irradiation. Environ. Sci. Technol. **44**:5098–5103.

Houlding, T. K., P. Gao, V. Degirmenci, K. Tchabanenko, and E. V. Rebrov. 2015. Mechanochemical synthesis of $TiO_2/NiFe_2O_4$ magnetic catalysts for operation under RF field. Mater. Sci. Eng.-B **193**:175-180.

Hu, A., X. Zhang, D. Luong, K. D. Oakes, M. R. Servos, R. Liang, S. Kurdi, P. Peng, and Y. Zhou. 2012. Adsorption and photocatalytic degradation kinetics of pharmaceuticals by TiO_2 nanowires during water treatment. Waste Biomass Valori. **3**:443-449.

Hu, L., H. M. Martin, and T. J. Strathmann. 2010. Oxidation kinetics of antibiotics during water treatment with potassium permanganate. Environ. Sci. Technol. **44**:6416-6422.

Hu, L., F. Yang, W. Lu, Y. Hao, and H. Yuan. 2013. Heterogeneous activation of oxone with CoMg/SBA-15 for the degradation of dye rhodamine B in aqueous solution. Appl. Catal. B-Environ. **134-135**:7-18.

Hu, L. H., H. M. Martin, O. Arcs-Bulted, M. N. Sugihara, K. A. Keatlng, and T. J. Strathmann. 2009. Oxidation of carbamazepine by Mn(VII) and Fe(VI): reaction kinetics and mechanism. Environ. Sci. Technol. **43**:509-515.

Hu, X., J. Yang, and J. Zhang. 2011. Magnetic loading of TiO_2/SiO_2/Fe_3O_4 nanoparticles on electrode surface for photoelectrocatalytic degradation of diclofenac. J. Hazard. Mater. **196**:220-227.

Huang, X., Y. Feng, C. Hu, X. Xiao, D. Yu, and X. Zou. 2015. Mechanistic QSAR models for interpreting degradation rates of sulfonamides in UV-photocatalysis systems. Chemosphere **138**:183-189.

Hussain, I., M. Li, Y. Zhang, Y. Li, S. Huang, X. Du, G. Liu, W. Hayat, and N. Anwar. 2017. Insights into the mechanism of persulfate activation with nZVI/BC nanocomposite for the degradation of nonylphenol. Chem. Eng. J. **311**:163-172.

Hussain, S., S. Gul, J. R. Steter, D. W. Miwa, and A. J. Motheo. 2015. Route of electrochemical oxidation of the antibiotic sulfamethoxazole on a mixed oxide anode. Environ. Sci. Pollut. Res. Int. **22**:15004-15015.

Ibrahim, I., I. O. Ali, T. M. Salama, A. A. Bahgat, and M. M. Mohamed. 2016. Synthesis of magnetically recyclable spinel ferrite (MFe_2O_4, M=Zn, Co, Mn) nanocrystals engineered by sol gel-hydrothermal technology: High catalytic performances for nitroarenes reduction. Appl. Catal. B-Environ. **181**:389-402.

Iliades, P., S. R. Meshnick, and I. G. Macreadie. 2004. Dihydropteroate synthase mutations in *Pneumocystis jiroveci* can affect sulfamethoxazole resistance in a *Saccharomyces cerevisiae* model. Antimicrob. Agents Chemother. **48**:2617-2623.

Iovino, P., S. Chianese, S. Canzano, M. Prisciandaro, and D. Musmarra. 2016. Degradation of ibuprofen in aqueous solution with UV light: the effect of reactor volume and pH. Water Air Soil Poll. **227**:1-9.

Isidori, M., M. Lavorgna, A. Nardelli, L. Pascarella, and A. Parrella. 2005. Toxic and genotoxic evaluation of six antibiotics on non-target organisms. Sci. Total. Environ. **346**:87-98.

Ji, Y., Y. Fan, K. Liu, D. Kong, and J. Lu. 2015. Thermo activated persulfate oxidation of antibiotic sulfamethoxazole and structurally related compounds. Water Res. **87**:1-9.

Ji, Y., C. Ferronato, A. Salvador, X. Yang, and J. M. Chovelon. 2014. Degradation of ciprofloxacin and sulfamethoxazole by ferrous-activated persulfate: implications for remediation of groundwater contaminated by antibiotics. Sci. Total. Environ. **472**:800-808.

Jiang, J.-Q., Z. Zhou, S. Patibandla, and X. Shu. 2013. Pharmaceutical removal from wastewater by ferrate(VI) and preliminary effluent toxicity assessments by the zebrafish embryo model. Microchem. J. **110**:239-245.

Jiang, J., S. Y. Pang, and J. Ma. 2009. Oxidation of triclosan by permanganate (Mn(VII)): importance of ligands and in situ formed manganese oxides. Environ. Sci. Technol. **43**:8326-8331.

Jiang, J. Q., and Z. Zhou. 2013. Removal of pharmaceutical residues by ferrate(VI). PLoS One **8**:e55729.

Jiang, L., X. Yuan, Y. Pan, J. Liang, G. Zeng, Z. Wu, and H. Wang. 2017. Doping of graphitic carbon nitride for photocatalysis: a reveiw. Appl. Catal. B-Environ. **217**:388-406.

Jin, X., H. Xu, S. Qiu, M. Jia, F. Wang, A. Zhang, and X. Jiang. 2017. Direct photolysis of oxytetracycline: influence of initial concentration, pH and temperature. J. Photochem. Photobio. A-Chem. **332**:224-231.

Karthikeyan, K. G., and M. T. Meyer. 2006. Occurrence of antibiotics in wastewater treatment facilities in Wisconsin, USA. Sci. Total. Environ. **361**:196-207.

Keen, O. S., N. G. Love, and K. G. Linden. 2012. The role of effluent nitrate in trace organic chemical oxidation during UV disinfection. Water Res. **46**:5224-5234.

Kemper, N. 2008. Veterinary antibiotics in the aquatic and terrestrial environment. Ecol. Indic. **8**:1-13.

Kester, D. R., I. W. Duedall, D. N. Connors, and R. M. Pytkowicz. 1967. Preparation of artificial seawater. Limnol. Oceanogr. **12**:176-179.

Kharisov, B. I., H. V. R. Dias, and O. V. Kharissova. 2014. Mini-review: ferrite nanoparticles in the catalysis. Arab. J. Chem.

Kim, H. Y., T. H. Kim, and S. Yu. 2015. Photolytic degradation of sulfamethoxazole and trimethoprim using UV-A, UV-C and vacuum-UV (VUV). J. Environ. Sci. Health A: Tox. Hazard. Subst. Environ. Eng. **50**:292-300.

Kim, T. K., B. R. Moon, T. Kim, M. K. Kim, and K. D. Zoh. 2016. Degradation mechanisms of geosmin and 2-MIB during UV photolysis and UV/chlorine reactions. Chemosphere **162**:157-164.

Kim, Y., K. Choi, J. Jung, S. Park, P. G. Kim, and J. Park. 2007. Aquatic toxicity of acetaminophen, carbamazepine, cimetidine, diltiazem and six major sulfonamides, and their potential ecological risks in Korea. Environ. Int. **33**:370-375.

Klavarioti, M., D. Mantzavinos, and D. Kassinos. 2009. Removal of residual pharmaceuticals from aqueous systems by advanced oxidation processes. Environ. Int. **35**:402-417.

Knoll/BASF. 1995. Pharmaceutical safety data sheet (issue/ revision 06/04/94).*in* K. Pharmaceuticals, editor., Nottingham, UK.

Kokkali, V., I. Katramados, and J. D. Newman. 2011. Monitoring the effect of metal ions on the mobility of *Artemia salina* nauplii. Biosensors (Basel) **1**:36-45.

Kontos, A. I., I. M. Arabatzis, D. S. Tsoukleris, A. G. Kontos, M. C. Bernard, D. E. Petrakis, and P. Falaras. 2005. Efficient photocatalysts by hydrothermal treatment of TiO_2. Catal. Today **101**:275-281.

Koplin, D. W., E. T. Furlong, M. T. Meyer, E. M. Thurman, S. D. Zaugg, L. B. Barber, and H. T. Buxton. 2002. Pharmaceuticals, hormones, and other organic wastewater contaminants in U.S. streams, 1999−2000: a national reconnaissance. Environ. Sci. Technol. **36**:1202-1211.

Krishnakumar, P. K., A. P. Dineshbabu, and G. Sasikumar. 2007. Toxicity evaluation of treated refinery effluent using bring shrimp (*Artemia salina*) egg and larval bioassy. Fish. Technol. **44**:85-92.

Kubo, M., K. Matsuoka, A. Takahashi, N. Shibasaki-Kitakawa, and T. Yonemoto. 2005. Kinetics of ultrasonic degradation of phenol in the presence of TiO_2 particles. Ultrason. Sonochem. **12**:263-269.

Kummerer, K. 2009. Antibiotics in the aquatic environment--a review--part II. Chemosphere **75**:435-441.

Lapworth, D. J., N. Baran, M. E. Stuart, and R. S. Ward. 2012. Emerging organic contaminants in groundwater: A review of sources, fate and occurrence. Environ. Pollut. **163**:287-303.

Larsen, P. S., C. V. Madsen, and H. U. Riisgård. 2008. Effect of temperature and viscosity on swimming velocity of the copepod *Acartia tonsa*, brine shrimp *Artemia salina* and rotifer *Brachionus plicatilis*. Aquat. Bio. **4**:47-54.

Lee, H. U., G. Lee, J. C. Park, Y.-C. Lee, S. M. Lee, B. Son, S. Y. Park, C. Kim, S. Lee, S. C. Lee, B. Nam, J. W. Lee, D. R. Bae, J.-S. Yoon, and J. Lee. 2014a. Efficient visible-light responsive TiO_2 nanoparticles incorporated magnetic carbon photocatalysts. Chem. Eng. J. **240**:91-98.

Lee, S.-w., J. Drwiega, D. Mazyck, C.-Y. Wu, and W. M. Sigmund. 2006. Synthesis and characterization of hard magnetic composite photocatalyst—barium ferrite/silica/titania. Mater. Chem. Phys. **96**:483-488.

Lee, S.-w., J. Drwiega, C.-Y. Wu, D. Mazyck, and W. M. Sigmund. 2004. Anatase TiO_2 nanoparticle coating on barium ferrite using titanium bis-ammonium lactato dihydroxide and its use as a magnetic photocatalyst. Chem. Mater. **16** 1160-1164.

Lee, Y., L. Kovalova, C. S. McArdell, and U. von Gunten. 2014b. Prediction of micropollutant elimination during ozonation of a hospital wastewater effluent. Water Res. **64**:134-148.

Lee, Y., and U. von Gunten. 2010. Oxidative transformation of micropollutants during municipal wastewater treatment: comparison of kinetic aspects of selective (chlorine, chlorine dioxide, ferrate VI, and ozone) and non-selective oxidants (hydroxyl radical). Water Res. **44**:555-566.

Li, C., X. Z. Li, and N. Graham. 2005. A study of the preparation and reactivity of potassium ferrate. Chemosphere **61**:537-543.

Li, F., Y. Dai, M. Gong, T. Yu, and X. Chen. 2015. Synthesis, characterization of magnetic-sepiolite supported with TiO_2, and the photocatalytic performance over Cr(VI) and 2,4-dichlorophenol co-existed wastewater. J. Alloy. Compd. **638**:435-442.

Li, F., Y. Kang, M. Chen, G. Liu, W. Lv, K. Yao, P. Chen, and H. Huang. 2016. Photocatalytic degradation and removal mechanism of ibuprofen via monoclinic $BiVO_4$ under simulated solar light. Chemosphere **150**:139-144.

Li, H., Y. Zhang, S. Wang, Q. Wu, and C. Liu. 2009a. Study on nanomagnets supported TiO_2 photocatalysts prepared by a sol–gel process in reverse microemulsion combining with solvent-thermal technique J. Hazard. Mater. **169**:1045-1053.

Li, J., Y. Ren, F. Ji, and B. Lai. 2017. Heterogeneous catalytic oxidation for the degradation of p-nitrophenol in aqueous solution by persulfate activated with $CuFe_2O_4$ magnetic nano-particles. Chem. Eng. J. **324**:63-73.

Li, R., W. Chen, and W. Wang. 2009b. Magnetoswitchable controlled photocatalytic system using ferromagnetic Fe-doped titania nanorods photocatalysts with enhanced photoactivity. Sep. Purif. Technol. **66**:171-176.

Li, X., Y. Wang, S. Yuan, Z. Li, B. Wang, J. Huang, S. Deng, and G. Yu. 2014. Degradation of the anti-inflammatory drug ibuprofen by electro-peroxone process. Water Res. **63**:81-93.

Li, W. C. 2014. Occurrence, sources, and fate of pharmaceuticals in aquatic environment and soil. Environ. Pollut. **187**:193-201.

Lichtenthaler, H. K., and C. Buschmann. 2001. Chlorophylls and carotenoids: measurement and characterization by UV-VIS spectroscopy. Curr. Protoc. Food Analyt. Chem.:F4.3.1-F4.3.8.

Lin, C. Y., and S. D. Huang. 2008. Application of liquid-liquid-liquid microextraction and high-performance liquid-chromatography for the determination of sulfonamides in water. Anal. Chim. Acta **612**:37-43.

Liu, C., J. Wang, W. Chen, C. Dong, and C. Li. 2015a. The removal of DON derived from algae cells by Cu-doped TiO_2 under sunlight irradiation. Chem. Eng. J. **280**:588-596.

Liu, C. H., C. Y. Chang, Q. Liao, X. Zhu, and J. S. Chang. 2013a. Photoheterotrophic growth of *Chlorella vulgaris* ESP6 on organic acids from dark hydrogen fermentation effluents. Bioresource Technol. **145**:331-336.

Liu, G., X. Li, B. Han, L. Chen, L. Zhu, and L. C. Campos. 2017. Efficient degradation of sulfamethoxazole by the Fe(II)/HSO_5^- process enhanced by hydroxylamine: Efficiency and mechanism. J. Hazard. Mater. **322**:461-468.

Liu, H., and L. Gao. 2006. Preparation and properties of nanocrystalline alpha-Fe_2O_3-sensitized TiO_2 nanosheets as a visible light photocatalyst. J. Am. Ceram. Soc. **89**:370-373.

Liu, H., S. Ji, Y. Zheng, M. Li, and H. Yang. 2013b. Porous TiO_2-coated magnetic core-shell nanocomposites: preparation and enhanced photocatalytic activity. Chinese J. Chem. Eng. **21**:569-576.

Liu, H., Z. Jia, S. Ji, Y. Zheng, M. Li, and H. Yang. 2011. Synthesis of $TiO_2/SiO_2@Fe_3O_4$ magnetic microspheres and their properties of photocatalytic degradation dyestuff. Catal. Today **175**:293-298.

Liu, J., Z. Zhao, P. Shao, and F. Cui. 2015b. Activation of peroxymonosulfate with magnetic Fe_3O_4–MnO_2 core–shell nanocomposites for 4-chlorophenol degradation. Chem. Eng. J. **262**:854-861.

Liu, J., S. Zuo, L. Yu, Y. Yu, B. Li, and P. Chen. 2013c. Visible light photodegradation of methylene blue by AgBr–$TiO_2/SiO_2@Fe_3O_4$ magnetic photocatalysts. Particuology **11**:728-731.

Liu, W., N. B. Sutton, H. H. M. Rijnaarts, and A. A. M. Langenhoff. 2016. Pharmaceutical removal from water with iron- or manganese-based technologies: A review. Crit. Rev. Environ. Sci. Tec. **46**:1584-1621.

Loos, R., R. Carvalho, D. C. Antonio, S. Comero, G. Locoro, S. Tavazzi, B. Paracchini, M. Ghiani, T. Lettieri, L. Blaha, B. Jarosova, S. Voorspoels, K. Servaes, P. Haglund, J. Fick, R. H. Lindberg, D. Schwesig, and B. M. Gawlik. 2013. EU-wide monitoring survey on emerging polar organic contaminants in wastewater treatment plant effluents. Water Res. **47**:6475-6487.

Lu, A. H., E. L. Salabas, and F. Schuth. 2007. Magnetic nanoparticles: synthesis, protection, functionalization, and application. Angew. Chem. Int. Ed. **46**:1222-1244.

Lucas, M. S., P. B. Tavares, J. A. Peres, J. L. Faria, M. Rocha, C. Pereira, and C. Freire. 2013. Photocatalytic degradation of reactive black 5 with TiO_2-coated magnetic nanoparticles. Catal. Today **209**:116-121.

Ma, J., N. Graham, and G. Li. 1997. Effect of permanganate preoxidation in enhancing the coagulation of surface waters laboratory case studies. J. Water Supply: Res. Technol. -Aqua. **46**:1-10.

Ma, Y., N. Gao, and C. Li. 2012. Degradation and pathway of tetracycline hydrochloride in aqueous solution by potassium ferrate. Environ. Eng. Sci. **29**:357-362.

Ma, Y., K. Zhang, C. Li, T. Zhang, and N. Gao. 2015. Oxidation of sulfonamides in aqueous solution by UV-TiO_2-Fe(VI). Biomed Res. Int. **2015**:973942.

Madhavan, J., F. Grieser, and M. Ashokkumar. 2010. Combined advanced oxidation processes for the synergistic degradation of ibuprofen in aqueous environments. J. Hazard. Mater. **178**:202-208.

Maeng, S. K., S. K. Sharma, K. Lekkerkerker-Teunissen, and G. L. Amy. 2011. Occurrence and fate of bulk organic matter and pharmaceutically active compounds in managed aquifer recharge: a review. Water Res. **45**:3015-3033.

Majewsky, M., D. Wagner, M. Delay, S. Brase, V. Yargeau, and H. Horn. 2014. Antibacterial activity of sulfamethoxazole transformation products (TPs): general relevance for sulfonamide TPs modified at the para position. Chem. Res. Toxicol. **27**:1821-1828.

Marce, M., B. Domenjoud, S. Esplugas, and S. Baig. 2016. Ozonation treatment of urban primary and biotreated wastewaters: Impacts and modeling. Chem. Eng. J. **283**:768-777.

Marsili, R. 2011. Flavor, fragrance, and odor analysis, second edition. CRC press, Boca Raton London New York.

Martin, Y. C. 1996. Exploring QSAR: hydrophobic, electronic, and steric constants C. Hansch, A. Leo, and D. Hoekman. American Chemical Society, Washington, DC. 1995. Xix+ 348 pp. 22× 28.5 cm. Exploring QSAR: fundamentals and applications in chemistry and biology. C. Hansch and A. Leo. American Chemical Society, Washington, DC. 1995. Xvii+ 557 pp. 18.5× 26 cm. ISBN 0-8412-2993-7 (set). $99.95 (set). J. Med. Chem. **39**:1189-1190.

Martins, R. C., M. Cardoso, R. F. Dantas, C. Sans, S. Esplugas, and R. M. Quinta-Ferreira. 2015a. Catalytic studies for the abatement of emerging contaminants by ozonation. J. Chem. Technol. Biotechnol. **90**:1611-1618.

Martins, R. C., R. F. Dantas, C. Sans, S. Esplugas, and R. M. Quinta-Ferreira. 2015b. Ozone/H_2O_2 performance on the degradation of sulfamethoxazole. Ozone-Sci. Eng. **37**:509-517.

Masoumi, S., G. Nabiyouni, and D. Ghanbari. 2016a. Photo-degradation of azo dyes: photo catalyst and magnetic investigation of $CuFe_2O_4$–TiO_2 nanoparticles and nanocomposites. J. Mater. Sci.-Mater. El. **27**:9962-9975.

Masoumi, S., G. Nabiyouni, and D. Ghanbari. 2016b. Photo-degradation of Congored, acid brown and acid violet: photo catalyst and magnetic investigation of $CuFe_2O_4$–TiO_2–Ag nanocomposites. J. Mater. Sci.-Mater. El. **27**:11017-11033.

Mcfarland, J. W. 1970. On the parabolic relationship between drug potency and hydrophobicity. J. Med. Chem. **13**:1192-1196.

McKendricka, C. A. G., and M. K. Pai. 1912. XLV.—The rate of multiplication of micro-organisms: a mathematical study. P. Roy. Soc. Edinb. **31**:649–653.

McMurdie, H. F., and E. Golovato. 1948. Study of the modifications of manganese dioxide. J. Res. Natl. Bur. Stand. **41**:589-600.

Mendez-Arriaga, F., S. Esplugas, and J. Gimenez. 2010. Degradation of the emerging contaminant ibuprofen in water by photo-Fenton. Water Res. **44**:589-595.

Miao, H. F., M. Cao, D. Y. Xu, H. Y. Ren, M. X. Zhao, Z. X. Huang, and W. Q. Ruan. 2015. Degradation of phenazone in aqueous solution with ozone: influencing factors and degradation pathways. Chemosphere **119**:326-333.

Miege, C., J. M. Choubert, L. Ribeiro, M. Eusebe, and M. Coquery. 2009. Fate of pharmaceuticals and personal care products in wastewater treatment plants. Conception of a database and first results. Environ. Pollut. **157**:1721-1726.

Milhem, M. M., A. S. Al-Hiyasat, and H. Darmani. 2008. Toxicity testing of restorative dental materials using brine shrimp larvae (*Artemia salina*). J. Appl. Oral Sci. **16**:297-301.

Minh, T. B., H. W. Leung, I. H. Loi, W. H. Chan, M. K. So, J. Q. Mao, D. Choi, J. C. Lam, G. Zheng, M. Martin, J. H. Lee, P. K. Lam, and B. J. Richardson. 2009. Antibiotics in the Hong Kong metropolitan area: Ubiquitous distribution and fate in Victoria Harbour. Mar. Pollut. Bull. **58**:1052-1062.

Mompelat, S., B. Le Bot, and O. Thomas. 2009. Occurrence and fate of pharmaceutical products and by-products, from resource to drinking water. Environ. Int. **35**:803-814.

Monteagudo, J. M., A. Duran, J. Latorre, and A. J. Exposito. 2016. Application of activated persulfate for removal of intermediates from antipyrine wastewater degradation refractory towards hydroxyl radical. J. Hazard. Mater. **306**:77-86.

Moreira, E., L. A. Fraga, M. H. Mendonça, and O. C. Monteiro. 2012. Synthesis, optical, and photocatalytic properties of a new visible-light-active $ZnFe_2O_4$–TiO_2 nanocomposite material. J. Nanopart. Res. **14**.

Mou, F., L. Xu, H. Ma, J. Guan, D. R. Chen, and S. Wang. 2012. Facile preparation of magnetic gamma-Fe_2O_3/TiO_2 Janus hollow bowls with efficient visible-light photocatalytic activities by asymmetric shrinkage. Nanoscale **4**:4650-4657.

Naddeo, V., C. S. Uyguner-Demirel, M. Prado, A. Cesaro, V. Belgiorno, and F. Ballesteros. 2015. Enhanced ozonation of selected pharmaceutical compounds by sonolysis. Environ. Technol. **36**:1876-1883.

Nguyen, T. P., and C. F. Clarke. 2012. Folate status of gut microbiome affects Caenorhabditis elegans lifespan. BMC Biol. **10**:1-4.

Nie, Y., L. Zhang, Y. Y. Li, and C. Hu. 2015. Enhanced Fenton-like degradation of refractory organic compounds by surface complex formation of $LaFeO_3$ and H_2O_2. J. Hazard. Mater. **294**:195-200.

Niu, J., L. Zhang, Y. Li, J. Zhao, S. Lv, and K. Xiao. 2013. Effects of environmental factors on sulfamethoxazole photodegradation under simulated sunlight irradiation: Kinetics and mechanism. J. Environ. Sci. **25**:1098-1106.

Nohara, K., H. Hidaka, E. Pelizzetti, and N. Serpone. 1996. Dependence on chemical structure of the production of NH_4^+ and/or NO_3^- ions during the photocatalyzed oxidation of nitrogen-containing substances at the titania/water interface. Catal. Lett. **36**:115-118.

Oh, B. T., Y. S. Seo, D. Sudhakar, J. H. Choe, S. M. Lee, Y. J. Park, and M. Cho. 2014. Oxidative degradation of endotoxin by advanced oxidation process (O_3/H_2O_2 & UV/H_2O_2). J. Hazard. Mater. **279**:105-110.

Ohno, T., K. Sarukawa, K. Tokieda, and M. Matsumura. 2001. Morphology of a TiO2 Photocatalyst (Degussa, P-25) Consisting of Anatase and Rutile Crystalline Phases. J. Catal. **203**:82-86.

Olmez-Hanci, T., D. Dursun, E. Aydin, I. Arslan-Alaton, B. Girit, L. Mita, N. Diano, D. G. Mita, and M. Guida. 2015. $S_2O_8^{2-}$/UV-C and H_2O_2/UV-C treatment of Bisphenol A: assessment of toxicity, estrogenic activity, degradation products and results in real water. Chemosphere **119 Suppl**:S115-123.

Pal, A., K. Y. Gin, A. Y. Lin, and M. Reinhard. 2010. Impacts of emerging organic contaminants on freshwater resources: review of recent occurrences, sources, fate and effects. Sci. Total Environ. **408**:6062-6069.

Pan, Y., M. Zhou, X. Li, L. Xu, Z. Tang, X. Sheng, and B. Li. 2017. Highly efficient persulfate oxidation process activated with pre-magnetization Fe^0. Chem. Eng. J. **318**:50-56.

Pang, H., Y. Li, L. Guan, Q. Lu, and F. Gao. 2011. TiO_2/Ni nanocomposites: biocompatible and recyclable magnetic photocatalysts. Catal. Commun. **12**:611-615.

Parker, A. M., Y. Lester, E. K. Spangler, U. von Gunten, and K. G. Linden. 2017. UV/H_2O_2 advanced oxidation for abatement of organophosphorous pesticides and the effects on various toxicity screening assays. Chemosphere **182**:477-482.

Pearl, R., and L. J. Reed. 1920. On the rate of growth of the population of the United States since 1790 and its mathematical representation. P. Natl. Acad. Sci. **6**:275-288.

Peng, L., T. Xie, Y. Lu, H. Fan, and D. Wang. 2010. Synthesis, photoelectric properties and photocatalytic activity of the Fe_2O_3/TiO_2 heterogeneous photocatalysts. Phys. Chem. Chem. Phys. **12**:8033-8041.

Pereira, A. V., and Q. B. Cass. 2005. High-performance liquid chromatography method for the simultaneous determination of sulfamethoxazole and trimethoprim in bovine milk using an on-line clean-up column. J. Chromatogr. B **826**:139-146.

Petronella, F., A. Truppi, T. Sibillano, C. Giannini, M. Striccoli, R. Comparelli, and M. L. Curri. 2017. Multifunctional $TiO_2/Fe_xO_y/Ag$ based nanocrystalline heterostructures for photocatalytic degradation of a recalcitrant pollutant. Catal. Today **284**:100-106.

Pieper, C., D. Risse, B. Schmidt, B. Braun, U. Szewzyk, and W. Rotard. 2010. Investigation of the microbial degradation of phenazone-type drugs and their metabolites by natural biofilms derived from river water using liquid chromatography/tandem mass spectrometry (LC-MS/MS). Water Res. **44**:4559-4569.

Pietrini, F., D. Di Baccio, J. Acena, S. Perez, D. Barcelo, and M. Zacchini. 2015. Ibuprofen exposure in *Lemna gibba L.*: evaluation of growth and phytotoxic indicators, detection of ibuprofen and identification of its metabolites in plant and in the medium. J. Hazard. Mater. **300**:189-193.

Pillai, S. C., U. L. Štangar, J. A. Byrne, A. Pérez-Larios, and D. D. Dionysiou. 2015. Photocatalysis for disinfection and removal of contaminants of emerging concern. Chem. Eng. J. **261**:1-2.

Police, A. K. R., S. Basavaraju, D. K. Valluri, S. Muthukonda V, S. Machiraju, and J. S. Lee. 2014. $CaFe_2O_4$ sensitized hierarchical TiO_2 photo composite for hydrogen production under solar light irradiation. Chem. Eng. J. **247**:152-160.

Pomati, F., A. G. Netting, D. Calamari, and B. A. Neilan. 2004. Effects of erythromycin, tetracycline and ibuprofen on the growth of *Synechocystis* sp. and Lemna minor. Aquat. Toxicol. **67**:387-396.

Provasoli, L. 1958. Nutrition and ecology of protozoa and algae. Annu. Rev. Microbiol. **12**:279-308.

Puckowski, A., K. Mioduszewska, P. Lukaszewicz, M. Borecka, M. Caban, J. Maszkowska, and P. Stepnowski. 2016. Bioaccumulation and analytics of pharmaceutical residues in the environment: A review. J. Pharm. Biomed. Anal. **127**:232-255.

Qian, H., J. Li, L. Sun, W. Chen, G. D. Sheng, W. Liu, and Z. Fu. 2009. Combined effect of copper and cadmium on *Chlorella vulgaris* growth and photosynthesis-related gene transcription. Aquat. Toxicol. **94**:56-61.

Quero-Pastor, M. J., M. C. Garrido-Perez, A. Acevedo, and J. M. Quiroga. 2014. Ozonation of ibuprofen: a degradation and toxicity study. Sci. Total Environ. **466-467**:957-964.

Quinn, B., F. Gagne, and C. Blaise. 2008. An investigation into the acute and chronic toxicity of eleven pharmaceuticals (and their solvents) found in wastewater effluent on the cnidarian, *Hydra attenuata*. Sci. Total. Environ. **389**:306-314.

Radke, M., C. Lauwigi, G. Heinkele, T. E. Murdter, and M. Letzel. 2009. Fate of the antibiotic sulfamethoxazole and its two major human metabolites in a water sediment test. Environ. Sci. Technol. **43**:3135-3141.

Raj, K. J. A., and B. Viswanathan. Effect of surface area, pore volume and particle size of P25 titania on the phase transformation of anatase to rutile. Indian J. Chem. **48A**:1378-1382.

Rajabi, S., A. Ramazani, M. Hamidi, and T. Naji. 2015. Artemia salina as a model organism in toxicity assessment of nanoparticles. J. Pharm. Sci. **23**:20.

Rao, Y., and W. Chu. 2013. Visible light-induced photodegradation of simazine in aqueous TiO_2 suspension. Ind. Eng. Chem. Res. **52**:13580-13586.

Rao, Y. F., D. Xue, H. m. Pan, J. t. Feng, and Y. j. Li. 2016. Degradation of ibuprofen by a synergistic UV/Fe(III)/Oxone process. Chem. Eng. J. **283**:65-75.

Reddy, P. V., and K. H. Kim. 2015. A review of photochemical approaches for the treatment of a wide range of pesticides. J. Hazard. Mater. **285**:325-335.

Rezaei-Vahidian, H., A. R. Zarei, and A. R. Soleymani. 2017. Degradation of nitro-aromatic explosives using recyclable magnetic photocatalyst: catalyst synthesis and process optimization. J. Hazard. Mater. **325**:310-318.

Roberts, P. H., and K. V. Thomas. 2006. The occurrence of selected pharmaceuticals in wastewater effluent and surface waters of the lower Tyne catchment. Sci. Total Environ. **356**:143-153.

Rodayan, A., P. A. Segura, and V. Yargeau. 2014. Ozonation of wastewater: removal and transformation products of drugs of abuse. Sci. Total .Environ. **487**:763-770.

Roderick, M. S., J. L. Adcock, J. M. Terry, Z. M. Smith, S. Parry, S. M. Linton, M. T. Thornton, C. J. Barrow, and P. S. Francis. 2013. Chemiluminescence evidence supporting the selective role of ligands in the permanganate oxidation of micropollutants. J. Phys. Chem. A **117**:10286-10293.

Rodil, R., J. B. Quintana, and R. Cela. 2012. Transformation of phenazone-type drugs during chlorination. Water Res. **46**:2457-2468.

Rodriguez, E., M. E. Majado, J. Meriluoto, and J. L. Acero. 2007. Oxidation of microcystins by permanganate: reaction kinetics and implications for water treatment. Water Res. **41**:102-110.

Sa, X., J. Wa, G. Xa, H. Ya, and C. Za. 2009. Magnetically separable Fe_3O_4/TiO_2 hollow spheres: fabrication and photocatalytic activity. J. Phys. Chem. C **113**:553-558.

Salma, A., H. V. Lutze, T. C. Schmidt, and J. Tuerk. 2017. Photolytic degradation of the beta-blocker nebivolol in aqueous solution. Water Res. **116**:211-219.

Sanderson, H., R. A. Brain, D. J. Johnson, C. J. Wilson, and K. R. Solomon. 2004. Toxicity classification and evaluation of four pharmaceuticals classes: antibiotics, antineoplastics, cardiovascular, and sex hormones. Toxicology **203**:27-40.

Santoke, H., and W. J. Cooper. 2017. Environmental photochemical fate of selected pharmaceutical compounds in natural and reconstituted Suwannee River water: Role of reactive species in indirect photolysis. Sci. Total. Environ. **580**:626-631.

Sarmah, A. K., M. T. Meyer, and A. B. Boxall. 2006. A global perspective on the use, sales, exposure pathways, occurrence, fate and effects of veterinary antibiotics (VAs) in the environment. Chemosphere **65**:725-759.

Sathishkumar, P., R. V. Mangalaraja, S. Anandan, and M. Ashokkumar. 2013. $CoFe_2O_4/TiO_2$ nanocatalysts for the photocatalytic degradation of Reactive Red 120 in aqueous solutions in the presence and absence of electron acceptors. Chem. Eng. J. **220**:302-310.

Scheideler, J., K. Lekkerkerker-Teunissen, J. Verberk, and H. v. Dijk. 2011. Combination of O_3/H_2O_2 and UV for multiple barrier micropollutant treatment and bromate formation control – an economic attractive option. Water Pract. Tech. **6**.

Schultz, T. W., A. P. Bearden, and J. S. Jaworska. 1996. A novel QSAR approach for estimating toxicity of phenols. SAR QSAR Environ. Res. **5**:99-112.

Serna-Galvis, E. A., J. Silva-Agredo, A. L. Giraldo-Aguirre, O. A. Florez-Acosta, and R. A. Torres-Palma. 2016. High frequency ultrasound as a selective advanced oxidation process to remove penicillinic antibiotics and eliminate its antimicrobial activity from water. Ultrason. Sonochem. **31**:276-283.

Shahidi, D., A. Moheb, R. Abbas, S. Larouk, R. Roy, and A. Azzouz. 2015. Total mineralization of sulfamethoxazole and aromatic pollutants through Fe^{2+}-montmorillonite catalyzed ozonation. J. Hazard. Mater. **298**:338-350.

Sharma, V. K., S. K. Mishra, and A. K. Ray. 2006. Kinetic assessment of the potassium ferrate(VI) oxidation of antibacterial drug sulfamethoxazole. Chemosphere **62**:128-134.

Shi, Y., K. Zhou, B. Wang, S. Jiang, X. Qian, Z. Gui, R. K. K. Yuen, and Y. Hu. 2014. Ternary graphene–$CoFe_2O_4$/CdS nanohybrids: preparation and application as recyclable photocatalysts. J. Mater. Chem. A **2**:535-544.

Shirokova, L. S., O. S. Pokrovsky, S. N. Kirpotin, and B. Dupré. 2009. Heterotrophic bacterio‐plankton in thawed lakes of the northern part of Western Siberia controls the CO_2 flux to the atmosphere. Int. J. Environ. Stu. **66**:433-445.

Skoumal, M., R. M. Rodríguez, P. L. Cabot, F. Centellas, J. A. Garrido, C. Arias, and E. Brillas. 2009. Electro-Fenton, UVA photoelectro-Fenton and solar photoelectro-

Fenton degradation of the drug ibuprofen in acid aqueous medium using platinum and boron-doped diamond anodes. Electrochim. Acta **54**:2077-2085.

Smith, D. G. 2001. Pennak's freshwater invertebrates of the United States: Porifera to Crustacea, 4th Edition. John Wiley and Sons, Inc., Canada.

Spongberg, A. L., J. D. Witter, J. Acuna, J. Vargas, M. Murillo, G. Umana, E. Gomez, and G. Perez. 2011. Reconnaissance of selected PPCP compounds in Costa Rican surface waters. Water Res. **45**:6709-6717.

Srinivasan, S. S., J. Wade, and E. K. Stefanakos. 2006. Synthesis and characterization of photocatalytic TiO_2-$ZnFe_2O_4$ nanoparticles. J. Nanomater. **2006**:1-4.

Srithep, S., and S. Phattarapattamawong. 2017. Kinetic removal of haloacetonitrile precursors by photo-based advanced oxidation processes (UV/H_2O_2, UV/O_3, and UV/H_2O_2/O_3). Chemosphere **176**:25-31.

Staiger, C., J. d. Vries, and E. Walter. 1980. A rapid and sensitive method for the determination of phenazone (antipyrine®) using Gas-Liquid-Chromatography with nitrogen detection. J. Clin. Chem. Clin. Biochem. **18**:817-819.

Standards, J. C. o. P. D. 1995a. Powder Diffraction File, Card No. 21-1272. Swarthmore, PA.

Standards, J. C. o. P. D. 1995b. Powder Diffraction File, Card No. 21-1276. Swarthmore, PA.

Standards, J. C. o. P. D. 1995c. Powder Diffraction File, Card No. 22-1086. Swarthmore, PA.

Stone, A. T. 1987. Reductive dissolution of manganese (III/IV) oxides by substituted phenols. Environ. Sci. Technol. **21**:979-988.

Subramonian, W., T. Y. Wu, and S. P. Chai. 2017. Photocatalytic degradation of industrial pulp and paper mill effluent using synthesized magnetic Fe_2O_3-TiO_2: Treatment efficiency and characterizations of reused photocatalyst. J. Environ. Manage **187**:298-310.

Szot, M., 2014. Toxicity of the ibuprofen degradation product 4'-IBAP. Department of Biology. Lund University (Less).

Tan, C., N. Gao, Y. Deng, W. Rong, S. Zhou, and N. Lu. 2013a. Degradation of antipyrine by heat activated persulfate. Sep. Sci. Technol. **109**:122-128.

Tan, C., N. Gao, Y. Deng, Y. Zhang, M. Sui, J. Deng, and S. Zhou. 2013b. Degradation of antipyrine by UV, UV/H_2O_2 and UV/PS. J. Hazard. Mater. **260**:1008-1016.

Tang, Y., G. Zhang, C. Liu, S. Luo, X. Xu, L. Chen, and B. Wang. 2013. Magnetic TiO_2-graphene composite as a high-performance and recyclable platform for efficient photocatalytic removal of herbicides from water. J. Hazard. Mater. **252-253**:115-122.

Tay, K. S., and N. Madehi. 2015. Ozonation of ofloxacin in water: by-products, degradation pathway and ecotoxicity assessment. Sci. Total Environ. **520**:23-31.

Taylor, D., and T. Senac. 2014. Human pharmaceutical products in the environment - the "problem" in perspective. Chemosphere **115**:95-99.

Teel, A. L., and R. J.Watts. 2002. Degradation of carbon tetrachloride by modified Fenton's reagent. J. Hazard. Mater. **B94**:179-189.

Tekle-Rottering, A., K. S. Jewell, E. Reisz, H. V. Lutze, T. A. Ternes, W. Schmidt, and T. C. Schmidt. 2016. Ozonation of piperidine, piperazine and morpholine: Kinetics, stoichiometry, product formation and mechanistic considerations. Water Res. **88**:960-971.

Tong, A. Y. C., R. Braund, D. S. Warren, and B. M. Peake. 2012. TiO_2-assisted photodegradation of pharmaceuticals — a review. Cent. Eur. J. Chem. **10**:989-1027.

Torres, R. A., C. Petrier, E. Combet, M. Carrier, and C. Pulgarin. 2008. Ultrasonic cavitation applied to the treatment of bisphenol A. Effect of sonochemical parameters and analysis of BPA by-products. Ultrason. Sonochem. **15**:605-611.

Trawinski, J., and R. Skibinski. 2017. Photolytic and photocatalytic degradation of tandospirone: determination of kinetics, identification of transformation products and in silico estimation of toxicity. Sci. Total Environ. **590-591**:775-798.

Trovo, A. G., R. F. Nogueira, A. Aguera, A. R. Fernandez-Alba, C. Sirtori, and S. Malato. 2009a. Degradation of sulfamethoxazole in water by solar photo-Fenton. Chemical and toxicological evaluation. Water Res. **43**:3922-3931.

Trovo, A. G., R. F. Nogueira, A. Aguera, C. Sirtori, and A. R. Fernandez-Alba. 2009b. Photodegradation of sulfamethoxazole in various aqueous media: persistence, toxicity and photoproducts assessment. Chemosphere **77**:1292-1298.

Truong, G. L., J. De Laat, and B. Legube. 2004. Effects of chloride and sulfate on the rate of oxidation of ferrous ion by H_2O_2. Water Res. **38**:2383-2393.

Turner, J. T. 2015. Zooplankton fecal pellets, marine snow, phytodetritus and the ocean’s biological pump. Prog. Oceanog. **130**:205-248.

Underwood, J. C., R. W. Harvey, D. W. Metge, D. A. Repert, L. K. Baumgartner, R. L. Smith, T. M. Roane, and L. B. Barber. 2011. Effects of the antimicrobial sulfamethoxazole on groundwater bacterial enrichment. Environ. Sci. Technol. **45**:3096-3101.

Veith, G. D., N. Austin, and R. Morris. 1979. A rapid method for estimating log P for organic chemicals. Water Res. **13**:43-47.

Wammer, K. H., T. M. Lapara, K. Mcneill, W. A. Arnold, and D. L. Swackhamer. 2006. Changes in antibacterial activity of triclosan and sulfa drugs due to photochemical transformations. Environ. Toxicol. Chem.:1480–1486.

Wan, J., L. Zhou, H. Deng, F. Zhan, and R. Zhang. 2015. Oxidative degradation of sulfamethoxazole by different MnO_2 nanocrystals in aqueous solution. J. Mol. Catal. A-Chem. **407**:67-74.

Wang, A., Y.-Y. Li, and A. L. Estrada. 2011. Mineralization of antibiotic sulfamethoxazole by photoelectro-Fenton treatment using activated carbon fiber cathode and under UVA irradiation. Appl. Catal. B-Environ. **102**:378-386.

Wang, C., L. Yin, L. Zhang, L. Kang, X. Wang, and R. Gao. 2009a. Magnetic (y-$Fe_2O_3@SiO_2)_n@TiO_2$ functional hybrid nanoparticles with activated photocatalytic ability. J. Phys. Chem. C. **113**:4008-4011.

Wang, G., L. Xu, J. Zhang, T. Yin, and D. Han. 2012. Enhanced photocatalytic activity of powders (P25) via calcination treatment. Internat. J. Photoenergy **2012**:1-9.

Wang, H., N. Wang, B. Wang, H. Fang, C. Fu, C. Tang, F. Jiang, Y. Zhou, G. He, Q. Zhao, Y. Chen, and Q. Jiang. 2016. Antibiotics detected in urines and adipogenesis in school children. Environ. Int. **89-90**:204-211.

Wang, J., Z. Jiang, Z. Zhang, Y. Xie, X. Wang, Z. Xing, R. Xu, and X. Zhang. 2008. Sonocatalytic degradation of acid red B and rhodamine B catalyzed by nano-sized ZnO powder under ultrasonic irradiation. Ultrason. Sonochem. **15**:768-774.

Wang, M., L. Sun, J. Cai, P. Huang, Y. Su, and C. Lin. 2013. A facile hydrothermal deposition of $ZnFe_2O_4$ nanoparticles on TiO_2 nanotube arrays for enhanced visible light photocatalytic activity. J. Mater. Chem. A **1**:12082.

Wang, R.-C., K.-S. Fan, and J.-S. Chang. 2009b. Removal of acid dye by $ZnFe_2O_4/TiO_2$-immobilized granular activated carbon under visible light irradiation in a recycle liquid–solid fluidized bed. J. Taiwan Inst. Chem. Eng. **40**:533-540.

Wang, Y., S.-y. Chen, X. Yang, X.-f. Huang, Y.-h. Yang, E.-k. He, S. Wang, and R.-l. Qiu. 2017. Degradation of 2,2′,4,4′-tetrabromodiphenyl ether (BDE-47) by a nano zerovalent iron-activated persulfate process: The effect of metal ions. Chem. Eng. J. **317**:613-622.

Wang, Y. R., and W. Chu. 2011a. Degradation of 2,4,5-trichlorophenoxyacetic acid by a novel electro-Fe(II)/oxone process using iron sheet as the sacrificial anode. Water Res. **45**:3883-3889.

Wang, Y. R., and W. Chu. 2011b. Degradation of a xanthene dye by Fe(II)-mediated activation of oxone process. J. Hazard. Mater. **186**:1455-1461.

Wang, Y. R., and W. Chu. 2012. Photo-assisted degradation of 2,4,5-trichlorophenoxyacetic acid by Fe(II)-catalyzed activation of oxone process: The role of UV irradiation, reaction mechanism and mineralization. Appl. Catal. B-Environ. **123-124**:151-161.

Watts, R. J., B. C. Bottenberg, T. F. Hess, M. D. Jensen, and A. L. Teel. 1999. Role of reductants in the enhanced desorption. Environ. Sci. Technol. **33**:3432-3437.

Webb, S. F. 2003. Pharmaceuticals in the environment: sources, fate, effects and risks. Springer, Berlin.

Wilde, M. L., W. M. Mahmoud, K. Kummerer, and A. F. Martins. 2013. Oxidation-coagulation of beta-blockers by K_2FeVIO_4 in hospital wastewater: assessment of degradation products and biodegradability. Sci. Total Environ. **452-453**:137-147.

Wu, Q., H. Shi, C. D. Adams, T. Timmons, and Y. Ma. 2012. Oxidative removal of selected endocrine-disruptors and pharmaceuticals in drinking water treatment systems, and identification of degradation products of triclosan. Sci. Total. Environ. **439**:18-25.

Wu, W., J. Changzhong, and V. A. Roy. 2015. Recent progress in magnetic iron oxide-semiconductor composite nanomaterials as promising photocatalysts. Nanoscale **7**:38-58.

Xu, L. J., W. Chu, and N. Graham. 2013a. Sonophotolytic degradation of dimethyl phthalate without catalyst: analysis of the synergistic effect and modeling. Water Res. **47**:1996-2004.

Xu, L. J., W. Chu, and N. Graham. 2013b. A systematic study of the degradation of dimethyl phthalate using a high-frequency ultrasonic process. Ultrason. Sonochem. **20**:892-899.

Xu, S., W. Shangguan, J. Yuan, M. Chen, and J. Shi. 2007. Preparation and photocatalytic properties of magnetically separable TiO_2 supported on nickel ferrite. Chinese J. Chem. Eng. **15**:190-195.

Xu, S., W. Shangguan, J. Yuan, M. Chen, J. Shi, and Z. Jiang. 2008. Synthesis and performance of novel magnetically separable nanospheres of titanium dioxide photocatalyst with egg-like structure. Nanotechnology **19**:1-7.

Yan, T., Y. Wang, L. Wang, Y. Chen, G. Han, and M. J. Zhou. 2009. Application of rotifer *Brachionus plicatilis* in detecting the toxicity of harmful algae. Chin. J. Oceanol. Limnol. **27**:376-382.

Yang, B., G. G. Ying, J. L. Zhao, S. Liu, L. J. Zhou, and F. Chen. 2012. Removal of selected endocrine disrupting chemicals (EDCs) and pharmaceuticals and personal care products (PPCPs) during ferrate(VI) treatment of secondary wastewater effluents. Water Res. **46**:2194-2204.

Yang, C.-C., C.-L. Huang, T.-C. Cheng, and H.-T. Lai. 2015. Inhibitory effect of salinity on the photocatalytic degradation of three sulfonamide antibiotics. Int. Biodeter. Biodegr. **102**:116-125.

Yang, J.-F., L.-M. Yang, S.-B. Zhang, L.-H. Ou, C.-B. Liu, L.-Y. Zheng, Y.-F. Yang, G.-G. Ying, and S.-L. Luo. 2017. Degradation of azole fungicide fluconazole in aqueous solution by thermally activated persulfate. Chem. Eng. J. **321**:113-122.

Yang, J. F., G. G. Ying, J. L. Zhao, R. Tao, H. C. Su, and Y. S. Liu. 2011. Spatial and seasonal distribution of selected antibiotics in surface waters of the Pearl Rivers, China. J. Environ. Sci. Health B **46**:272-280.

Yang, X., F. Chen, F. Meng, Y. Xie, H. Chen, K. Young, W. Luo, T. Ye, and W. Fu. 2013. Occurrence and fate of PPCPs and correlations with water quality parameters in urban riverine waters of the Pearl River Delta, South China. Environ. Sci. Pollut. Res. Int. **20**:5864-5875.

Yehia, F. Z., G. Eshaq, A. M. Rabie, A. H. Mady, and A. E. ElMetwally. 2015. Phenol degradation by advanced Fenton process in combination with ultrasonic irradiation. Egypt. J. Petro. **24**:13-18.

Yoon, M., Y. Oh, S. Hong, J. S. Lee, R. Boppella, S. H. Kim, F. Marques Mota, S. O. Kim, and D. H. Kim. 2017. Synergistically enhanced photocatalytic activity of graphitic carbon nitride and WO_3 nanohybrids mediated by photo-Fenton reaction and H_2O_2. Appl. Catal. B-Environ. **206**:263-270.

Yu, H. W., T. Anumol, M. Park, I. Pepper, J. Scheideler, and S. A. Snyder. 2015. On-line sensor monitoring for chemical contaminant attenuation during UV/H_2O_2 advanced oxidation process. Water Res. **81**:250-260.

Yu, J., and G. Wang. 2008. Hydrothermal synthesis and photocatalytic activity of mesoporous titania hollow microspheres. J. Phys. Chem. Solids **69**:1147-1151.

Yu, Y.-Y., and H.-Q. Zhang. 2016. Reduced graphene oxide coupled magnetic $CuFe_2O_4$-TiO_2 nanoparticles with enhanced photocatalytic activity for methylene blue degradation. J. Struct. Chem. Mater. **35**:472-480.

Yuan, F., C. Hu, X. Hu, J. Qu, and M. Yang. 2009. Degradation of selected pharmaceuticals in aqueous solution with UV and UV/H_2O_2. Water Res. **43**:1766-1774.

Yuan, J., L. Yong-kang, L. Yu, and L. Jun-ping. 2010. Synthesis and characterization of magnetic TiO_2/SiO_2/$NiFe_2O_4$ composite photocatalysts. Chem. Res. **26** 278-282.

Yuan, Z.-h., and L.-d. Zhang. 2001. Synthesis, characterization and photocatalytic activity of $ZnFe_2O_4$/TiO_2 nanocomposite. J. Mater. Chem. **11**:1265-1268.

Zhan, J., H. Zhang, and G. Zhu. 2014. Magnetic photocatalysts of cenospheres coated with Fe_3O_4/TiO_2 core/shell nanoparticles decorated with Ag nanopartilces. Ceram. Int. **40**:8547-8559.

Zhang, B., J. Zhang, and F. Chen. 2008. Preparation and characterization of magnetic $TiO_2/ZnFe_2O_4$ photocatalysts by a sol–gel method. Res. Chem. Intermed. **34**:375-380.

Zhang, D., B. Pan, H. Zhang, P. Ning, and B. Xing. 2010a. Contribution of different sulfamethoxazole species to their overall adsorption on functionalized carbon nanotubes. Environ. Sci. Technol. **44**:3806-3811.

Zhang, G.-Y., Y.-Q. Sun, D.-Z. Gao, and Y.-Y. Xu. 2010b. Quasi-cube $ZnFe_2O_4$ nanocrystals: hydrothermal synthesis and photocatalytic activity with TiO_2 (Degussa P25) as nanocomposite. Mater. Res. Bull. **45**:755-760.

Zhang, H., and C.-H. Huang. 2003. Oxidative transformation of triclosan and chlorophene by manganese oxides. Environ. Sci. Technol. **37**: 2421-2430.

Zhang, J., and X. Guan. 2013. Ru(III)-catalyzed permanganate oxidation of bisphenol A. Desalin. Water Treat. **52**:4592-4601.

Zhang, J., B. Sun, and X. Guan. 2013a. Oxidative removal of bisphenol A by permanganate: Kinetics, pathways and influences of co-existing chemicals. Sep. Purif. Technol. **107**:48-53.

Zhang, J., B. Sun, X. Guan, H. Wang, H. Bao, Y. Huang, J. Qiao, and G. Zhou. 2013b. Ruthenium nanoparticles supported on CeO_2 for catalytic permanganate oxidation of butylparaben. Environ. Sci. Technol. **47**:13011-13019.

Zhang, J., B. Sun, X. Xiong, N. Gao, W. Song, E. Du, X. Guan, and G. Zhou. 2014a. Removal of emerging pollutants by Ru/TiO_2-catalyzed permanganate oxidation. Water Res. **63**:262-270.

Zhang, J., Y. Zhang, H. Wang, and X. Guan. 2014b. Ru(III) catalyzed permanganate oxidation of aniline at environmentally relevant pH. J. Environ. Sci. **26**:1395-1402.

Zhang, K., Z. Luo, T. Zhang, N. Gao, and Y. Ma. 2015a. Degradation effect of sulfa antibiotics by ptassium frrate cmbined with utrasound (Fe(VI)-US). Biomed Res. Int. **2015**:169215.

Zhang, L., Y. He, Y. Wu, and T. Wu. 2011. Photocatalytic degradation of RhB over $MgFe_2O_4$/TiO_2 composite materials. Mater. Sci. Eng.-B **176**:1497-1504.

Zhang, Q. Q., G. G. Ying, C. G. Pan, Y. S. Liu, and J. L. Zhao. 2015b. Comprehensive evaluation of antibiotics emission and fate in the river basins of China: source analysis, multimedia modeling, and linkage to bacterial resistance. Environ. Sci. Technol. **49**:6772-6782.

Zhang, R., P. Sun, T. H. Boyer, L. Zhao, and C. H. Huang. 2015c. Degradation of pharmaceuticals and metabolite in synthetic human urine by UV, UV/H_2O_2, and UV/PDS. Environ. Sci. Technol. **49**:3056-3066.

Zhang, R., Y. Yang, C. H. Huang, N. Li, H. Liu, L. Zhao, and P. Sun. 2016. UV/H_2O_2 and UV/PDS treatment of trimethoprim and sulfamethoxazole in synthetic human urine: transformation products and toxicity. Environ. Sci. Technol. **50**:2573-2583.

Zhang, X., and L. Lei. 2008. Preparation of photocatalytic Fe_2O_3–TiO_2 coatings in one step by metal organic chemical vapor deposition. Appl. Surf. Sci. **254**:2406-2412.

Zhang, Y., J. Zhang, Y. Xiao, V. W. Chang, and T. T. Lim. 2017. Direct and indirect photodegradation pathways of cytostatic drugs under UV germicidal irradiation: process kinetics and influences of water matrix species and oxidant dosing. J. Hazard. Mater. **324**:481-488.

Zhang, Z., and W. Wang. 2014. Solution combustion synthesis of $CaFe_2O_4$ nanocrystal as a magnetically separable photocatalyst. Mater. Lett. **133**:212-215.

Zhao, J., Y. Zhang, X. Quan, and S. Chen. 2010. Enhanced oxidation of 4-chlorophenol using sulfate radicals generated from zero-valent iron and peroxydisulfate at ambient temperature. Sep. Purif. Technol. **71**:302-307.

Zhao, Y., J. Kuang, S. Zhang, X. Li, B. Wang, J. Huang, S. Deng, Y. Wang, and G. Yu. 2017. Ozonation of indomethacin: kinetics, mechanisms and toxicity. J. Hazard. Mater. **323**:460-470.

Zheng, J., Y. Wu, Q. Zhang, Y. Li, C. Wang, and Y. Zhou. 2016. Direct liquid phase deposition fabrication of waxberry-like magnetic Fe_3O_4@TiO_2 core-shell microspheres. Mater. Chem. Phys. **181**:391-396.

Zhong, Y., X. Liang, W. Tan, Y. Zhong, H. He, J. Zhu, P. Yuan, and Z. Jiang. 2013. A comparative study about the effects of isomorphous substitution of transition metals (Ti, Cr, Mn, Co and Ni) on the UV/Fenton catalytic activity of magnetite. J. Mol. Catal. A-Chem. **372**:29-34.

Zhou, L., C. Ferronato, J.-M. Chovelon, M. Sleiman, and C. Richard. 2017. Investigations of diatrizoate degradation by photo-activated persulfate. Chem. Eng. J. **311**:28-36.

Zhou, L. J., G. G. Ying, S. Liu, R. Q. Zhang, H. J. Lai, Z. F. Chen, and C. G. Pan. 2013a. Excretion masses and environmental occurrence of antibiotics in typical swine and dairy cattle farms in China. Sci. Total Environ. **444**:183-195.

Zhou, L. J., G. G. Ying, S. Liu, J. L. Zhao, B. Yang, Z. F. Chen, and H. J. Lai. 2013b. Occurrence and fate of eleven classes of antibiotics in two typical wastewater treatment plants in South China. Sci. Total Environ. **452-453**:365-376.

Zhou, Q., J. Li, M. Wang, and D. Zhao. 2016. Iron-based magnetic nanomaterials and their environmental applications. Crit. Rev. Environ. Sci. Tec. **46**:783-826.

Zhou, X. T., H. B. Ji, and X. J. Huang. 2012. Photocatalytic degradation of methyl orange over metalloporphyrins supported on TiO_2 Degussa P25. Molecules **17**:1149-1158.

Zhou, Y., J. Jiang, Y. Gao, J. Ma, S. Y. Pang, J. Li, X. T. Lu, and L. P. Yuan. 2015a. Activation of peroxymonosulfate by benzoquinone: A novel nonradical oxidation process. Environ. Sci. Technol. **49**:12941-12950.

Zhou, Z., and J. Q. Jiang. 2015. Treatment of selected pharmaceuticals by ferrate(VI): performance, kinetic studies and identification of oxidation products. J. Pharm. Biomed. Anal. **106**:37-45.

Zhou, Z., Y. Yang, and X. Li. 2015b. Effects of ultrasound pretreatment on the characteristic evolutions of drinking water treatment sludge and its impact on coagulation property of sludge recycling process. Ultrason. Sonochem. **27**:62-71.

Zorita, S., L. Martensson, and L. Mathiasson. 2009. Occurrence and removal of pharmaceuticals in a municipal sewage treatment system in the south of Sweden. Sci. Total. Environ. **407**:2760-2770.

Zrinyi, N., and A. L. Pham. 2017. Oxidation of benzoic acid by heat-activated persulfate: effect of temperature on transformation pathway and product distribution. Water Res. **120**:43-51.

Zuehlke, S., U. Duennbier, B. Lesjean, R. Gnirss, and H. Buisson. 2006. Long-term comparison of trace organics removal performances between conventional and membrane activated sludge processes. Water Environ. Res. **78**:2480-2486.